SIMULATION OF SPATIAL AND TEMPORAL VARIABILITY OF METHYLMERCURY CONCENTRATION WITHIN CHANNEL BANKS AND SURFACE WATERS OF THE CARSON RIVER, NEVADA

By

DANIEL E. CRAWFORD

A THESIS PRESENTED TO THE GRADUATE SCHOOL
OF THE UNIVERSITY OF FLORIDA IN PARTIAL FULFILLMENT
OF THE REQUIREMENTS FOR THE DEGREE OF
MASTER OF ENGINEERING

UNIVERSITY OF FLORIDA

2003

This thesis is dedicated to the graduate students of the University of Florida.

ACKNOWLEDGMENTS

I would like to thank the National Science Foundation for their generous support of this project through grant # 4510586-12. I wish to acknowledge the time, effort, and continued support of my advisor John J. Warwick. The well-being of his students always remained a priority. Special thanks go to Andy James for his support and guidance throughout this research, most notably during the 7 months after John's departure. I also thank Bill Wise and Jean-Claude Bonzongo for serving on my committee and providing invaluable feedback. I thank my peers and closest friends for helping me (through countless hours of frustration) with words of encouragement; and for always being there. Lastly, I would like to thank my parents and family. Although the research may not have been their forte, their support, encouragement, and sense of pride in my accomplishments never waned. My time at this university has been long-lived, but the experience was greater than ever expected and has truly prepared me for the future.

TABLE OF CONTENTS

APPENDIX

LIST OF TABLES

LIST OF FIGURES

Abstract of Thesis Presented to the Graduate School
of the University of Florida in Partial Fulfillment of the
Requirements for the Degree of Master of Engineering

SIMULATION OF SPATIAL AND TEMPORAL VARIABILITY OF METHYLMERCURY CONCENTRATION WITHIN CHANNEL BANKS AND SURFACE WATERS OF THE CARSON RIVER, NEVADA

By

Daniel E. Crawford

August 2003

Chair: John J. Warwick
Major Department: Environmental Engineering Sciences

The USEPA designated the Carson River, Nevada as part of a Superfund site in 1990. Between 1860 and 1890, elemental mercury was used at over 70 mill sites to recover gold and silver via mercury amalgamation, introducing 7000 tons of mercury to the Carson River watershed. Contaminated sediments line channel banks downstream of these mill sites, with mercury concentrations two to three orders of magnitude above regional background levels. Mercury concentrations in both the Carson River and Lahontan Reservoir are among the highest known worldwide. Mercury methylation within sediments (accompanied by diffusion, advection, and erosion processes) introduces toxic methylmercury to the water column for ultimate transport into Lahontan Reservoir. Methylmercury concentrations in the bank are not spatially and temporally constant; but are instead a function of moisture history.

A computer simulation model, Integrated Fluvial Mercury Transport and Fate Model (IFMTFM), was developed to simulate bank erosion and diffusion from bottom

sediments. A new bank element was developed and incorporated into the previous IFMTFM, to relate flow history within the channel to moisture-content levels observed within the channel banks. Zones of varying moisture affect methylation and demethylation kinetics; and therefore affect temporal concentrations of methylmercury available to the water column.

Global positioning system (GPS) data were used to construct a detailed, temporal model of three-dimensional river hydrodynamics for a specific reach of the model domain, using Surface Water Modeling System (SMS) software. Streamflow and water table data show a tight coupling between the Carson River and the surficial aquifer. The nearly instantaneous water table response to streamflow oscillations (as observed in a monitoring well set back 5 feet from the channel bank) serves as the foundation for bank element functionality.

Incorporation of the bank element into the complete Carson River model of hydrodynamics, sediment transport, and mercury transport and cycling (IFMTFM) provides a new capability to simulate temporally variable mercury concentrations within the channel bank; reduces the number of model calibration parameters from three to two; and increases the accuracy of in-stream mercury predictions. The height of bank saturation and zone of active microbial methylation are continuously updated as river stage changes. Contacted bank sediments release mercury to the water column through erosion, advection, and diffusion processes; with no threshold height for methylation. Hydrodynamic components of IFMTFM (RIVMOD) and SMS were compared to show the value of high-resolution transect data.

CHAPTER 1
RESEARCH LOCATION: AN INTRODUCTION TO THE CARSON RIVER

Carson River Basin

The Carson River, located in the southwestern corner of Nevada, drains from the eastern Sierra Nevada Mountains just south of the Lake Tahoe Basin (NDWP, 1996). The Sierra Nevada Mountains thus serve as the river basin's primary source of precipitation. Precipitation in the Carson River Basin is attenuated by the rainshadow of the Sierra Nevada. In the modeled portion of the Carson River (downstream of Carson City, Figure 1-1), the climate is semi-arid, with typical annual precipitation of less than 5 inches (Covay et al., 1996). Vegetation near the river is largely sagebrush or similar species, with cottonwood trees growing along the riparian zone immediately adjacent to the river.

The Carson River Basin encompasses an area of approximately 3,966 square miles in the states of California and Nevada (Figure 1-1). The basin is topographically closed. A closed basin has no outlet, and water entering such a basin discharges only by evapotranspiration or loss to groundwater (Covay et al., 1996). The upper portion of the Carson River Basin is drained by the Carson River's East and West Forks. The Carson River's two forks merge in the northern part of Carson Valley and form the Carson River mainstem, which then continues on toward the river system's terminus in the Carson Sink. The Carson Valley agricultural area diverts water from both river forks and from the Carson River mainstem, to provide irrigation for approximately 35,000 acres. Lahontan Reservoir, completed in 1915 with the construction of Lahontan Dam, serves as a major sediment trap upstream of the Carson Sink. The Truckee Canal diverts water

from the Truckee River Basin into the reservoir, to meet the agricultural water demands associated with the Newlands Irrigation Project (downstream of Lahontan Dam). United States Geological Survey (USGS) streamflow gages are available at Carson City (CCG station #10311000), Fort Churchill (FCH #10312000), Lahontan Dam (LDM #10312150), and the Truckee Canal (TRC #10351400).

Of the Carson River Basin's total surface area, approximately 606 square miles (387,840 acres; or just over 15%) lie within the State of California. The remaining 3,360 square miles (2,149,680 acres; or almost 85%) lie within the State of Nevada (NDWP, 1996). While most of the basin's surface area is in the State of Nevada, most of the basin's precipitation originates in the State of California. The geographic separation between the Carson River Basin's principal supply of water and its principal demands has historically resulted in controversy surrounding the rights to and uses of water resources. The lower Carson River Basin begins at the head of Dayton Valley and ends at the furthermost extent of the Carson Sink (NDWP, 1996). The geology of this region (Lahontan Valley), the bottom of a prehistoric lake, is characterized by sediment deposits between 3,000 and 8,000 feet in thickness. The present-day Lahontan Valley and Carson Desert, now considerably drier, is characterized by a number of important and varied hydrologic features including lakes, marshes and wetlands, cultivated farmlands and pastures, barren desert sinks, alkali flats, and playas.

Carson River Streamflow

The rain-shadow effect of the Sierra Nevada Mountains to the west allows little precipitation to fall within the Lahontan Valley (NDWP, 1996). Average annual precipitation is only about 5 inches, while annual potential evaporation exceeds 60 inches.

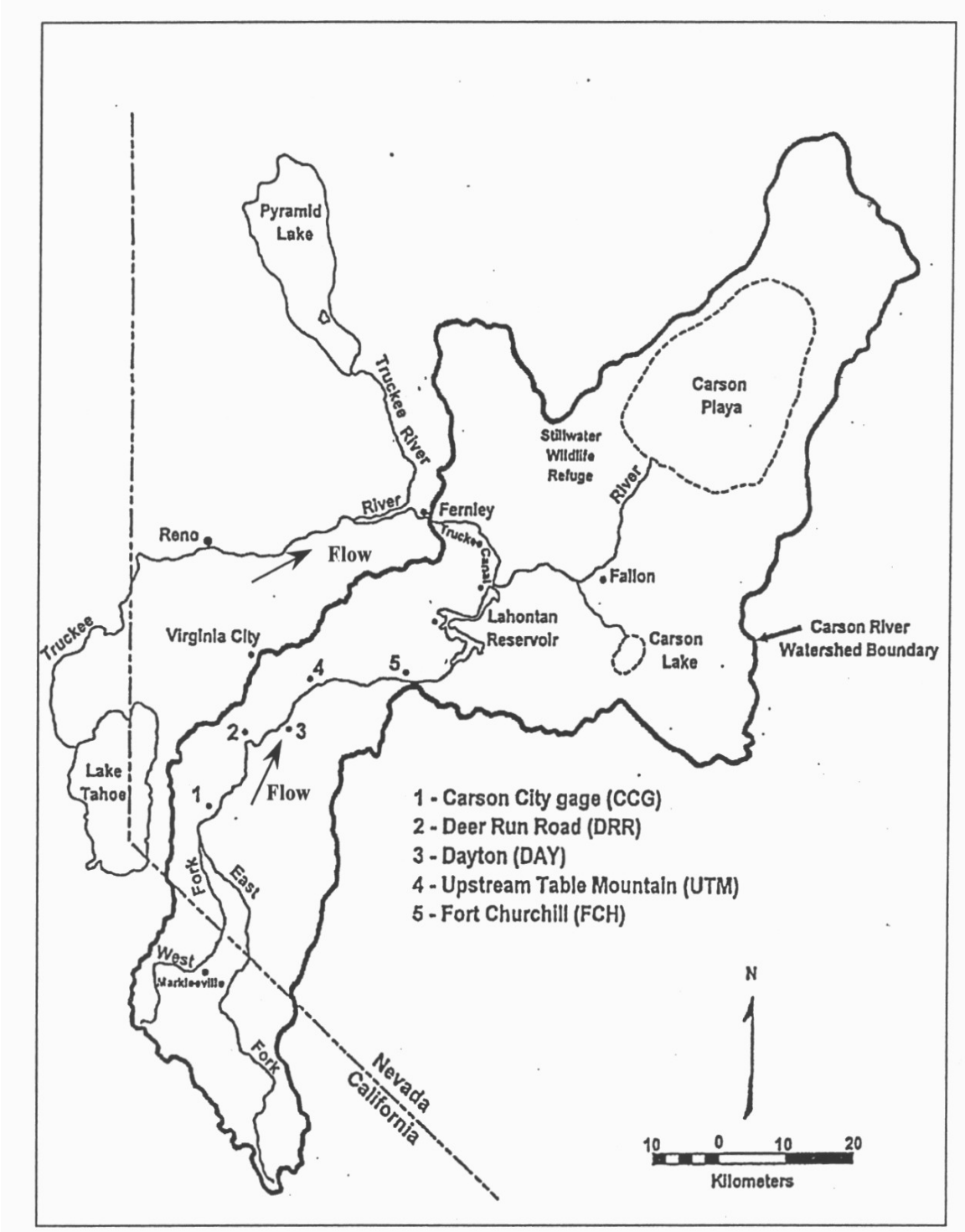

Figure 1-1. Map of the Carson River drainage and selected sampling sites. (Reprinted with permission from Carroll, R.W.H., 1999. Simulation of Mercury Transport and Fate in the Carson River, Nevada. Masters Thesis. University of Nevada-Reno, Reno, Nevada. Figure 1.1, pp. 9)

Before extensive upstream storage and water diversions, the Lahontan Valley was generally inundated in late winter and early spring by the unhindered runoff of the melting snow pack from the Sierra Nevada Range. After this runoff period, a drying pattern would ensue during the remainder of the year until the winter precipitation period commenced again in October-November. This highly seasonal pattern of wet and dry has been disrupted since the completion of the Newlands Project in the valley in 1903, and particularly after the completion of Lahontan Reservoir in 1915.

Carson River flow is primarily from snowmelt, but the effects of upstream storage and storage in Lahontan Reservoir have tended to moderate flow magnitudes. The cycle of seasonal high flows in the spring (due to snowmelt) and low flows during the remainder of the year in the Carson River upstream of the Lahontan Reservoir continues, but the flow magnitudes no longer reflect pre-development conditions. Snowmelt, whether immediate or from upstream reservoir releases, is the source of Carson River streamflow; this observation, along with the semi-arid Nevada climate and the extensive diversion of water for agricultural use along the entire Carson River, results in a highly variable streamflow pattern.

Carson River flows may vary by three to four orders of magnitude on an annual basis. During late summer and early fall, streamflow in downstream reaches of the Carson River may be nonexistent. By contrast, consider the rain-on-snow flood event of January 1997; the Carson River extended well into the floodplain, with peak discharge values of 24,000 cubic feet per second (cfs) and 22,300 cfs estimated at Carson City Gage (CCG) and Fort Churchill Gage (FCH), respectively (USGS, 1997).

Carson River Aquifer Systems

Principal aquifers in the Carson River Basin are unconsolidated basin-fill deposits of interbedded gravel, sand, silt, and clay (Covay et al., 1996). Aquifers within the basin readily receive, transmit, and store large volumes of water. Detailed hydrologic investigations of the Carson River Basin have been performed as part of the USGS National Water-Quality Assessment (NAWQA) program. General areas along the Carson River underlain by basin-fill aquifers include Carson Valley, Eagle Valley, Dayton Valley, and Churchill Valley.

Unconsolidated deposits occur in all valleys of the Carson River Basin and are the primary water-bearing units (Covay et al., 1996). Carson Valley contains unconsolidated Quaternary basin-fill sediments (mostly fine- to coarse-grained Carson River alluvium), and semiconsolidated Tertiary sediments (mostly lake and stream deposits) (Maurer, 1986). Eagle Valley contains Quaternary semiconsolidated and unconsolidated alluvium (including deposits of sand, silt, and coarse materials; and clay confining units) (Trexler, 1977; Arteaga, 1986). Basin-fill deposits in Dayton and Churchill Valleys include Cenozoic sedimentary deposits (500 to 3000 ft thick); alluvial fans and pediments; and lake, river, delta, and floodplain deposits (consisting of a mixture of clays, silts, sands, and gravel) (Schaefer and Whitney, 1992). The sediments within the modeled reach of the Carson River Valley clearly may be defined as typical alluvium.

Historical Mining Operations

Historical mining activities have contaminated lower reaches of the Carson River, Lahontan Reservoir, and Stillwater Marsh with mercury. Extensive milling and ore processing operations were situated within Dayton Valley during the era of the Comstock Lode during the late 1800s (NDWP, 1996). Here the Carson River passes through a

canyon and loses 240 feet of elevation over a distance of 10 miles. With its proximity to the Comstock mines to the north and the available hydropower, this was an ideal location to establish the mills. During the peak of the Comstock era, more than 75 mills operated along the Carson River.

Gold Canyon and Sixmile Canyon (Figure 1-2) mark the geologic boundaries of one of this nation's richest silver strikes—the Comstock Lode. Known mill tailings deposits are found in areas along the Carson River from just downstream of Carson City to Dayton and in areas along the Carson River tributaries from Virginia City (Wayne et al., 1996), as shown by the crosshatched areas in Figure 1-2. “Efforts to extract this vast body of silver wealth would begin a period of natural resource exploitation (timber cutting and water diversions) and environmental degradation (deforestation, soil erosion, water pollution, arsenic and mercury spills), the effects of which have carried forward to the present day” (NDWP, 1996). During the Comstock's peak years of production (1862 to 1880), approximately $296,400,000 worth of silver and gold were removed from the mines. Over its entire active mining period, which lasted from 1857 to 1921, the Comstock yielded $386,346,931 (historical value) in total mineral production (of which $222,315,814 was in silver; $164,023,917 was gold; and $7,200 was copper and lead).

Mining operations associated with the Comstock Lode resulted in the production of an extensive volume of mine tailings (waste rock material). It has been estimated that during some peak periods of mining, more than 600 tons of tailings material were released to the surrounding area on a daily basis (Miller et al., 1998). Liquid elemental mercury was used to extract gold and silver from the mined material using an amalgamation process. This introduced an estimated 7000 tons of mercury into the

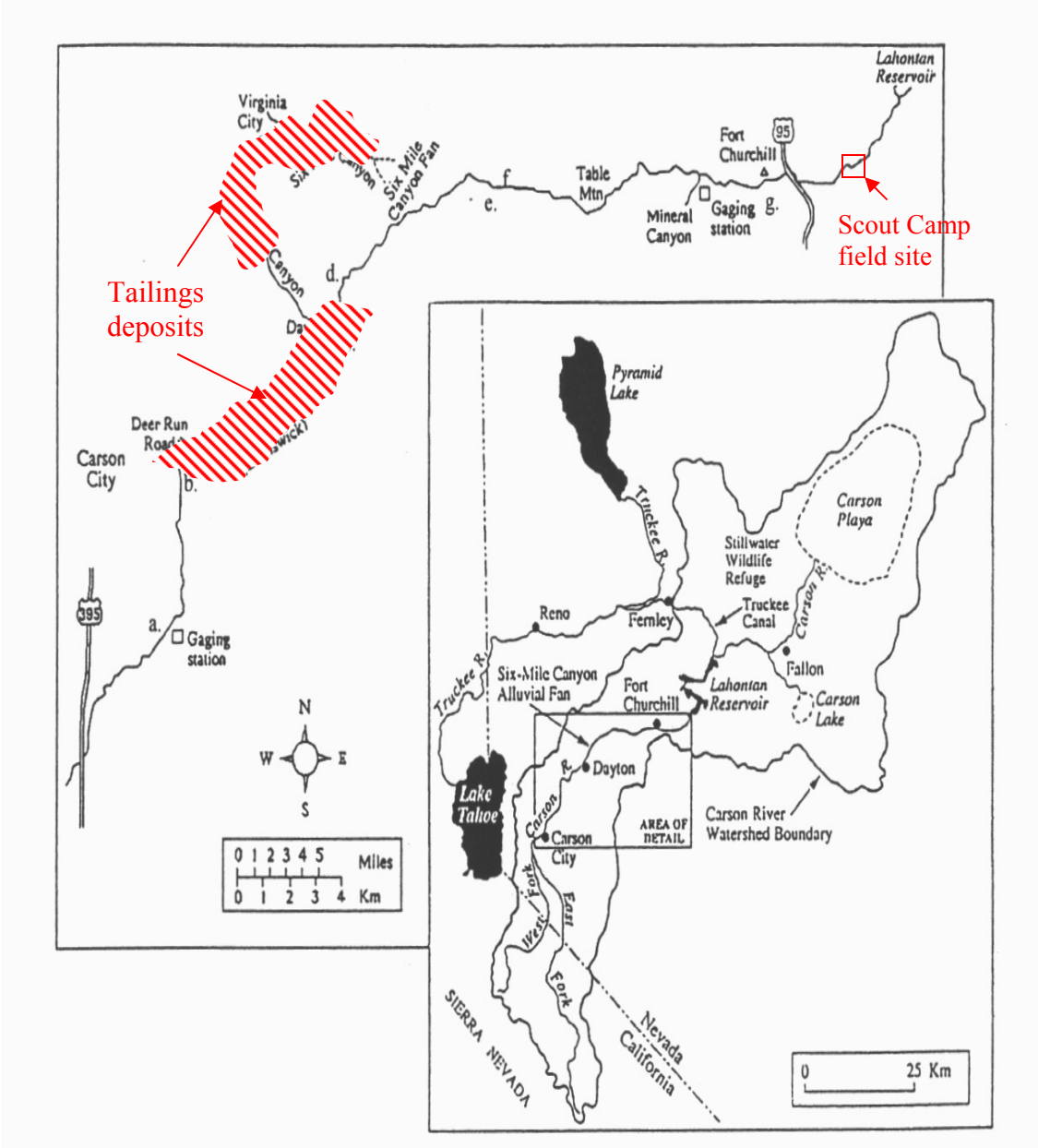

Figure 1-2. General locations of known mill tailings deposits and Scout Camp field site

Carson River system through mercury residual within the mine tailings (Carroll, 1999), along with the immense, immeasurable volume of associated sediment. At the mills, mined ores were pulverized and mixed with mercury, forming a mercury-silver/gold amalgam because of the high affinity of mercury for these metals (a method known as the Washoe process). Float tanks were used to separate the amalgam from the waste rock.

Roasting the amalgam, releasing the mercury from the complex as a vapor, would then produce a pure form of the precious metals. Although most of the mercury vapor was recovered, it was estimated that as much as 0.68 kg of mercury was released to the environment with mill tailings for every ton of ore that was processed (Miller et al., 1996). During the past 140 years, mercury-contaminated sediments were eroded from the mill sites, transported downstream by fluvial processes, and re-deposited in specific localities, thereby expanding the influence of mercury pollution (Miller et al., 1996).

Carson River Geomorphology

Analysis of historical documents and alluvial stratigraphy indicate that the Carson River underwent significant changes in channel form and process during the period of the Comstock Lode (Miller et al., 1998). The increased sediment load resulting from the constant supply of mine tailings, along with sediment introduced from clear-cut headwater areas used for timber production during this period, caused the river to aggrade (on the order of several meters); and to experience lateral instability and meander abandonment. The valley floor and abandoned channels subsequently filled with contaminated debris. The end result of these processes was the storage of mercury-enriched sediments within a complexly structured alluvial sequence located all along the Carson River valley downstream of Carson City (Miller et al., 1999). Mercury concentrations in the alluvial valley fill deposits exhibit great spatial variability (longitudinally and laterally along the river; and vertically within sediment deposits), but the concentrations are generally two to three orders of magnitude greater than regional background levels of 0.01 to 0.10 μg/L (Miller et al., 1998).

The eventual reduction of mining operations decreased the sediment load and caused the river to downcut through these contaminated sediments. Today, the Carson River continues to reclaim its original floodplain in an attempt to establish a new equilibrium. Mercury-contaminated sediment is believed to enter the system primarily during higher flow events when water levels reach overlying contaminated sediments (notably within the floodplain) and erosional processes become significant. Initially, mercury released from mines represented a point-source contaminant problem. Modern mercury pollution of the Carson River must be considered a distributed-source problem because of the contaminated sediment stored within channel banks.

CHAPTER 2
MERCURY CONTAMINATION AND MERCURY CYCLING

Mercury Cycling within Surface Water Systems

Mercury is introduced to surface waters through atmospheric deposition, surface runoff (erosion), and diffusion. After mercury enters into surface water, it enters a complex cycle of transformations—primarily according to redox chemistry and microbes. A schematic drawing of mercury cycling in an aquatic ecosystem is shown in Figure 2-1 (USGS, 1995). Mercury may remain in the water column or be lost through drainage or advection. Mercury can be incorporated into the bed sediments by particle settling, perhaps only to be later released by diffusion or resuspension. The formation of methylmercury can introduce mercury into the food chain, or volatilization may exile the mercury back to the atmosphere. Divalent mercury and methylmercury, critical components of the Carson River system, can be transported to water bodies in runoff, typically bound to suspended soil/humus or attached to DOC (dissolved organic carbon), or Hg(II) and methylmercury can leach into the water body from groundwater flow in the upper soil layers (USEPA, 1997). Research has shown that both DOC and pH can play a significant role in the fate of mercury within a system. Studies have shown that DOC concentration and pH levels have a strong effect on mercury fate, with increasing acidity (decreasing pH) and increasing DOC content resulting in higher body burdens in fish (USGS, 1995). The movement of mercury will vary within each given body of water. Mercury concentrations are typically reported for the water column (dissolved or

particulate), the underlying sediment (surface or deep sediments), and biota (generally fish) (USEPA, 1997).

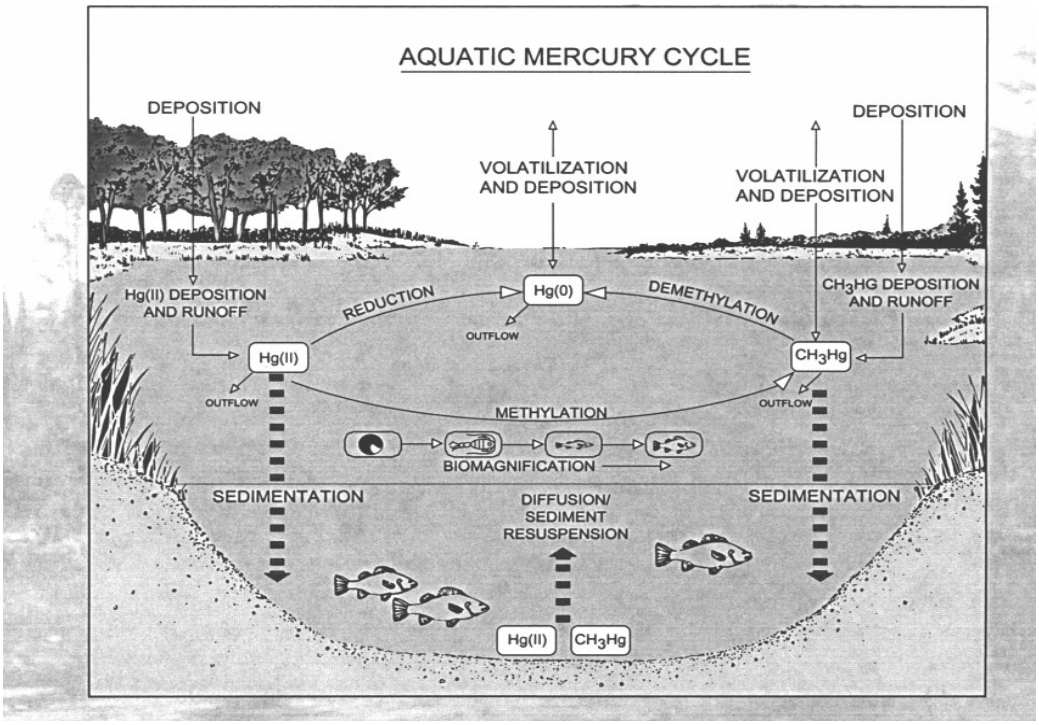

Figure 2-1. The aquatic mercury cycle. (USGS, 1995. Mercury Contamination of Aquatic Ecosystems. U.S. Geological Survey Fact Sheet 216-95. Figure 6, pp. 3)

Quantification of Mercury Levels in the Carson River System

The major water issue for the lower Carson River Basin focuses not on quantity but rather quality (NDWP, 1996; Carroll, 1999; Miller et al., 1998). Mercury is introduced into the river from the contaminated mine tailings distributed throughout the riverbank sediments and floodplain deposits. Mercury concentrations in the tailings are two to three orders of magnitude greater than background concentrations in the region. Sampling by the United States Environmental Protection Agency (USEPA) found mercury concentrations as high as 4,600 parts per million (ppm) in the fine-grained materials of the tailings piles. Mercury dispersal from these tailings is extensive. Concentrations exceeding 100 ppm have been measured more than 60 kilometers (km) downstream of

the mining operations. During the most intense period of mining activity, the Carson River emptied directly onto an extensive wetland now known as the Stillwater Wildlife Management Area (SWMA). The completion of Lahontan Dam in 1915 created a new settling basin for sediments derived from the mercury-contaminated mine tailings, but a large amount of mercury had already been introduced to the wetland habitat downstream of the dam.

Several extensive site-characterization studies addressed mercury contamination along the Carson River System. Total mercury (Hg) in three mountain streams indicates background levels of < 2 nanograms per liter (ng/L) for this region of Nevada (Wayne et al., 1996). Water samples collected in 1992 and 1993 showed the following:

- Elevated (e.g., > 20 ng/L) mercury levels first appear downstream from accumulations of mill tailings.
- Total mercury concentrations in unfiltered and filtered water increase downstream.
- Mercury concentrations in both the Carson River and Lahontan Reservoir are among the highest known worldwide (100 to 1000 ng/L); filtered water samples suggest that the >0.4 μm particle fraction constitutes over 60% of the total water-borne mercury (Wayne et al., 1996).

Abnormally high levels of Hg, Au, and Ag occur in sediments downstream of former ore milling operations. Systematic trends are apparent from the analysis of bank and bed samples (Wayne et al., 1996): mine tailings have the highest Hg, Au, and Ag contents, and fine-grained silts and muds from the river banks typically have higher Hg contents than coarser sands and gravel from the river channel; and mercury contents in both channel and bank deposits increase with increasing distance from CCG. Potential explanations for the high mercury levels in the Carson River system when compared to other contaminated sites include the large quantity of elemental mercury introduced to the

system and the time period of over 100 years allowed for physical dispersal and chemical alteration (Wayne et al., 1996).

Introduction of Mercury to the Carson River System

The original elemental form of mercury released to the environment remains the prevalent form in highly contaminated soils, sediments, and tailings (Lechler et al., 1997). Subaerial (buried) tailings typically contain greater than 95% elemental mercury; downstream of the influence from the tailings, along the Carson River, the percentage of total mercury as elemental mercury increases to slightly greater than 90% before decreasing further downstream (Lechler et al., 1997). Elemental mercury possesses a high volatility and low water solubility, and equilibrium conditions of exposed sediments does result in both volatilization and some dissolution. The species of primary interest in terms of mercury toxicity are the organo-mercury compounds such as methylmercury (CH_3Hg^+ or MeHg) (Wayne et al., 1996). However, methylmercury is the end product of the methylation of inorganic divalent mercury (Hg(II) or Hg^{2+}). Elemental mercury (Hg(0) or Hg^0) is the mercury form introduced to the Carson River System. The low reactivity of the prevalent Hg(0) species does not allow for direct methylation of this species. Therefore, the environmental transformations of elemental mercury are next considered.

Starting with elemental mercury, the two potential pathways for mercury oxidation involve volatilization and dissolution. Following its introduction and transport in the atmosphere (after volatilization), Hg(0) (gas) can undergo transformation to Hg(II) (gas) and Hg(II) (particulate) within cloud water (USEPA, 1997). This mechanism has been proposed as an explanation for the global nature of mercury pollution, as it can result in mercury deposition to land and water. The circulation of air masses on the global scale has the potential to take Hg(0) emissions from their point of origin and carry them to

anywhere on the globe before transformation and deposition occur. The slow oxidation of Hg(0) to Hg(II) results in Hg(0) having an atmospheric residence time on the order of 1 year. Other forms of mercury are likely deposited before they are ever able to dilute within the global atmosphere. The end result of these atmospheric transformations is that mercury released to the atmosphere deposits mainly as Hg(II), whether from the direct deposition of emitted Hg(II) or transformation of emitted Hg(0) to Hg(II) by the above process (USEPA, 1997). Elevated deposition rates therefore occur around emission sources, but regional or global transport and deposition also occurs. In other words, even though the principal emissions of mercury are from point sources concentrated in industrial areas, mercury pollution is truly a global concern.

While this is a pathway that does occur, the arid climate, and hence lack of rainfall, of the Carson River region and the likelihood of wider atmospheric transport make it an unlikely source for the large-scale introduction of Hg(II) to this system. Rather, a small fraction of the liquid Hg(0) that is associated with the mill tailings is dissolved out of the amalgam particles and subsequently adsorbed to fine-grained sediments. These sediments are then deposited in downstream, low-energy reaches of the river and reservoir (Lechler et al., 1997). Research by de Magalhaes and Tubino (1995) has shown that Hg(0) can be easily oxidized by molecular oxygen in aqueous solution in the presence of species such as chloride, which complex Hg(II); high chloride activities in Carson River and Lahontan Reservoir sediments are a product of the prevailing arid climate conditions and subsequent evapo-concentration processes (Wayne et al., 1996). This mechanism facilitates mercury oxidation to occur in sediments that remain moist or in suspension, including channel bed sediments and bank sediments under certain moisture conditions.

Other oxidizing agents within the sediment matrix and in the water, however, are likely at work as well. The presence of sulfur within the ores of the Comstock era results in the precipitation of some of the oxidized divalent mercury as relatively insoluble HgS in highly-reducing environments, such as within the reservoir or buried portions of the soil profile (Lechler et al. 1997). This mechanism serves to limit methylation of all oxidized mercury, although very limited methylation of HgS may occur. Note that the prevalent mercury species within the system remains the elemental form. The key item to take from the above discussion, though, is the presence of inorganic, divalent mercury (Hg(II) or Hg^{2+}) within the near-channel and in-channel sediments of the Carson River system.

Chemistry of Mercury in Soil

Divalent mercury within soil is subject to many chemical and microbial reactions (USEPA, 1997). For typical ranges of pH, temperature, and humic content in soils, conditions generally favor the formation of inorganic Hg(II) compounds such as $HgCl_2$, $Hg(OH)_2$, and inorganic Hg(II) compounds complexed with organic anions. These inorganic Hg(II) compounds possess high water solubility, but this theoretical mobility is heavily limited by the tendency of these compounds to form complexes with soil organic matter, primarily humic and fulvic acids, because of the affinity of Hg(II) and its inorganic compounds for sulfur-containing functional groups. Because of the high affinity of mercury species for soil, soil acts as a large reservoir for mercury introduced to the environment and a leaching source that will continue for many years after the cessation of mercury loading. Partition coefficients (K_d = concentration of Hg in dry sediment, soil, or suspended matter divided by the dissolved concentration in water) have been calculated for the relative affinity of Hg(II) and MeHg for sediment over water. Typical values are 10 to 100,000 milliliters (mL) per gram(g) of soil, 100,000 mL/g of

sediment, and 100,000+ mL/g for suspended matter, indicative of a strong preference Hg(II) and MeHg to remain in these phases (USEPA, 1997). In aquatic systems with significant mercury loadings, it is possible for a significant amount of Hg(II) to partition into the water column, especially in those instances where the concentration of suspended material in the water column is high, as in the case of a flood event. Alluvial sediments within the Carson River system are generally mineral-rich soils with low organic content. In the absence of large amounts of organic material, complexation with these compounds is limited; studies have suggested that enhanced mercury mobility within the Carson River and Lahontan Reservoir system may also result from locally high chloride activities (Wayne et al., 1996). Divalent mercury compounds and complexes can undergo reduction to elemental mercury, processes mediated by both humic substances and light (USEPA, 1997). These processes will bring about diffusion of the gas and re-emission to the atmosphere. Microbial activity on certain Hg(II) substances can result in MeHg formation, which typically makes up between 1 and 3 percent of mercury found in soil (USEPA, 1997). Most of the remaining mercury (97 to 99%) will be present as Hg(II) species. Contaminated sediments may contain MeHg levels far greater than these typical observations.

Mercury Transformation and Toxicity

Heavy metals, including mercury, possess a strong affinity for sorption onto particulate matter given the E_h and pH conditions found in most aquatic environments (Morel and Hering, 1993). Several contaminated river systems convey roughly 90% of their total heavy metal load via sediment transport (Babiarz at al., 1998; Balogh et al., 1997; Gill and Bruland, 1990; Hurley et al., 1995; Meade et al., 1995). The Carson River

is no exception in that more than 95% of total mercury can be removed from water column samples by filtration (Bonzongo et al., 1996a).

Several forms of mercury are present within the sediments and waters of the Carson River system. Due to its high volatility, only very low concentrations of elemental mercury are detected in the surface waters of the Carson River (Bonzongo et al., 1996a). Inorganic mercury and methylmercury in sediments along the Carson River are transported into the water column through diffusion and erosion processes (Figure 2-2). Mercury bound to particulate matter is generally considered unavailable for any chemical or biological reaction and will be susceptible to sedimentation processes. The presence of a state of sorption equilibrium (partitioning between sorbed and dissolved phases) does, however, ensure the presence of a small quantity of free ionic mercury (Hg^{2+}) within the water column and pore water of saturated bed sediments and moist bank sediments. Free ionic mercury is available for transformation. Within bottom sediments, a positive but weak correlation between the ratio of total MeHg to total Hg and organic matter has been observed (Hoffman and Thomas, 2000).

Sulfate-reducing bacteria (SRB) methylate free ionic mercury into the organic mercury species methylmercury (CH_3Hg) and dimethylmercury ($(CH_3)_2Hg$) (Gilmour and Henry, 1991; Gilmour et al., 1992; Matilainen, 1995; Bonzongo et al., 1996a). The production of MeHg by SRB is primarily controlled by SO_4^{2-} concentrations required for SRB activity. Optimal concentrations for the biotransformation of inorganic mercury by SRB are estimated in the 200 to 500 μM/L range; above this range, methylation is inhibited by high production of sulfide, while lower concentrations inhibit methylation because of sulfate availability (Bonzongo et al., 1996a). Evidence is available to support

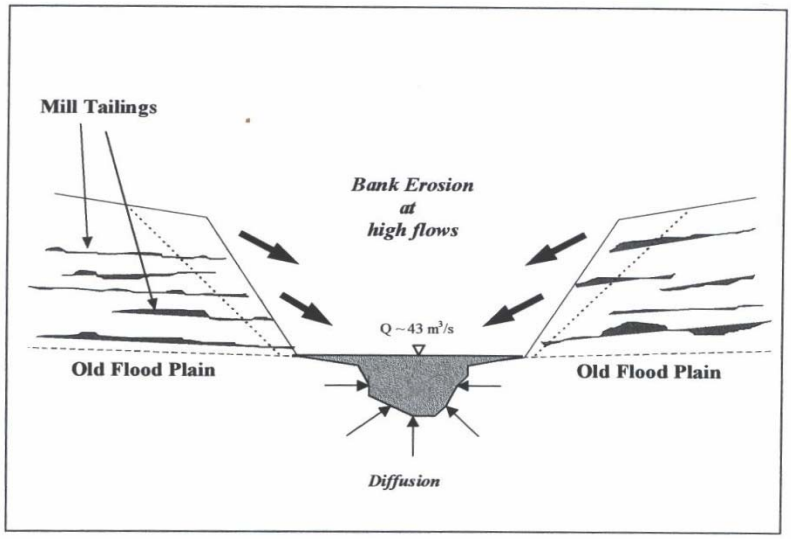

Figure 2-2. Processes that transport mercury into the water column along the Carson River. (Reprinted with permission from Carroll, R.W.H., 1999. Simulation of Mercury Transport and Fate in the Carson River, Nevada. Masters Thesis. University of Nevada-Reno, Reno, Nevada. Figure 1.2, pp. 11)

abiotic contributions to the methylation and demethylation processes as well, but the exact mechanisms remain poorly understood (Chen et al., 1996). While all mercury species possess intrinsic toxic properties, it is only the organic mercury species that are lipophilic and can bioaccumulate through the food chain (Fitzgerald and Clarkson, 1991; Zillioux et al., 1993). Within freshwater systems, methylmercury accounts for the majority, if not all, of the organic mercury species; the lack of dimethylmercury accumulation in freshwater systems may be related to both its high volatility and photochemical destruction (Fitzgerald and Mason, 1997). Methylmercury is therefore the principal species of concern for both ecosystems and human health.

Sulfate-reducing bacteria are widespread in anaerobic bottom sediments but may also reside within the anoxic hypolimnion of large lakes (Gilmour and Henry, 1991; Matilainen, 1995; Watras et al., 1995b). Fluvial systems contain mostly oxic waters; within the context of this study, only the anoxic channel bottom sediments and the moist

or saturated bank sediments (potentially anoxic environments) will be considered as sites for mercury methylation.

The reader should further note that methylation and demethylation processes occur simultaneously. Methylation refers to the biologically- or abiotically-mediated transformation of free ionic (inorganic) Hg(II) to MeHg; demethylation is the conversion of MeHg back to inorganic Hg. While demethylation reactions are kinetically unfavorable, due in part to the presence of partially covalent metal-to-carbon bonds, the unfavorable kinetics can be overcome through microbial enzymatic or photochemical mechanisms (Amyot, 1998). While both processes must be modeled, interest is centered on the net rate of MeHg production, as this is the determining factor for methylmercury concentrations in channel bottom and bank sediments and (through subsequent diffusion and erosion) the water column, the latter of which is available for introduction to the food chain. The balance between methylation and demethylation processes may be critical to maintaining low levels of MeHg in some surface waters. Processes which reduce the availability of inorganic Hg(II) for methylation can further limit the potential for biological uptake. Examples of these processes include the following: sedimentation of inorganic Hg(II) compounds resulting in the precipitation of insoluble HgS as the sediments become increasingly anaerobic; photochemical or microbial reduction of Hg(II) to Hg(0), which is removed by volatilization, within aerobic surface waters; and microbial or abiotic reduction of Hg(II) within anaerobic sediments (Amyot, 1998).

Methylmercury in the Water Column

The result of the chemical transformation of free ionic Hg^{2+} to MeHg is the introduction of methylmercury into the water column by diffusion and erosion processes. Large flow events, when the Carson River erodes significant quantities of contaminated

bank material, are believed to be the principal pathway by which mercury enters into the water column (and ultimately the Lahontan Reservoir and Wildlife Refuge areas). Because mercury is adsorbed to the sediment, the increased erosion associated with high flow events and the higher quantity of mercury present within the floodplain (compared to the channel bottom) results in more mercury getting into the water column. Particulate Hg is typically greater than 50% of total Hg and increased downstream; by contrast, the dissolved fraction of MeHg constituted a larger fraction of total MeHg than particle-associated MeHg (Bonzongo et al., 1996b). Flood events also contribute greatly to the continued dispersal of mercury contaminated sediments throughout the river system. Concentrations of both total Hg and MeHg in water are strongly influenced by flow regimes and well correlated with concentrations of suspended solids, as result from erosion (Bonzongo et al., 1996a; Bonzongo et al., 1996b).

Observations of MeHg and total Hg in the water column and bank sediments indicate that the MeHg and total Hg concentrations measured in surface waters were discharged in large part from Hg-contaminated bank materials, which are not in permanent contact with the water body (Bonzongo et al., 1996a). Contaminants entering the water column that are associated with silt and clay are transported to the reservoir, while mercury associated with amalgam grains and other sand-sized sediment are incorporated into the materials found beneath the channel floor (Miller et al., 1998). Mercury also enters the water column by diffusion from the channel bed and contacted bank sediments (Carroll, 1999; Carroll et al., 2000; Wayne et al., 1996). This source term is thought to be particularly important for the introduction of MeHg to the water column when the discharge is low and erosion is minimal. For water samples, positive but weak

correlations between total MeHg concentration and water temperature, pH, and total organic carbon have been observed; in addition to a positive, moderate correlation between total MeHg and total Hg concentrations. A strong positive correlation between total MeHg in water and total Hg in sediment has also been observed (Hoffman and Thomas, 2000).

The distribution and occurrence of Hg species in aquatic environments are probably regulated by key limnological and chemical parameters. While significant concentrations of methylmercury (MeHg) exist within the surface waters and biota of the Carson River, the ratio of total MeHg to total Hg is much smaller than other contaminated sites (Bloom and Effler, 1990; Bonzongo et al., 1996a; Gill and Bruland, 1990). The ratio of total MeHg to total Hg decreases downstream, reaching values of less than 1% below the mine tailing sites. This suggests both a high percentage of inorganic mercury input from point sources and a low net product of methylation-demethylation within the system (Bonzongo et al., 1996b). There is a strong indication that net methylation rates increase with decreasing pH in both the water column and at the sediment-water interface (Watras et al., 1995b; Xun et al., 1987). The alkaline nature of the Carson River (pH 7.5 to 9.0) may limit the MeHg production. Naturally occurring Group VI oxyanions (W, Mo, and Se) also inhibit the methylation process by SRB, and the extremely high levels of inorganic mercury found in the Carson system during winter and spring flood events may actually be toxic for SRB as well (Bonzongo et al., 1996a; Chen et al., 1996; Chen et al., 1997).

The Carson River has a very low organic content (<2%) (Miller et al., 1998; Wayne et al., 1996), and no correlation exists between DOC and total mercury or methylmercury

concentrations (Bonzongo et al., 1996a). Low levels of DOC limit complexation of dissolved MeHg to dissolved organic ligands, and lead to the assumption that a large fraction of dissolved MeHg is available for conversion processes and uptake by aquatic organisms (Bonzongo et al., 1996b). Increased temperatures result in increased methylation rates along the Carson River (Carroll, 1999; Carroll et al., 2000); this direct relationship is strongly supported with several studies of other systems (Callister and Winfrey, 1986; Matilainen, 1995; Stordal and Gill, 1995; Watras et al., 1995a).

Methylmercury within the water column is available for introduction to the aquatic food chain. MeHg is introduced to the water column through bank erosion and diffusion from contacted channel bank and bed sediments. Analysis of water samples from the Carson River indicates that only a very small fraction of mercury found in the water is available for conversion processes, including methylation, demethylation, and Hg(0) (or Hg^0) formation (Bonzongo et al., 1996b).

Total Hg and total dissolved mercury concentrations in the contaminated part of the Carson River are 5 to 100 times higher than the following recently studied systems polluted with mercury: Davis Creek, California; Clear lake, California; Lake San Antonio, California; Pyramid Lake, Nevada; Onondage Lake, New York; and Clay Lake, Ontario (Bonzongo, 1996b). Mercury concentrations in the Carson River are likely among the highest in any aquatic systems, even those with known histories of Hg contamination. However, the reactive fraction is observed to be lower within the Carson system. This data is used to justify the exclusion of methylation-demethylation processes within the surface waters of the Carson River model, limiting these reaction sites only to bed sediments and saturated or moist bank sediments.

Methylation and demethylation kinetics are variable spatially within the Carson River system and vary with the time of year. Preliminary findings from the USGS study on methylmercury formation and degradation in sediments of the Carson River system (CRS) include the following (Marvin-DiPasquale and Oremland, 1999):

- High rates of MeHg production in upstream river sediments and low rates in wetland sediments;
- Low rates of MeHg degradation in the upstream river sediments and high rates in the wetlands;
- Gross MeHg degradation strongly impacts net MeHg production;
- Microbial sulfate reduction and resulting reduced-S concentrations play an important role in mediating Hg-transformations;
- Oxidative demethylation is the dominant degradation pathway in the CRS
- Agricultural drains are a potentially important source of mercury to the larger wetland areas;
- Distinct spatial trends in microbial Hg-dynamics reflect the immediate environmental conditions with respect to organic matter, sediment redox, pore-water anions, and overall anaerobic microbial activity.

Note that most of these observations were discussed at greater length within earlier portions of this document.

Mercury in the Aquatic Food Chain

The quantity of mercury transformed to methylmercury (methylated) can vary greatly between water bodies because of several factors; some of these factors, other than mercury loading rate, include the following: environmental setting (climate, geology, land use, land cover), water chemistry, and wetland density, with the latter being the most important determinant of methylmercury production at the basin scale (USEPA, 2000).

Methylation is a key step in the entrance of mercury into the food chain. This methylation process occurs principally through biological processes in the aquatic sediment or water column, but also perhaps through abiotic processes involving humic

and fulvic acids in solution. Demethylation reactions, volatilization of elemental mercury and dimethylmercury, and bonding to particulate matter and settling prevent all of the mercury loaded into a system from being bioavailable in the aquatic environment (USEPA, 2000).

Microbial uptake of mercury is the first step for both possible methylation processes and bioaccumulation considerations. Methylation by sulfate-reducing bacteria or entry into the aquatic food chain via phytoplankton or bacteria first mandates the transport of mercury across the lipid membrane that surrounds unicellular organisms (Amyot, 1998). The microbial uptake of inorganic Hg(II) and methylmercury are affected by elements of water chemistry. High chloride concentrations and low pH conditions that favor the uncharged chloride complexes $HgCl_2$ and CH_3HgCl, mercury complexes which possess the highest lipid solubility, have been shown in field data to promote the accumulation of inorganic Hg and MeHg at the microbial level by phytoplankton and bacteria. Other non-polar mercury species, including dimethylmercury and elemental mercury, also diffuse rapidly through cell membranes, but they are not bioaccumulated. Bioaccumulation refers to organisms taking up contaminants more rapidly than their bodies can eliminate them, allowing the amount in the body to increase over time.

In order for high concentrations to occur in fish, mercury must be efficiently taken up by microorganisms at the bottom of the food chain, retained by these organisms, and passed on to their predators (Amyot, 1998). Although trace metals are often accumulated at the bottom of the food chain, concentrations in biomass do not often increase up the food chain (a process called biomagnification). Biomagnification is the incremental increase in contaminant concentration at each level of the food chain; this phenomenon is

the result of higher concentration of contaminant in the food sources for organisms higher on the food chain (USGS, 1995). Methylmercury is very bioavailable and accumulates in fish through the aquatic food web, with nearly 100 percent of mercury found in fish muscle tissue in the methylated state (USEPA, 2000). Elemental mercury and dimethylmercury are not bioaccumulated at the microbe level because they are non-reactive and tend to diffuse out just as easily as they diffused into the cell membrane.

Further explanations are needed as to why MeHg bioaccumulates and Hg(II) does not, despite both $HgCl_2$ and CH_3HgCl diffusing into cells at similar rates, reacting with components of the cell, and being efficiently retained (Amyot, 1998). Research was conducted to explain this phenomenon on copepods feeding on marine diatoms. What was shown is that Hg(II) is primarily bound to particulate cellular material of the diatom, while MeHg is associated with the soluble portion within the diatom cell. Because the particulate material is excreted by the copepod rather than absorbed, only the MeHg associated with the soluble fraction is efficiently incorporated into the copepod. Other field data has shown this difference in transfer efficiency as applicable to other microorganism predator relationships, although perhaps counter-intuitive based on the relative abundance of Hg(II) compared to MeHg found in water bodies.

This process continues up the food chain through zooplankton, and the lipid solubility of MeHg allows it to be retained in fat tissues of these organisms. Further explanation is, however, needed since once the trophic level of fish is reached, MeHg burden in muscle tissue is of greater significance that in fat tissue (Amyot, 1998). In fish, MeHg absorption occurs principally along the intestinal wall, whereas inorganic Hg(II) is adsorbed at the microvilli interface (located on immune system lymphocytes that are

carried within the bloodstream); this results in a very low uptake rate of inorganic mercury in comparison with methylmercury. This cycle results in increases in the proportion of MeHg to total Hg from about 10% in the water column, to 15% in phytoplankton, to 30% in zooplankton, and to 95% in fish. In fact, bioconcentration factors (BCF = concentration of MeHg in biota divided by concentration of MeHg in water column) are on the order of 10^5 to 10^6 (USEPA, 2000). The food chain structure therefore plays a key role in mercury biomagnification, because the accumulation of MeHg results mainly from the consumption of MeHg-containing food rather than uptake from the water itself. As the number of trophic levels within an aquatic system is increased, so too is the mercury concentration in the top predators of the food chain (Amyot, 1998). Large saltwater fish with long life cycles, most notably sharks, tuna, and swordfish, are likely to accumulate the highest amounts of MeHg (USDHHS, 1997). Higher methylmercury contents are also typically found in fish species in more acidic lakes (lower pH) (USEPA, 2000). Studies have shown that DOC concentration and pH levels have a strong effect on mercury fate, with increasing acidity (decreasing pH) and increasing DOC content resulting in higher body burdens in fish, perhaps by enhancing the mobility of mercury in the environment and thus the likelihood of entering the food chain (USGS, 1995).

Even though mercury loadings to some remote areas may be very low, the strong absorption by microbial bacteria and plankton found in floating material make the possibility of biomagnification increasingly likely if other conditions are suitable (USGS, 1995). Although mercury is a globally dispersed pollutant, problems do not arise everywhere. With the exception of grossly polluted areas, mercury is generally only a

problem where the rate of natural formation of methylmercury from inorganic mercury is greater than the reverse reaction (USGS, 1995). Specific environments known to favor the production of methylmercury include certain types of wetlands, dilute low-pH lakes in the northeast and north central United States, parts of the Florida Everglades, newly flooded reservoirs, and coastal wetlands, particularly along the Gulf of Mexico, Atlantic Ocean, and San Francisco Bay (USGS, 1995). Because methylmercury is the mercury species of concern with regard to bioaccumulation and biomagnification within the food chain, quantification of MeHg contamination within the Carson River is of great importance.

Carson River Superfund Site

In August 1990, the stretch of the Carson River through Dayton Valley and extending downstream to Lahontan Reservoir, to include Carson Lake, Stillwater National Wildlife Refuge (NWR), and Indian Lakes in Lahontan Valley, along with adjoining tributaries stretching nearly to Virginia City itself, was declared a Superfund site by the U.S. Environmental Protection Agency (USEPA). The remediation strategy for these sites remains unresolved. Lahontan Valley's wetland system encompasses a large portion of the lower Carson River Basin and includes the Stillwater NWR, the Fallon NWR, and Stillwater Wildlife Management Area. This area serves as a key production, migration, and wintering area for up to one million waterfowl, shorebirds, and raptors (NDWP, 1996). Mercury concentrations in soil samples are found to be some 200 times greater below the mill sites than above them, with the highest concentrations found just upstream from Lahontan Reservoir (the principal area for sediment deposition). Fish within the Carson River system have been found to have total mercury levels four times greater than the Federal Action Limit for consumption of 1 μg/g (Miller

et al., 1996; Carroll, 1999). Mercury levels in fish (up to 9.5 μg/g) and waterfowl (>3.6 μg/g) caught in and near the SWMA (Stillwater Wildlife Management Area) have also been found to be well above the FDA limits for human consumption. The recreational value of Lahontan Reservoir, which includes commercial and recreational fishing, and the SWMA are severely impacted by the continued input of mercury. Abnormally high Hg concentrations in sediments and fauna from the SWMA support a scenario of Hg mobilization, transport, and methylation within the Carson-Lahontan system (Wayne et al., 1996).

Health Effects of Mercury Contamination

Airborne and waterborne mercury may undergo several biological transformations that can yield methylmercury. In this form, mercury efficiently accumulates in the aquatic food web. Nearly all of the mercury that accumulates in fish in rivers, lakes, and reservoirs is present in its methylated form. The methylmercury concentrations found in fish specimens may be several orders of magnitude greater than concentrations in the water column, the direct result of the bioaccumulation and biomagnification processes. Inorganic mercury tends to not bioaccumulate (USEPA, 2000). The efficient accumulation of methylmercury up the aquatic food web poses risks to both humans and ecosystems. Other forms of mercury can also impact human health.

Toxic effects associated with methylmercury include permanent damage to the brain and kidneys; and damage to the nervous system (USEPA, 2000). Mercury effects many different brain functions and symptoms may occur which include the following: personality changes (irritability, shyness, nervousness), tremors, changes in vision or hearing, loss of sensation, and memory loss (United States Department of Health and

Human Services (USDHHS), 1997). Consumption of large amounts of methylmercury-containing fish or seed grains treated with methylmercury or other organic mercury compounds may cause permanent brain and kidney damage, as well as damage to the brain of a developing fetus. Methylmercury exposure is most dangerous to young children because a greater amount of the chemical passes into the brain and interferes with brain development. Adding to the problem is that since methylmercury is concentrated in fish muscle tissue (unlike organic contaminants like PCBs and dioxins, which concentrate in the skin and fat), mercury cannot be filleted or cooked out of consumed fish (USGS, 1995).

CHAPTER 3
PREVIOUS MODEL STRUCTURE

Mercury fate and transport within the Carson River are simulated using three computer models: RIVMOD (RIVer MODule), WASP5 (Water Quality Analysis Simulation Program), and MERC4 (MERCury). These models were originally chosen and linked by Heim and Warwick (1997). Currently, RIVMOD is a subroutine within the WASP5 code and is executed during each model time step. Sediment transport is simulated within the WASP5/MERC4 system of models and not within the RIVMOD code. The resulting model framework is referred to as the Integrated Fluvial Mercury Transport and Fate Model, or IFMTFM.

Hydrodynamic Modeling Using RIVMOD

RIVMOD (Hosseinipour and Martin, 1990) is a USEPA one-dimensional (1D) hydrodynamic and sediment transport routine that simultaneously solves the standard fluid equations of continuity and momentum throughout the system being simulated, utilizing the Gauss-Seidel iterative scheme. Finite difference equations are solved by the Newton-Raphson method to determine fluid velocity and depth given unsteady flow conditions. RIVMOD's input requirements include bed elevation, cross-sectional geometry, roughness coefficients, and initial conditions for water depth and discharge. Discharge is specified at the upstream and downstream boundary. The model domain includes the Carson River from the USGS Carson City Gage (CCG) through Lahontan Reservoir. The 115-km, or 71.4 mile, reach is subdivided into 273 segments. The location of each model segment is specified by model stations located at both the upstream and

downstream ends of the segment, resulting in a total of 274 stations. Station 1 is located at CCG and Station 274 at the base of Lahontan Dam. Station spacing is generally 0.50 km throughout the modeled reach, although station spacing is reduced to 0.25 km in the transition region between the river and reservoir for stability reasons.

Discharge is specified at the upstream boundary based on CCG data. At the downstream boundary, discharge from Lahontan Reservoir is specified with data from the USGS gaging station below the dam (LDM #10312150). Inflow from the Truckee Canal into Lahontan Reservoir is specified with data from the USGS gaging station on the Truckee Canal near Hazen, Nevada (TRC #10351400). Data available from the USGS gage at Fort Churchill (FCH #1031200) is used to define a time-varying lateral outflow at this location (IFMTFM station 128); the flow difference between what is predicted and what is measured at FCH is removed, thereby accounting for irrigation diversions and loss/gain due to groundwater interaction between the upstream and downstream boundaries. Here it is important to note that no diversion ditches are in operation downstream of the FCH gaging station.

Two major modifications have been made to RIVMOD. The original RIVMOD code was capable of modeling sediment transport, but geometry was limited to a simple rectangular channel or a first- or second-order polynomial. The first modification implemented a more complex cross-sectional geometry. Figure 3-1 presents the channel representation incorporated into the modified version of RIVMOD (Warwick and Heim, 1995). Note the cross-section is divided into two basic components: the main channel (parameter BW2) and floodplain (depth greater than D2). The inner channel and low-medium flow transition slope portions of the cross-section represent the channel bed.

The portion of D2 above the low-medium flow transition slope represents what will be referred to as the channel bank; the modeled portion of the Carson River is characterized by steep, nearly-vertical channel banks. The RIVMOD input file includes values for each parameter at each model station, the combined result of averaged field measurements and approximate values as taken from USGS topographic maps. The modified version of the code is able to consider changing flow and cross-sectional area between adjacent stations. The second modification applied a divided channel approach to the momentum equation, thus allowing for a separate floodplain roughness coefficient and the computation of overbank depths and velocities (Carroll, 1999). A smaller modification was also made to allow for the inclusion of evaporative losses, which are potentially significant in the semi-arid region of the Carson River system.

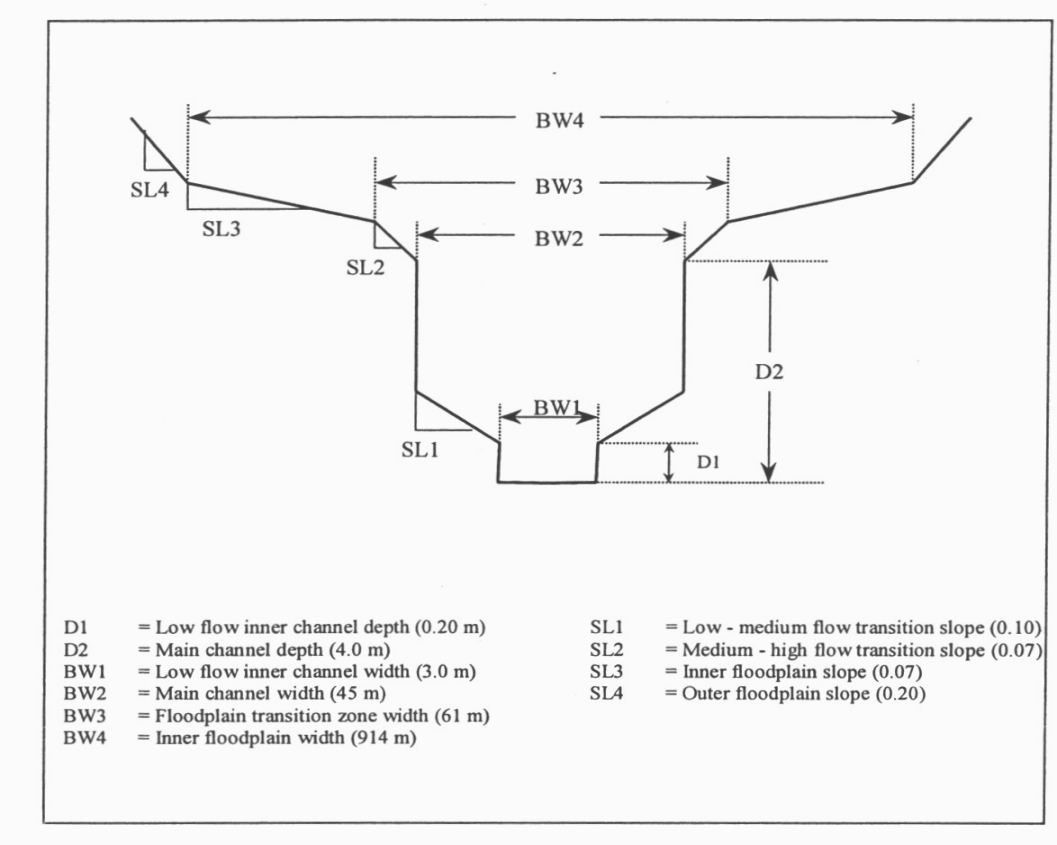

Figure 3-1. Modified channel geometry

The WASP5 and MERC4 Programs

WASP5 is the USEPA Water Quality Analysis Simulation Program-5 that was developed to simulate the transport and transformation of various water body constituents (Ambrose et al., 1991). Mass balance equations account for all material entering and leaving model segments through direct and diffuse loading, advective and dispersive transport, and any physical or chemical transformation. Input parameters required by WASP5 include simulation and output control, model segmentation (same as RIVMOD), advective and dispersive transport variables, boundary concentrations, point and diffuse source waste loads, and initial conditions.

Several modifications have been made to the WASP5 numeric code. The RIVMOD model is currently a subroutine within the WASP5 program. This linkage allows for sediment transport information, as related to hydrodynamic characteristics, to be incorporated into the WASP5 mass flux calculations (Heim and Warwick, 1997). The current WASP5 model simulates the transport of three distinct solid types: washload (diameter < 0.063 mm), coarse suspended sediment, (diameter > 0.063 mm), and bedload. Washload and CSS (coarse suspended sediment) are carried in suspension, while bedload is defined as coarse material that travels by rolling, skipping, and/or sliding along the riverbed. Washload and CSS boundary conditions are modeled by making use of measured rating curves at CCG; by contrast, bedload is modeled using van Rijn's transport theory (van Rijn, 1984a; van Rijn, 1984b; Carroll, 1999). USGS data indicate that CSS is held constant between CCG and FCH. While exchange is modeled between water column and bed segments, there is no net increase in CSS. However, data also show that on average 70% of the bank material is considered coarse (Heim and Warwick, 1997). Thus, for the purpose of modeling the system, it is assumed that eroded

coarse bank material settles onto the bed segment and is transported as bedload. The exchange between bedload and CSS is modeled by satisfying the water column CSS concentrations as defined by the measured rating curves. Equations governing the erosion of washload were originally developed by Carroll (1999). Modifications to these erosion equations and additional relationships for modeling overbank deposition during extreme flood conditions were later introduced by Carroll et al. (in press). It is assumed that the river is in vertical equilibrium with erosion and/or deposition occurring only laterally across the floodplain and not along the channel bed. Channel bank and floodplain are subject to dynamic erosion processes within the IFMTFM, while channel bed is assumed to remain constant. It is further noted that channel geometry is not updated within the RIVMOD code following modeled sediment erosion.

MERC4 is a subroutine contained within WASP5 (Martin, 1992). It was developed to compute mercury speciation and kinetic transformation. MERC4 is capable of simulating up to four mercury species: elemental Hg(0), Hg(2+), inert Hg, and Methylmercury (MeHg). The MERC4 model is also capable of simulating up to three solids types: washload, CSS, and bedload in this case. For this study, only inorganic mercury and methylmercury are modeled. Note that only the soluble forms of these mercury species are available for chemical transformation. The simulation of solids is critical because of the strong tendency of mercury to sorb onto solids. The mercury speciation and kinetics algorithms are based on the Mercury Cycling Model (MCM) developed by Tetra Tech, Inc. (Hudson et al., 1994) for the Electric Power Research Institute. The MERC4 model resulted in the coupling of chemical speciation and kinetics,

based on the MCM model, with the transport capabilities of the WASP4 modeling system.

Within the MERC4/WASP5 program, mass balance equations are written for each form of mercury and solids being modeled. The initial total concentrations for each of these state variables are specified to the model. New total concentrations are computed based on transport, transformations, and reaction kinetics, which vary depending on the species present (Martin, 1992). In addition to the state variables, other chemicals which affect mercury speciation are input to the model but not predicted, including the following: pH and concentrations of free sulfide, sulfate, chloride, dissolved organic carbon, and dissolved oxygen. The chemical species considered by MERC4 include dissolved, sorbed, and precipitated forms.

Measured rating curves at CCG for inorganic mercury and methylmercury in the water column were written into WASP5 as an upstream boundary condition (Carroll, 1999). Reaction constants for sorption (Bonzongo et al., 1996a); and methylation and demethylation reactions (Carroll, 1999; Carroll et al., 2000), which are input into the model, are based on field data collected along the Carson River system. Initial conditions for mercury bed concentrations are described by fitting a three-point moving average through data collected by Miller and Lechler (1998). Initial concentrations for mercury in the banks were based on calibrated parameters and were not dynamic in nature. The previous version of WASP5/MERC4 does not simulate diffusion other than from the bed sediments. These shortcomings of the model in terms of simulating field conditions will be addressed later in this chapter.

Stages of Model Development

The modified and linked RIVMOD/WASP5/MERC4 model, as described above, makes up the framework of the IFMTFM. Model development has occurred in three distinct, but ongoing phases (Heim and Warwick, 1997). The first phase of the project applied RIVMOD to the Carson River and Lahontan Reservoir system (CRLR) to simulate a variety of river flows and reservoir stages (Warwick and Heim, 1995). The second phase incorporated sediment transport and characterization of the association of mercury with sediment transport. The third phase seeks to incorporate the results of the first two phases with MERC4 to determine areas of potential mercury methylation, define important transport mechanisms, isolate sources or times of increased mercury contamination, and allow application of the model to different hydrologic scenarios. A working model may then be used to test the outcome of mitigation strategies, such as the removal of mercury sources. This effort may ultimately lead to an effective way to reduce mercury concentrations in the water column, and ultimately the food chain.

While much of this research was previously completed (Heim and Warwick, 1997; Carroll, 1999; Carroll et al., 2000; Carroll et al., in press), this thesis improves the capabilities of the IFMTFM through the incorporation of bank elements. The purpose behind the development of the bank elements to be integrated into the current IFMTFM code is to develop a means to simulate the spatial and temporal variability of methylmercury within the channel banks of the Carson River system by better simulating the actual physical and biological processes which are occurring in the field. Methylmercury concentrations in the bank are not spatially and temporally constant but are instead a function of moisture history. A modified Carson River model is developed to include the relation between flow history and moisture levels observed within the

banks. Zones of varying moisture impact methylation and demethylation kinetics, and therefore the temporal concentrations of methylmercury available to the water column.

CHAPTER 4
CHANNEL BANK ELEMENTS: LINKING SURFACE WATER AND GROUNDWATER

Modeling the Carson River

The USEPA designated the Carson River, Nevada as part of a Superfund site in 1991. Between 1860 and 1890, elemental mercury was used at over 70 mill sites to recover gold and silver via mercury amalgamation, introducing 7000 tons of mercury to the Carson watershed. Contaminated sediments line channel banks downstream of these mill sites, with mercury concentrations two to three orders of magnitude above background levels. Mercury methylation within sediments, accompanied by diffusion and erosion, introduces methylmercury to the channel. Methylmercury concentrations in the bank are not spatially and temporally constant but are instead a function of moisture history. A modified Carson River model is developed to relate flow history to moisture levels observed within the banks. Zones of varying moisture impact methylation and demethylation kinetics, and therefore the temporal concentrations of methylmercury available to the water column.

Methylmercury concentrations within the Carson River channel banks vary with both spatial location and time. The temporal variability in methylmercury concentrations was not previously considered by the IFMTFM. The previous modeling approach (prior to this thesis) considered methylmercury bank concentrations as temporally constant and inversely related to the square root of channel bottom slope (S_0) (Carroll, 1999):

$$[Hg_{MeHg}] = \frac{\lambda_2}{S_0^{0.5}} \quad \text{(Eq. 4-1)}$$

A calibrated threshold flow of 1000 cfs was developed, below which methylmercury is available to be eroded from the channel banks. This threshold flow was later modified to a threshold depth of 1.00 meters. Diffusion of methylmercury was only allowed to occur from the channel bottom of the main channel. No efforts are included within the previous model to simulate groundwater hydrodynamics in response to flow history within the river channel. It is this temporal variability in bank saturation zones that controls the kinetics underlying the microbial production of methylmercury within the channel banks, thereby influencing MeHg available for introduction to the water column. Research concerning the relation between soil wetting and drying cycles; and methylation / demethylation kinetics is ongoing at other academic institutions.

The end product of this thesis research is the introduction of channel banks into the IFMTFM code as areas for active mercury transformation. Channel bank elements are created within the IFMTFM, conceptually similar in functionality to bed elements within the IFMTFM. Bank element size is dynamic and equal to the saturated portion of the bank. Methylation and demethylation will occur within channel banks, resulting in dynamic methylmercury concentrations. As in the previous IFMTFM version, channel banks are eroded, but the methylmercury concentrations within the eroded material are no longer temporally constant. The code was already able to predict flow magnitudes and depths along the Carson River from the Carson City Gage through the Lahontan Reservoir. The creation of bank elements, along with the accompanying coding modifications, allows the model to predict the zone of saturation within the channel banks. The functionality of these bank elements is determined based on analysis of the

following: river stage predictions as computed from a 3-dimensional (3D) hydrodynamic model, water table data from three groundwater wells, and the time lag between river stage oscillations and observed water table response.

Available Data

To obtain more precise channel geometry data, a GPS (global positioning system) unit, the Leica GPS System 500 (Leica Geosystems, Atlanta, Georgia), was purchased and used to collect detailed data for a 0.5 km reach of the lower Carson River, with this reach encompassing the location three installed groundwater wells (Scout Camp field site). Signals from at least four satellites are needed by a GPS receiver on the ground to resolve measurement ambiguities and obtain the location (latitude, longitude, and elevation) of a given observed point. Without getting into the complexities of the system, observations from four satellites are sufficient to resolve ambiguities and obtain spatial location on the surface of the earth. The repetition of this procedure allows for the collection of detailed channel morphology data for this small reach of the Carson River. Vertical resolution of data points, based on system specifications, is reported to be on the order of a few centimeters.

Flow data (magnitude and depth) from the USGS gaging station at Fort Churchill, water table data (March 2001 through present) from the three wells installed along a channel transect, and GPS survey data are used to construct a detailed surface-water model and to integrate channel and groundwater hydrodynamics. Specifically, the goal was to develop simple relationships between flow history (specifically rising and falling water depths) in the channel to moisture content values (specifically the height of saturation) within the channel banks. The simple relationships discovered from modeling efforts and data analysis were incorporated into the IFMTFM modeling of channel bank

elements. With the IFMTFM model then able to predict bank moisture content both spatially (due to variable channel geometry) and temporally, microbial kinetics data was included to allow the model to predict spatial gradients and temporal variability of methylmercury concentrations within the banks of the Carson River. The inclusion of bank elements allows the IFMTFM to more accurately simulate mercury concentrations present in eroded bank material and methylmercury gradients for diffusion processes. Calibration and verification of the model is used to compare the updated IFMTFM model with data collected within the Carson River system. Although the bank element is conceptually simple, a historical perspective with regard to modeling of surface water and groundwater interaction is important to gain additional insight prior to a discussion on data analysis.

Introduction to the Hyporheic Zone

Historically, much ecological and hydrological research on groundwater and rivers has treated the two systems as distinct entities. River and groundwater systems are, in fact, characterized by marked differences (Boulton et al., 1998). Rivers typically have currents generating turbulence; short water residence time; variable discharge and physicochemical conditions; dynamic channel morphology; unidirectional transport of nutrients, sediments, and biota; and are open to sunlight. By contrast, alluvial groundwater environments tend to offer increased stability, longer water residence times, laminar flow regimes, little change in sediment bed structure, and permanent darkness. Despite these differences, the interface between surface streams and alluvial groundwater represents a region of active interchange of water, nutrients, biota, and other materials. This intervening zone is termed the hyporheic zone. Exchange occurs because of variations in discharge, bed topography, and porosity (Boulton et al., 1998). Upwelling

groundwater supplies nutrients to stream organisms, while downwelling stream water provides dissolved oxygen and organic matter to microbes and invertebrates in the hyporheic zone (where photoautotrophic production is not possible). Dynamic gradients exist at all scales (due largely to sediment heterogeneity), and the boundaries of the hyporheic zone vary in both time and space. Flow occurs in three dimensions: longitudinally down the channel, vertically between the channel and underlying sediments, and laterally to or from the riparian zone (Jones and Holmes, 1996). Subsurface regions are classified as hyporheic or groundwater zones based on hydrologic exchange with surface waters; one definition proposes the division between the hyporheic zone and groundwater to be where less than 10% of the subsurface water originated from the surface channel (Fuller and Harvey, 2000; Jones and Holmes, 1996).

The dynamics of the hyporheic zone are particularly important for mercury speciation. As the extent of the hyporheic zone fluctuates with stream stage and the associated changes in hydraulic gradients, so too do the anoxic zones where the methylating population is able to thrive. Flow rates through sediments are much slower than on the surface, thus constraining the import of dissolved oxygen. If oxygen demand from aerobic metabolism and other chemical reactions exceeds the influx, anoxic regions will develop and have two important effects on hyporheic zone processes (Jones and Holmes, 1998). First, organic matter decomposition occurs via anaerobic pathways, such as denitrification, sulfate-reduction, and methanogenesis. Secondly, the oxic-anoxic interface is the site of redox/precipitation reactions, such as the oxidation of methane or ferrous iron. Additionally, methylating SRB thrive in these anoxic environments. The active exchange of water in the hyporheic zone with water in the stream enables

methylmercury introduction to the biota of the channel and offers an additional introduction pathway to bank erosion. The contribution of hyporheic zone processes to the stream ecosystem function is determined by the rate of chemical transformations in the sediments and the proportion of stream discharge flowing through sediments (Jones and Holmes, 1996). It should be further noted that flow of surface water in the hyporheic zone increases the effective reactive site density per volume of surface water by providing contact of dissolved metals with potential reaction or sorption sites, thus potentially enhancing metal attenuation by transport into zones where removal processes are more favorable (Fuller and Harvey, 2000).

Modeling Surface-Subsurface Interactions: A Historical Perspective

A number of different approaches were taken over the years in the effort to quantify stream-aquifer hydraulics. Individual efforts to obtain analytical expressions to relate stream and aquifer hydraulic heads are each based on the same starting point, the continuity equation. The differences arise in the assumptions made and the consideration of different boundary conditions. In the interest of completeness, a number of these approaches are summarized within this section.

Groundwater levels in alluvial valley aquifers vary with stage changes in the associated surface streams. A rise or fall of stream stage over a short time period imparts a flow reversal within the aquifer, a result of the change in gradient between the stream and the aquifer (Serrano and Workman, 1998). The distance of influence within the aquifer is dependent on the aquifer transmissivity and porosity, the change in stream stage, and the length of time that conditions for a flow reversal exist (Serrano and Workman, 1998). The hydraulic gradient is also spatially variable; river stage typically does not increase uniformly over a long reach because of variations in channel geometry

and bottom slope (Squillace, 1996). When water quality within the stream differs from that within the aquifer, the spread of contaminants (e.g. methylmercury) is a problem directly connected to the hydraulics of the stream-aquifer system.

A rise in river stage, as associated with downstream movement of a flood wave, is accompanied by lateral stream losses to bank sediments. As the flood wave passes, the volume of water held in bank storage is gradually released to sustain baseflows between flood events. Channel banks and floodplains thus mitigate against extreme hydrologic phenomena by storing substantial volumes of water which would otherwise increase flood volumes, a process known as bank storage (Whiting and Pomeranets, 1997; Hantush et al., 2001). While this interaction between surface streams and groundwater has often been studied in the interest of flood control, the underlying equations remain the same for gradually varied stage changes within the stream.

The discussion to follow includes mention of a number of solutions developed for unconfined aquifers. Yeh (1970) and Marino (1975) provide numerical solutions by accounting for streams as time-varying boundary conditions. Further numerical solutions have been developed modeling the stream and aquifer as interacting dynamic systems, including work by Pinder and Sauer (1971) and Zitta and Wiggert (1971). One-dimensional open channel flow equations are coupled with the two-dimensional (2D) ground water flow equation. Assumptions embedded within these solutions may bring about questions as to their practicality. Despite being more restrictive, practical analytical solutions have also been developed. Several authors have presented analytical solutions to the linearized Boussinesq equation, subject to a fluctuating stream stage. Cooper and Rorabaugh (1963) derived an analytical solution for the changes in

groundwater head when the river stage can be approximated as a damped sinusoid, as in the case of a passing flood wave. A finite difference expression of the analytical solution developed by Cooper and Rorabaugh was developed by Hornberger (1970). Hall and Moench (1972) and Moench et al. (1974) use the convolution integral to expand applicability to flood waves of arbitrary shape, as described by a step function. A more general solution developed by Workman et al. (1997) includes the effects of transient redistribution of water levels in the aquifer from the previous day. Govindaraju and Koelliker (1994) assessed the accuracy of these analytical solutions compared with numerical solutions of the nonlinear equation, finding as much as 10% error.

The analytical solutions do not consider the simultaneous interactions that are inherent to a dynamically coupled stream-aquifer system; rather, their use is based on a prior knowledge of the stream-stage fluctuations, and they cannot be used for routing streamflows without iterative procedures (Hantush et al., 2001). One key source of difficulty in the efficient numerical coupling of streamflow and aquifer equations is the intrinsic difference in the time scales of water movement in the two systems (Perkins and Koussis, 1996). Analytical solutions to simultaneously couple the governing equations of stream flow and groundwater flow are developed by Morel-Seytoux (1975), Hunt (1990), and Harada et al. (2000). Analytical solutions to the non-linear Boussinesq equation are later presented by and Serrano and Workman (1998). Each of the above solutions was developed starting from the following standard assumptions, with additional assumptions included as needed (Sharp, 1977):

- The alluvial aquifer is homogeneous, isotropic, and infinite in extent.
- The alluvium's bottom boundary is horizontal and impermeable.
- The Dupuit-Forchheimer conditions are valid. These conditions are:
    - In any vertical section the groundwater flow is horizontal;

  - The velocity is uniform over the depth of flow;
  - The slope (α) of the free surface (unconfined flow) is small enough that $\tan(\alpha) \approx \sin(\alpha)$.
- All media are saturated.
- Water from storage is discharge instantaneously upon reduction in head.
- Fully-penetrating streams (i.e., the streams penetrate to the bottom of the alluvium, or alternatively, the heads in the alluvium beneath the river bed are all times equal to the river stage.
- A solely unconfined or solely confined groundwater system.

Some authors have sought to develop more general solutions by relaxing some of these assumptions. Solutions derived through use of linearization techniques applied to the nonlinear Boussinesq equation are naturally expected to contain some error, caused by the nonlinear nature of the original equation (Gill, 1985). This being the case, one may choose to use even simpler solutions, using suitably calibrated values of the aquifer constants to obtain reasonable results. Gill (1985) deduced limiting solutions for finite aquifers of long-thin and short-thick dimensions, rather than assuming aquifers of infinite thickness. Hantush (1967) derived 2D, time-dependent equations for a stream-leaky aquifer system subject to an instantaneous rise in stream water level, with a constant water level thereafter. Dever and Cleary (1979) advanced Hantush's approach with general solutions for any stream stage hydrograph that can be represented by a continuous or piecewise continuous function of time. An analytical model of stream-aquifer interaction that considers the effects from a small degree of aquifer penetration and low-permeability sediments on the head response to an arbitrary stream stage hydrograph was proposed by Zlotnik and Huang (1999).

The progression of research into the area of stream-aquifer interaction led to the development of numerical models, which became required tools as assumptions were relaxed and solutions became increasingly complex and realistic. Neuman and

Witherspoon (1971) developed an iterative, finite element method applicable to a wide variety of problems involving complex boundaries and arbitrary degrees of heterogeneity and anisotropy. This approach, which considers 2D flow within channel banks (and thereby does not encompass the limitations of Dupuit assumptions), was used in the development of a bank storage model (WaTab2D) by Whiting and Pomeranets (1997). Two-dimensional flow within channel banks for unconfined aquifers, of either semi-infinite or finite width and without a semipervious streambank, was further considered in work by Moench and Barlow (2000). It was necessary to assume that water table fluctuations were small relative to the saturated thickness and that vertical flow into or out of the zone above the water table occurred instantaneously, therefore neglecting the effects of hysteresis in the moisture distribution above the water table. In addition to considering stream interaction with anisotropic, homogeneous unconfined aquifers, Moench and Barlow (2000) also considered stream interaction with various homogeneous confined and leaky aquifer types. The computer programs STLK1 and STWT1 were developed for simulations of confined and leaky aquifers and confined and water-table aquifers, respectively (Barlow et. al., 2000). It was noted that a water-table aquifer (unconfined) may respond very much like a confined aquifer if the unsaturated zone is thin and the specific yield is small, the result of the non-instantaneous release of water from storage following a reduction in head. Freeze (1971) was one of the earliest researchers to consider the integration of the saturated and unsaturated zones into a transient model. One common failure with the use of non-integrated fully saturated flow models is that slower water table responses are predicted than are actually observed (Wise et al., 1994).

In the choice of a model for a given system, it is important to consider the assumptions upon which the model is based. Assumptions made for some of these solutions are likely to be questionable in some instances and can yield erroneous results. These questionable assumptions include Dupuit-Forcheimer conditions, homogeneity, full penetration of streams, and systems that are solely confined or unconfined (Sharp, 1977). Sharp used data collected from major alluvial valleys in the central United States to assess the validity of these assumptions; his findings are listed below:

- The assumption of homogeneity is clearly invalid as demonstrated by the exponential increase in hydraulic conductivity with depth.

- Isotropy assumptions might be justified in the deep alluvium; anisotropic conditions may occasionally be present at shallower depths.

- Valley bottoms may be adequately represented by a horizontal surface; the extremely high hydraulic conductivities of the deep alluvium also justify the assumption of impermeable boundaries, at least for first approximations.

- It is clearly shown that Dupuit-Forcheimer assumptions are not valid in the major alluvial systems considered. Flow is predominantly vertical in the vicinity of the river bed; groundwater flow is also not uniform with depth. While the approach reduces the problem's dimension by one, it does not allow accounting for the vertical component of the seepage velocity or accurate prediction of a significantly sloped free surface (Whiting and Pomeranets, 1997).

- The assumption of saturated flow is legitimate and typical conductivities allow for very rapid (instantaneous) release of water from storage upon head reduction.

- The rivers of the major alluvial aquifers studied are not fully penetrating. Presumably, most groundwater flow between the river and bank storage is through the river bed and not the banks because:

    - The river bed has greater surface area, and
    - The river bed is closer to the zone of greater hydraulic conductivity.

  Additionally, the banks and bed, in general, will have differing hydraulic conductivity because of smaller sediment sizes and higher clay percents in the bank than in the bed, further decreasing the contribution of the banks to the river-aquifer interaction. This condition leads, in part, to the invalidity of the Dupuit-Forcheimer

assumptions and makes most 1D models suspect. The simulation of bank storage using semi-permeable stream banks is not directly applicable.

- Alluvial aquifers may be confined and unconfined and these conditions may vary both spatially and temporally.

Based on the above discussion, it becomes apparent that many bank storage models are based on assumptions that do not correspond to observed field conditions. As noted by Sharp, this does not necessarily invalidate the models. Rather, the validity of a model and its assumptions rests on two divergent sets of criteria: "The positivistic view states that any assumption which leads to a useable predictive model is a valid assumption…the assumptions are valid regardless of any correspondence to observed or theoretical processes. The normative view states that assumptions should correspond to the actual processes or the true relationships between variables. If not, the assumptions are invalid because they yield or are faulty interpretations" (Sharp, 1977). The listed assumptions fall into both classifications, with difficulty arising when positivistic assumptions are used to infer the actual hydrogeologic processes or when data from a positivistic model is extrapolated to a situation where conditions differ by any significant degree (Sharp, 1977). "The problems involved in modeling without simplifying assumptions are self-evident. Hydrogeologic variability insures that models cannot precisely correspond to real-world processes. Nevertheless, the hydrologist or geologist who is attempting to describe or model and bank-storage situation must be aware of the limitations of his assumptions. The degree to which invalid (in the normative sense) assumptions reduce the accuracy or interpretation or prediction will depend on the degree of divergence from the real world and cannot be predicted a priori" (Sharp, 1977).

Modeling Simplifications

Despite the probable presence of a regional groundwater flow perpendicular to the Scout Camp groundwater well transect, limiting data requires the assumption that water fluxes along the front and back boundaries of this cross-section are negligible in comparison to fluxes along the cross-section (perpendicular to the stream). River stage and water table levels are then able to be analyzed as a 2D model. It is essentially assumed that changes in hydraulic head within the aquifer are due primarily to the pressure head gradients associated with the changing river stage, rather than changes in aquifer head levels further upstream. This phenomenon is shown schematically in Figure 4-1.

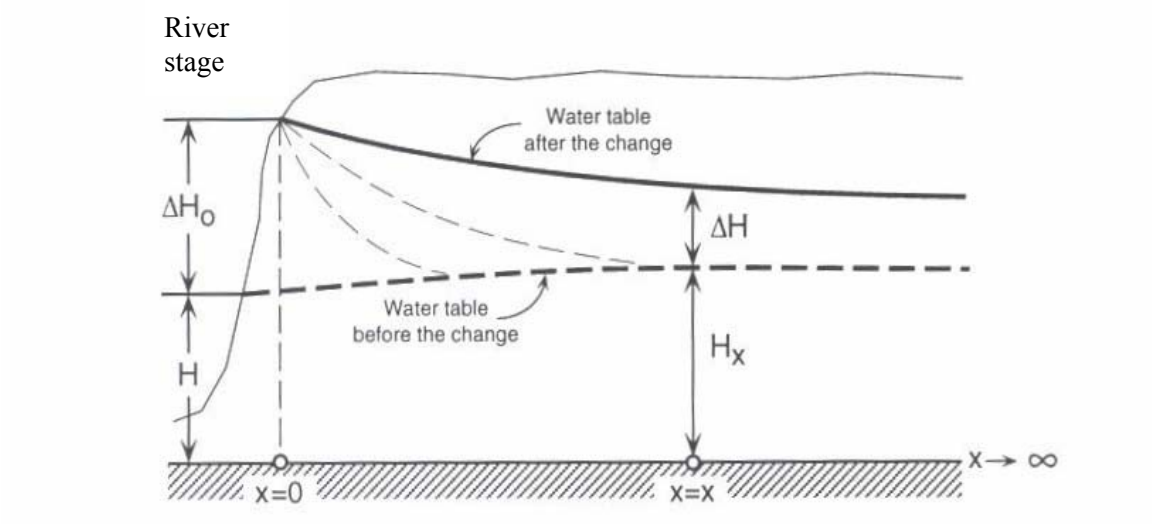

Figure 4-1. Water table response to changing river stage

Using IFMTFM Modifications to Track Bank Saturation: Bank Element Functionality

Knowledge in hand, the functionality of the IFMTFM model is next considered; specifically, how the model previously operated is compared with the updated model

with incorporated bank elements. Sediment transport and mercury transport and kinetics within WASP5/MERC4 are reviewed. The previous IFMTFM includes two types of elements: water column elements and bed elements. The modeling of mercury cycling within channel banks required the creation of a new type of element: the bank element. The bank element is used to track moisture content levels within the channel banks. As moisture contents change within bank elements, properties of these elements relating to mercury modeling are updated. The ability to model moisture content variability within the channel banks, utilizing the newly-developed bank elements, allows for a more detailed analysis of microbial behavior concerning methylation and demethylation.

Mercury modeling within the previous IFMTFM was accomplished as follows (Carroll, 1999). The Carson City Gage (CCG) measured rating curves for washload and coarse suspended sediment, along with a calculated bedload rating curve, are written directly in the WASP5 code as upstream boundary conditions, or rather, input to the model domain. Measured rating curves for inorganic mercury and methylmercury in the water column are also directly written into the WASP5 code as upstream boundary conditions. Mercury concentrations within the channel banks were chosen to calibrate the water column concentrations of inorganic mercury and methylmercury. Miller et al. (1999) found a statistically significant correlation between mercury concentrations and the percentage of fine sediment (washload, diameter < 0.063 mm), with the implication being that the contaminated material is primarily associated with the fine sediment. This fine sediment is deposited along the lower reaches of the Carson River where the stream gradient is shallow and velocities are slow. The assumption was therefore made that

concentrations of inorganic mercury and methylmercury within the bank sediments are inversely related to the slope of the channel:

$$[Hg_{in}]_{bank} = \frac{\lambda_1}{S_0^{0.5}} \quad \text{(Eq. 4-2)}$$

$$[Hg_{MeHg}]_{bank} = \frac{\lambda_2}{S_0^{0.5}} \quad \text{(Eq. 4-1)}$$

S_0 is the channel bottom slope and λ_1 and λ_2 are calibration parameters adjusted to match water column mercury concentration data. Bank mercury concentrations (inorganic and methylmercury) are not dynamically changed in the previous version of the model. This IFMTFM version includes a threshold flow depth (based on segment geometry and calibrated Q_T = 1000 cfs) above which methylmercury does not occur in the channel banks because methylating microbial communities cannot survive.

Within the confines of the previous model, methylation and demethylation (resulting in dynamic concentrations of MeHg and inorganic Hg(II)) are allowed to occur in the channel bed sediments (confined by the main channel) and these kinetic reactions are governed by the equations 4-3 and 4-4:

$$\frac{\partial[C_p]}{\partial t} = f_{temp} K_{20} [C_r] \quad \text{(Eq. 4-3)}$$

$$f_{temp} = Q_{10}^{\frac{T-20}{10}} \quad \text{(Eq. 4-4)}$$

For mercury methylation, the reactant (C_r) is soluble Hg^{2+} and the product (C_p) is soluble methylmercury. In the case of demethylation, soluble methylmercury serves as the reactant and soluble Hg^{2+} serves as the product. K_{20} is the reaction rate (day^{-1}), f_{temp} is a temperature multiplier to correct for temperatures deviating from 20ºC (dimensionless), t is time in days, and reactant and product concentrations are in units of milligrams per liter

(mg/L). The spatial variability of the constants K_{20} and Q_{10} are summarized in Table 4-1 (Carroll, 1999; Carroll et al., 2000).

Table 4-1. Spatial variability of reaction constants within IFMTFM

Range	Methylation		Demethylation	
(distance from CCG in km)	K_{20} (day^{-1})	Q_{10}	K_{20} (day^{-1})	Q_{10}
0.00 - 79.25	0.0041	2.03	0.4483	2.32
79.25 - 95.40	0.0011	2.03	1.3291	2.32
95.40 - 115.00	0.0028	2.03	1.1753	2.32

Initial mercury concentrations in bed sediments were determined by fitting a three-point moving average through data collected by Miller and Lechler (1998) (Carroll, 1999). Inorganic mercury and methylmercury were introduced to the water column through the following mechanisms (Figure 2-2): erosion of channel bank (vertical portion of channel at BW2 in Figure 3-1) sediments; and diffusion from bottom sediments within the confines of the main channel (BW2 in Figure 3-1) (inner channel is assumed in dynamic vertical equilibrium and therefore not subject to erosion). Only deposition, not erosion, is considered to occur during flows which contact the floodplain (BW2 to BW3 and BW3 to BW4 in Figure 3-1). Mercury concentrations within the eroded sediments remain constant over time, although concentrations are spatially variable based on the λ_1 and λ_2 calibration parameters. Water column concentrations are based on measured partitioning constants between dissolved and adsorbed phases. MeHg and inorganic Hg(II) are the only species modeled, based on the high volatility of elemental mercury. Methylation and demethylation only occur within the water-contacted bed sediments of the main channel, based on the predicted free ionic MeHg and free ionic inorganic Hg(II) concentrations. Free ionic (~soluble) concentrations are considered to represent the bioavailable fraction of total mercury, with soluble fraction defined as the fraction able to pass through a 0.45 μm sieve. Partitioning coefficients are shown in Figure 4-2.

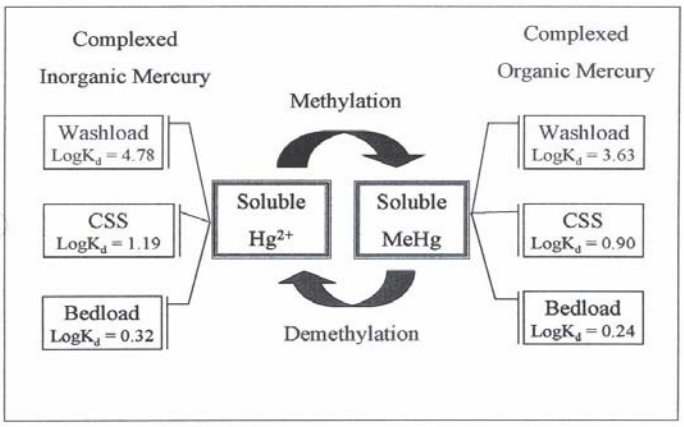

Figure 4-2. State variables measured with MERC4. (Reprinted with permission from Carroll, R.W.H., 1999. Simulation of Mercury Transport and Fate in the Carson River, Nevada. Masters Thesis. University of Nevada-Reno, Reno, Nevada. Figure 1.4, pp. 16)

Based on these considerations, the previous IFMTFM version was calibrated to provide a best-fit to field observations of water column mercury and sediment concentrations. This approach, however, is clearly not entirely representative of actual field processes. The calibrated methylmercury function predicts methylmercury bank concentrations over two orders of magnitude higher than the methylmercury bank data collected under conditions of near-zero flow (Carroll, 1999). The samples, from October 1994, were collected high up on the bank at the estimated point of river contact during spring floods. Examination of water column data shows that, unlike other systems, increased discharge does not always cause a dilution in MeHg. Instead, an increase from low to medium flow causes a significant increase in MeHg water column concentrations. These results strongly suggest that given medium flows, bank erosion, and not diffusion, acts as the principal pathway for MeHg into the water column. This trend of MeHg increase with increasing flow begins to reverse when flows go from medium to high conditions. The resulting dilution at higher flows suggests that the availability of MeHg

from erosion of the upper bank is limited, and this observation was used to justify the inclusion of a threshold height got bank MeHg in the previous model version. This limitation is not observed for inorganic mercury (Carroll, 1999).

Modeling MeHg concentrations as constant over time is not representative of field conditions, which depend on microbe populations and therefore moisture levels. Mercury methylation is stimulated if soils are fully saturated and anoxic conditions are achieved (Gilmour and Henry, 1991; Porvari and Verta, 1994). Low flow conditions, which characterize the Carson River during most of the year, do not result in inundation of channel banks or the attainment of anoxic conditions. It is probable that high flow rates are too infrequent and short in duration to allow anaerobic microbes to develop in the upper portions of the bank sediments. Given these considerations, MeHg concentrations within the channel banks are not expected to be vertically uniform; rather, MeHg concentrations are expected to display a dependence on soil moisture conditions (Carroll, 1999). Flow history and the rates at which river stages are rising or falling will, in turn, impart time-dependent and vertically variable MeHg concentrations within the channel banks along the Carson River. This hypothesis is borne-out in soil samples collected at Deer Run Road. Four soil samples were collected in triplicate from the bank profile at this location, with sampling locations shown in Figure 4-3(A). Evaluation of sample water content and percent methylmercury resulted in the relationship shown in Figure 4-3(B), which clearly shows a direct relationship between the percent of MeHg in the bank profile and the soil moisture content (Carroll, 1999).

As mentioned previously, the previous version of IFMTFM utilizes temporally constant MeHg bank concentrations and a threshold flow depth above which MeHg does not occur

in the channel banks, both of which were determined through calibration procedures. The incorporation of the bank element into the IFMTFM attempts to remedy this and other discrepancies between the model and physical observations; and reduce the number of calibration parameters. Modeling efforts using the Finite Element Surface-Water Modeling System: Two-Dimensional Flow in a Horizontal Plane (FESWMS-2DH) model and analysis of water table data from the installed groundwater monitoring wells allowed for the determination of a temporally-variable zone of saturation (as critical for methylation) within the channel banks of the updated IFMTFM version. The zone of saturation is a function of time history of channel stage, as computed within RIVMOD. The saturated extent of channel banks is also a function of spatial location within the model domain, resulting from variable channel geometry, and hence computed stage, for any given flow magnitude. The creation of the new bank element type within IFMTFM allows for moisture content within the banks will be continuously simulated and updated as required throughout the model domain from CCG to Lahontan Reservoir.

Within the domains of RIVMOD/WASP5/MERC4, each bank element includes the channel bank between adjacent stations (Carson River model includes 274 stations). Recall that different channel geometry is assigned for each station within the input files. This geometrical configuration inside each model segment (between adjacent stations) is determined through linear interpolation of the properties of the two bordering stations. Symmetry is specified for opposite channel banks. A single bank element is therefore sufficient for each IFMTFM model segment.

Flow history must be tracked. The combined vertical extent of the capillary fringe and the partially saturated zone will depend on whether river stage is rising or falling. A

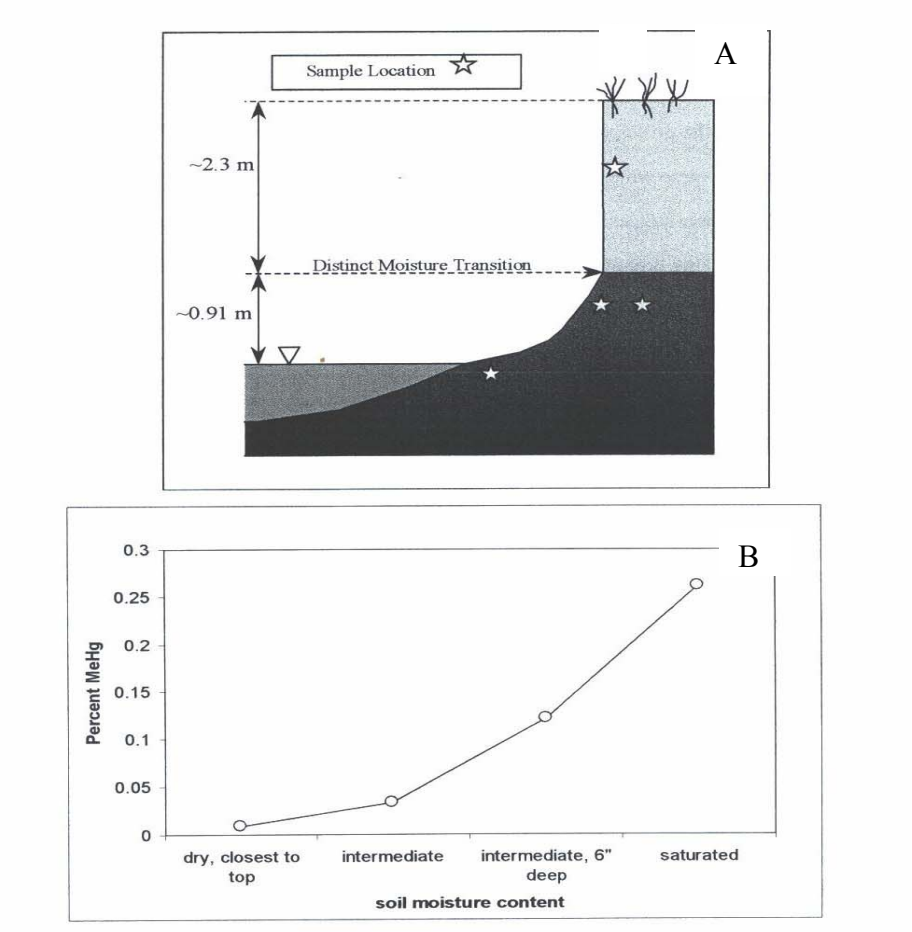

Figure 4-3. Dependency of methylmercury concentration on soil moisture. (A) Schematic of bank profile at DRR with sampling locations marked. (B) Percent MeHg versus percent moisture content found in the bank profile at DRR. (Reprinted with permission from Carroll, R.W.H., 1999. Simulation of Mercury Transport and Fate in the Carson River, Nevada. Masters Thesis. University of Nevada-Reno, Reno, Nevada. Figure 1.13, pp. 38)

smaller distance would be expected if the river stage is rising (bank not recently inundated) and a larger distance if river stage is falling (bank recently inundated). This is a by-product of the variable relationships between pressure head (ψ) and moisture content (θ), based on whether a given soil is wetting or drying. This relationship is commonly referred to as hysteresis and can be represented by scanning curves (Tindall and Kunkel, 1999).

Two soil samples were collected along the channel bank at the location of the groundwater wells during October 2002. While possible to obtain a steady-state estimate for the size of the capillary fringe using these samples, incorporation of this value into the IFMTFM would require the assumption of equilibrium attainment within bank sediments. Given the nature of Carson River streamflow, equilibrium conditions will rarely be reached (except perhaps during flood events). Ideally, data would be collected relating the extent of the capillary fringe to the rates at which channel stage is rising or falling. Realistically, this data collection is impractical and, given the spatial heterogeneity of sediments within the Carson River system, unilaterally applying these functional relationships to all bank sediments within the model domain is incorrect. Alternatively, it will be kept in mind that a capillary fringe does exist, that MeHg concentrations within channel bank sediments are likely underestimated, and, by neglecting this fringe, that the final calibration to match observed MeHg water column concentrations will be conservatively low. Because mass failure along channel banks is not a modeled erosion process within IFMTFM, mercury enters the water column only through erosion or diffusion from contacted (by stream stage) portions of the bank. Mercury concentrations within the capillary fringe will only impact the model if these portions of the bank become contacted in the immediate future. Relative to the contacted portion of the channel bank, the extent of the capillary fringe is predicted to be small. With these considerations in mind, attempts are only be made to track the saturated portion of the channel bank elements.

Soil heterogeneity, the lack of available data regarding soil properties relating to soil moisture, the presumed minimal impact of the capillary fringe on water column

mercury concentrations, and data analysis suggesting a nearly instantaneous response time from channel to wells ultimately pushed modeling efforts away from the inclusion of unsaturated zone modeling. The possibility of a variable time lag, from river stage change to water table response, based on whether the bank sediments are wetting or drying, however, was continually considered throughout the data analysis portion of this project.

By tracking the size of the saturated zone over time as river flows change, the updated IFMTFM begins to remove itself from the unrealistic assumption of static MeHg concentrations within the channel banks and no MeHg above a given depth threshold, as present in the previous model version. By allowing the model to run for a sufficient length of time prior to generating used output, initial conditions (bank concentrations) effectively wash out of the system, thereby removing the dependence of output on initial conditions. The addition of the bank element allows for user specification of different methylation and demethylation rates within the channel banks, as compared to the channel bed. This is expected based on the higher percentage of fine particles within channel bank sediments. Data has been presented to suggest that methylation is dependent on moisture content and, specifically, the presence of anoxic regions within the channel banks. Ongoing research at other institutions is seeking to determine these rates as a function of soil moisture content and the time duration of saturation conditions necessary for maximum MeHg production by microbes; preliminary results are used in this thesis research.

As moisture content within the bank elements change over time, the concentrations of methylmercury within the channel banks become dynamic, variable with respect to

time, spatial location within the model domain, and vertical location within the bank. Variable concentrations are then used in the model to determine methylmercury amounts introduced to the water column via erosion, diffusion, and advection (during receding hydrographs) from the banks. Note also that while erosion of channel bank MeHg and inorganic Hg(II) was previously simulated by the IFMTFM, diffusion of these chemicals from channel banks is an addition to the code. The inclusion of bank diffusion could be a significant contributor to MeHg concentrations in the water column under medium to low flow conditions. Diffusion was previously only modeled from the bed sediments, which include a much larger contact area for diffusion than do the channel banks. However, mercury concentrations within the channel banks are observed to be two to three orders of magnitude greater than the concentrations within the channel bed sediments. Additional considerations were also needed to determine the impact of moisture content history on methylation and demethylation rates. Although the rates are a function of moisture content, the microbially-mediated nature of these chemical reactions does suggest that response time for each microbial community should be considered and somehow modeled. For example, how long does a portion of the bank need to be wet before the observed net methylation rate reflects this moisture change? These considerations are later discussed in chapter 7. Additionally noted is that water temperature, which impacts the kinetics, is known by the model.

Final Considerations and Comparative Analysis

The completion of modeling efforts allows for an improved understanding of the relationship between river stage change and water table. Based on the high degree of spatial heterogeneity within the system, the simple relationships developed for the Scout Camp reach are unlikely to precisely duplicate the field conditions observed elsewhere

within the Carson River system. The detailed FESWMS-2DH and groundwater data were only tools used in developing the relationships between flow history and bank saturation levels. The IFMTFM simulates the hydrodynamics within the system based on user-input data from the USGS gages and through application of RIVMOD. RIVMOD is capable of predicting the temporal and spatial variability of river stage. The water table observations are not known to the IFMTFM model, as the groundwater wells were not installed during periods of historical data collection (used for model calibration and verification). Modified input data file structure and a new portion of FORTRAN code are added to the IFMTFM to incorporate bank elements and dynamically compute and update MeHg concentrations in the channel banks.

With the bank element concept presented to the reader, it is possible to move forward to the model development and data analysis portions of this thesis. Following the discussion of the data modeling and data analysis, the final component of this thesis research is a comparative analysis to compare RIVMOD and FESWMS-2DH (SMS) predictions for river stage and flow velocity as functions of flow magnitude. Ideally, the results would be in perfect agreement. Regardless of the results, it must be realized that the IFMTFM will still only have available to it the stage output from RIVMOD (a 1D hydrodynamic model based on coarse, simplified channel geometry). However, the potential use for higher resolution channel geometry data (for future model inclusion) can be assessed.

Bank elements are used to model the spatial and temporal variability of bank moisture conditions (over a range of flow conditions and scenarios) to determine bank MeHg concentrations; these bank concentrations are then the determining factors for

water column concentrations and, ultimately, the availability of MeHg for uptake within the aquatic food chain. The development and inclusion of bank dynamics within the IFMTFM will assist in the modeling efforts for the mercury-contaminated Carson River system, with the long-term goal of assisting in the determination of an appropriate remediation strategy. Should additional data regarding methylation kinetics as they relate to soil moisture content become available, the basic IFMTFM code structure needed for its inclusion is in place following the completion of this thesis research.

CHAPTER 5
SURFACE WATER MODELING

Site Selection

The starting point for all field research is site selection. In the case of this study of the Carson River, one of the goals is the quantification of the interaction between surface water and groundwater. Months in advance of the first field expedition, it was decided that this would be accomplished through a combination of surface water modeling and analysis of data collected from near-channel groundwater wells. Site selection therefore hinged on two critical elements: the ability to gain vehicular access to the site for the survey equipment and the drill rig for well installation, and permission of the landowner to install the wells. Additionally, the site needed to have the characteristic vertical banks and a site layout conducive to and stable enough for getting a drill rig as close to the channel as possible.

Much of the land along the lower Carson River is privately owned by cattle farmers and agricultural interests, landowners with no real reason to justify access to their land and not interested in supporting a water quality study. Fortunately, a portion of the lands adjacent to the lower Carson River are public lands under the administration of Fort Churchill State Historic Park of the Nevada Division of State Parks. On March 5, 2001, accompanied by Mr. James Prida of the Fort Churchill State Park, a suitable site was located at a Boy Scout Camp approximately 10 km downstream of the Fort Churchill USGS Gaging Station (Figure 1-2). On March 8, 2001, three groundwater wells were installed along the south bank of the Carson River at the Scout Camp field site. The three

wells were installed along a transect, perpendicular to streamflow direction, at distances from the vertical channel bank of approximately 5, 25, and 100 feet. The 6-inch diameter, PVC wells are cased to a depth of 20 feet. Pressure transducers monitor the position of the water table within each well, data which is recorded by data loggers at 1-hour sampling intervals.

Collection of GPS Survey Data

The channel geometry used in RIVMOD can be described as coarse, based only on outdated USGS topographic maps. The construction of a surface water model required more precise channel geometry data. The Leica GPS System 500 was used to conduct a detailed bathymetric survey of the Carson River channel for a reach centered on the three installed groundwater wells. The system utilized a base station and a rover unit. Survey data was collected over two periods: March 6-9, 2001 and July 2-6, 2001.

The complete set of surveyed elevation data points is shown in Figure 5-1. Data points could be divided into several classifications: transects (100 through 500), top of vertical banks, water surface, channel thalweg, or general channel bed points. Surveyed elevations are expected to be accurate to within +/- 3.0 centimeters (cm), with horizontal accuracy closer to +/- 1.0 cm . The total surveyed reach measured approximately 500 meters along the thalweg.

The bathymetric data collected was used as the framework for a surface water model. As the raw surveyed data will later be refined, a few shortcomings of the survey process are herein noted. Recall that GPS is based on travel times and distances from receiver to at least four satellites. The large canopy of the cottonwood trees situated along the channel banks often caused a loss of signal with the required satellites, resulting in incomplete data along the top of the channel banks and effectively limiting the ability to

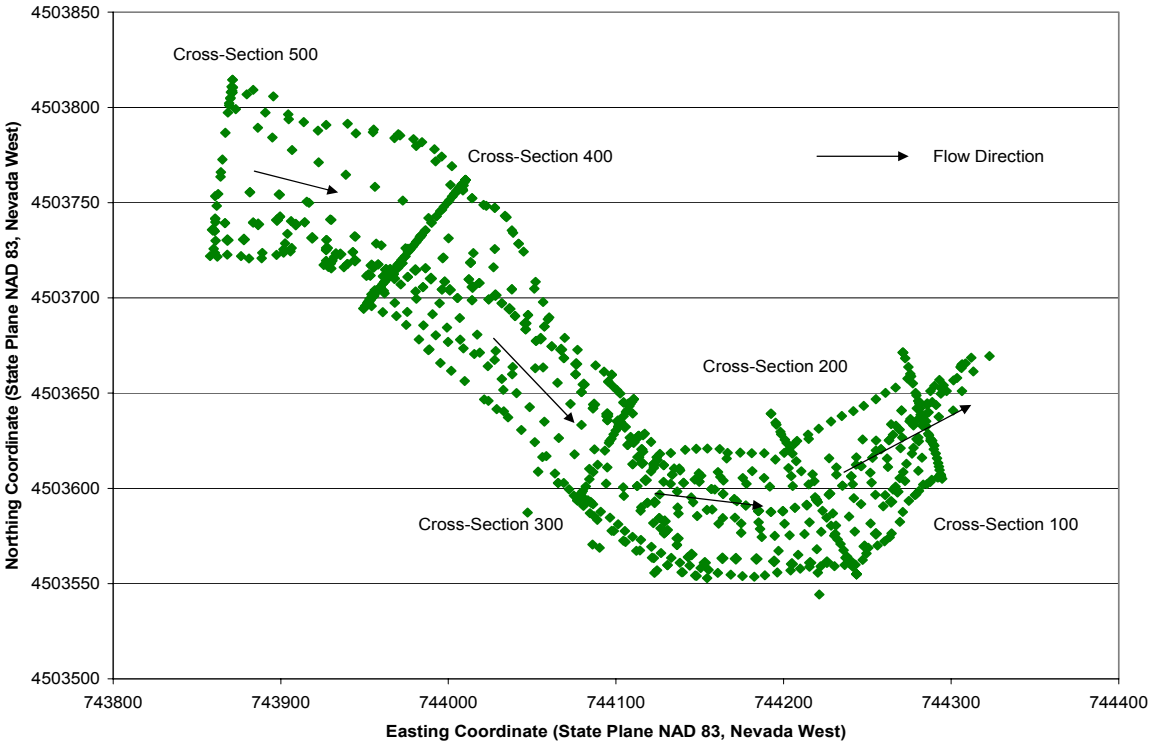

Figure 5-1. Spatial location of survey points and cross-sections at Scout Camp site

collect precise elevation data for the floodplain. Vertical banks between two and three meters in height additionally limited the ability to collect elevation data adjacent to the base of the vertical banks. Observed streamflows during March ranged from 165 to 215 cfs, while those in July were between 8 and 9 cfs. Given that flows of interest are those high enough to contact the channel banks (thereby causing erosion and introducing MeHg to the water column), the water surface data collected in March is of particular interest for surface water model calibration. However, the high flows at this time prevented the acquisition of thalweg elevations along the channel, and thus prevented an analysis of any relation between water surface slope and representative bed slope. For this reason, most channel bed data was collected during the period of significantly lower flows. All data collected are associated with measurement errors. This error is reported during the post-processing stage. Unfortunately, some of the data points required multiple attempts at this

collection, as a result of errors outside of the acceptable range. These limitations, in addition to time constraints, resulted in a surveyed reach of basically 500 meters, including 5 complete transects. The spatial extent of the model domain is an important component to SMS model development.

Surface Water Model Selection

Based on cost considerations, research, and consultation with the model developers, it was decided that Surface Water Modeling System, Version 8.0 (SMS 8.0) would be the modeling system of choice for developing a surface water model of the surveyed reach of the Carson River. Within the SMS model, several modules are available. The module of choice is FESWMS-2DH. The FESWMS model executable code, FLO2DH, is written in the Fortran 77 computing language. FLO2DH was originally developed by the USGS (Water Resources Division) and later modified by the Federal Highway Administration of the U.S. Department of Transportation.

FESWMS-2DH applies the finite element method to solve the system of equations that describes 2D depth-averaged flow in a horizontal plane. The system can be used to simulate flow in rivers and floodplains and other surface-water bodies where vertical accelerations are small in comparison to horizontal motion (Froehlich, 2000). The hydrodynamic modeling code of FESWMS supports both super- and sub-critical flow analyses, including area wetting and drying. Use of this model is justified because one is not interested in the vertical variability of flow properties, but rather only the horizontal distribution of flow quantities. The temporal variability of flow within the Carson River channel also mandates the ability of the chosen model to account for wetting and drying patterns within grid elements along the channel boundary. Within this document, the

surface water hydrodynamic model will be interchangeably referred to as SMS, FESWMS, or FLO2DH.

Functionality of the FESWMS Model

Several steps were involved in the development of a functioning surface water hydrodynamic model. GPS data (Figure 5-1) was used to generate a quasi-3D finite element model of the reach of the Carson River immediately surrounding the Scout Camp and the groundwater wells. Channel bathymetry data, from the field survey, was first used to generate a 2D finite element network (or mesh) using the DIN2DH program. The finite element network was then refined through node addition and deletion, elevation modifications, and node spacing adjustments. With the model domain carefully planned, the final step was to simulate water flow through the model domain. Though the procedure is straightforward, the execution of this process for the Carson River model proved far more complicated. Several months of research was placed into the development of this model, and each step of model development will be reviewed in turn.

The primary equations governing the hydrodynamics are summarized by equations 5-1, 5-2, and 5-3 (Froehlich, 2000):

- Vertically-integrated momentum equation in the x direction:

$$\frac{\partial(HU)}{\partial t}+\frac{\partial}{\partial x}\left(\beta_{uu}HUU+(\cos\ \alpha_x\ \cos\ \alpha_z)^2\frac{1}{2}gH^2\right)+\frac{\partial}{\partial y}(\beta_{uv}HUV)$$
$$+\cos\ \alpha_x\ gH\frac{\partial z_b}{\partial x}-\Omega HV+\frac{1}{\rho}\left[\tau_{bx}-\tau_{sx}-\frac{\partial(H\tau_{xx})}{\partial x}-\frac{\partial(H\tau_{xy})}{\partial y}\right]=0 \qquad \text{(Eq. 5-1)}$$

- Vertically-integrated momentum equation in the y direction:

$$\frac{\partial(HV)}{\partial t}+\frac{\partial}{\partial y}\left(\beta_{vv}HVV+(\cos\ \alpha_y\cos\ \alpha_z)^2\frac{1}{2}gH^2\right)+\frac{\partial}{\partial x}(\beta_{uv}HVU)$$

$$+\cos\ \alpha_y\ gH\frac{\partial z_b}{\partial y}+\Omega HU+\frac{1}{\rho}\left[\tau_{by}-\tau_{sy}-\frac{\partial(H\tau_{yx})}{\partial x}-\frac{\partial(H\tau_{yy})}{\partial y}\right]=0 \qquad \text{(Eq. 5-2)}$$

- Continuity equation

$$\frac{\partial H}{\partial t}+\frac{\partial(HU)}{\partial x}+\frac{\partial(HV)}{\partial y}=q \qquad \text{(Eq. 5-3)}$$

where variables are defined as follows (units: [L] = length, [T] = time, [M] = mass):

H = water depth [L]
z_b = bed elevation [L]
$z_s = z_b + H$ = water-surface elevation [L]
U = depth-averaged velocity in the horizontal x direction [L / T]
V = depth-averaged velocity in the horizontal y direction [L / T]
β_{uv},β_{vu},β_{vv} = momentum flux correction coefficients that account for the variation of velocity in the vertical direction; coefficients result from the vertical integration of the momentum transport equations and account for the vertical variations of U and V
$\alpha_x = \arctan(\partial z_b / \partial x)$
$\alpha_y = \arctan(\partial z_b / \partial y)$
$\alpha_z = \arccos(1 - \cos^2\alpha_x - \cos^2\alpha_y)$
g = gravitational acceleration [L / T^2]
Ω = Coriolis parameter [T^{-1}]
ρ = water mass density, which is considered constant [M / L^3]
τ_{bx}, τ_{by} = bed shear stresses acting in the x and y directions, respectively [$M / T^2 L$]
τ_{sx}, τ_{sy} = surface shear stresses acting in the x and y directions, respectively [$M / T^2 L$]
τ_{xx}, τ_{yx}, τ_{yy} = shear stresses caused by turbulence where, for example, τ_{xy} is the shear stress acting in the x direction on a plane perpendicular to the y direction [$M / T^2 L$]
q = unit source (inflow) or unit sink (outflow) term [$L^3/T / L^2$]

These governing equations are solved by the FLO2DH program using the Galerkin finite element method applied to the user-defined grid network. The method is carried out using

Newton-Raphson iteration and Gaussian quadrature integration for all elements (triangular or quadrangular shapes defined by nodes at vertices and mid-side points) within the model domain. FLO2DH is capable of simulating both steady and unsteady (time-dependent) 2D (in a horizontal plane) surface-water flow to obtain depth-averaged velocities and flow depths. The effects of bed friction and turbulent stresses are included, as are, optionally, surface wind stresses and the Coriolis force (though the latter two are not used here). The postprocessor program ANO2DH is used to present the results of flow simulations either graphically or as reports. Graphic plots of velocity and unit-flow vectors; ground-surface and water-surface level isolines; and velocity, unit flow, or stage (water-surface elevation) time-history plots at a computation point can be created.

The principal gain from creation of this model is the generation of time-history plots of river stage at the location of the groundwater well transect. An assessment can be made as to the agreement between river stage over this reach as predicted by RIVMOD and FESWMS-2DH; this will be discussed in the comparative analysis portion of this document (chapter 8). Recall that the former (RIVMOD) is based on a generalized channel shape and data interpolated from topographic maps, while the latter (FESWMS-2DH) is based on precise data collected using GPS. The ultimate requirement for bank elements is to predict moisture content variability within the channel banks, as a function of temporally- and spatially-varying river stage, as predicted by the current RIVMOD portion of IFMTFM. The FESWMS-2DH model was used to develop simple relationships between flow history and bank moisture, but the FESWMS model is not directly incorporated into the IFMTFM; the simple relationships are rather applied to river stage as predicted by RIVMOD.

Creation of Scatter Point Data Set

Data points for a finite element mesh can be generated directly from topographic data, such as a list of survey points within a text file, imported into SMS. The Leica GPS software allows for the extraction of data point latitudes, longitudes, and elevations in the form of a simple text file. In this instance, the text file was a compilation of the survey data collected during March and July of 2001. Survey point data from the Leica output text files were first imported into Excel. Using examples of .xyz files included in the FESWMS documentation, the raw survey data was copied and manipulated within Excel to match the required input file format for FESWMS.

Pre-Processing of Data Prior to Mesh Construction

The FESWMS mesh was constructed by making use of the available survey data. Before mesh creation, a moderate degree of pre-processing was required to account for shortcomings of the data set. Limited data downstream of cross-section 100 suggests that this cross section will serve as the downstream boundary for the surface water model. Surveyed points downstream of this cross-section were therefore deleted. Erosion and deposition processes result in dynamic bed forms (high and low spots) and seasonal changes to exact thalweg location. In the interest of consistency (and with the most complete data available in July), survey points along the channel bed collected during March (water surface elevations) were removed from the scatter data set. To preserve the valuable detail provided from the cross-section surveys, however, the data points from the four downstream cross-sections collected in March are retained. Duplicate data points collected at nearly the same spatial location, as evidenced through visual inspection, were selected and deleted. While the software does include options for duplicate point removal, these means could not be used because of the spatial proximity of desirable

points at the top and base of steep banks. One is generally seeking a uniform nodal spacing in the range of 3 to 10 meters. Finer resolution is needed in areas where the element slopes are steep, such as along the banks, and lower resolution is adequate for flatter regions, or where survey data is less extensive. The identification of points to be removed was tedious as each point must be identified by coordinates only, but trial and error indicated this to provide the best starting point for mesh generation, as these points determine the mesh boundary and the first cut for the mesh layout.

With the point set modestly trimmed down, the Excel file was saved as a text file, and the file extension was changed to .xyz. The survey points are now able to be read into FESWMS using the 'File / Open' command. Within the File Import Wizard dialog box, the option was selected to open file as mesh and the coordinate systems are set to match the survey data (Horizontal System: State Plane NAD 83, State Plane Zone: Nevada West – 2703, Vertical System: NAVD 88, Units: meters) before the file was opened. The data points from the file were converted to mesh nodes, points representing locations of known position and elevation. The key components to a finite element mesh are the elements themselves, which connect the nodes to define the flow area, or model domain.

The network of scatter data points (the dots) and the associated mesh boundary is shown in Figure 5-2. For reference, the elevation contours created from this initial data set have also been overlain. All SMS-generated figures are in color, with the scale and type of plotted contours (water surface elevation, water depth, ground elevation / bathymetry, or velocity) indicated by the legend. A few items are of particular note. Vertical banks are poorly represented due to the inability to properly survey the base of the banks, or the top of the banks, in certain instances. Evidence of the channel thalweg

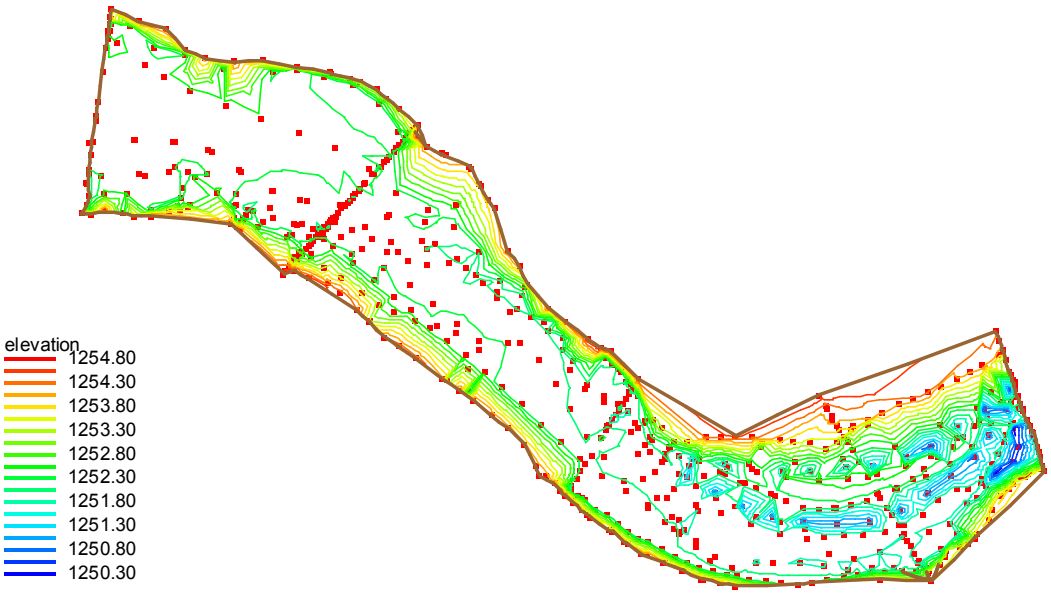

Figure 5-2. Original survey points after import into SMS scatter module

(or low-flow inner channel) is present, but many of these points are disjointed. Additionally, the linear interpolation scheme of the model does not necessarily connect those points which should logically be connected. The plethora of points along the five channel cross-sections is also very clear, as is the paucity of points along some portions of the channel banks and bed. Clearly, nodal spacing is also far removed from uniform. The resolution of these shortcomings is discussed at length in Appendix A.

Mesh Construction and Editing as Discussed in Appendix A

The mesh construction and editing process is discussed in Appendix A (separate from the main body of text) not because it was not a critical part of this thesis, but rather because the material is not needed for the reader to understand and appreciate the results of this research. The material is available for the reader's reference for three main reasons: to provide proof that mesh construction was completed under a carefully planned set of guidelines, to provide explanation for the mesh's limitation regarding the modeling

of overbank flows and the simulation of dynamic streamflows, and to justify the time spent getting the model to simulate Carson River hydrodynamics.

The development of a functioning model based on this set of scattered survey data points proved to be far more labor-intensive task than initially believed. Model development required several months before the model was able to simulate streamflow conditions ranging from bank full levels to levels at which flow was confined to the channel thalweg. Efforts were made to retain channel morphology information contained within the survey data set. Attempts to model stage levels above bank full and on the floodplain proved unsuccessful. Several problem areas were encountered as next listed: model parameterization, including element wetting and drying and specification of boundary conditions; steep channel banks, including modified mesh boundaries and slope transitions; irregular channel morphology, as result from erosion and deposition processes; drying of elements internal to the wet / dry boundary; jagged wet / dry boundaries; element re-wetting; supercritical flow conditions along boundary nodestrings; nodal velocity and water surface divergence; non-uniform node spacing and limited data availability for some portions of the mesh, resulting in poor element construction; and approaches for attaining model convergence. The mesh was constructed to accurately portray the geometry of the channel, as based on a combination of survey points, field measurements of channel bank dimensions, photographs, and personal recollection. The desired end-product was a model able to wet and dry as would be observed in the field. When the mesh editing process was complete, the FLO2DH hydrodynamic model was able to simulate element drying from bank-full to flows confined to the channel bed.

Summary of Mesh Editing

No amount of written explanation can explain the frequent frustration associated with getting this model to simulate the range of flows from bank-full to nearly zero. Any change in mesh geometry, regardless of how trivial, required the model to be initialized with all elements submerged. Water surface lowering needed to be performed gradually to allow the time for model convergence. Iteration after iteration, attempts were put forth to identify as many potential problem areas as possible, but it was never known if the problem was corrected until the water surface was able to be lowered beyond a previous threshold. It remained uncertain if this was the last round of mesh editing or if many more divergence problems awaited discovery. Eventually, however, the mesh was completed. The water surface was able to be lowered to minimum levels at which flow could no longer pass through the model domain, due to interior elements along the thalweg becoming dry. After all the frustration, repetition, and uncertainty, the sense of satisfaction and accomplishment that is worthy of note. The final edited mesh (bathymetry) is shown in Figure 5-3. The well transect is indicated in the figure. For reference, the minimum flow levels able to be modeled are also shown in Figure 5-4. The flow magnitude at this condition is not discussed here as this early result was based on a 0.2-meter head gradient between the upstream and downstream boundary condition nodestrings, a gradient originally chosen for no other reason than to be conservative. With the model able to simulate element drying under these conditions, the model was predicted to be stable for any larger head gradient and the associated higher mean velocity. Admittedly, most of the required mesh editing was due to the manner in which the mesh was constructed, that being from a random network of survey points. While the model might have performed better had less detail been included, this would also have

significantly altered the reliability of the model results. After all, the modeled reach of the Carson River is only 500 meters in length, and the goal was to accurately simulate the hydrodynamics (and thus river stage) down to low flows within the channel thalweg, which necessarily requires a high degree of model detail.

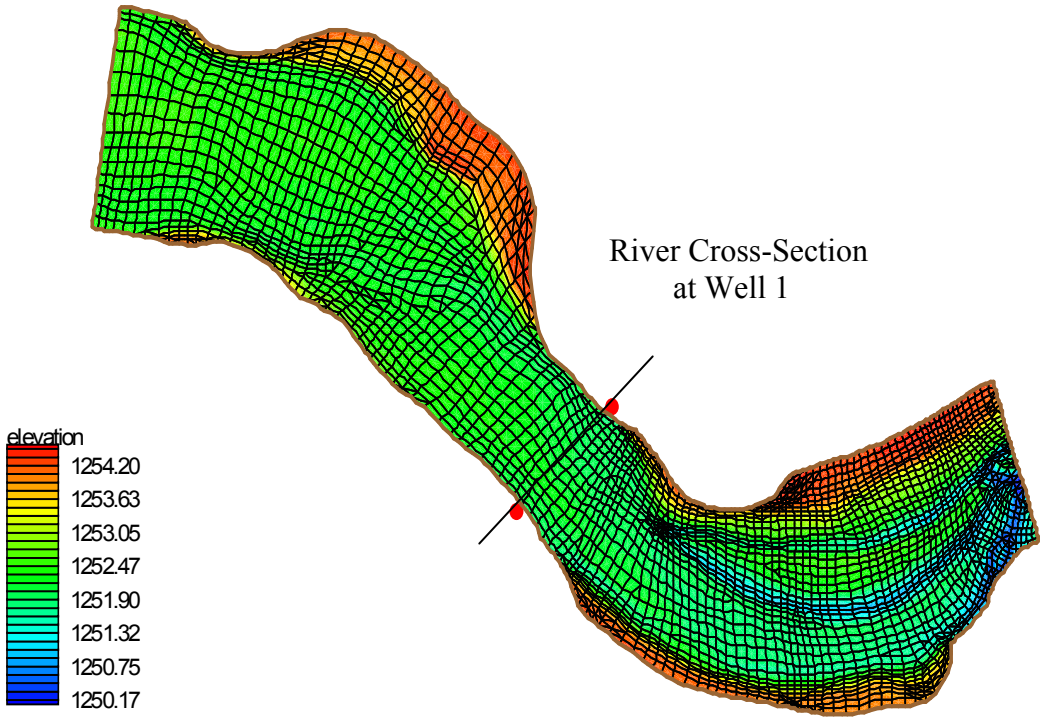

Figure 5-3. Bathymetry of Scout Camp reach after mesh editing found in Appendix A

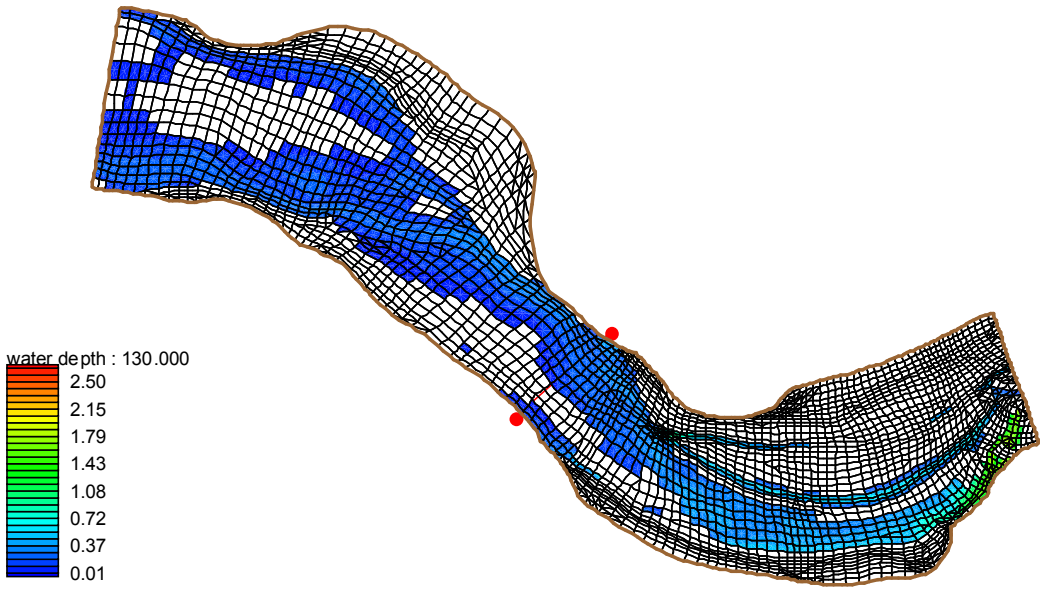

Figure 5-4. Minimum flow levels able to be modeled, subject to a 0.2-meter head gradient

CHAPTER 6
WATER TABLE RESPONSE TO STREAMFLOW VARIABILITY

Linking Surface Water Modeling and Groundwater Data

When the SMS model was selected as the surface water model for this project, two distinct end-products were envisioned. The first was to develop a simple relationship to relate stage in the channel to water table level within the bank. This relationship was then to be incorporated into a new IFMTFM bank element functionality to predict saturation conditions within the channel bank immediately adjacent to the channel, as a function of flow depth and channel geometry known by RIVMOD. The second end-product, to be discussed in chapter 8, was a comparative analysis between RIVMOD predictions and SMS predictions. For the modeled Scout Camp reach, a comparison between the two models was sought for flow depths and mean velocity to see if the simplified channel geometry and 1D nature of RIVMOD results in consistently high or low predictions relative to a more detailed and calibrated model.

Data Availability

A GPS survey was conducted to provide channel bathymetry input data to the SMS model, which was used to model Carson River streamflows and predict river stage. After site selection in March 2001, the survey operation began. With the groundwater wells sited, the intention was to survey channel cross-sections both upstream and downstream of the well transect, with roughly equivalent survey areas in both directions. Complications arose with loss of satellite lock caused by cottonwood trees, vertical banks, and, at times, less-than-ideal satellite configurations. Further complications arose

when post-processing indicated points with unacceptable error values, which would have to be surveyed again. After two channel survey operations in March 2001 and July 2001, five channel cross-sections and approximately 500 meters of channel length were surveyed. Three groundwater wells are situated along a transect, approximately 275 meters downstream of the upstream boundary condition of the mesh, as indicated in Figure 5-3.

The SMS mesh was constructed (Appendix A) to predict the relationship between streamflow and river stage, specifically the stage adjacent to the vertical bank at the well transect. Three gages along the Carson River monitor streamflow levels. The RIVMOD module in IFMTFM incorporates dynamic streamflow values from the Carson City and Fort Churchill gages to perform hydraulic routing. Upstream irrigation withdrawals are accounted for using the Fort Churchill streamflow values. With no known withdrawals downstream of Fort Churchill, RIVMOD is capable of routing flows and predicting average streamflows for all RIVMOD segments downstream of Fort Churchill.

Generation of Boundary Condition for FESWMS Surface Water Model

To develop a relationship between river stage and water table level, the river stage needed to be accurately modeled within the FESWMS module of SMS. Following mesh creation, editing, and refinement; but before simulating the hydrodynamics through the mesh reach, boundary conditions must be specified. The FLO2DH model requires an upstream and a downstream boundary condition.

During the mesh construction process (Appendix A), it became evident that the finite-element mesh was not suitable for the simulation of dynamically rising and falling flows. The decision was made to use head boundary conditions at both the upstream and downstream extents of the model spatial domain. Nodestrings along the boundaries and

strategically located at cross-sections within the mesh interior were used along with the model solutions for flow depth to identify the flow through any given cross-section. Water surface elevations from a FESWMS model solution are, therefore, relatable to streamflow through the model domain.

Within FESWMS, the head boundary conditions are incrementally lowered to generate a series of water surface solutions. The FESWMS module can stably operate with a head or flow upstream boundary condition, but the model requires a head downstream boundary condition. Because the Scout Camp site is not located at a gaged location, a rating curve at the downstream boundary was not available. The head gradient between upstream and downstream boundary conditions must, instead, be specified and held at a constant value, based on the lack of stage data for the downstream boundary and a lack of data for the variability of water surface slope with streamflow magnitude, as later discussed. Though an upstream head boundary is used in the surface-water model, the flow hydrograph at the upstream boundary channel cross-section must also be known in order to later link surface water modeling of river stage to the corresponding water table elevations from the wells within the channel bank.

Streamflow routing: testing the validity of instantaneous translation

Water table data collected via the groundwater wells is a time series of water table elevation (NAVD 88). Flow in the channel also varies over time, as evidenced by the hydrographs of USGS gaging stations at Carson City and Fort Churchill. This flow must be specified to develop a correlation between water table and river stage. Two options to obtain this time series were considered. First is the possibility of an evapotranspiration (ET) forcing function. Under this scenario, streamflow would simultaneously rise and fall at all locations along the Carson River. Peak flow would occur everywhere at the same

time of day. Differences in streamflow magnitude with distance are the result of irrigation withdrawals and tributary additions. Given the arid environment and the prevalence of transpiring cottonwood trees along the entire river length, this seemed a viable possibility. Streamflow withdrawals for irrigation are believed to be nonexistent downstream of the Fort Churchill gaging station. If the ET forcing function was indeed present, so that streamflow oscillation is solely due to flow withdrawals, then the streamflow time series at Fort Churchill could be instantaneously translated (no consideration of travel time) and used as the upstream boundary condition for the Scout Camp reach. This instantaneous downstream translation by a distance of 10 km may not seem intuitively correct, as a reasonable velocity of 0.5 m/s would translate to a 6-hour travel time. However, it would simplify the effort to obtain the streamflow time series at the upstream boundary, and the option was investigated.

To validate or invalidate the assumption of instantaneous translation and an ET forcing function, streamflow data from three Carson River gages were compared for the period of available well data (March 2001 through September 2002). The three USGS gages, Carson City Gage (CCG), Deer Run Road Gage (DRR), and Fort Churchill Gage (FCH), record streamflow at 15-minute intervals. This set of data was obtained from the USGS with the assistance of USGS Hydrologist Jim Crompton in Carson City, Nevada. The streamflow time series are graphed in Figure 6-1 (2001) and Figure 6-2 (2002). The data is separated by calendar year. A logarithmic scale is used to better capture the high degree of streamflow variability over this period of interest. Streamflow data available at 15-minute resolution should capture the diel (within day) variability at these respective locations.

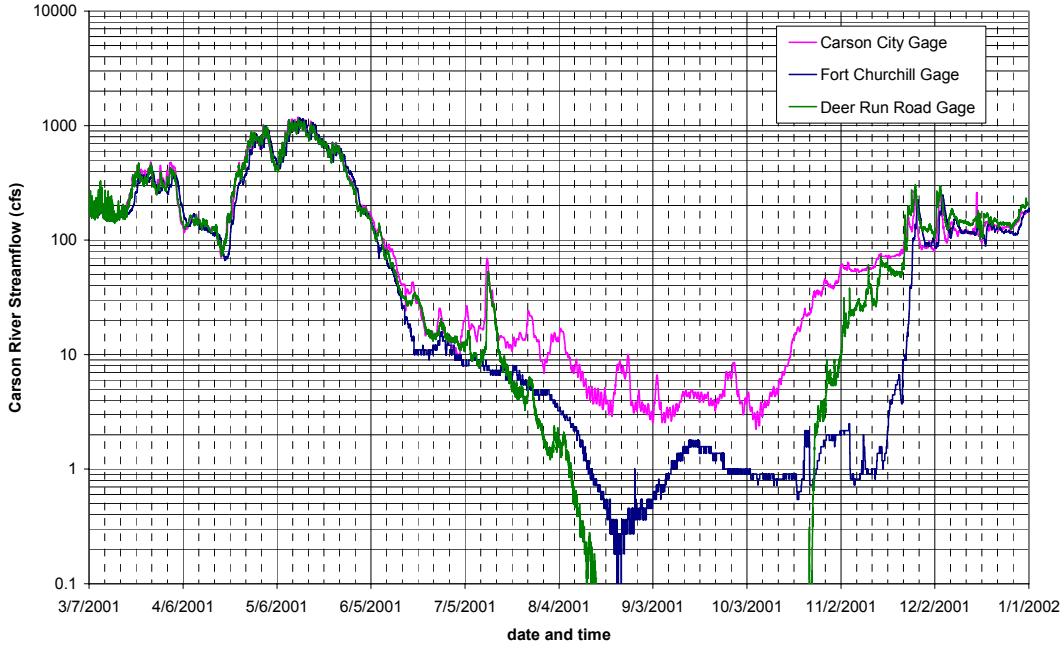

Figure 6-1. 2001 USGS streamflow gage comparison: 15-minute data

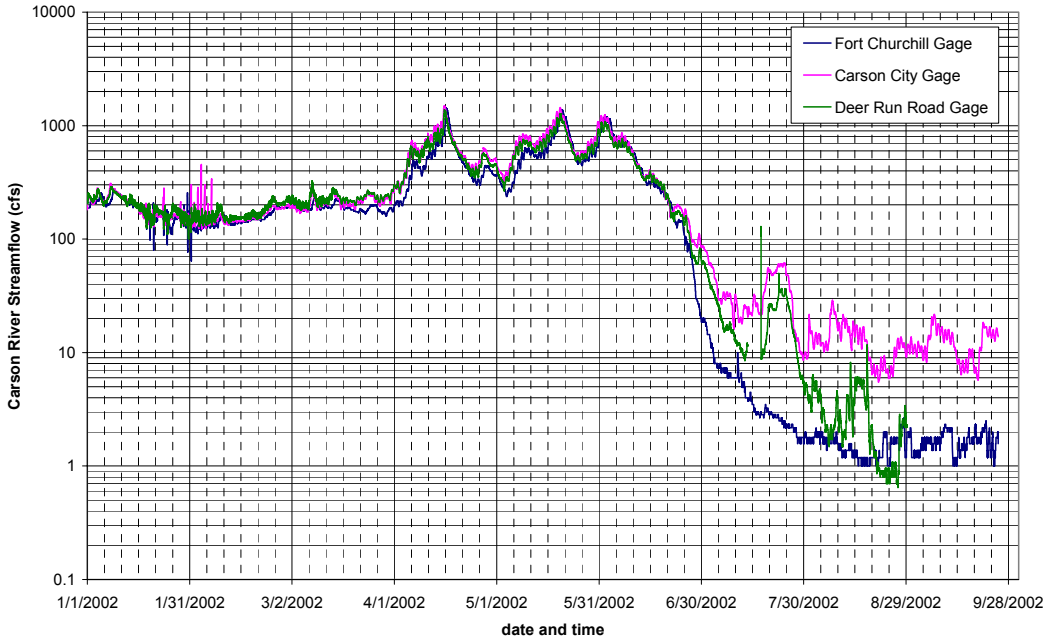

Figure 6-2. 2002 USGS streamflow gage comparison: 15-minute data

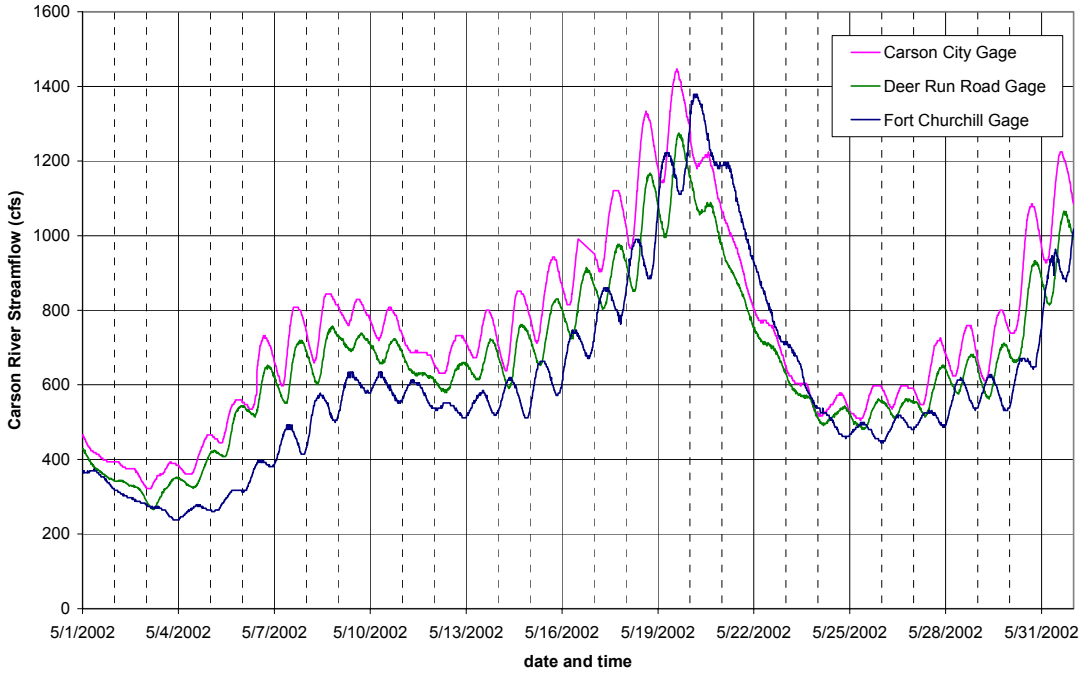

Figure 6-3. May 2002 Carson River streamflow at USGS gages

The complete set of data provides evidence of a travel time for flow peaks from upstream gaging stations to Fort Churchill. A more noticeable time lag is evident for DRR to FCH as compared to CCG to DRR, as reasonably expected given the 6-km versus 52-km distance between the respective stations. A subset of the data, for May 2002, is used to illustrate this point, appearing in Figure 6-3. Note the diel variations in streamflow. The daily peaks do not occur consistently at the same time of day, but rather occur at times dictated by travel time from upstream. During times of year when streamflow is primarily due to snowmelt, higher melt rates would be observed during the early afternoon when the day is at its hottest. As the melt rates slow overnight, the result is a diel streamflow variability which will then characterize the observed streamflow further downstream. Despite the arid climate, the diel streamflow variability caused by ET is clearly overshadowed by the influence of travel time. The observed streamflow

reduction from CCG to FCH is due to irrigation withdrawal; no known irrigation ditches or tributaries occur from Fort Churchill to the study reach at the Scout Camp. The Scout Camp site is approximately 10 km downstream from FCH, so a lag time is expected between these two locations. Fort Churchill streamflows will need to be hydraulically routed to create the upstream boundary condition for the SMS model. The assumption of instantaneous translation would have the effect of artificially impacting the observed time lag between modeled river stage (a function of streamflow) and water table oscillations. In the extreme case of rapidly rising flow and rapid response time between channel and bank, the assumption of instantaneous translation could presumably cause the well response to precede the river stage oscillation. This approach was discarded.

Streamflow routing: hydraulic routing using RIVMOD

Streamflow was instead routed using RIVMOD. RIVMOD performs hydrodynamic computations using a 60-second time step. Being only interested in the hydrodynamic output from IFMTFM, there was no need to accurately simulate reservoir stage, which impacts the mercury computations. This alleviated the need to obtain and process 15-minute data for the USGS gage in Lahontan Reservoir at the dam (LRD). A time series for flow must still be input to RIVMOD at LRD, but the values were simply set equal to the time series for flow at FCH. This approach ensures that backwater conditions from the reservoir do not impact the hydraulic routing from Fort Churchill to the reservoir, between which the Scout Camp is located.

Within IFMTFM, streamflow values input to RIVMOD are average daily flows. To be consistent with the 1-hour interval at which water table data is collected by the well data loggers, a 1-hour time interval was selected for streamflow input to RIVMOD for the hydrodynamic routing. To create the RIVMOD input data files, macros were written

to extract hourly flow data from the smaller 15-minute data sets. Data from CCG and FCH were extracted, and, as mentioned, flows at LRD are taken as equal to those at FCH. Inflow to the reservoir from the Truckee Canal was modeled as zero. Care was taken to ensure that the flow values at the respective stations within any given input file row corresponded to the same point in time, as needed to compensate for the intermittent data gaps within the 15-minute data files. Flows lower than 8.0 cfs were changed to 8.0 cfs, as this value represents the minimum allowable flow input for RIVMOD within IFMTFM. Periods of lower flow are therefore not accurately simulated by RIVMOD. Before simulating real-time hourly streamflow data, RIVMOD was run at steady state for a period of 10 days to create a valid initial solution throughout the RIVMOD model domain from CCG to Lahontan Reservoir. Hydrodynamics were then simulated for the period from March 2001 through August 2002 using hourly gage data, and the solution time series for flow are output, to a text file, for RIVMOD segments 148 through 155 (segments near Scout Camp reach). It is also noted that two separate hydrodynamic simulations were necessary because of file size limitations in RIVMOD; a 30 day overlap was used to ensure flow continuity when the simulation results were later combined.

Latitude and longitude of all survey points are known from the survey data set in Nevada West State Plane Coordinates. RIVMOD segments have previously been recorded on a USGS topographic map, which utilizes the 1927 North American Datum (NAD 27) as the horizontal reference. Within SMS, the mesh coordinates (surveyed date points) are easily converted to an alternate coordinate system from the Edit menu. This feature was used to identify the NAD 27 coordinates corresponding to the upstream and downstream boundary conditions, as well as the location of the well transect. The

upstream and downstream boundary conditions are located within RIVMOD segments 151 and 153, respectively. The groundwater well transect is approximately centrally located within RIVMOD segment 152. Segment spacing for model segments 144 through 240 is equal to 250 meters.

RIVMOD flow computations were used to construct the flow time series at the upstream boundary condition of the FESWMS model. With no significant inflows or flow withdrawals downstream of Fort Churchill, hydraulic routing results in hydrograph attenuation and delay due to channel resistance. RIVMOD does not model hydrograph attenuation due to storage capacity within channel banks. RIVMOD is able to smooth the FCH hydrograph, which can oscillate significantly during periods of rapidly changing streamflow or under low flow conditions (because of inherent gage limitations). The hydrograph input into RIVMOD uses hourly time steps. The routed hydrograph output from RIVMOD is extracted at hourly intervals, but all RIVMOD computations are completed at 60-second time steps.

Groundwater Well Data

General Well Information

Three groundwater monitoring wells were installed in March 2001, approximately centrally located within the surveyed Scout Camp reach. The 6-inch diameter, 20-foot deep wells are located along the south streambank at distances from the vertical bank of approximately 5 (Well 1), 25 (Well 2), and 100 (Well 3) feet. The three wells are situated along a transect perpendicular to streamflow direction. Pressure transducers situated at the base of each well monitor the water table level, with data continuously recorded by data loggers. With the notable exception of the middle well, continuous water table data is generally available dating back to the time of well installation.

Data Limitations

Although well installation was completed on March 9, 2001, time was allowed for the water to clarify prior to data logger insertion. Collection of water table data began on March 12, 2001, after the March 2001 field survey work was completed. Water table elevations, relative to the NAVD 88 vertical datum, are measured in each well at hourly intervals. The probe installed in Well 2 failed to function properly, and this data set is therefore unavailable. After the failure of this probe, the remaining two probes were also removed on May 29, 2001 for preventative maintenance, to ensure no similar problems in the future. The probes were unable to be returned to the wells before the field work period in July 2001. For this reason, a data gap appears in the water table data sets for Well 1 and Well 3 between May 29 and July 5, 2001. During the reinstallation process, the cable for holding up the probe in Well 1 was insufficiently stabilized. Duct tape failed to hold the looped cable in place, and the probe weigh resulted in the probe falling to the base of the well. As this process occurred gradually, a uniform correction is unable to be applied to the well data. Probe slippage is evident in the well data for this time period, as shown in Figure 6-4, and was verified by well inspection in October 2002 (note the sudden rise in water table, inconsistent with water table oscillations observed in Well 3, associated with the increased water pressure felt by the transducer as it moved down the well). With the probe slippage complete and the probe at the base of Well 1, the slip distance was calculated and applied as a uniform correction to the water table data for Well 1 after August 1, 2001. The 2001-2002 water table elevations in Figure 6-4 are plotted relative to the thalweg elevation at the well transect (1252.01 meters (NAVD 88) set as point of zero-reference); additionally included for reader reference are the top of bank elevation (1254.15 meters), the top of casing elevation for Well 1 (1253.95 meters),

and the high point of the channel bed along the well transect (1252.27 meters), which is indicative of the elevation at which the channel bank closest to Well 1 will no longer be in contact with water actively flowing through the main channel.

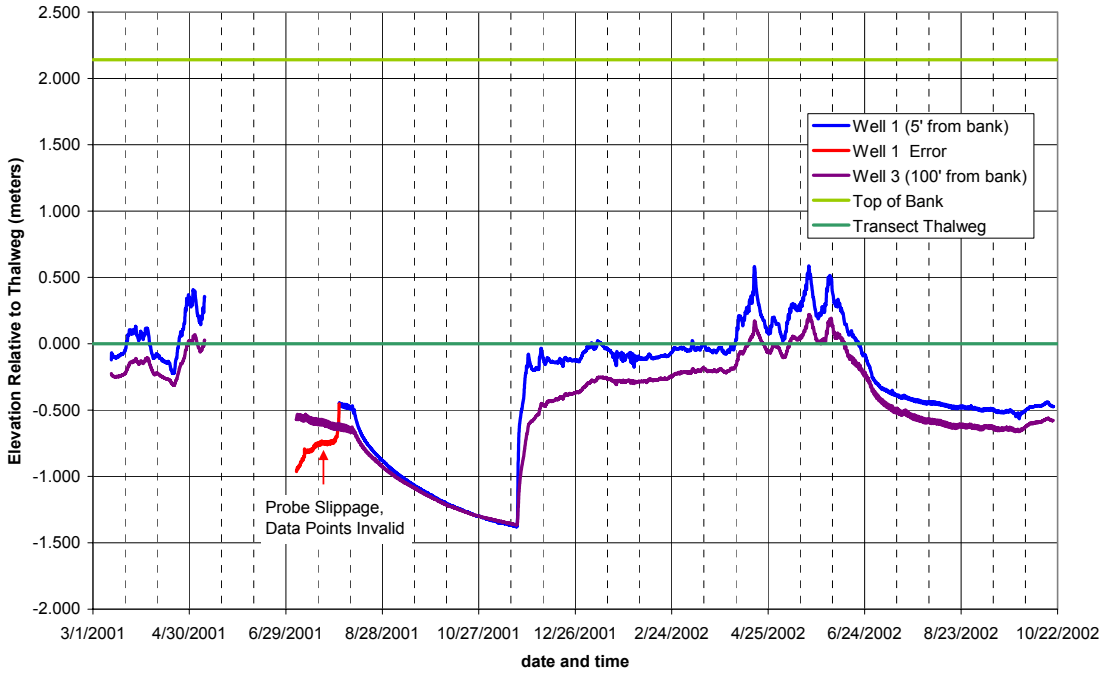

Figure 6-4. Complete water table data from Well 1 and Well 3 at Scout Camp site

Concern with computing the hydraulic gradient between the river and the bank sediments directed the selection of the useable set of well data, as data is only selected from time periods in which water table data is available in both Well 1 and Well 3. This data set is used in the later analysis of the coupling of river stage and water table level. Complete water table data is available for the following time periods: March 12, 2001 through May 9, 2001 and August 1, 2001 through October 22, 2002, the date of the final site visit. The loss of data from May 9, 2001 through July 5, 2001 was unavoidable, and the loss of data from July 5, 2001 through August 1, 2001 was for a period of low streamflow, below the point of contact with the banks. Recall, the relationship between

river stage and saturated bank levels is of particular interest, so the latter data loss is considered trivial. Fifteen-minute streamflow data, obtained for the period from March 1, 2001 through August 29, 2002, was used to create RIVMOD input data files for hydraulic routing and to develop a hydrograph at the upstream boundary of the SMS mesh. Assimilation of this data took place in September of 2002. Given that flows after August 29, 2002 are very low and below the point of bank contact, no effort was deemed necessary to update the 15-minute data set following the download of additional well data in October 2002. Water table response to streamflow oscillations after August 29, 2002 will not be considered in the data analysis portion of this project. The complete set of overlapping well data for Well 1 and Well 3 is shown in Figures 6-5. Note that the water table elevations appear relative to the NAVD 88 vertical datum (not thalweg elevation). The thalweg and bed high point elevations along the well transect are again shown for reference. The graphs do evidence a travel time, related to hydraulic conductivity of bank sediments and signal dampening with increasing distance from the channel.

Observed Hydraulic Gradient within Bank Sediments

Before any data was collected, it was assumed that the river stage would influence the water table levels within the channel bank, as observed at the groundwater wells. This direct response relationship requires the hydraulic gradient to be in the direction away from the channel. The hydraulic gradient between Well 1 and Well 3 is computed as the difference in the respective water table elevations for each hourly sample interval, such that a positive value indicates a gradient away from the channel. As shown in Figure 6-6, the hydraulic gradient is indeed away from the channel, with the singular exception of October 23, 2001 through November 19, 2001, during which the value is barely negative. During this time period, the measured flow at FCH is less than 2.0 cfs. This low flow

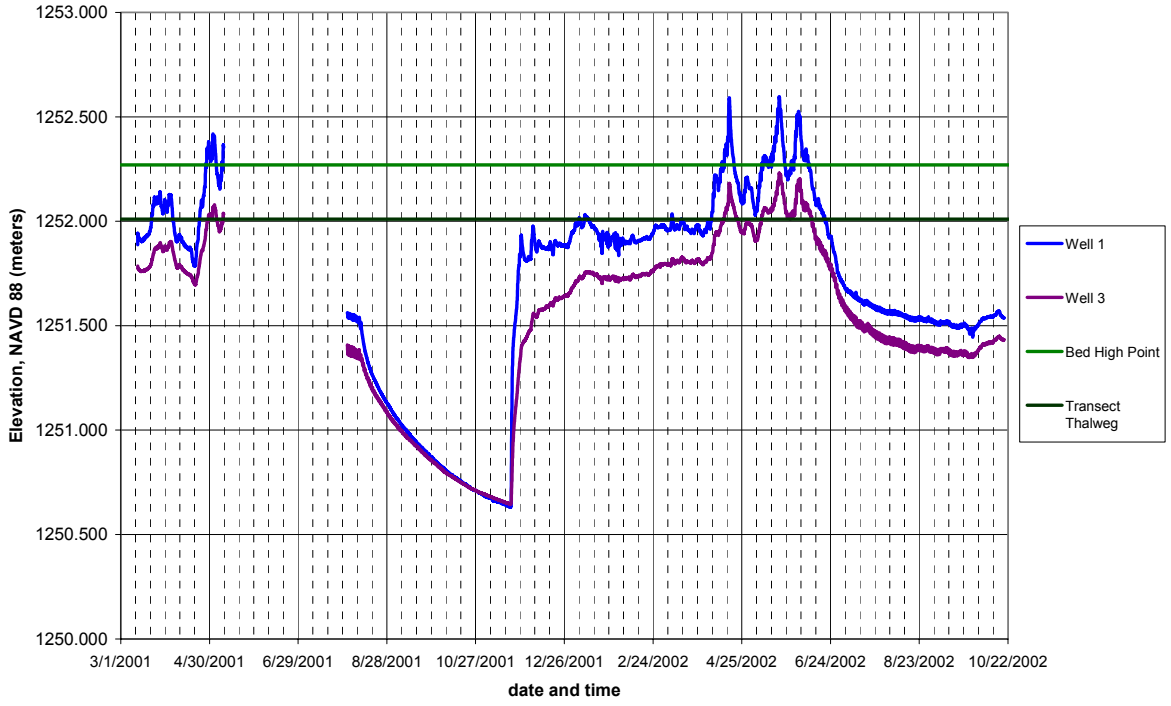

Figure 6-5. Transient water levels in Well 1 and Well 3, 2001-2002

cannot be routed using RIVMOD, but it is likely that the river is no longer flowing at the Scout Camp. Any water in the channel is likely the result of baseflow from the connected surficial aquifer, which may explain the brief gradient towards the river. For all periods for which the channel banks are contacted (periods of interest), the hydraulic gradient is away from the river. This verifies the original assumption that saturation conditions within the channel banks are determined in response to changes in river stage.

Pump Test Analysis

Additional field data for the analysis of water table response to streamflow oscillations was obtained from a pump test conducted at the Scout Camp site in October 2001. A submersible pump was lowered to near the bottom of Well 1. Pressure transducers with data loggers were used in Well 1 and Well 3 to record the water table

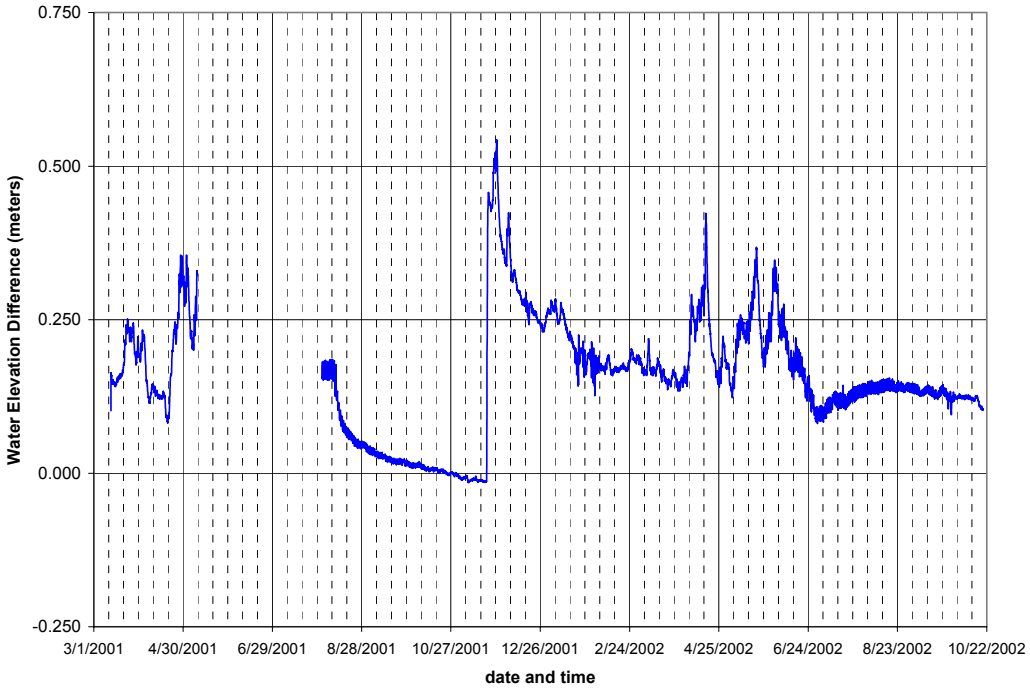

Figure 6-6. Hydraulic differential from Well 1 to Well 3, 2001-2002

response within the wells during the pump test. The data logger in Well 1 was attached to a laptop so that water levels could be monitored throughout pump test duration. Flow rate was adjusted to ensure the drawdown level would not fall below the pump intake, while also allowing the drawdown to approach steady state within a reasonable time duration. Prior to recording pump test data, the pumping flow rate was allowed to stabilize, given that a constant flow rate is necessary for data analysis.

The drawdown versus time relationship observed for Well 1 during the pump test is shown in Figure 6-7. The pump test was conducted for a duration of 112 minutes at a flow rate of 1 gallon per 32 seconds (0.00418 cfs), sufficient time for the water table to approach steady state. Generally, three approaches can be followed in analyzing the response of water levels in an unconfined aquifer during a pump test (Fetter, 2001). The

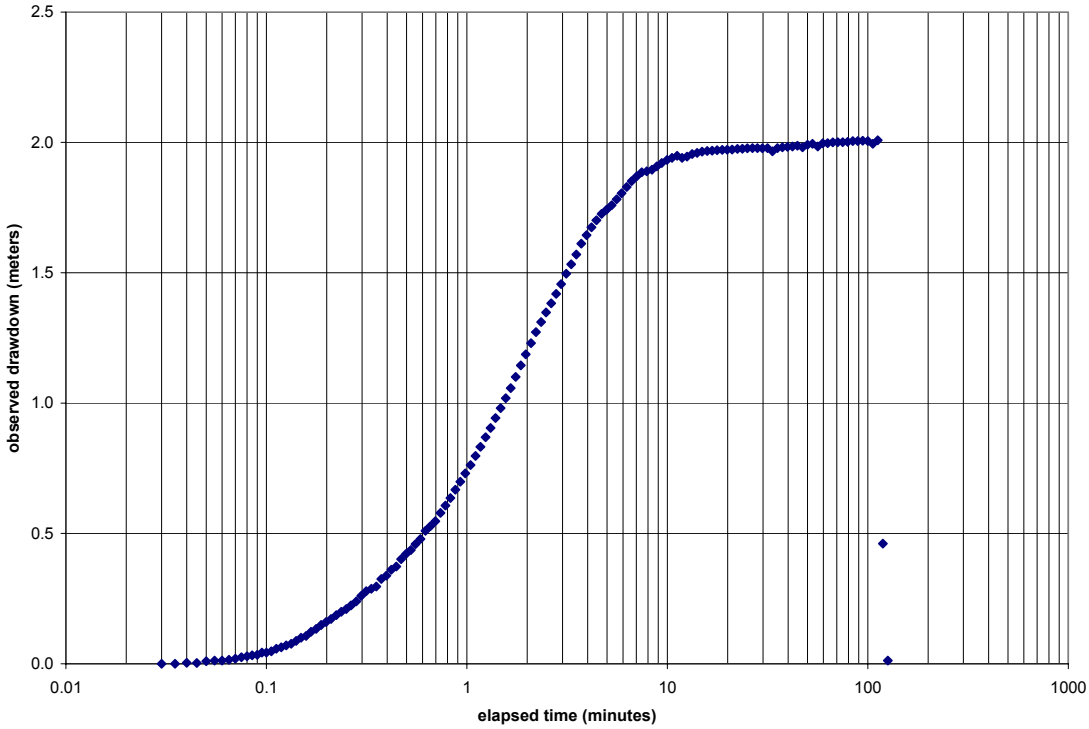

Figure 6-7. Pump test drawdown data collected for Well 1 in October 2002

first approach uses a 2D- or 3D-variably saturated flow model, but the detailed soil characteristic data needed for this type of analysis is not available for this study. The second approach requires the assumption of small drawdown for an observation well some specified distance away from the pumped well. To validate this assumption, two pieces of data are necessary: observed drawdown versus time data for an observation well and knowledge of the saturated thickness of the unconfined aquifer. For the Scout Camp field site along the Carson River, no drawdown was observed at Well 3 (likely the result of the small pumping rate), at a distance of 95 feet from Well 1; and the well penetration is only 25 feet, with the total saturated thickness unknown. The third option, as will be used in this analysis, bases calculations on a match point between the time-drawdown data and theoretical curves.

The flow of water in an unconfined aquifer toward a pumping well is described by equation 6-1 (Neuman and Witherspoon, 1969):

$$K_r \frac{\partial^2 h}{\partial r^2} + \frac{K_r}{r}\frac{\partial h}{\partial r} + K_v \frac{\partial^2 h}{\partial z^2} = S_s \frac{\partial h}{\partial t} \qquad \text{(Eq. 6-1)}$$

where h is the saturated thickness of the aquifer [L], r is the radial distance from the pumping well [L], z is the elevation above the base of the aquifer [L], S_s is the specific storage [1/L], K_r is the radial hydraulic conductivity [L/T], K_v is the vertical hydraulic conductivity [L/T], and t is time [T]. Neuman (1975) has published a solution to the above equation. The solution included two parts, one for the time just after pumping has begun (water is coming from specific storage) and one for much later (when the water is coming from gravity drainage of aquifer pores) (Fetter, 2001). Neuman's solution is written as equation 6-2:

$$h_0 - h = \frac{Q}{4\pi T} W(u_A, u_B, \Gamma) \qquad \text{(Eq. 6-2)}$$

where $(W(u_A,u_B,\Gamma))$ is the well function for the water table aquifer, based on the dimensionless parameters defined by equations 6-3, 6-4, and 6-5:

$$u_A = \frac{r^2 S}{4Tt} \qquad \text{(early time drawdown data)} \qquad \text{(Eq. 6-3)}$$

$$u_B = \frac{r^2 S_y}{4Tt} \qquad \text{(late time drawdown data)} \qquad \text{(Eq. 6-4)}$$

$$\Gamma = \frac{r^2 K_v}{b^2 K_h} \qquad \text{(Eq. 6-5)}$$

where $(h_0 - h)$ is the drawdown [L], Q is the pumping rate $[L^3/T]$, T is the aquifer transmissivity $[L^2/T]$, S is the storativity [dimensionless], S_y is the specific yield

[dimensionless], b is the initial saturated thickness of the aquifer [L], and other parameters are as previously defined.

After plotting pump test drawdown versus time using a log-log scale, the data was overlaid on the theoretical curves presented by Neuman, and a match point was determined. The following parameter values describe the selected match point for the early time drawdown data: $W(u_A,u_B,\Gamma) = 1.80$, $1/u_A = 5.5E10^{-5}$, $\Gamma = 0.017$, $t = 0.10$ minutes, and $(h_0 - h) = 1.0$ meters. Utilizing the presented equations and these parameter values, with the pumping rate, it is possible to solve for aquifer transmissivity:

$$T = \frac{Q}{4\pi(h_0 - h)} W(u_A, \Gamma) = 1.46 \ \frac{m^2}{day} \qquad \text{(Eq. 6-6)}$$

Obtaining an estimate for hydraulic conductivity requires knowledge of the saturated aquifer thickness. With field measurements of the water table immediately before pumping and the elevation of the base of the pumped well, a minimum saturated thickness is calculated as 5.2 meters. A low-end estimate for horizontal hydraulic conductivity is then calculated:

$$K_h = \frac{T}{b_{\min imum}} = 0.28 \frac{m}{day} = 3.25 * 10^{-4} \frac{cm}{s} \qquad \text{(Eq. 6-7)}$$

Principal aquifers in the Carson River Basin are unconsolidated basin-fill deposits of interbedded gravel, sand, silt, and clay (Covay et al., 1996). The above estimate for horizontal hydraulic conductivity is a spatial average over the portion of the aquifer impacted by the pump test. Not surprisingly, the calculated value falls within typical ranges for the following sediment types: silt, sandy, silt, clayey sands, till (10^{-6} to 10^{-4}

cm/s); and silty sands, fine sands (10^{-5} to 10^{-3} cm/s) (sediments characteristic of typical alluvium) (Fetter, 2001; Freeze and Cherry, 1979).

Channel bank sediments are heterogeneous throughout the Carson River system, a point verified by inspection of bank soils along the Scout Camp site. Recall (chapter 1) that the Carson River underwent significant changes in both channel form and process during the period of the Comstock Lode, resulting in the storage of mercury-enriched sediments within a complexly structured alluvial sequence located all along the Carson River valley downstream of Carson City. Today, the Carson River continues to experience cycles of sediment erosion and deposition associated with high flow events, processes which continue to produce sediment heterogeneity.

The pump test estimate of average hydraulic conductivity is not used as a determining factor for water table response to streamflow variability. With detailed sediment cores unavailable for the field site, acceptance of this number as representative is difficult. It is conceivable that the pump test is only extracting water through a high hydraulic conductivity layer, such as a deposited layer of coarse sand or a sediment-filled meander of a historic channel within the hyporheic zone, rather than from sediments truly representative of the surficial aquifer. The calculated hydraulic conductivity from the pump test may not be representative of the surficial aquifer, a point further reinforced by the rapid water table recovery to zero drawdown within 15 minutes of the cessation of pumping, as shown by the late time data points in Figure 6-7. The pump test analysis was used only in a qualitative sense to gain insight to the system. A more useful analysis is provided from a direct comparison of routed streamflow and well data for the Scout Camp reach of the Carson River.

Quantifying the Relationship between River Stage and Water Table Elevation

It has been suggested that streamflow oscillations, with the associated changes in river stage, will result in an observed response in the water table within the channel bank. The water table level is not, admittedly, a perfect indicator of saturation conditions within the channel banks. The hydraulic conductivity of bank sediments will determine the rate at which the bank becomes saturated when river stage is rising and the rate at which the bank dries as river stage falls. Knowing that the SMS model would be unable to dynamically simulate river stage rising and falling, and given that the mesh remained incomplete, alternative means to analyze the degree of connectivity between channel and bank water levels began to be considered. Although the relationship between streamflow and river stage at the well cross-section could not yet be predicted using the SMS model, there was obviously a direct relationship between streamflow and river stage.

Comparison of Streamflow Hydrograph and Water Table Response

The routed streamflow hydrograph from RIVMOD is the only data available for streamflow in the vicinity of the groundwater wells within the surveyed Scout Camp reach. The streamflow values are not perfect substitutes for field measurements of streamflow because of the use of a 1D model, simple input channel geometry, no bank storage considerations, and spatial averaging over 250-meter segment lengths; but this data should be a reasonable representation of the routed hydrographs. Visual inspection of a portion of the routed RIVMOD hydrograph shows evidence of travel time and modest magnitude attenuation from the Fort Churchill gage to the Scout Camp reach. Hydrograph routing from Fort Churchill to the Scout Camp for the streamflows of 2001 and 2002 are shown in Figures 6-8 and 6-9, respectively. To show enhanced detail, hydrograph routing for streamflows of April 2002 are shown in Figure 6-10. RIVMOD

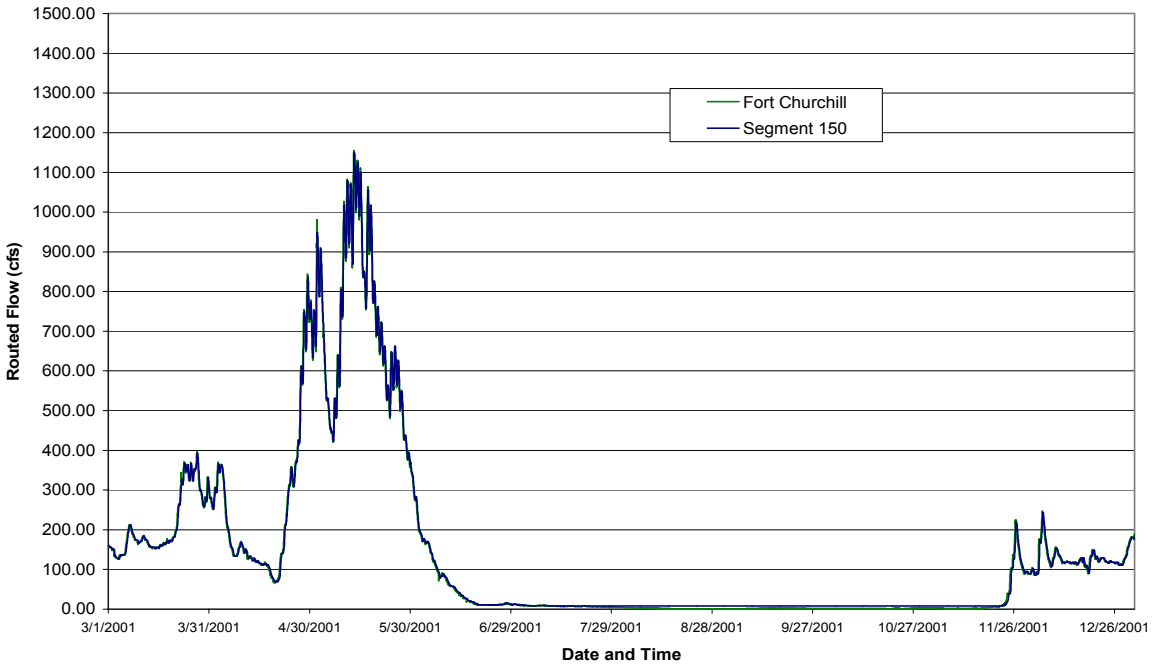

Figure 6-8. 2001 streamflow routing comparison: FCH gage data and RIVMOD simulation for upstream boundary condition

segment 150 is selected, as it is the first segment upstream of the modeled upstream boundary for the SMS mesh. Travel time from Fort Churchill to the Scout Camp, a distance of 10 km, ranged from 2 to 8 hours for the observed 2001-2002 streamflow magnitude range from 0 to 1500 cfs. The upstream boundary is situated in segment 151, the groundwater wells in segment 152, and the downstream boundary in segment 153. The hydrograph for segment 150 was selected for one additional reason. As it turns out, routed flows for segments 151 or 152 would predict well response to occur in advance of the associated streamflow change in a few instances. Given the simplifications inherent to RIVMOD (most notably no inclusion of hydrograph attenuation due to bank storage effects), noting that the RIVMOD segments are only 250 meters in length (indicative of a small travel time from one segment to the next), realizing that well data is collected only at 1-hour time intervals (leaving uncertainty between any consecutive data points), and noting that Well 1 is 5 feet removed from the vertical channel bank, this could certainly

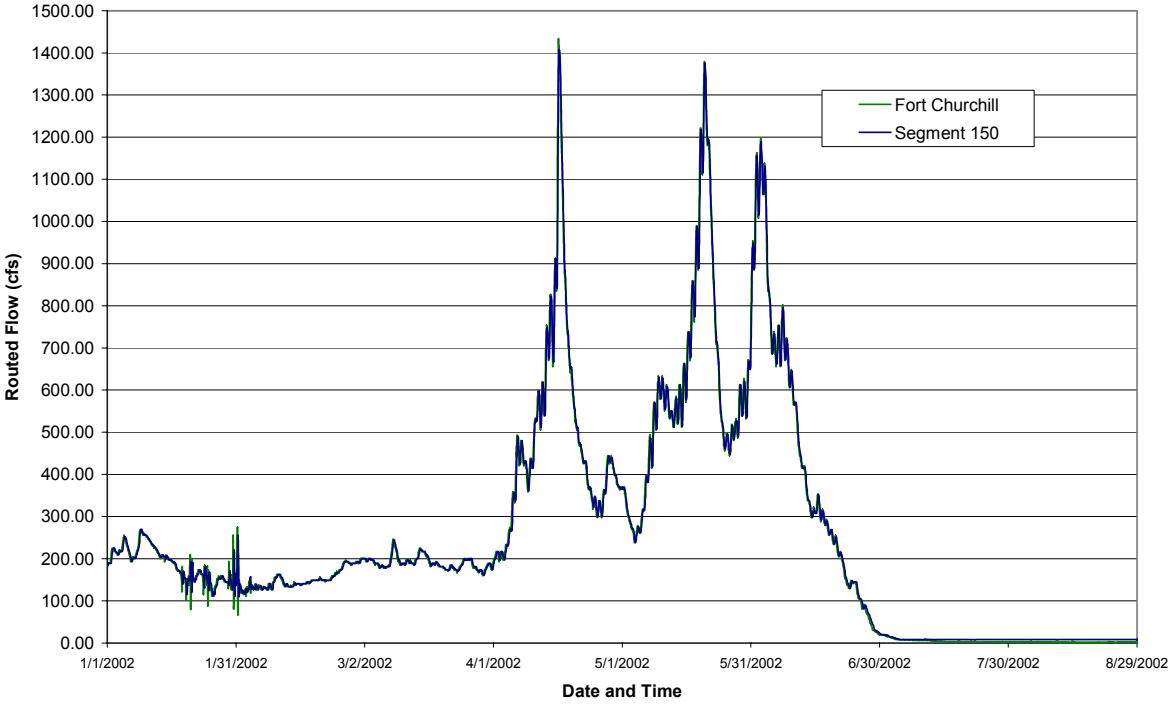

Figure 6-9. 2002 streamflow routing comparison: FCH gage data and RIVMOD simulation for upstream boundary condition

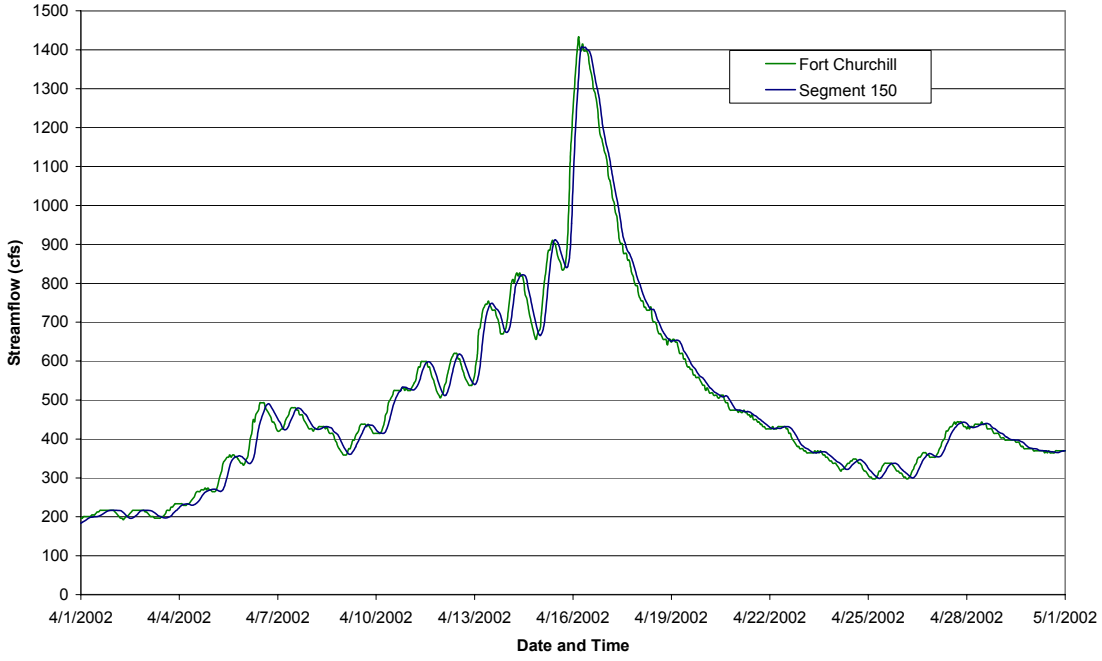

Figure 6-10. April 2002 streamflow routing comparison: FCH gage data and RIVMOD simulation for upstream boundary condition

have been predicted as a likely possibility. It has already been shown that the hydraulic gradient is away from the channel, so that water table levels will change in response to a rising or falling river stage. Stage change must therefore precede water table response.

The near-channel (Well 1) response to streamflow variability during calendar years 2001 and 2002 is shown in Figures 6-11 and 6-12. The routed hydrograph from RIVMOD segment 150 is indicated as the Scout Camp UBC (upstream boundary condition) in these and the following plots. To view the degree of connectivity between streamflow and Well 1 water levels, it is necessary to zoom in on these annual plots. A complete set of figures is found in Appendix B, in temporal order from March 2001 through June 2002. This collection of figures is used to show the following: RIVMOD hydrograph routing from Fort Churchill to the Scout Camp reach for each month of simultaneous record; Well 1 water table response to streamflow variability for each month of simultaneous record; and Well 1 water table response to streamflow variability for selected periods of interest on the order of a few days. These periods of interest are selected based on two characteristics: high degree of streamflow oscillation; and distinct peaks and troughs. Months excluded from the appendix are those in which streamflows are low in magnitude (such that banks are no longer contacted) and connectivity is less evident. Note the dual y-axes showing both Carson River streamflow and water table elevation; scales were adjusted as needed to best indicate the time lag between streamflow change and water table response. A sampling of these plots is shown in Figures 6-13 through 6-23. The selected figures demonstrate the water table response for streamflow variability for two specific flow classifications: flood events (example: April to May 2002, Figures 6-13 through 6-21), where flows are highly dynamic, and

periods of nearly constant flow (example: February 2002, Figures 6-22 and 6-23), where fluctuations are diurnal in nature and likely due to ET.

Indicated by this small sampling and the complete set of figures in Appendix B is the fact that peaks and troughs for routed streamflow and well data occur at essentially the same time. This time will not be exactly the same, but the time of peak or trough will occur during the same hour because RIVMOD and well data are both available hourly at times which do not exactly overlap. Streamflow changes in all instances precede well response. No evidence of a time lag from stage change to water table change (at least within the data frequency limitation of 1 hour), is found within the data. This observation does not state that the water level within the channel and within the bank will be the same (in fact, it cannot be the same given the 5-foot separation from channel to well and evidence of a hydraulic gradient away from the channel).

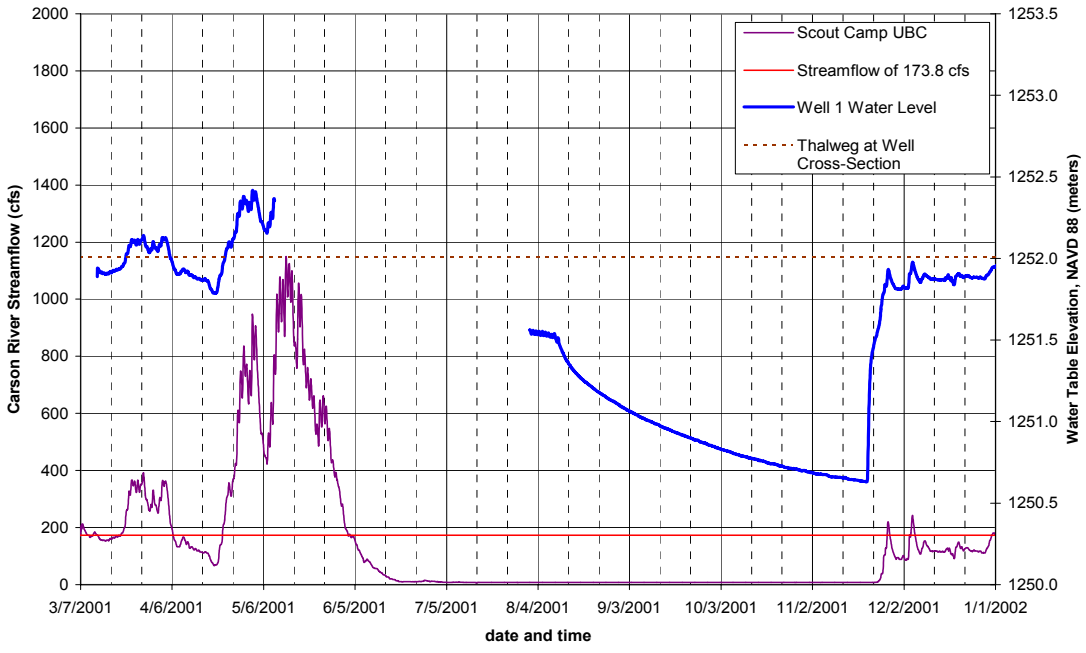

Figure 6-11. 2001: near-channel well response to streamflow variability

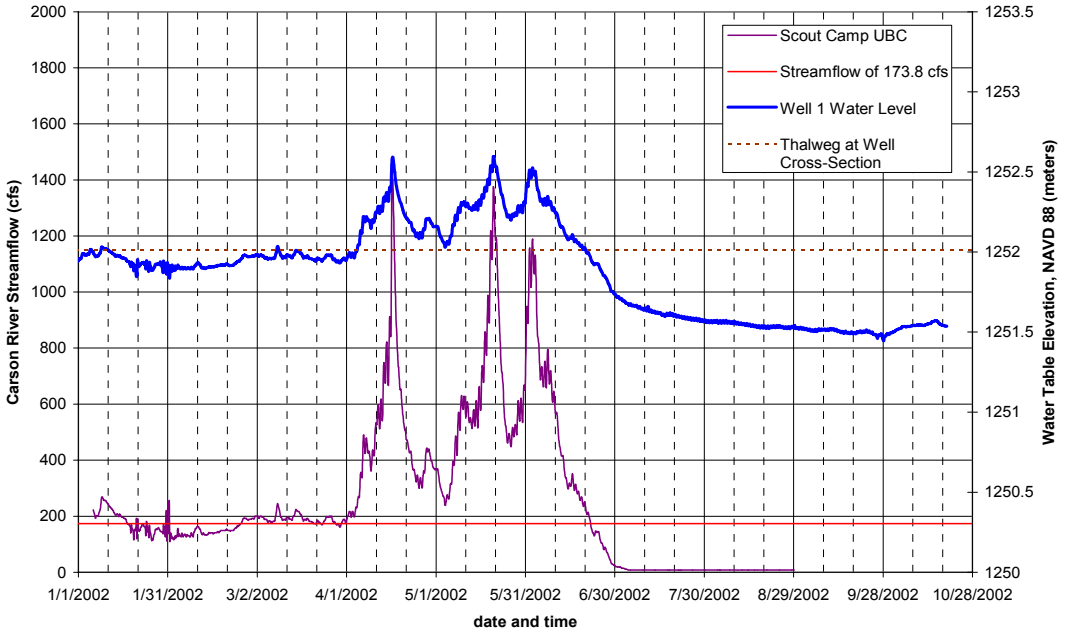

Figure 6-12. 2002: near-channel response to streamflow variability

Previously, there was thought of a time lag between river stage change and water table response, and the thought further stated that this time lag could vary depending on whether flows were rising or falling. For example, if the soil is wetting (river stage rising), clays in the bank sediments could swell and slow infiltration of water into the channel bank. After extended periods of low flow and dry conditions, surface crusting could impede water infiltration into the banks. Rapidly-rising streamflows could entrap air within the banks and effectively reduce the hydraulic conductivity of the bank sediments. Rapidly falling flows could show a lag time prior to water table dropping due to bank storage phenomena. With no visual evidence of a time lag for flow peaks or troughs, well response is clearly tightly coupled to streamflow variability. This high degree of coupling holds true during flood events, periods of nearly constant flow, and

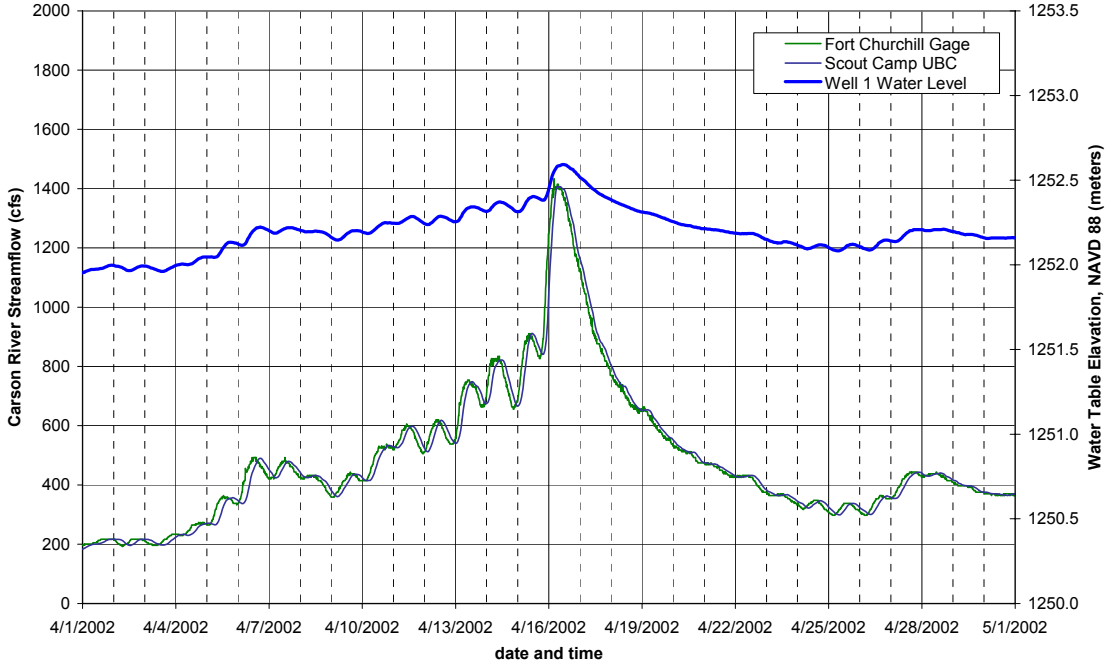

Figure 6-13. April 2002: near-channel response to streamflow variability

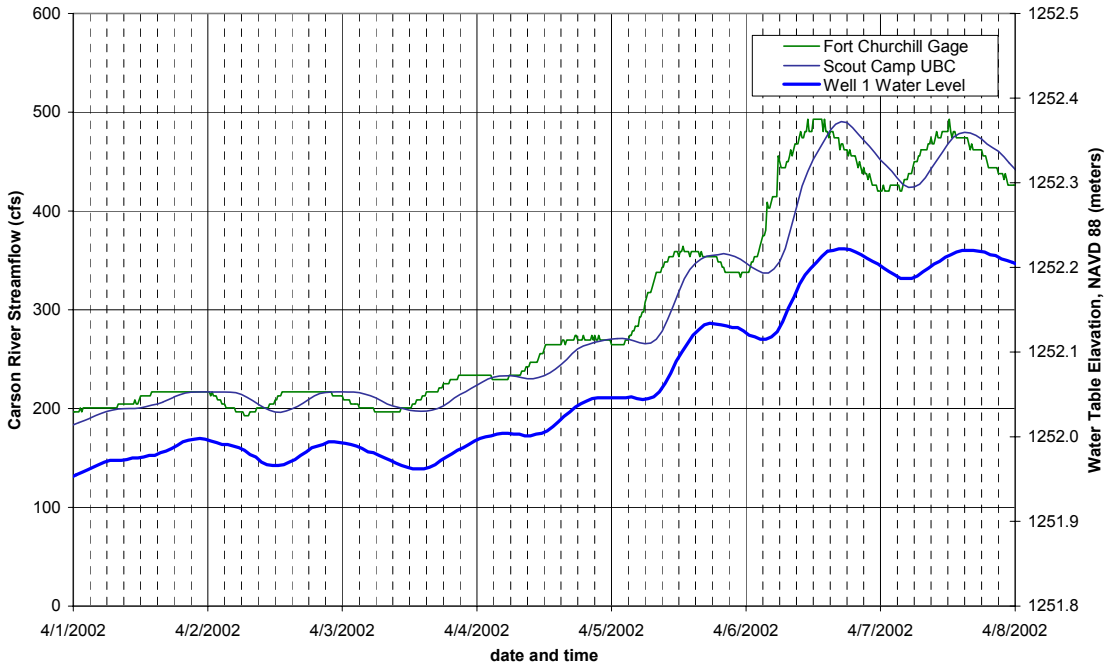

Figure 6-14. April 1-7, 2002: near-channel response to streamflow variability

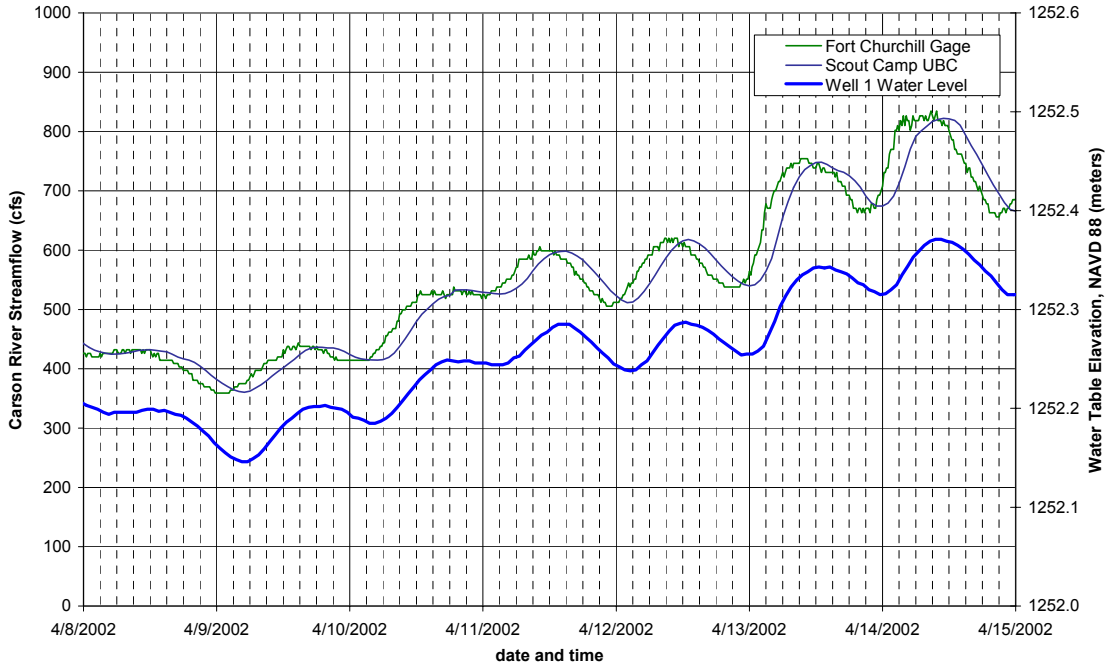

Figure 6-15. April 8-14, 2002: near-channel response to streamflow variability

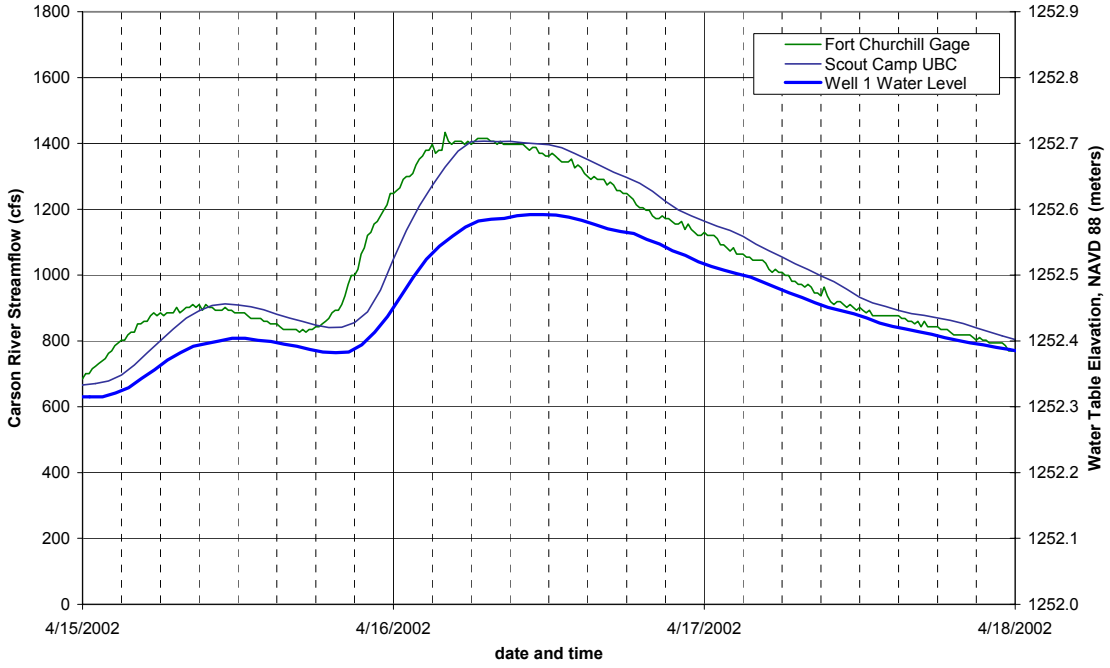

Figure 6-16. April 15-17, 2002: near-channel response to streamflow variability

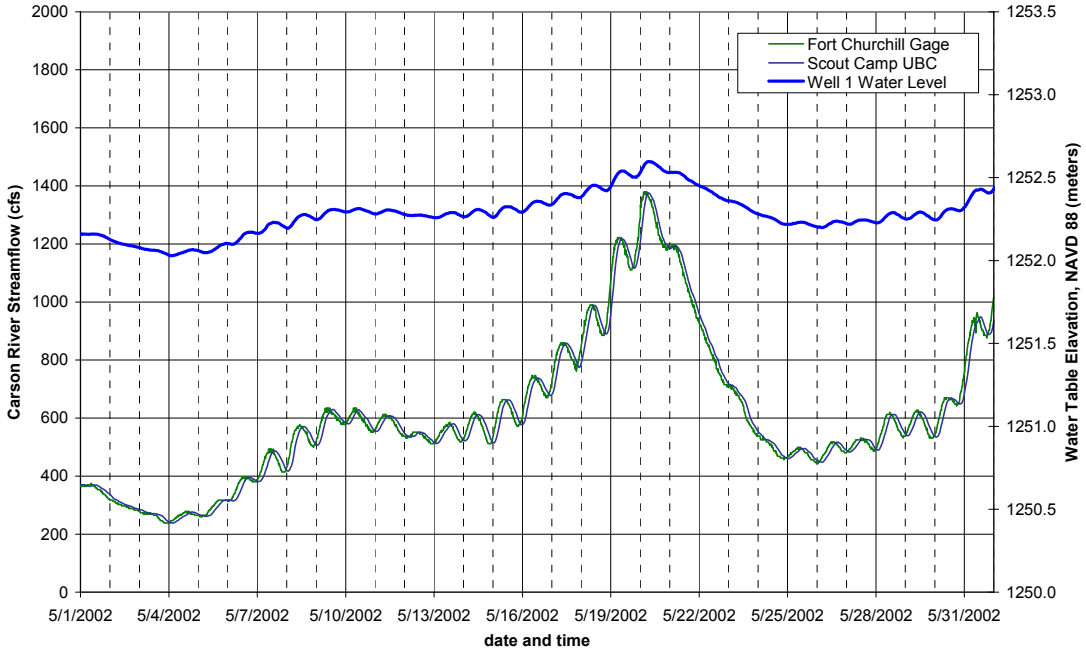

Figure 6-17. May 2002: near-channel response to streamflow variability

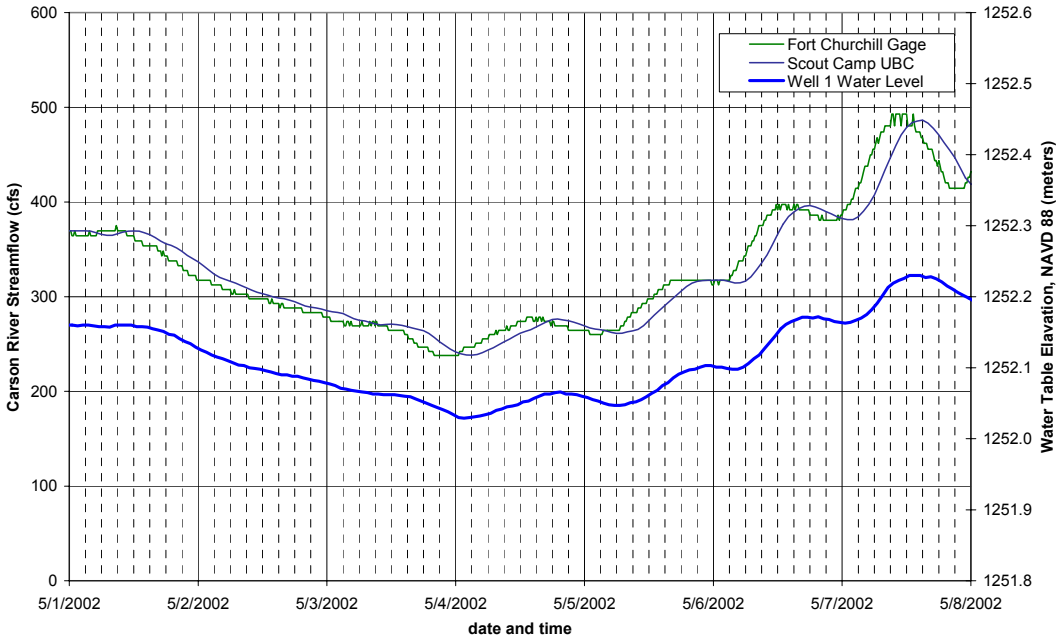

Figure 6-18. May 1-7, 2002: near-channel response to streamflow variability

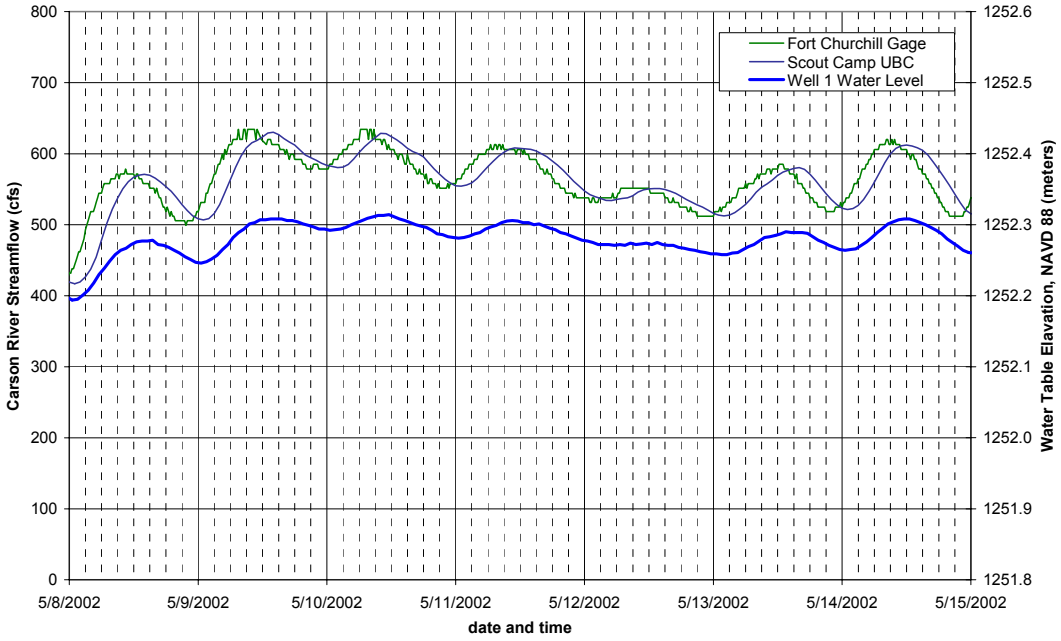

Figure 6-19. May 8-14, 2002: near-channel response to streamflow variability

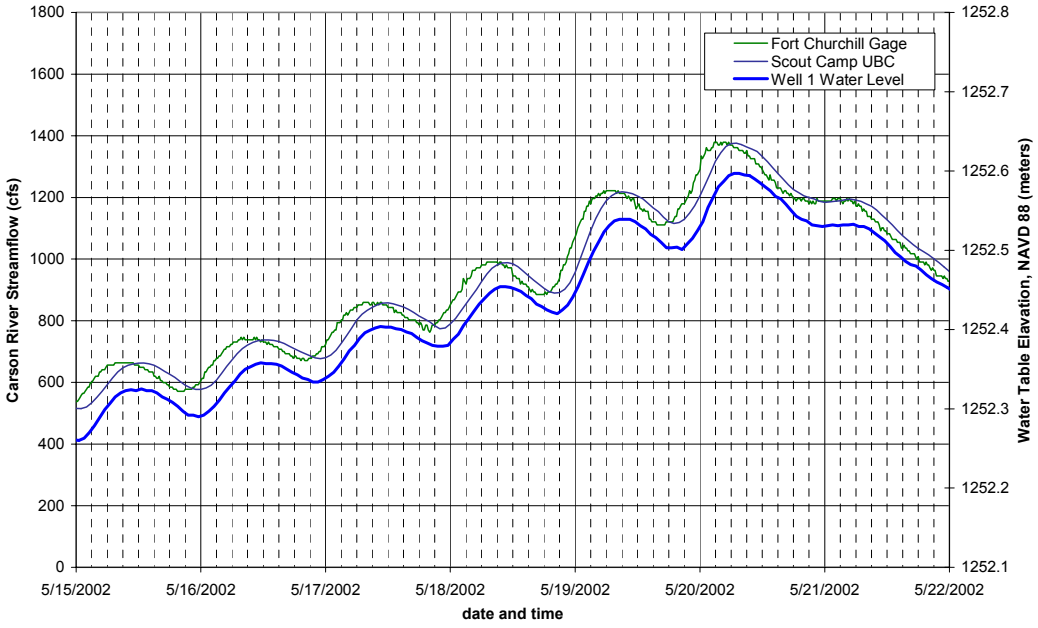

Figure 6-20. May 15-21, 2002: near-channel response to streamflow variability

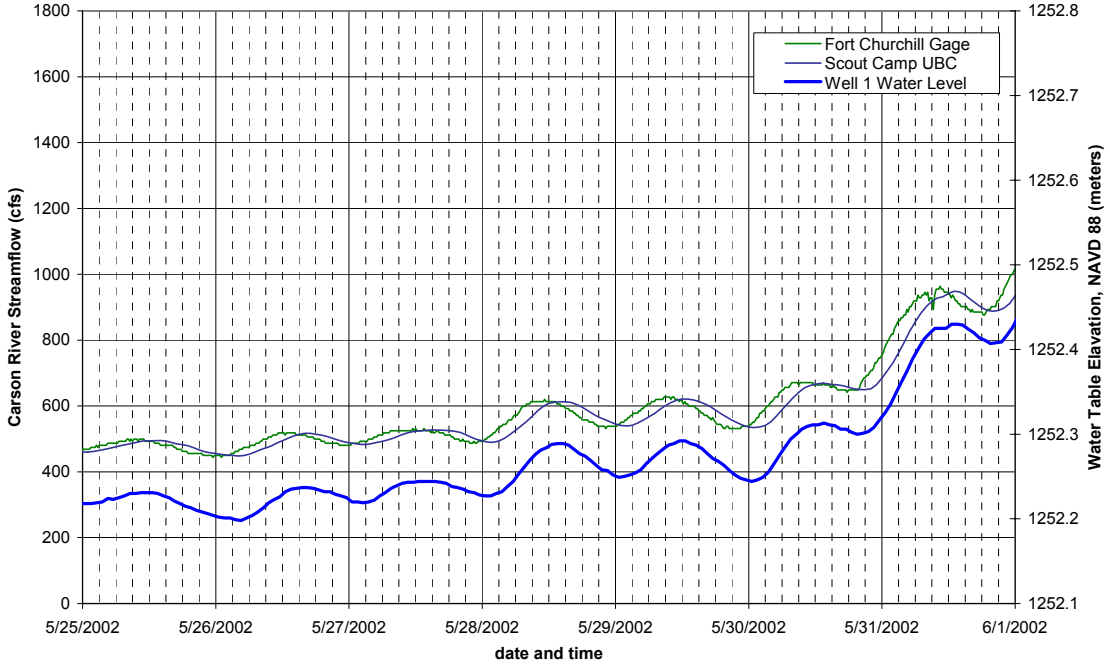

Figure 6-21. May 25-31, 2002: near-channel response to streamflow variabililty

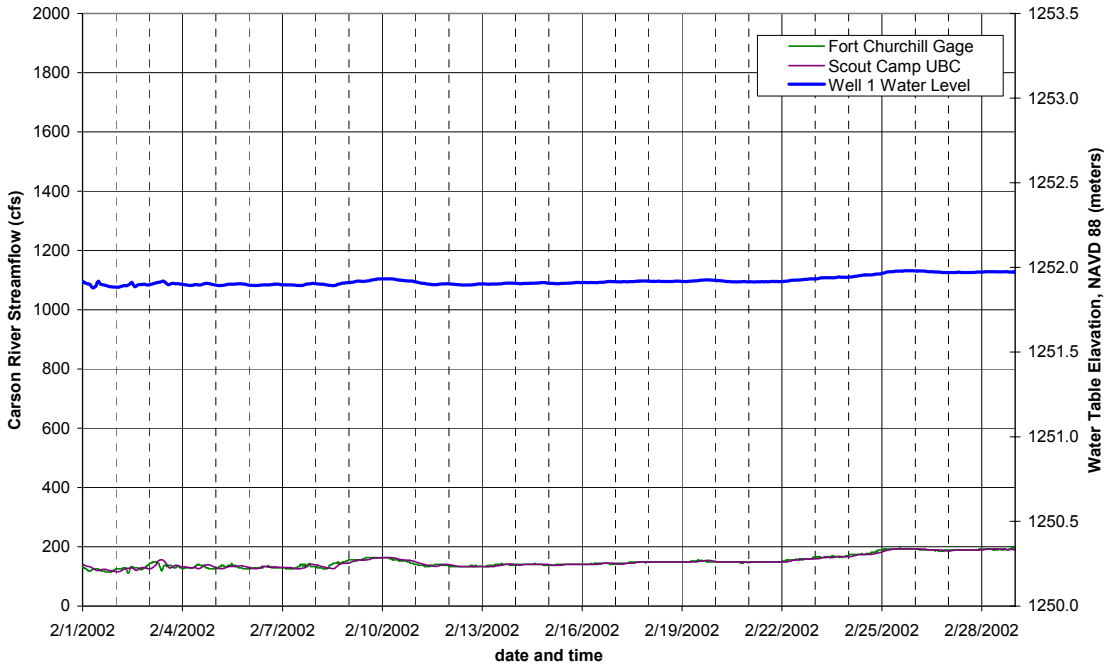

Figure 6-22. February 2002: near-channel response to streamflow variability

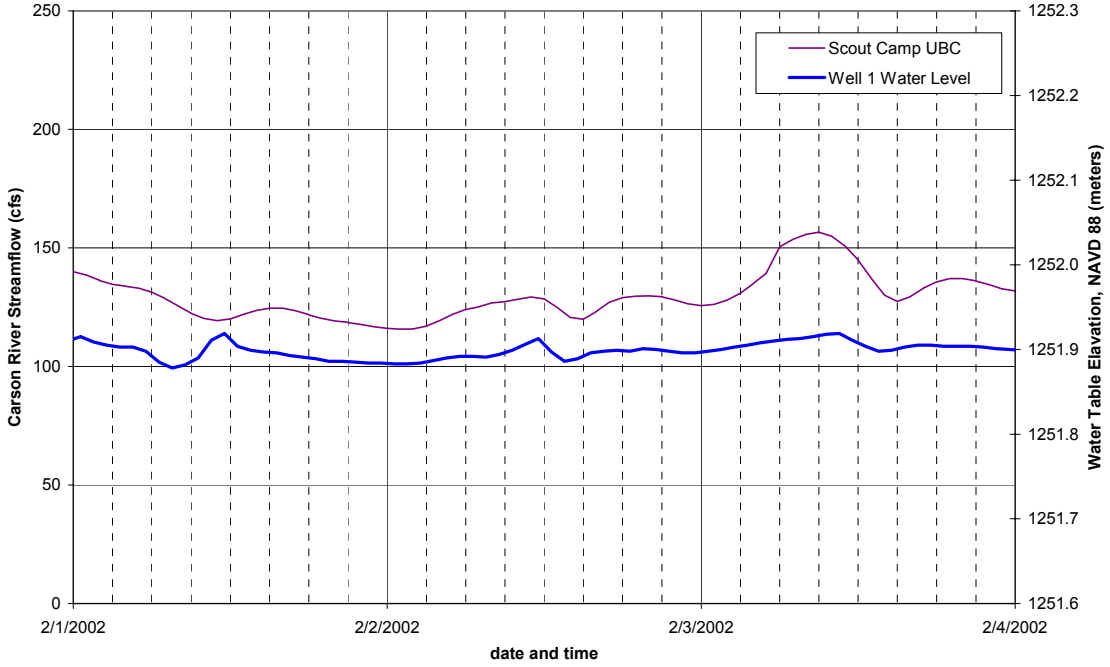

Figure 6-23. February 1-3, 2002: near-channel response to streamflow variability for intermediate streamflows during the period of record (2001-2002) at the Scout Camp site. RIVMOD is not the perfect tool for hydraulic routing because of the implicit simplifications, and the well data is not perfect because of the 1-hour data collection intervals, but, regardless, there is no evidence for a time lag on the order of hours (with 1 hour as the lower bound based on data collection frequency).

If this hydrograph for RIVMOD segment 150 were applied as the upstream boundary condition in the SMS model, a slight time lag would necessarily be added within SMS to translate the upstream boundary hydrograph to the well cross-section. This would further reduce the time lag shown in the above figures and Appendix B. This comparison is not perfect because RIVMOD routing is 1D and incorporates coarse channel geometry. The hydrograph from a model segment 500 meters upstream of the well cross-section is also being used for the comparison with the well data. The time lag

cannot be negative because the hydraulic gradient is away from the channel, and segment 150 is the first segment upstream of the well ensuring this to be true. The choice of segment 150 is assumed to offset the 1D routing used in RIVMOD. RIVMOD is the IFMTFM tool to model Carson River hydrodynamics. Therefore, as RIVMOD sees the Scout Camp reach, the water table response is effectively instantaneous.

Comparison of Surveyed Water Surface Elevations to Water Table Observations

Surface water streamflow oscillations and groundwater water table oscillations are tightly coupled. With the SMS model remaining unfinished (at this point in the research) and hence unable to provide stage predictions, it became necessary to turn to the available water surface survey data to aid in the coupling analysis. Given the particular interest in flows at which the banks are contacted and susceptible to erosion, the survey data from March 2001 is the focal point of this analysis, as channel flows were significantly lower during July of 2001.

Water surface elevations from March 2001 are taken as the starting point for this analysis. Field work was conducted from March 6 to March 9, 2001. The routed streamflows for this time period are shown in Figure 6-24, with flows at Fort Churchill included for reference. While the routed streamflows for RIVMOD segments 150 through 153 are shown, it will be assumed that the flows through the entire model reach can be approximated by those of Segment 152 (the RIVMOD segment containing the groundwater wells). Note the unperceivable time lag through these segments, due to the segment length of only 250 meters; segment 150 could also have been used.

During the GPS site survey, water surface elevations were collected along the water edge (in addition to the collected channel bathymetry). The surveyed water surface elevations are shown in Figure 6-25. The primarily east-west configuration of the channel

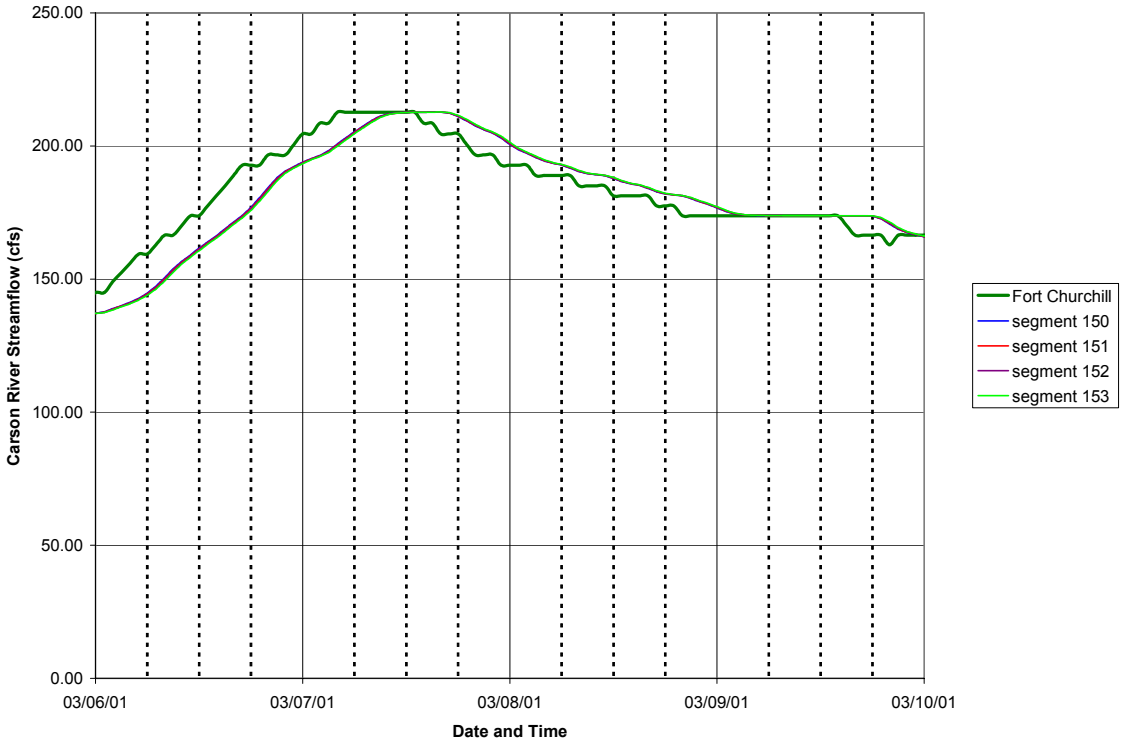

Figure 6-24. Hydrodynamic routing through RIVMOD segments within reach of interest

for the Scout Camp reach (Figure 5-1) allows the points to be plotted based on easting coordinate. For spatial reference, easting coordinates for the SMS upstream and downstream boundaries, Well 1, and extent of RIVMOD segment 152 are additionally indicated. Surveyed water surface elevations (WSEs) were classified based on the times during which they were collected, as shown in Table 6-1. Based on this classification scheme, first-cut approximations for water surface slope were computed with a simple linear regression. Regression equations in the standard form of $y = mx + b$, where m is the slope, with the associated R^2 value, are indicated in Figure 6-25. Although these water surface slopes are not plotted based on distance along the flow path, it is evident that the water surface slope will not be constant over all flow regimes or constant over the entire model domain for a given flow regime. Rather, water surface elevations are a function of both flow magnitude and spatial location. The most reliable surveyed

elevation is the indicated staff gauge. All other survey points were collected along the irregular water edge, thereby introducing human error associated with choosing the exact location of the water edge (as governed by features along the channel bed).

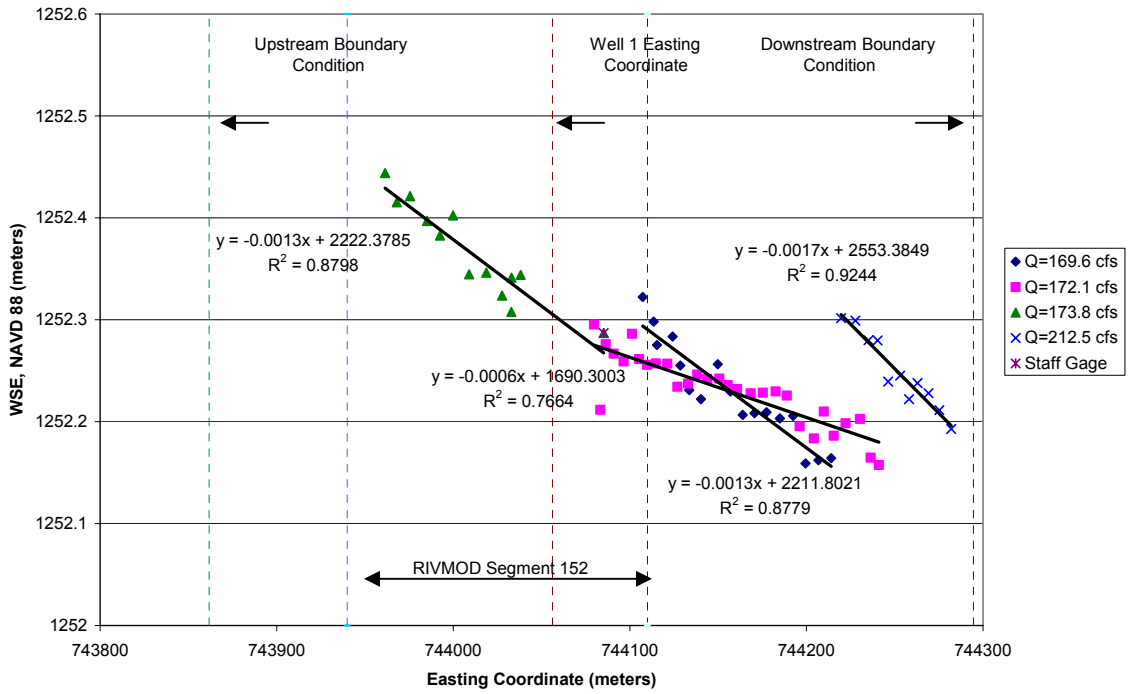

Figure 6-25. Water surface elevation (WSE) as a function of flow for March 2001 data

Table 6-1. Classification of surveyed water surface elevations according to time of collection

Survey start time, t_1	UBC flow at t_1 (cfs)	Survey end time, t_2	UBC flow at t_2 (cfs)	Average flow during survey (cfs)
3/6/01 15:00	168.3	3/6/01 16:00	170.8	169.6
3/6/01 16:00	170.8	3/6/01 17:00	173.3	172.1
3/7/01 11:00	212.4	3/7/01 12:00	212.6	212.5
3/9/01 10:00	173.8	3/9/01 13:00	173.8	173.8

In Figure 5-1, the flow path between cross-sections 300 and 400 is reasonably straight, contains the wells, and includes the set of water surface elevation points for the average flow of 173.8 cfs (Figure 6-25). Looking to relate channel stage to water table elevations and being unable to justify backward extrapolation of the surveyed water

surface elevations from further downstream (where channel morphology is markedly different), the 173.8 cfs water surface survey set from March 9, 2001 is singled out for further analysis. This set of data points approximates the energy grade line for the water surface in the vicinity of the wells. With the energy grade line corresponding to energy lost along the flow path, the channel thalweg between cross-sections 300 and 400 was used to estimate the flow direction. The locations of surveyed water surface elevations at a streamflow of 173.8 cfs are shown in Figure 6-26, in relation to mean flow direction and well siting (axes indicate easting and northing coordinates). By projecting water surface observations along the direction of flow, an improved approximation of the energy grade line is obtained, as the flow path is clearly not east-west only along this portion of the channel. By plotting this set of water surface elevations with respect to distance along the thalweg, shown in Figure 6-27, it is possible to interpolate the water surface elevation at the Well 1 cross-section (perpendicular to flow as indicated in the figure) with use of regression analysis. The water surface nearest Well 1 is approximately 1252.30 meters (NAVD 88) for a flow of 173.8 cfs.

Ideally, water table data from March 9, 2001 would be available to compare with this water surface elevation, in order to assess the hydraulic gradient from channel to Well 1. While the groundwater wells were installed on March 9, 2001, the pressure transducers and data loggers were not placed in the wells until March 12, 2001, days after the completion of the March survey work on site. In July 2001, the streamflows were between 8 and 9 cfs (lower than the levels of interest at which the banks are contacted). Stage data collected during July 2001 also cannot be compared with simultaneous water

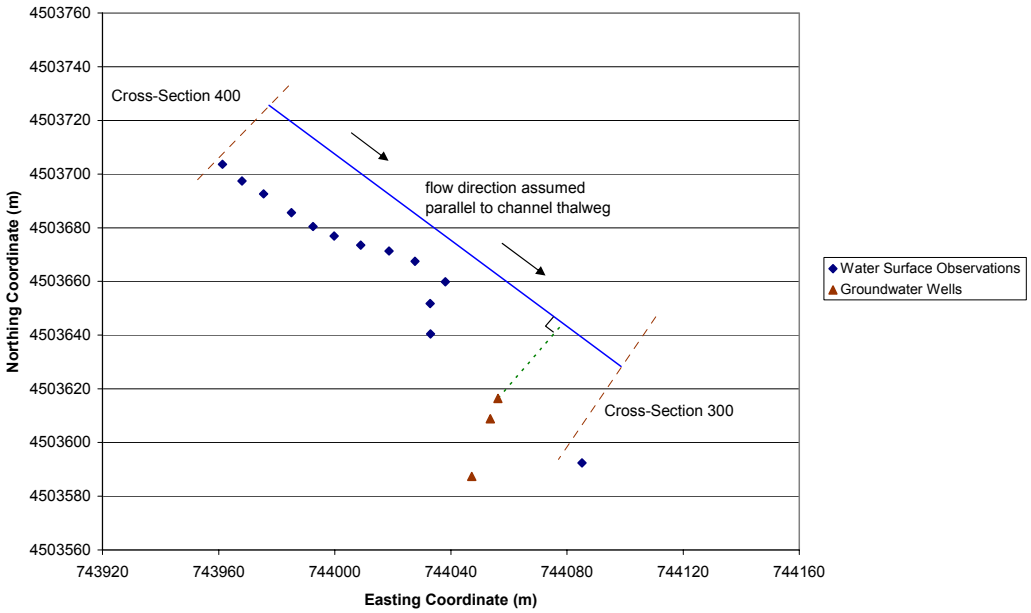

Figure 6-26. March 9, 2002: location of surveyed water surface observations in RIVMOD segment 152

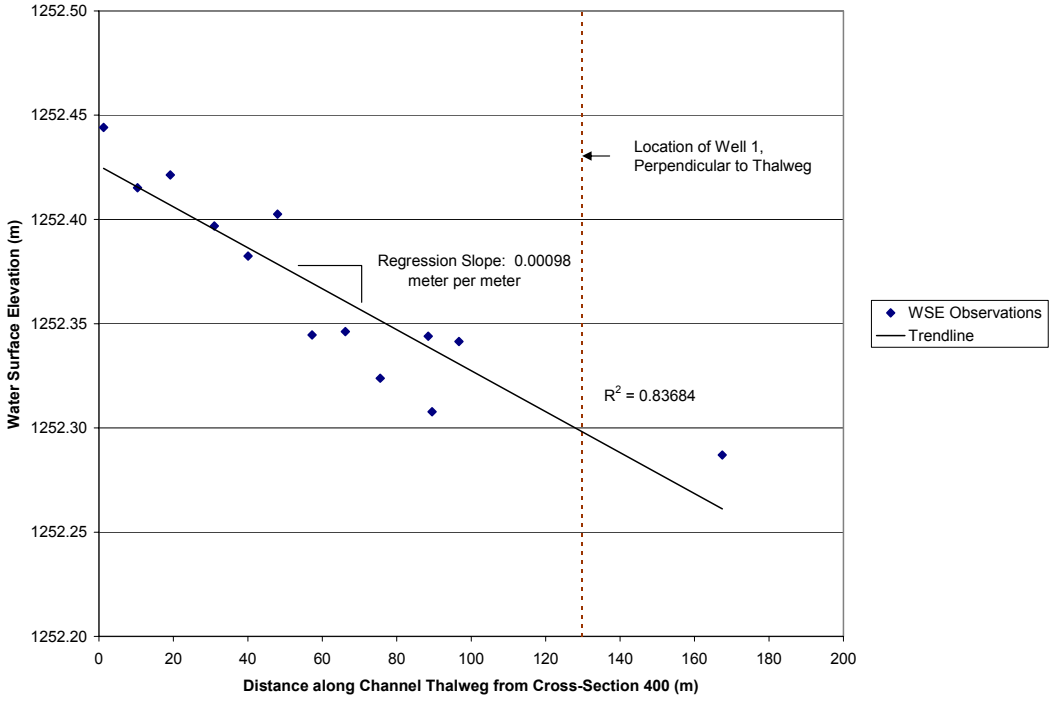

Figure 6-27. March 9, 2001: graphical approximation of channel water surface slope in RIVMOD segment 152

table observations, even though the probes were in the wells, because the probe in Well 1 was slipping toward the bottom of the well. The original belief, prior to data collection, was that the water table elevation would basically parallel the river stage, with only a small water surface elevation change from open channel to Well 1 (5 feet removed from the bank). What is indeed interesting and unnoticed in advance of this analysis, is that this is clearly not the case. Well 1 and channel water levels show a tight coupling over time (based on analysis of routed streamflows), but it is here suggested that the same type of hydraulic gradient evident between Well 1 and Well 3 (at a separation distance of 95 feet) also exists between the open channel and Well 1 over this 5-foot distance. Consider Figures 6-11 and 6-12. In these figures, the thalweg (NAVD 88 elevation = 1252.01 m) represents the lowest possible value for river stage, the stage which would occur at the well cross-section if the flow in the channel were essentially zero. These figures indicate that the water table observed in Well 1 is only situated above the thalweg elevation for flows in excess of approximately 200 cfs. At the well transect, the thalweg is also a close approximation for the observed elevation at the base of the vertical channel bank nearest the wells. For a streamflow of 200 cfs, river stage must be above the thalweg elevation. The SMS model is not needed to verify this point, and the need to use waders to cross the river during March 2001 provides additional assurance.

The water surface elevation from open channel to Well 1 is not a straight line, but, rather, there is a distinct hydraulic gradient. Quantifying this gradient was to be the use of SMS model output, but the model was not completed at the time of this analysis. Simultaneous water table and stage observations are also not available. As the SMS model would simulate, assume that river stage is a function of flow at any selected

location, specifically segment 152 near the wells. Based on the trendline from the March water surface elevations, in Figure 6-27, assume that the interpolated water surface elevation of 1252.30 meters (NAVD 88) is representative of a 173.8 cfs streamflow. With these assumptions in mind, this same streamflow magnitude occurs at other times within the data collection period for this project (March 2001 through August 2002). Antecedent streamflows, specifically rising versus falling stage, of course, vary. Streamflows are taken from the RIVMOD-generated hydrograph for segment 152. The streamflow magnitude of 173.8 cfs remained basically constant in the hydrograph during the survey hours on March 9, 2001 (Figure 6-24), the collection time for the water surface elevation data set under current consideration. The routed RIVMOD hydrograph output is available at hourly intervals. Simple linear interpolation is applied to the routed hydrograph to provide the exact times at which flows of 173.8 cfs occur at the well cross-section. These times can be seen in Figures 6-11 and 6-12 at the intersections of the horizontal line for Q =173.8 cfs and the hydrograph. Water table data is also collected at hourly intervals, but the exact times vary for each period of data collection (for example, 11 or 33 minutes after the hour). Linear interpolation was performed on the well data to obtain water table observations for times corresponding to the exact time of modeled 173.8 cfs streamflow.

For times at which modeled streamflows at the wells are equal to 173.8 cfs and for which the assumed river stage is therefore 1252.30 meters, the observed water table elevations are found to vary over an 11-centimeter range from 1252.85 to 1252.96 meters (NAVD 88). This data set was further classified based on whether streamflow is rising or falling, with the idea that a variable time lag might exist between stage change and water table response for rising versus falling river stage. This relates back to the possibility of

hydraulic conductivity being impacted by considerations such as soil swelling from clay content, surface crusting after prolonged dry conditions, or entrapped air during periods of stage rising. Figure 6-28 shows points with no time lag—water table elevations at the exact time of the 173.8 cfs streamflows; note that the x-axis indicates the times at which this streamflow occurs, and the y-axis indicates the water table elevation. In this plot, scatter is evident, but the average water table elevation in Well 1 is 1251.93 meters for both rising and falling portions of the hydrograph (dotted horizontal lines), providing some evidence of a typical stage-discharge relationship. The estimated river stage under this flow condition is 1252.30 meters, indicating an average head gradient from open channel to well of 37 centimeters, over a distance of only 5 feet. Within the data set, the minimum gradient is nearly 34 centimeters.

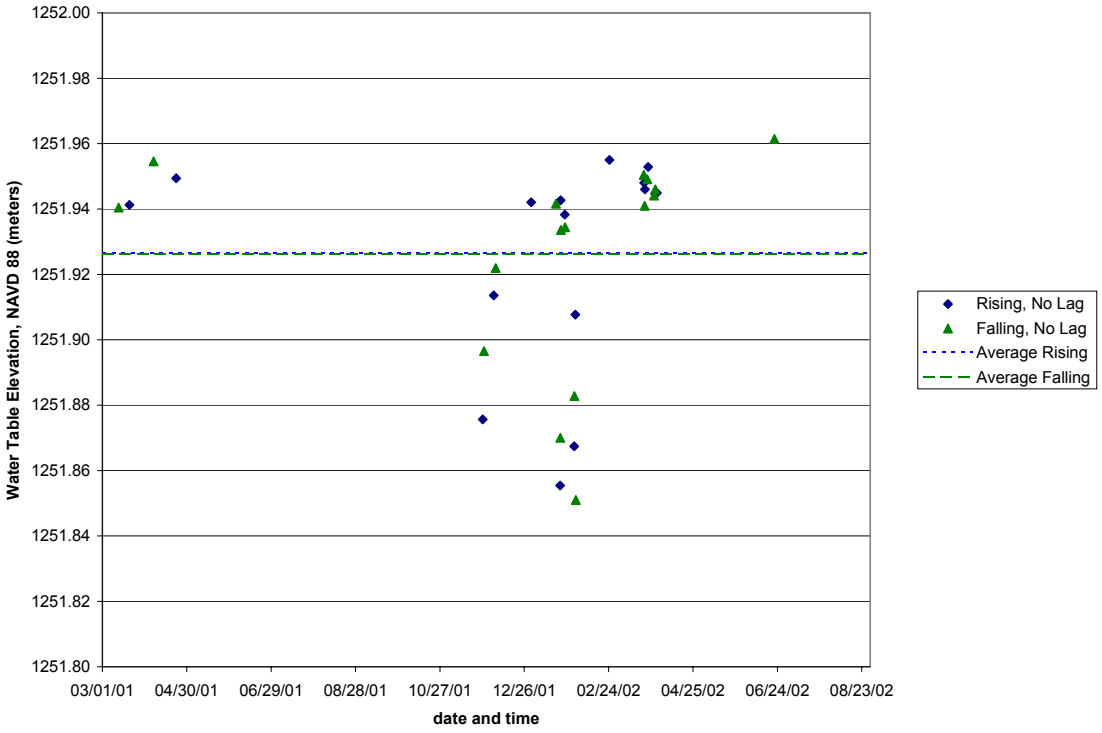

Figure 6-28. Zero time lag: temporal correlation between river stage and water table response in Well 1

Some of the points in Figure 6-28 are considered flow "spikes," whereby modeled flows are not really part of a distinct rising or falling trend, but only a brief oscillation. This explains why many of the points appear close in time. Removing these points, as shown in Figure 6-29, a slight increase in separation of the average water table between rising and falling flows is observed, but the separation remains significantly less than one centimeter (note y-axis scale). Time lags were also considered. For example, streamflow magnitude is 173.8 cfs at time x, but one is interested in the water table response 1 or 2 hours after this change. One expects the average difference between the mean water table observations for rising versus falling flows to increase as the time lag is increased. This is indicative of a nearly instantaneous water response to streamflow oscillation, or at least a response time of less than the one-hour data collection interval. In fact, this expectation is borne out by the data. Figures 6-30 and 6-31 are for 1 and 2 hour time lags, respectively. In the figures, flow "spikes" are included, but calculations show that average rising versus falling separation distance increases with increasing time lag if "spike" points are removed as well. Note the elevation scale is the same in Figures 6-28, 6-29, 6-30, and 6-31.

Surface Water Modeling and Rating Curve Development

Initially, surface water modeling with SMS was to predict river stage based on a realistic input hydrograph. River stage would be dynamically modeled. A regression analysis would then be performed to determine the relationship between river stage and water table level. By incorporating various time lags in the water table data and comparing the regression fit, two possibilities could be assessed: 1. the indication of a positive time lag for rising flows, falling flows, or both; and 2. if present, the potential of different time lags for rising and falling flow conditions.

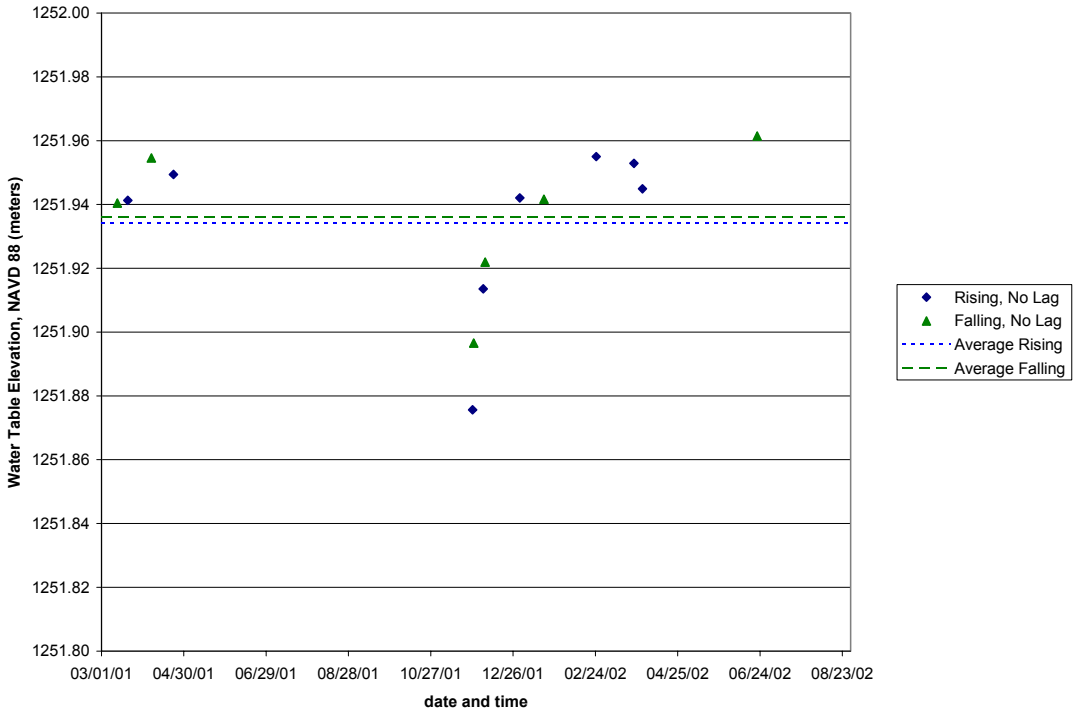

Figure 6-29. Zero time lag, flow spikes removed: temporal correlation between river stage and water table response in Well 1

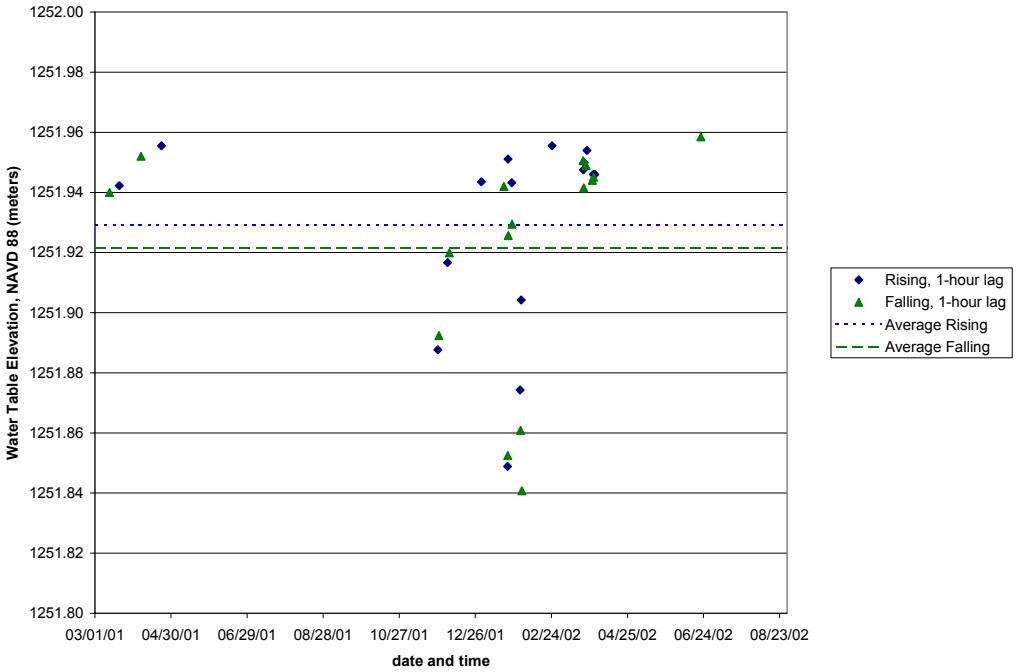

Figure 6-30. One hour time lag: temporal correlation between river stage and water table response in Well 1

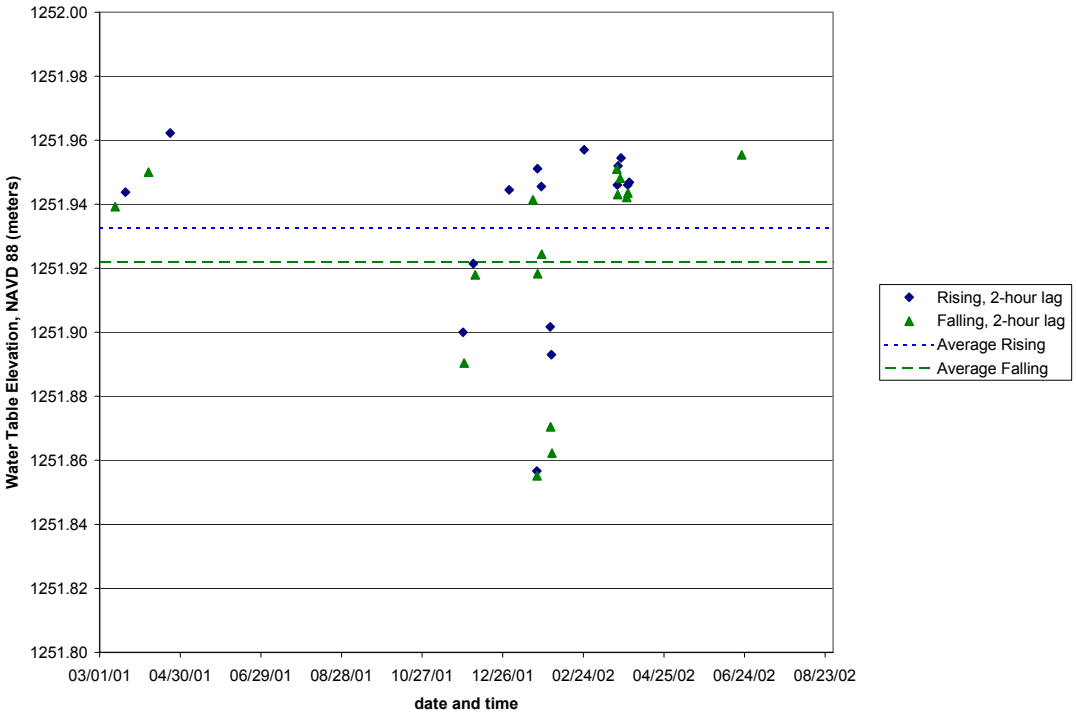

Figure 6-31. Two hour time lag: temporal correlation between river stage and water table response in Well 1

Justification for a change in strategy

Ultimately, the modeling limitations of the SMS model required an adjustment to be made to this original approach. Variable-sloped banks, a steep inner-channel thalweg, and irregular bed and bank morphology features resulted in jagged wet / dry boundaries and recurrent loss of model stability because of divergence problems. Divergence problems resulted in extended model run time, model crashes, and invalid solutions beyond reasonable ranges for velocity or depth. An iterative, time-consuming procedure involved with mesh refinement and editing, accompanied by the strategic manipulation of model parameters, required several months of effort to overcome these obstacles and enable the model to simulate a fairly simple lowering of the water surface elevation.

Eventually, in March 2003, the SMS mesh was deemed complete and was capable of simulating a lowering water surface from bank-full conditions to almost zero-flow conditions, subject to a head gradient of 0.2 meters from the upstream to downstream boundaries of the mesh.

It was necessary to abandon the simulation of overbank stage levels and real-time dynamic streamflow hydrographs within the SMS model domain. Experience with the FLO2DH model within SMS indicated that element re-wetting could not be simulated along the Scout Camp reach without the model experiencing a crash or divergence problem causing an invalid solution. Only the falling portions of the routed hydrograph could be simulated with accurate regard for antecedent flow conditions. Recalling that no rating curve relationship is available at the downstream boundary, no means are available to use the SMS mesh subject to an upstream flow boundary condition. Use of a flow upstream boundary would require specification of a downstream rating curve; of course, even if rating curve data was available, the rating curve option within SMS was found to not function properly. Instead, head boundary conditions were used to gradually lower the water surface elevations across the model domain, with flow values computed from depth and velocity output along nodestrings. Mesh editing was completed using a conservative head gradient of 0.2 meters, but this value was not based on any known data.

The limited availability of water surface elevation survey data prevented model calibration or verification, and the flaws of using a constant head gradient between the model flow boundaries should be noted. Most notably, stage-discharge relationships are assumed independent of antecedent flow conditions, and head loss from upstream

boundary to downstream boundary is assumed constant over the entire range of modeled flow magnitudes. The presence of a low-flow inner channel, a channel bed characterized by erosion and deposition features, channel banks of variable slopes ranging from flat to vertical, and rapid zones of slope transition in both longitudinal and lateral directions along the channel virtually guarantees that these will not be the case in reality. That said, the assumptions remain necessary given the intrinsic data limitations.

By the time the SMS model was fully operational, alternative approaches to a regression analysis of modeled river stage versus water table elevation had been used to circumvent the use of the SMS model as a component for regression analysis. By comparing routed streamflow hydrographs to continuous water table observations and making use of the limited water surface survey data that is available, it was shown that river stage and water table levels are tightly coupled, and the water table response to streamflow oscillations is effectively instantaneous. No evidence of a time lag on the order of hours was indicated for either rising or falling flow conditions. This conclusion was used (chapter 7) for the design of bank elements and determination of bank element functionality. Note that the same questions originally to have been answered through regression analysis (and making use of SMS) were answered with these alternative analysis approaches.

No utility is found for a regression analysis of SMS stage predictions versus water table observations. To establish utility to the months spent developing the SMS model, the decision was made to use the model output to generate a rating curve at the well cross-section and compare rating curve stage predictions to surveyed water surface data. The 0.2-meter head gradient used for mesh refinement was arbitrary and selected to be

conservative, but model operation does require user specification of a head gradient. Determination of an applicable gradient to be used in rating curve development for the Scout Camp reach is the subject of the next section.

Determination of FESWMS longitudinal hydraulic gradient

The decision was made to simulate lowering of the water surface and element drying subject to a physically-meaningful head gradient. The model parameterization, as reviewed in Appendix A, remained unchanged. Simulations were to range from bank-full conditions to the minimum level the mesh could handle. Uniform flow is considered. Under conditions of uniform flow, one assumes the water surface slope, energy grade line slope, and bed slope as equal. Based on survey data, and, as would be expected given the bend internal to the modeled reach, the bed slope is not uniform between any consecutive cross-sections. Only two boundary conditions are input into the SMS model, eliminating the possibility of user specification of multiple water surface slopes within the model domain. Instead, a representative bed slope for the 500-meter modeled reach was determined using regression analysis. This slope is based on surveyed thalweg elevations along the channel, as extracted from the complete set of surveyed data points.

The thalweg is a connection of the points of lowest elevation for all cross-sections, representing minimum flow level in the channel. The latitude and longitude coordinates of all points along the thalweg are shown in Figure 6-32, as is their location relative to other points within the surveyed reach. Linear segments were used to connect the data points and compute a distance along the thalweg, or distance along the flow direction, for each point. The thalweg point located along cross-section 500 (Figure 5-1) is used as the point of zero distance. By performing a regression of bed elevation versus

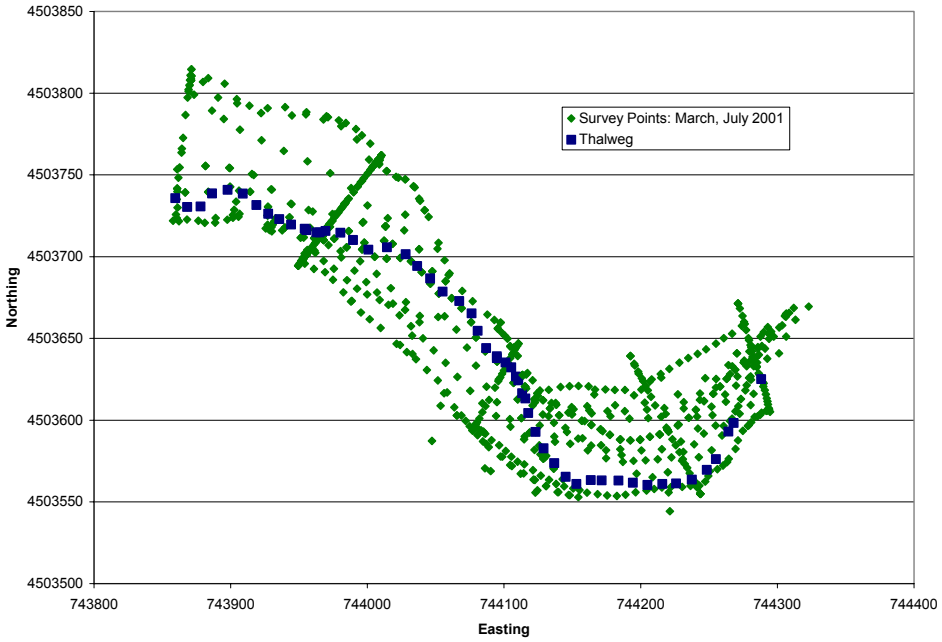

Figure 6-32. Channel thalweg location based on survey points from March and July, 2001

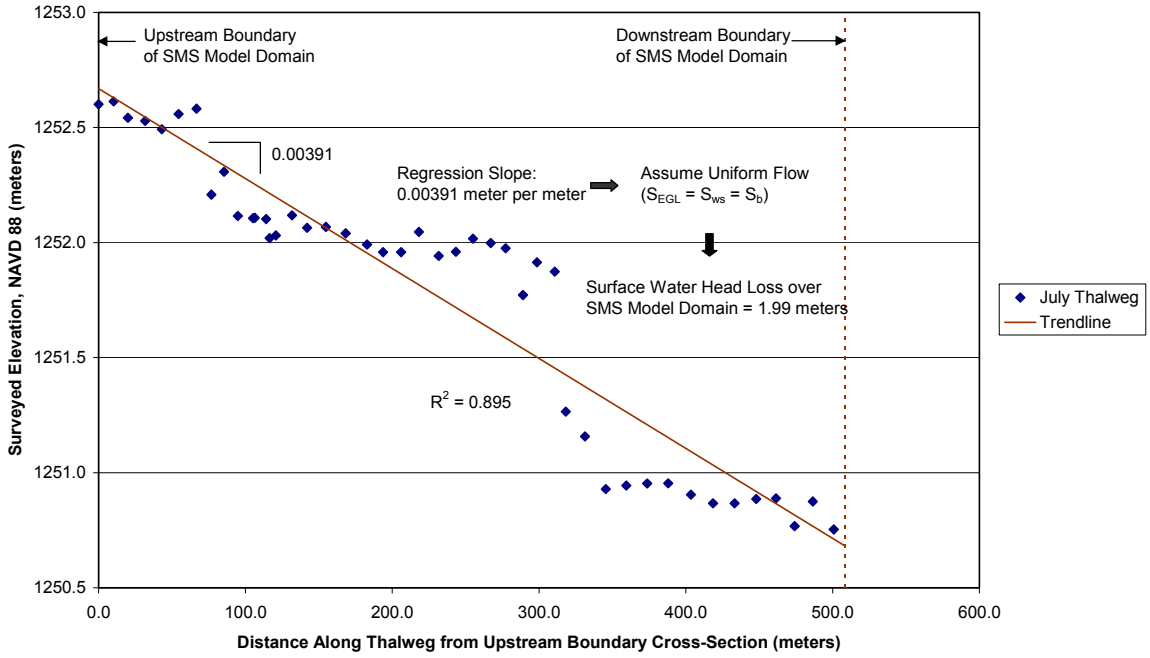

Figure 6-33. Linear regression of March, July 2001 surveyed bed elevations for use in determination of hydraulic gradient for SMS model

distance along the thalweg, the channel is effectively straightened, and a mean bed slope is computed. The results of the regression analysis can be found in Figure 6-33. The figure shows that bed slope is variable over the model domain, but the R^2 value of 0.895 does indicate a good fit and a definite trend for elevation loss moving downstream. Regression analysis, based on the slope of the trendline in Figure 6-33 (S = 0.00391 m/m), indicates a net elevation loss of 1.99 meters through the 510-meter flow path of the Scout Camp model domain, from cross-section 500 upstream to cross-section 100 downstream. Cross-sections 100 and 500 coincide with the upstream and downstream boundary nodestrings within the SMS mesh.

Hydrodynamic simulation and rating curve development using FESWMS

Based on the assumption of uniform flow, the head gradient across the model domain was assumed equal to the mean bed slope. The 1.99-meter head gradient does not mandate a uniform water surface slope within the mesh interior, as the SMS model will perform these computations based on the mesh geometry. Visual inspection of the points' locations relative to the regression line indicates that the SMS model will predict smaller flow depths in the central portion of the modeled reach and larger flow depths downstream. This observation is consistent with conditions observed in the field, and also suggests eventual flow discontinuity within the SMS mesh interior, indicating a minimum attainable level for flow simulations. It is noted that this is not a perfect solution because water surface slope is not constant with respect to flow or location, but rather the assumption is a product of limited data. This was previously suggested from the analysis of surveyed water surface elevations in Figure 6-25. Complex, dynamic channel geometry and lack of velocity observations prevent artificial development of a downstream rating curve using a relationship such as Manning's equation. Additionally,

the single known accurate water surface elevation data point from the staff gauge, is not sufficient for use in SMS calibration for the channel bed and channel bank roughness coefficients. Rather, the bed and bank roughness values are assumed equivalent, with this value equal to the 0.045 value used in RIVMOD. Notably, this value is likely set high because of the 1D modeling approach embodied in RIVMOD.

The head gradient across the model domain was used to develop a rating curve at the well cross-section. The SMS model was initialized for the 1.99-meter head gradient with all nodes initially submerged. After the initial water surface was lowered to 1255.0 meters at the upstream model boundary and 1253.01 meters at the downstream boundary (note head gradient equal to 1.99 meters), rating curve computations were initialized. The water surface elevations were simultaneously lowered at both boundary nodestrings, at the same rate, to maintain a constant head gradient. To maintain model stability and limit output file size, the boundary conditions were lowered continuously by a series of simulations and hotstarts. When the water surface could no longer be lowered because of flow discontinuity within the mesh interior (wet elements are no longer connected), the simulation was necessarily stopped. Examples from the time series of element drying due to the lowering water surface are shown in Appendix C, including the minimum attainable boundary condition levels.

After the water surface was lowered to minimum attainable levels, the intermediate solution files were used as starting points for a series of steady state simulations. Hotstart files were used to start these steady state conditions at 0.25-meter head increments (chosen to generate a sufficient number of data points). During mesh construction, nodestrings were constructed along cross-sections of the mesh interior, to

be used for obtain streamflow as a function of head boundary conditions. Steady state simulations were run consecutively using hotstart files until the following criteria is met: flow across the upstream boundary and well cross-section nodestrings have stabilized (flows may not be exactly the same as flow direction is not exactly perpendicular to the well nodestring, but they will be very close; range was later determined as 0.15 – 0.60 cubic meters per second (cms)); and the water surface elevation at the well cross-section node along the vertical bank adjacent to the wells is no longer changing between simulations. With jagged wet / dry boundaries within the model domain, convergence criteria were difficult to attain. The working definition for attainment of steady state was therefore necessarily adopted. At the well cross-section, steady state flows and water surface elevations were recorded after each simulation for later use in rating curve development. Boundary condition increments of 0.25 meters were used until minimum flow levels were reached. The steady state outputs from the SMS model are summarized in Table 6-2 (UBC / DBC = upstream / downstream boundary condition).

Table 6-2. Steady-state output for depth and discharge from final SMS model

		Equilibrium Flow at Well Transect			Water Surface Elevation Adjacent to Well 1 (GZF = 1252.01 m)		
UBC Stage, NAVD 88 (m)	DBC Stage, NAVD 88 (m)	Q_1 (cms)	$\log_{10} Q_1$	Q (cfs)	NAVD 88 (meters)	Depth (above GZF, m)	$\log_{10}$ (Depth)
1255.00	1253.01	226.80	2.36	8014	1254.50	2.49	0.40
1254.75	1252.76	190.20	2.28	6721	1254.28	2.27	0.36
1254.50	1252.51	152.20	2.18	5378	1254.05	2.04	0.31
1254.25	1252.26	109.60	2.04	3873	1253.96	1.95	0.29
1254.00	1252.01	84.20	1.93	2975	1253.74	1.73	0.24
1253.75	1251.76	63.70	1.80	2251	1253.49	1.48	0.17
1253.50	1251.51	45.30	1.66	1601	1253.23	1.22	0.09
1253.25	1251.26	20.80	1.32	735	1253.14	1.13	0.05
1253.00	1251.01	15.20	1.18	537	1252.81	0.80	-0.10
1252.75	1250.76	6.85	0.84	242	1252.45	0.44	-0.36
1252.525	1250.54	0.80	-0.10	28	1252.40	0.39	-0.41

The upstream and downstream stage boundary conditions were input to the SMS model based on the 1.99-meter mean gradient determined from regression. With the SMS model parameterized in metric units, the streamflow / discharge (Q) through the well cross-section and water surface elevation for the node along this transect closest to Well 1

are extracted from steady-state model output in units of cms and meters (NAVD 88 vertical datum), respectively.

The procedure used for rating curve development was based on techniques practiced by the USGS (Kennedy, 1984). The stage that would occur at a gaging station if the discharge were infinitesimal is the gage height of zero flow (GZF). For this analysis, the GZF was defined as the elevation of the channel thalweg (the minimum bed elevation) along the well transect, a value of 1252.01 meters (NAVD 88 datum). The stage versus discharge relationship is shown in Figure 6-34, with each point taken from a steady-state SMS model simulation in Table 6-2.

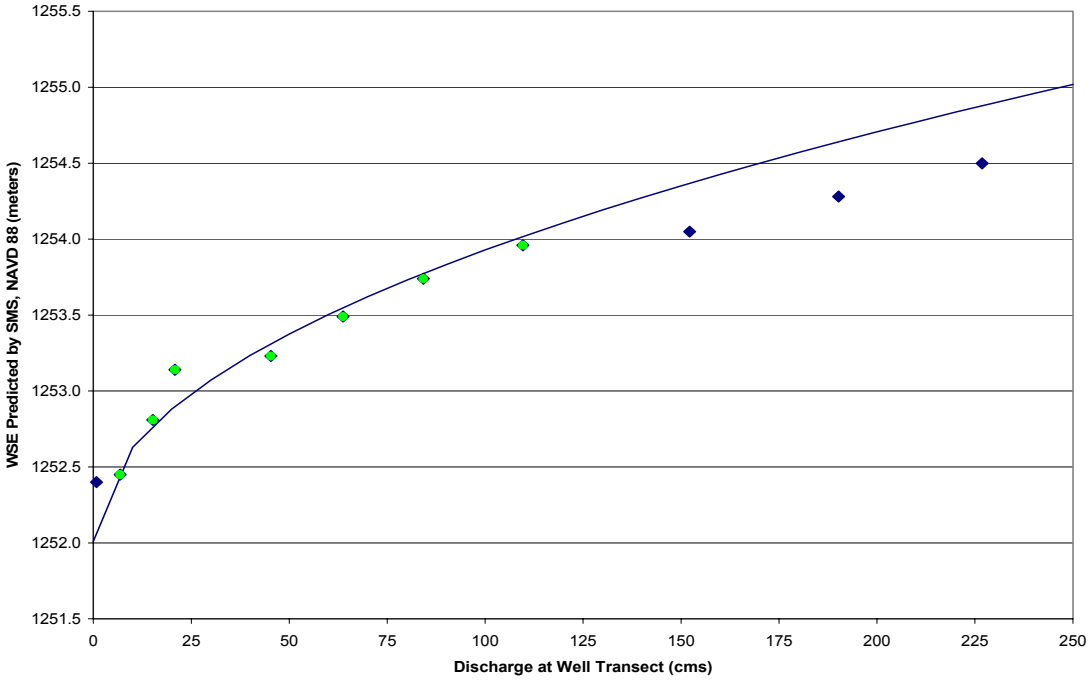

Figure 6-34. Stage – Discharge Relationship for Steady State Lowering of SMS Water Surface Elevation

Rating curve analysis is based on fitting a straight line through the stage-discharge relationship in log-log space. Stage is first normalized to depth (above the GZF datum). The log transforms of flow and depth data points are included in Table 6-2. Before

determination of a rating curve equation, limitations of the data were noted. First, the top of the channel bank is situated at an elevation of 1254.15 meters. Stage elevations greater than this value correspond to flows on the floodplain, beyond the specified upper limit (for accurate stage modeling) of the constructed SMS mesh. It is also evident from Figure 6-34 that the data point corresponding to the third-highest discharge (152.2 cms) does not follow the trend observed for lower discharge values. Given the irregular nature of top-of-bank elevations along the channel, this data point was also presumed to correspond to floodplain flows for some areas of the model domain. Recalling that the maximum observed flow between March 2001 and September 2002 is less than 1500 cfs (42.5 cms), the range of flow magnitudes for the period of interest will be entirely included by regression of the remaining points. Additionally noted is the fact that the final data point in Table 6-2 does not correspond to the 0.25-meter boundary condition lowering interval. The data point noted at a flow of 0.80 cms, as shown in Figure 6-34, is the lowest available modeled stage for which flow is able to be transported through the model domain. At this flow level, the water surface elevation immediately adjacent to the wells is disconnected from the actively flowing portion of the channel, representing a backwater location, and this data point was therefore also excluded from the rating curve analysis. The lowest streamflow for which elements adjacent to this bank remain hydraulically connected to the active flow path is 1.91 cms. The applicable flow range for the rating curve equation was therefore defined as 1.91 cms (67.5 cfs) to 109.6 cms (3871 cfs). The rating curve analysis included the 7 middle data points highlighted in Figure 6-34. The log transforms of these data points were plotted and fitted with a regression line. Regression results are found in Figure 6-35. The regression line is extrapolated back to

show the complete applicable discharge range. The stage-discharge relationship predicted from this regression line is shown in Figure 6-35. The techniques to generate this curve are next discussed. The three largest flow magnitudes represent floodplain flows outside the rating curve applicable flow range, so the poor match to these data points is expected.

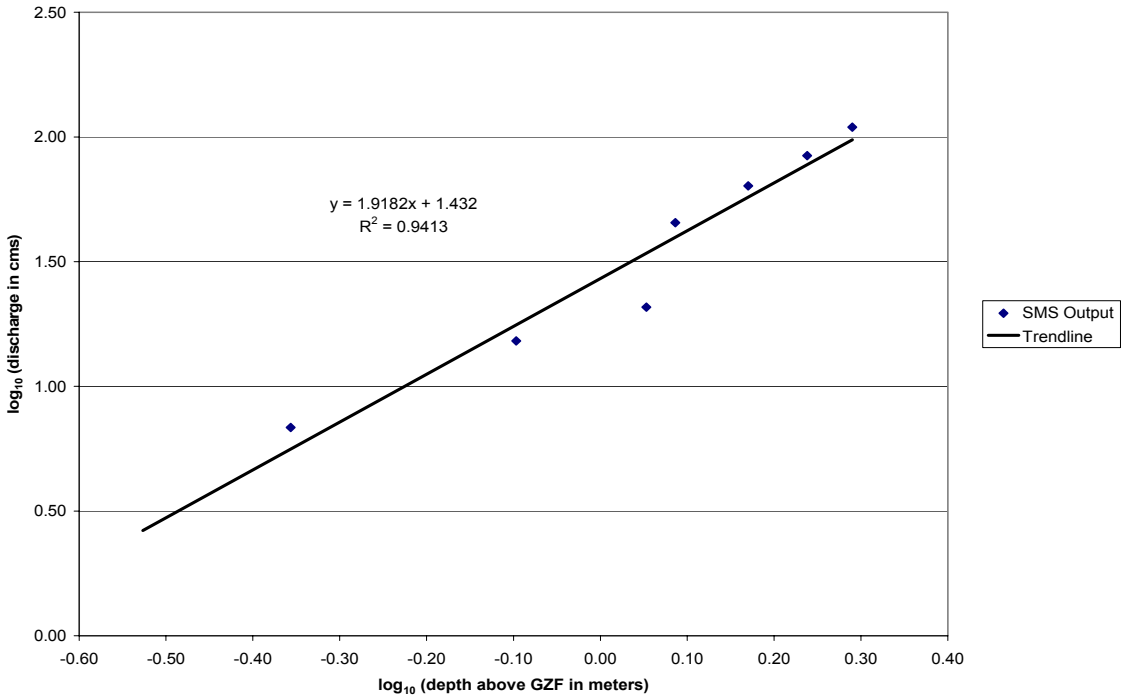

Figure 6-35. Linear regression for determination of discharge as a function of depth

The straight-line fit through the data points assumes a simple power law relationship for discharge as a function of depth above the GZF datum:

$$Q = \alpha \ D^{\beta} \qquad \text{(Eq. 6-8)}$$

where Q is discharge (cms), D is normalized depth (meters), and α and β are constants computed using the straight-line regression in Figure 6-35. The constants are determined directly from the slope and intercept of the regression equation, as determined from equation 6-9:

$$\log_{10}(Q) = \log_{10}\alpha \ + \ \beta \log_{10} D \qquad \text{(Eq. 6-9)}$$

This equation has the form of a straight line: y = mx + b. Plotting the log of normalized depth on the x-axis and the log of flow on the y-axis, it is noted that the y-intercept of the regression line corresponds to log α and the slope of the regression line corresponds to β. The values of the constants are computed to be the following:

$$\alpha = 10^{1.432} = 27.040$$

$$\beta = 1.918$$

The power law rating curve function for the Scout Camp well cross-section is therefore described by equation 6-10:

$$Q = 27.040\ D^{1.918} \qquad \text{(Q in cms, D in meters above GZF = 1252.01)} \qquad \text{(Eq. 6-10)}$$

An inverse relationship for depth as a function of flow (flow being the known parameter from RIVMOD routing through the well reach) can be calculated in several ways. A power law relationship is computed in the same manner as above by switching the axes on which discharge and depth are plotted, as in Figure 6-36. Without showing the details, the power law relationship for depth (above GZF) as a function of discharge is described by equation 6-11:

$$D = 0.200\ Q^{0.491} \qquad \text{(Q in cms, D in meters above GZF = 1252.01)} \qquad \text{(Eq. 6-11)}$$

The power law relationship, as previously discussed, in only applicable for the streamflow range between 1.91 cms (67.5 cfs) to 109.6 cms (3871 cfs). The groundwater well transect is approximately centrally located within IFMTFM segment 152. Making use of the streamflow hydrograph through this segment as routed by RIVMOD and the relationship for depth as a function of streamflow (equation 6-11), plots were prepared to show SMS-modeled river stage versus water table levels in Well 1, noting the 5-foot separation distance between channel and well. For routed streamflows within the

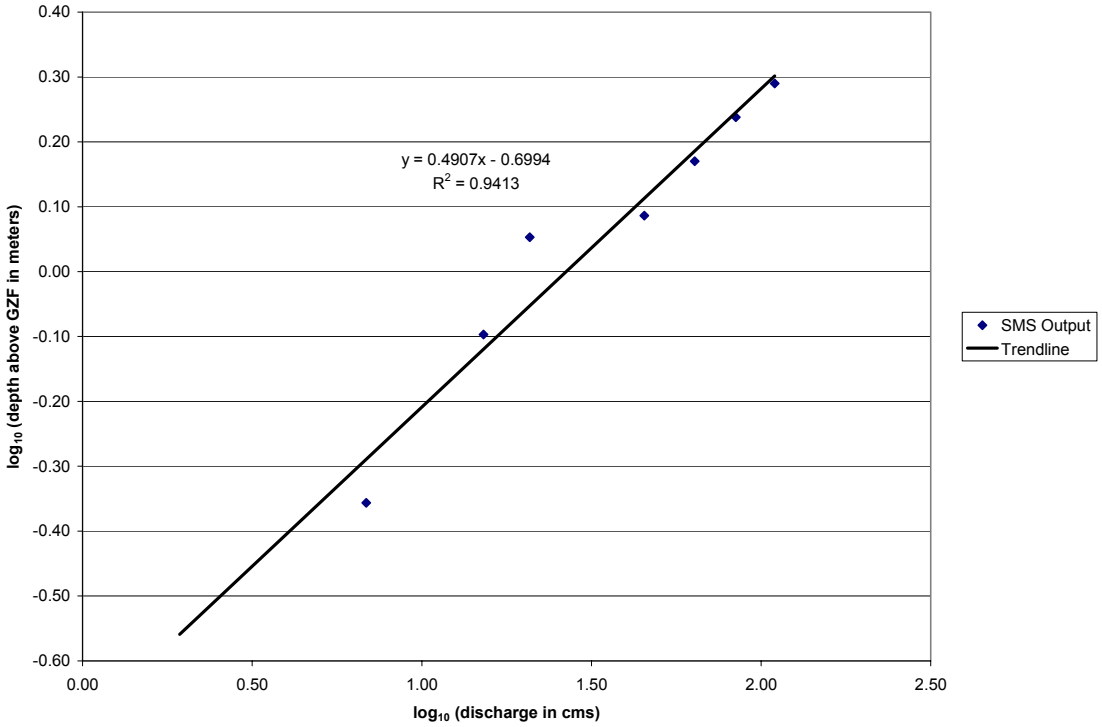

Figure 6-36. Linear regression for determination of depth as a function of discharge acceptable magnitude range, water surface elevation along the well transect is calculated for comparison with observed water table recordings from Well 1. As indicated in Figures 6-37 and 6-38, a positive hydraulic gradient ranging between 0.4 and 0.6 meters exists between the water surface elevation in the channel (adjacent to the channel bank) and the water table observation in Well 1.

It is important to compare the rating curve predictions with the limited field data available for water surface elevation in the channel, in the vicinity of the wells. In Figure 6-27, a regression equation approximated the water surface elevation at the well transect as 1252.30 meters (NAVD 88). The water surface elevation survey data used was collected on March 9, 2001 for streamflow conditions of 173.8 cfs. Using equation 6-11 or by inspection of Figure 6-37 on this date, it is noted that the rating curve predicts a water surface elevation of 1252.45 meters at this flow magnitude. The water surface

estimates from these two approaches are not in good agreement, differing by 15 centimeters. This result was not unexpected. Greater reliability is placed on the estimate based on the surveyed elevations for four main reasons: the surface water model used to develop the rating curve is not properly calibrated based on the lack of available data; the rating curve calculations assume streamflows routed (from FCH to the Scout Camp well transect) using RIVMOD to be correct (these are the discharge values plugged into the rating curve equation), although RIVMOD does not consider losses to ET or groundwater; the bed roughness used in the quasi-3D SMS model is set equal to the value used in the 1D RIVMOD, possibly causing model stage predictions to be higher than for a lower bed roughness value; and the SMS model assumes a head gradient that does not vary over time, equal to the 1.99-meter average bed slope. With these considerations in mind, the 15-centimeter difference was reasonably expected. Unfortunately, additional comparisons for alternate flow regimes are not possible without additional water surface elevation data. However, it is important to note that the water surface elevations predicted from SMS output with this rating curve approach (Figures 6-37 and 6-38) in fact represent maximum water surface elevations that could be observed in the channel, based on the above-listed assumptions. Alternative model runs for different bed roughness values are not completed given poor data availability regarding the setting of this parameter, the required model run time of several days, and the inconsequential value of these results on the conclusions reached for bank element functionality.

Water surface oscillations appear to precede water table oscillations in figures 6-37 and 6-38. With previous evidence presented of a hydraulic gradient away from the

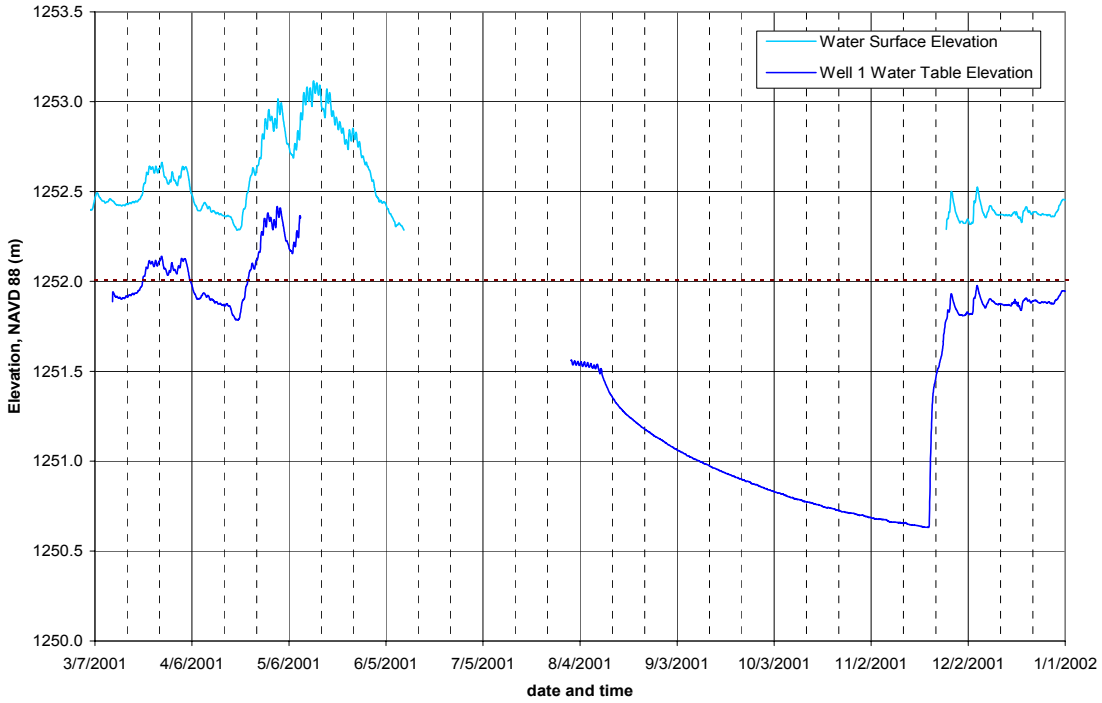

Figure 6-37. 2001 rating curve-based estimates for water surface elevation in the channel compared to water table level in Well 1

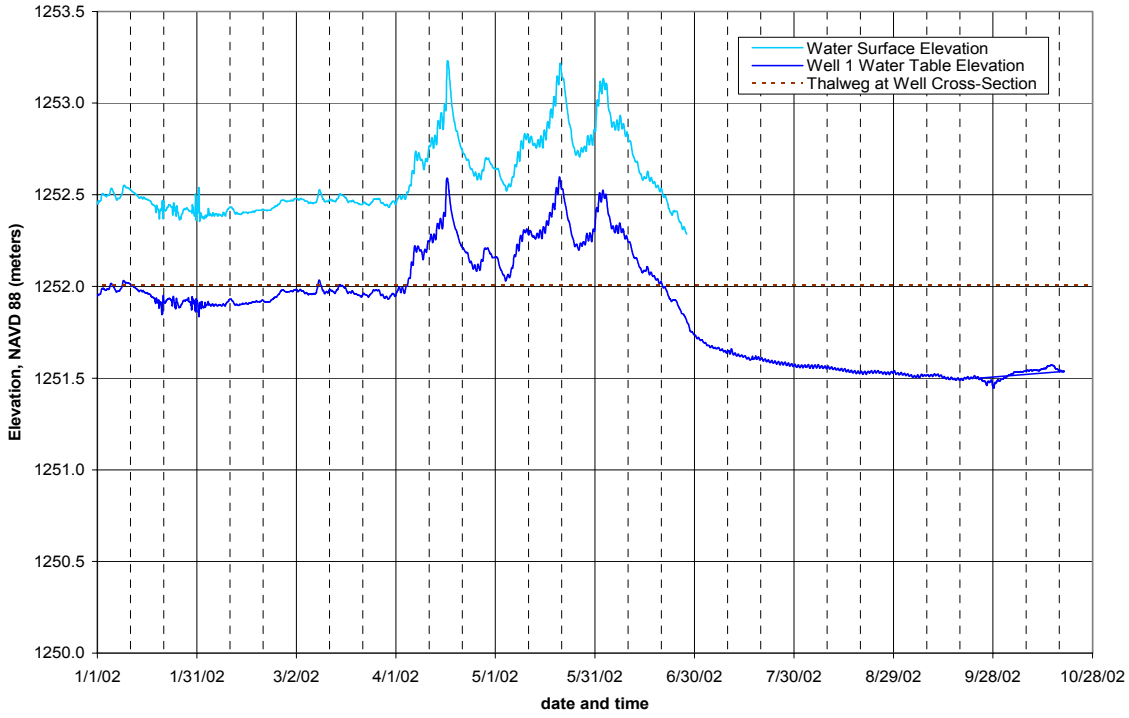

Figure 6-38. 2002 rating curve-based estimates for water surface elevation in the channel compared to water table level in Well 1

channel, this response should be reversed. Recall, this same problem was encountered when streamflow oscillations for segments 151 or 152 were compared with water table oscillations. This is the result of the 1D channel routing approach used by RIVMOD. The common thread between the two comparisons is that the same streamflow hydrograph from RIVMOD segment 152 was used with the rating curve equation to predict the plotted water surface elevations shown in Figures 6-37 and 6-38.

Completion of a more detailed regression analysis of water surface predictions from SMS versus water table oscillations seen in the well was not warranted and would prove meaningless without accurate routed hydrographs and additional data for use in model calibration for the Scout Camp reach. Bank storage, evaporation, and groundwater losses downstream of Fort Churchill are not considered within RIVMOD. The surface water model is not properly calibrated based on the absence of sufficient water surface data, and, as such, the rating curve computations are only approximate. Sufficient evidence has been presented to justify the assumption of an instantaneous saturation height response to streamflow changes within the erodable face of the channel bank, and this evidence was the basis for bank element design.

Limitations of FESWMS and impacts on this thesis research

The SMS modeling package was purchased for this thesis research based on its reasonable cost and stated ability to simulate areal wetting and drying for a riverine system, including the capability to handle steep channel banks. As thoroughly documented, model development for the Scout Camp reach of the Carson River was neither straightforward nor simple. Use of the SMS software began in June of 2002, and a useable model was not completed until March 2003. The SMS model package includes two possible modules for 3D hydrodynamic modeling: RMA 2 and FESWMS. FESWMS

was ultimately chosen based on its support of both subcritical and supercritical flow analysis. The high degree of variability in element slopes and river stage levels create a high likelihood of supercritical flow conditions at the mesh boundary conditions and within the mesh interior. In fact, this premonition was supported by supercritical flow warnings encountered during many model simulations.

The FESWMS module and the FLO2DH code possess some notable limitations. Recall, when this thesis research began, one was looking to use FESWMS to simulate a continuous hydrograph through the surveyed reach and extract water surface elevation data. The model shortcomings are briefly reviewed. First, a downstream boundary condition must be specified, rather than computed by the model. With no available downstream rating curve, the model could only be run under conditions of a constant longitudinal head gradient for all flow regimes, despite field data indicating this as an invalid assumption. This is also a result of a distant field site (Nevada) and a limited ability to collect detailed water surface data over time. The mesh generation process does not favor the use of detailed survey data over a relatively small reach. In this instance, the high node density, with typical spacing of 3 to 5 meters, and irregular nature of the channel morphology causes extreme divergence with the finite difference algorithm used by FLO2DH. The surface variability, due to erosion and deposition cycles, is present in the field and therefore enters into the mesh. Large irregularities understandably cause divergence problems, but localized variability on the order of a couple of centimeters should be better handled within the model. Ideally for the model, data points (model nodes) would fall along contour lines for improved drying performance; and spatial heterogeneity, such as highly variable bank slopes ranging from gradual to vertical,

would not exist. The fact remains, however, that in order to develop an accurate water surface solution within the SMS model, high spatial resolution is needed (as opposed to perhaps a simple linear interpolation between cross sections).

Steep channel banks cannot be simulated by the FESWMS model, unless vertical wall boundaries are used. This eliminates the model ability to simulate floodplain level flows. The transition zones from steep vertical banks to gradual sloping banks within the model domain also required a large degree of mesh editing. Divergence was also a problem when multiple material types were used to indicate variable roughness values for bed, banks, and floodplain areas. While the tools for mesh editing are acceptable, mesh quality indicators, warning messages, and error explanations could be improved upon to better identify potential problem areas. Typical of many models, the available documentation, although extensive, is vague, and the physical meanings of model parameters are often unexplained. Technical support through ems-i, the company through which the SMS model was purchased, should also not be commended.

The most substantial model shortcomings relate to wetting and drying. The model would be suitable to simulating modest stage fluctuations across a large river area, but the model is not very useful for simulating large stage oscillations and repeated element wetting and drying across a small river area (i.e. the Carson River). The parameters to determine if an element is wet or dry—storativity and depth tolerance for drying—perform poorly when some mesh elements are steep and element slopes are highly variable, even across short distances. The end result for the Scout Camp mesh is a jagged wet / dry boundary. When the boundary takes this jagged shape, convergence requirements are seldom attained and model run time is increased. The jagged boundary

also increases the likelihood for element re-wetting, with the usual end result a model crash. With no guidance available for setting these parameters in model documentation, a discernable fine line exists between experimenting with these parameters to accurately predict the wet / dry boundary (likely causing a model crash) and loosely setting these parameters to eliminate element re-wetting (thereby bringing into question the accuracy of the wet / dry boundary and the solution water surface elevation). Priority was given to accurately simulating the wet / dry boundary when possible, with the trade-off being no ability to simulate a rising river stage.

Lastly, a comment on model simulation time is needed. Model simulations must begin with all mesh nodes submerged. This is a waste of time during the mesh editing process. When a node is identified as causing a model failure or divergence, the mesh must be edited. Even if only one node is altered, all previous solution data for the other 12000+ nodes must be discarded and the model simulation started again. By attempting to minimize the magnitude of elevation corrections (to preserve the original field measurements), it is never certain that a given correction will be successful until the water surface reaches the previous problem level. Based on limited explanations regarding the cause of a model crash or divergence, mesh editing is iterative with only a limited number of problem nodes able to be corrected following a given simulation. When starting with all nodes submerged, the rate at which the water surface can be lowered serves as a further constraint, as model stability must be maintained throughout the process. By editing the solution file, nodes can be manually turned off (forced to be dry). This is particularly useful to manage disjoint wet elements caused by jagged wet / dry boundaries and element re-wetting. After the solution file is edited, the simulation

can be hotstarted from this edited solution, and a model crash can be averted (thereby saving the need to start over completely).

The SMS model would be better suited to modeling large riverine systems from coarse bathymetry data. The spatial heterogeneity of Carson River bathymetry, vertical banks, and bed features proved to be significant obstacles for the software program. Conceivably, based on this user's experience with the SMS model, particularly the FESWMS module, the program would work well to simulate a river system with greater bathymetric uniformity and could simulate small-scale wetting and drying in which only a small portion of the model mesh is undergoing wetting and drying. The channel size and streamflow variability of the Carson River was a poor match for the SMS software package.

CHAPTER 7
BANK ELEMENT DEVELOPMENT AND COMPARISON TO PREVIOUS IFMTFM

General Considerations for Bank Element Design and Operations

Methylation within channel banks is dependent on the presence of anoxic regions within the sediments. The size of the saturated, anoxic zone of channel bank sediments changes with river stage, in response to the induced hydraulic gradient away from the channel. Bank sediments which are characterized by these conditions long enough for the microbial populations to become established are able to support an active zone of methylation and demethylation. By tracking the size of the active zone of methylation as river flows change over time, the updated IFMTFM is able to remove itself from the unrealistic assumptions of static MeHg concentrations within the channel banks and no MeHg above a given depth threshold. By allowing the model to run for a sufficient length of time prior to generating used output, initial conditions (bank concentrations) can effectively wash out of the system, thereby removing the dependence of output on initial conditions.

The spatial heterogeneity of Carson River sediments proved to be an obstacle for detailed unsaturated zone and groundwater modeling. Visual inspection of soils on site verified sediment heterogeneity, as did the pump test results indicating the presence of high conductivity layers. To develop and validate a 2D groundwater and unsaturated zone model, detailed soil data is required. The modeling of flow in the unsaturated zone requires user specification as to how moisture content, relative conductivity, and specific moisture capacity vary as a function of pressure head. Ideally, these curves are

determined directly by performing a series of tests on the soils involved in the study. In many cases, they can be approximated using a set of measured or approximated constants and a set of empirical relationships, an example being the van Genuchten functions (Lin et al., 1996). In fact, one would ideally possess data relating channel bank capillary fringe characteristics to the rate at which an adjacent head boundary (river stage) is rising or falling. The combined vertical extent of the partially saturated zone will depend on whether river stage is rising or falling. A smaller distance would be expected if the river stage is rising (bank not recently inundated) and a larger distance if river stage is falling (bank recently inundated). In the end, time constraints and the conclusion that such detailed sediment data could not justifiably be extrapolated over the IFMTFM model domain prevented this type of analysis from being undertaken.

Analysis of the coupling of routed streamflow and water table response; surveyed water surface elevations; and pump test data indicated a nearly instantaneous response time between river stage fluctuations and observed water table changes in Well 1. A hydraulic gradient away from the river channel is evident for periods of river contact with channel banks within the modeled reach. Given the nearly instantaneous response observed at a distance of 5 feet into the channel bank (location of Well 1), it is assumed that the saturated portion of the erodable face of the channel bank is in instantaneous equilibrium with the modeled river stage, as predicted within the IFMTFM by RIVMOD. In order to account for the microbial response time following a change in bank moisture, the saturated portion of the bank is tracked over time. The IFMTFM will consider the portion of the channel bank actively methylating to be a temporal average of this saturation height. The determination of this averaging window is later discussed.

Conceptually, however, if the river stage is rising over a few days time (time must exceed the averaging window), the actively methylating portion of the bank must be lower than the current river stage. Similarly, if river stage is falling for a consecutive number of days, the actively methylating portion of the bank will be higher than the final river stage. Erosion only occurs for portions of the bank contacted by the river, such that MeHg generated within the channel bank above the river stage will only be introduced to the water column if the stage again rises to contact these bank areas prior to the bank becoming dry. Within the model, microbial methylation and demethylation cease when bank sediments become dry. If the sediments are re-wetted, the sediments again require the same acclimation time for microbes to become established, regardless of how recently the sediments were saturated.

The use of a temporal averaging window to track the saturated portion of the bank requires the creation of bank elements within the IFMTFM. In following the original goals of this thesis, the ability to better simulate field processes by allowing methylmercury bank concentrations to change over time was added to the previous capabilities of the IFMTFM. Model calibration requirements are also reduced, as discussed in the upcoming sections of this chapter.

Updated Input Data Sets to Include Bank Elements

Model Functionality Prior to Addition of Bank Elements

The complete IFMTFM model includes 274 stations, with station 1 located at the Carson City Gage (CCG) and station 274 at Lahontan Dam. Channel cross-sectional geometry is specified in the RIVMOD input data file, based on the parameters defined in Figure 3-1. Linear interpolation of channel geometry is applied to segments, or river reaches between adjacent stations. Prior to modifications as part of this thesis research,

the IFMTFM included two element types, water column elements and bed elements. Segments 1 through 273 are classified as water column elements, and segments 274 through 546 are classified as channel bed elements. Each water column segment lies above a corresponding bed segment, as indicated in Figure 7-1. Bed segments encompass the channel bottom area, internal to the main channel (BW2 in Figure 3-1) between adjacent stations. Mercury methylation and demethylation within channel bed elements create dynamic mercury concentrations able to exchange with the overlying water column through sediment erosion and diffusion processes. The active depth for mercury transformations within channel bed elements is assumed to be 10 centimeters.

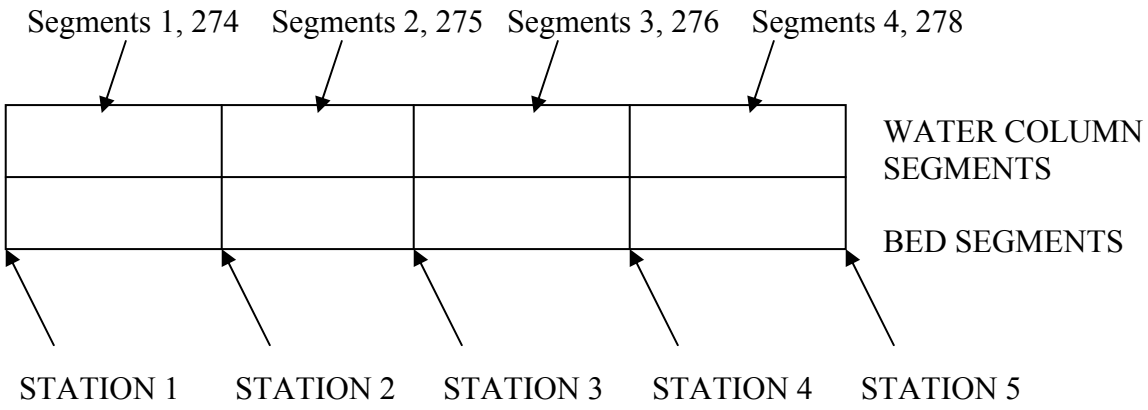

Figure 7-1. Station and segment definition within IFMTFM

Within the previous IFMTFM, channel banks (vertical portion of D2 in Figure 3-1 that is above the slope SL1) can be eroded (although geometry is not updated within the model), but mercury transformations do not occur within the channel banks. Rather, inorganic Hg(II) and organic MeHg concentrations within channel bank sediments remain constant, as determined by calibration on the parameters λ_1 and λ_2.

$$\left[Hg_{MeHg}\right]_{bank} = \frac{\lambda_2}{S_0^{0.5}} \qquad \text{(Eq. 4-1)}$$

$$[Hg_{in}]_{bank} = \frac{\lambda_1}{S_0^{0.5}} \quad \text{(Eq. 4-2)}$$

To model dynamic mercury concentrations within the channel banks, a new segment type was needed. Bank segments, incorporating the channel bank between adjacent stations, were created within the IFMTFM hydrodynamic input data file. These new segments within IFMTFM will be collectively referred to as bank elements.

The hydrodynamic portion of the IFMTFM (RIVMOD) predicts water depths and velocities for all segments throughout the Carson River model domain. Based on the specified cross-section geometry for any two adjacent stations, the model is able to compute the average contacted height of the water column on the channel banks for all segments. By tracking this height over time, the model estimates the saturated portion of the channel banks in each of the 273 water column segments. Within the saturated bank sediments, methylation and demethylation are modeled to occur. MERC4 modeling of mercury partitioning to bank sediments and pore water is used to incorporate diffusion and advection of mercury from the channel banks to the water column, in addition to the already-modeled bank erosion mechanism (unchanged). Bank element functionality is essentially the same as bed element functionality with respect to mercury modeling.

Rather than starting with the complete 273-segment IFMTFM model of the Carson River, a simple 10-segment model was constructed. Modifications to the IFMTFM code and input data files were first tested on a small scale with a smaller computation time. The simple model included 10 water column segments, 10 bed segments, and 10 bank segments; uniform cross-section geometry; and a uniform bed slope. Conceptually, the updated IFMTFM model was constructed as shown in Figure 7-2. Arrows indicate mercury and sediment exchange between the different element types

within the model for any given river segment, based on average values between two adjacent stations. Due to the geometric symmetry used to define all model segments, one bank segment corresponds to a single water column and bed segment for each model reach between adjacent stations. Total bank segment volume over a reach is simply the predicted bank volume for the single bank segment multiplied by two (left and right banks). This same approach is used to compute surface area for diffusion.

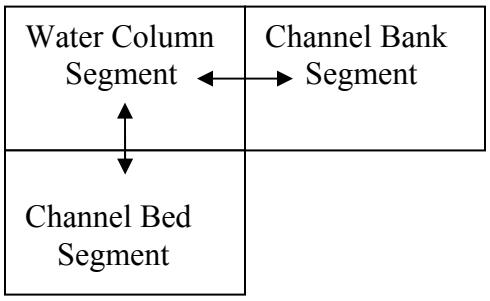

Figure 7-2. Conceptual IFMTFM segment interaction

Modified Input Data Files

Following the code modifications to the IFMTFM and testing and refinement based on the simple 10-segment model, updated input data files for the hydrodynamic (RIVMOD) and water quality (WASP5/MERC4) components of the IFMTFM were prepared to match the new requirements of the code. Based on the linkage structure between the three IFMTFM models and the unchanged channel geometry specified in the RIVMOD input data file, modifications are only necessary for the WASP input data file. The required changes are briefly discussed in their order of appearance within the WASP5 model documentation.

- Data Group A: Model Identification and Simulation Control
    - 819 model segments: 273 water column segments, 273 channel bed segments, and 273 channel bank segments

- Data Group B: Exchange Coefficients
    - 818 modeled exchanges: 272 water column segment to water column segment, 273 water column segment to bed segment, and 273 water column segment to bank segment
    - Characteristic length for diffusion for bank segments set equal to 0.01 m value used for bed and bank segments
    - Diffusion coefficient for bed and bank segments changed to 1.14E-10 to match field data for mercury flux out of channel bed

- Data Group C: Volumes
    - Defined new segment type, ITYPE = 5 for bank segments
    - 273 bank segments numbered as segments 547 through 819
    - Bank segments defined based on adjacent water column segments (segment 1 with segment 547, segment 2 with segment 548, etc.)

- Data Group G: Parameters
    - Three additional segment classifications added, including river bank segments, upstream reservoir bank segments, and downstream reservoir bank segments
    - Specified bank segment parameters same as corresponding bed segment parameters, with exception of methylation and demethylation rates (further discussed under Data Group I)

- Data Group I: Kinetic Time Functions
    - Model limitations dictate a maximum of 4 methylation / demethylation rates based on segment classification
        - Previously, rates varied for water column segments, river bed segments, upstream reservoir bed segments, and downstream reservoir bed segment
        - After changes, rates vary for water column segments, river bed segments, reservoir bed segments (average of previous upstream and downstream reservoir values), and bank segments

- Data Group J: Initial Concentrations
    - Initial mercury and sediment concentrations specified for bank segments
        - Hg(0) concentrations = 0.00 (not simulated)
        - Hg(2+) concentrations = 1.00E+01 (arbitrary as later calibrated on)
        - MeHg concentrations = 0.00 (no available data, methylation simulated by updated IFMTFM model and concentrations updated)
        - Hg(inert) concentrations = 0.00 (not simulated)
        - Coarse suspended solid (Solid 1) concentrations based on sediment samples from river banks and reservoir bed (total conc.=1.56E+06)
            - River segments 547-755: CSS = 1.08E+06 (69.5% of total)

        - Reservoir segments 756-819: CSS = 0.62E+06 (40% of total, same as corresponding bed segments)
    - Bedload (Solid 2) concentrations = 0.00 (bedload only present for water column segments)
    - Washload (Solid 3) concentrations based on sediment samples from river banks and reservoir bed (total conc.=1.56E+06)
        - River segments 547-755: WL = 0.48E+06 (30.5% of total)
        - Reservoir segments 756-819: WL = 0.94E+06 (60% of total, same as corresponding bed segments)

- No changes necessary for Data Groups D: Flows, E: Boundary Concentrations, F: Loads, and H: Constants

Comparison of Updated IFMTFM Code versus Previous Version

Code modifications were completed by John Warwick in 2003. While inspection of the final code changes are not needed for this discussion, it is important to understand how the updated code incorporates the new bank elements for improved mercury modeling; and the resulting benefits to model calibration. Throughout this discussion, the updated IFMTFM code with bank elements ('new' version) will be compared to the previous version of the model code without bank elements ('old' version). Changes to the IFMTFM by this thesis research only pertain to mercury modeling within the channel banks. Remaining model structure (chapter 4) was unchanged.

Mercury Modeling within 'Old' IFMTFM

Within the IFMTFM, the MERC4 model simulates inorganic Hg(II), methylmercury (MeHg), and the following three solids types: washload, CSS (coarse suspended solids), and bedload. Note that only the soluble forms of these Hg(II) and MeHg are assumed available for chemical transformation. The simulation of solids is critical because of the strong tendency of mercury to adsorb onto solids. The MERC4 model resulted in the coupling of chemical speciation and kinetics with the transport capabilities of the WASP4 modeling system. A brief overview of sediment transport

modeling within the IFMTFM was discussed in Chapter 3 of this document. Documentation of erosion and floodplain deposition modeling are available from Carroll et al. (in press). The details of these modeling processes are not here reviewed as they remain unchanged throughout the course of this research.

Additional details concerning mercury modeling within the IFMTFM are critical to the understanding of bank element functionality. MERC4 simulates methylation and demethylation reactions with a general equation for first-order kinetics (Martin, 1992):

$$\frac{\partial[C_P]}{\partial t} = f_{spec} f_{temp} K_{20}[C_R] \qquad \text{(Eq. 7-1)}$$

C_P is the concentration (mg/L) of product within a given model segment, free ionic (also referred to as dissolved or soluble) MeHg for methylation or free ionic Hg(II) for demethylation. C_R is the concentration of reactant (mg/L) within a given model segment, free ionic Hg(II) for methylation or free ionic MeHg for demethylation. The rate multiplier, f_{spec}, refers to the fraction of the total concentration of a mercury species (MeHg or Hg(II)) which is available for the reaction, the dissolved fraction in this case. Free ionic (~soluble) concentrations are considered to represent the bioavailable fraction of total mercury, with soluble fraction defined as the fraction able to pass through a 0.45 μm sieve. Dissolved fractions are based on measured partitioning constants (Bonzongo, 1996b) between dissolved and adsorbed phases, as indicated in Figure 4-2. Adsorption is a surface phenomena and is proportional to the amount of surface area available (Carroll, 1999). Given equal volumes of particles of differing diameter, the total surface area becomes greater the smaller the particle size; the rate of adsorption is indirectly related to the diameter of the adsorbent particles, an observation supported by data collected by

Miller et al. (1999). K_{20} values are the reaction rates (day^{-1}) as calculated from Carson River sediment samples (Carroll, 1999). To correct for water temperatures deviating from 20°C, the temperature multiplier f_{temp} is used, as governed by the following equation (Martin, 1992), where T is the ambient temperature in °C and Q_{10} values are constants calculated from Carson River sediment samples (Carroll, 1999):

$$f_{temp} = Q_{10}^{\frac{T-20}{10}} \qquad \text{(Eq. 7-2)}$$

Prior to the incorporation of bank elements within the IFMTFM, methylation and demethylation only occurred in channel bed sediments. Sediment data suggests that methylation and demethylation rates in bed sediments vary with respect to spatial location, as indicated in Table 7-1 (Carroll, 1999; Carroll et al., 2000). It is assumed that the chemical parameters that define each sample (pH being the only known parameter of significance) are not time dependant, so that no geochemical multipliers were used (Carroll and Warwick, 2001). In this study, the quotient of K_{20} (methylation) and K_{20} (demethylation) are referred to as the methylation / demethylation ratio (M / D).

Table 7-1. Spatial variability of M/D reaction constants within IFMTFM

Range	Segment Range,	Methylation		Demethylation	
(distance from CCG, km)	Bed / Overlying Water Column	K_{20} (day^{-1})	Q_{10}	K_{20} (day^{-1})	Q_{10}
0.00 - 79.25	274 - 448 / 1 - 175	0.0041	2.03	0.4483	2.32
79.25 - 95.40	449 - 513 / 176 - 240	0.0011	2.03	1.3291	2.32
95.40 - 115.00	514 - 546 / 241 - 273	0.0028	2.03	1.1753	2.32

The mass transfer of mercury from the channel bed sediments into the water column is calculated within the WASP5 code with equation 7-3, similar to Fick's law (Carroll and Warwick, 2001):

$$\frac{\delta M_i}{\delta t} = \frac{E_{ij} A_{ij} n_{ij}}{L_{ij} / n_{ij}} \left[\frac{f_{Di} C_j}{n_j} - \frac{f_{Di} C_i}{n_i} \right] \qquad \text{(Eq. 7–3)}$$

Equation parameters are defined as follows: M is mass (mg), t is time (days), A is interfacial area (m^2), C is the total chemical concentration (mg/L), f is the dissolved portion of the chemical available for diffusion, L is the characteristic mixing length (0.01 m; Thomann and Mueller, 1987), n is porosity, E is the diffusion coefficient (m^2/s), i is the 'to' segment, and j is the 'from' segment. The surface area (A) is dependant on the cross-sectional geometry and the hydraulic characteristics calculated in RIVMOD. The dissolved fraction of the chemical and concentration gradient for diffusion are determined in MERC4 based on the first-order kinetic reactions for methylation and demethylation.

The 'old' IFMTFM model is calibrated on three parameters for mercury, in order to best-fit limited water column samples for MeHg and inorganic Hg(II). Recall the assumed calibration relationships for inorganic Hg(II) and MeHg within channel bank sediments, as shown in equations 4-1 and 4-2 in chapter 4 and earlier in this chapter.

Mercury concentrations within eroded bank sediments remain constant over time, although concentrations are spatially variable based on the λ_1 and λ_2 calibration parameters. The calibrated methylmercury function predicted methylmercury bank concentrations over two orders of magnitude higher than the methylmercury bank data collected under conditions of near-zero flow (Carroll, 1999). The samples, from October 1994, were collected high up on the bank at the estimated point of river contact during spring floods. Examination of water column data shows that, unlike other systems, increased discharge does not always cause a dilution in MeHg. Instead, an increase from low to medium flow causes a significant increase in MeHg water column concentrations. These results strongly suggest that given medium flows, bank erosion, and not diffusion,

acts as the principal pathway for MeHg into the water column. This trend of MeHg increase with increasing flow begins to reverse when flows go from medium to high conditions. The resulting dilution at higher flows suggests that the availability of MeHg from erosion of the upper bank is limited. An additional calibration parameter, a threshold depth (H_T) above which MeHg bank concentration are taken as zero, was used to account for this observed dilution. Underlying this assumption was the idea that high flow rates are too infrequent and short in duration to allow anaerobic microbes (performing the methylation) to develop in the upper portions of the channel banks. This same limitation is not observed for inorganic mercury (Carroll, 1999). Modeling MeHg concentrations as constant along the vertical banks and over time is not representative of field conditions, which depend on microbe populations and therefore moisture levels.

The IFMTFM includes three additional calibration parameters for the erosion and sediment transport functions. These parameters, ψ_1, ψ_2, and ψ_3, remain unchanged throughout this research and are not further discussed. Detailed information regarding these parameters is available from Carroll et al. (2002).

Mercury Modeling within 'New' IFMTFM

The functionality of the new bank elements within the IFMTFM is similar to the bed elements. The 'new' IFMTFM includes both bed elements and bank elements, whereas only bed elements were included in the 'old' IFMTFM. Methylation and demethylation occur within bank elements, resulting in temporally-variable MeHg concentrations not present in the 'old' IFMTFM, in which bank MeHg was only allowed to vary with respect to spatial location according to the λ_2 calibration parameter. The parameters used to define bed elements remain unchanged from the 'old' IFMTFM, and

bed MeHg concentrations remain dynamic. Diffusion from contacted bank elements to the water column is modeled using the same parameter values and diffusion equation as the bed elements (equation 7-3).

Bank elements differ from bed elements because bank elements possess two additional features. Bank elements can erode, introducing mercury-laden sediment to the water column. This erosion process is contained within the 'old' model as well; the erosion functions and parameter values (ψ_1, ψ_2, ψ_3) remain unchanged from those used in the 'old' model. Within the 'new' version, however, mercury concentrations adsorbed to erodable sediment and present within bank pore water are not constant, but rather continuously updated based on methylation and demethylation within bank sediments and equilibrium phase portioning (dissolved and adsorbed). Advection is also modeled as a potential means for mercury transport from bank elements to the water column. Advection is not considered for bed segments.

Bank element volumes are dynamic and equivalent to the saturated portion of the channel bank. Recall the bank elements represent the vertical portion of the assumed channel cross-sectional geometry, above the low-medium transition slope in Figure 3-1. The saturated heights of bank elements are assumed equal to the 4-day moving average of the water surface elevation within the adjacent water column elements (Figure 7-3). Four days is the length of time required for methylating microbial populations to establish themselves and attain maximum methylation rates (Dr. Mark Hines, personal communication). Figure 7-3 shows a typical RIVMOD cross-section; note that the water surface elevation, as predicted by RIVMOD, at the current model time step is likely not equal to the 4-day moving average water surface elevation. If streamflow (and hence

river stage) is continually rising over the 4-day averaging window, the average water surface elevation will be lower than the current river stage; if streamflow (and hence river stage) is continually falling over the 4-day averaging window, the average water surface elevation will be higher than the current river stage. For a given model segment, between two adjacent stations, the saturated height is computed as the arithmetic average of the saturated heights at the stations on either end of the segment. Due to symmetry, bank volume (saturated portion of bank element) is computed as the product of this average saturated height, the segment length (distance between stations), and the assumed active depth into the channel bank of 10 cm (equal to active depth for bed elements), multiplied by a factor of two (left and right bank).

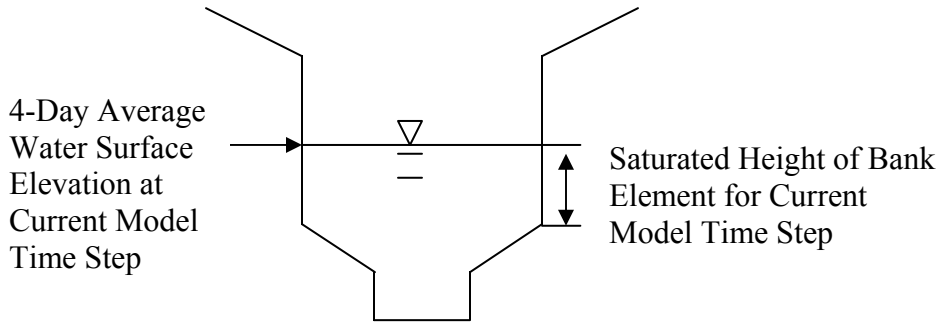

Figure 7-3. Relationship between temporally-averaged RIVMOD stage and bank saturation height

Predicted river stage for each model segment potentially changes with each 60-second IFMTFM time step. The hydrodynamic (RIVMOD) portion of the IFMTFM is driven by daily flow values easily obtained from the USGS gages at Carson City, Fort Churchill, Truckee Canal, and Lahontan Dam. Mean daily flow values are assigned at time midnight for each day. Streamflow values do not remain constant throughout the ensuing 24-hour period, but rather are linearly interpolated from the values for consecutive days at each model time step. This approach ensures that streamflow varies

gradually throughout the model domain. With flows updated for each time step, RIVMOD-predicted river stage also changes with each time step. The 4-day moving average for water surface elevation also therefore changes with each model time step. Bank segment volumes (saturated portion of channel banks), however, are updated only at hourly intervals using this 4-day moving average, in the interest of minimizing computation time without a loss of accuracy.

Within the saturated portion of a given channel bank segment, methylation and demethylation occurs at a prescribed rate, based on model calibration to be discussed. The portion of the channel bank contacted by the water column is subject to loss of mercury through diffusion and erosion processes. When bank element volumes are updated hourly, they are assumed to achieve instantaneous equilibrium with regard to volume and methylation rate. During a receding hydrograph, river stage is falling and bank element volume is decreasing. At this instant, the concentration of both total and soluble MeHg and Hg(II) in the channel bank segment will not change. However, the soluble mercury present in the now-dry portion of the bank segment (product of change in bank segment volume, MeHg or Hg(II) concentration, and fraction of total Hg that is soluble) must go somewhere if solute continuity is to be preserved. This soluble quantity of MeHg and Hg(2+) is therefore introduced to the adjoining water column segment through advection. In the interest of completeness, advection and diffusion from the channel banks are modeled. However, it is noted that erosion remains the dominant mechanism for the introduction of mercury to the water column.

Methylation within saturated channel bank elements requires a source of inorganic Hg(II) within the channel banks. As in the ‘old’ version of the IFMTFM code, the

concentration of Hg(2+) within the channel banks is assumed to be temporally constant and spatially-variable between segment, based on calibration to the model parameter λ_1:

$$[Hg_{in}]_{bank} = \frac{\lambda_1}{S_0^{0.5}} \quad \text{(Eq. 4-2)}$$

The value of λ_1 does not change from the 'old' version to the 'new' version. Model calibration is performed on the inorganic Hg(II) data set collected on May 16, 1994 under medium flow conditions of 600 cfs (27 cms). Model calibration is performed to achieve a simple visual best-fit through the limited number of sample data points. The calibration for λ_1 is shown in Figure 7-4, with a calibrated value of λ_1 = 1,900 μg-Hg^{2+} / Kg-Soil. Model verification is shown in Figure 7-5 for high flow conditions (1,960 cfs, 55.5 cms) on June 10, 1995 and in Figure 7-6 for low flow conditions (62 cfs, 1.76 cms) on June 16, 1994. In these three figures, the curve fit through the data points is the same for the 'old' and 'new' versions of the code, as no modifications were made with regard to the simulation of inorganic Hg(II). MeHg data is available for these same three data sets and is later used for MeHg calibration and verification of the 'new' IFMTFM. Note that all concentration data for model calibration and verification are mercury concentrations in the water column. For reader reference, the three farthest downstream data points in the high and low flow data sets; and the two farthest downstream in the medium flow data set were collected in Lahontan Reservoir at the river delta, the narrows, and the dam.

With a constant source of total inorganic Hg(II) within the channel banks, the soluble fraction of Hg(II) is determined based on the sediment composition and the equilibrium partitioning coefficients for the coarse suspended sediment (diameter > 0.063 mm) and washload (diameter < 0.063 mm) particle sizes. The soluble fraction of Hg(II) is

considered as the bioavailable fraction for methylation by sulfate-reducing bacteria. As previously discussed, methylation and demethylation are modeled according to the first-order kinetic equation:

$$\frac{\partial[C_P]}{\partial t} = f_{spec} f_{temp} K_{20}[C_R] \qquad \text{(Eq. 7-1)}$$

Methylmercury is created within the saturated channel bank elements. With a higher fraction of fine sediment within the channel banks as compared to the channel bed, the reaction rates are not assumed to be the same. Instead, the K_{20} reaction rate for methylation is used as a new calibration parameter. Since methylation and demethylation reactions occur simultaneously, the model is calibrated on the net methylation rate, or rather the methylation / demethylation ratio (M / D = K_{20} (methylation) / K_{20} (demethylation). With this in mind, the demethylation rate within channel banks is taken

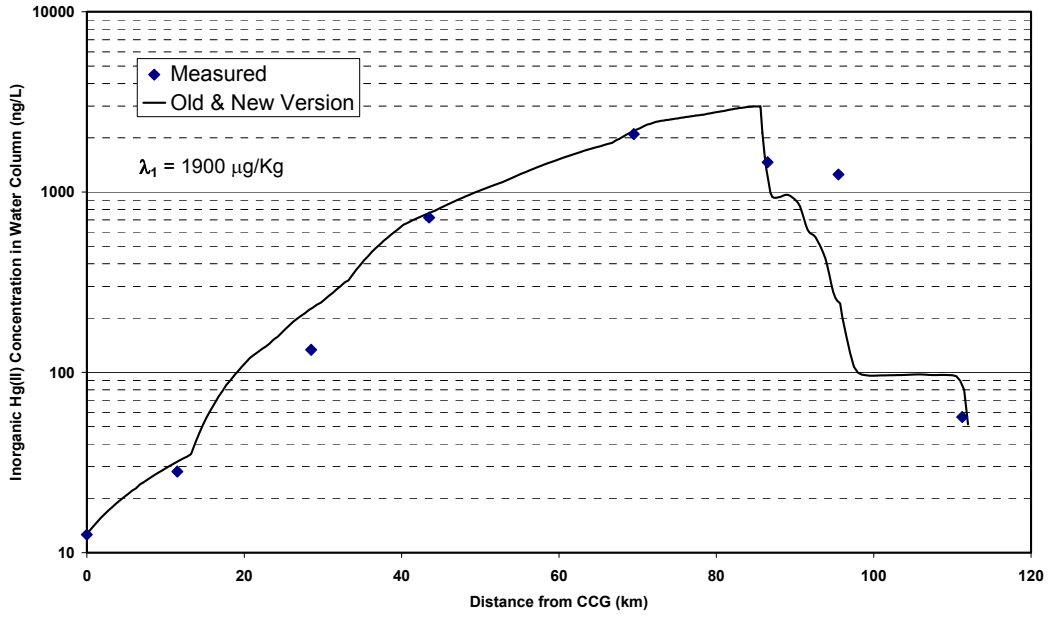

Figure 7-4. Medium flow (May 16, 1994) IFMTFM calibration for inorganic Hg(II) (parameter λ_1) in channel banks for 'old' and 'new' code versions

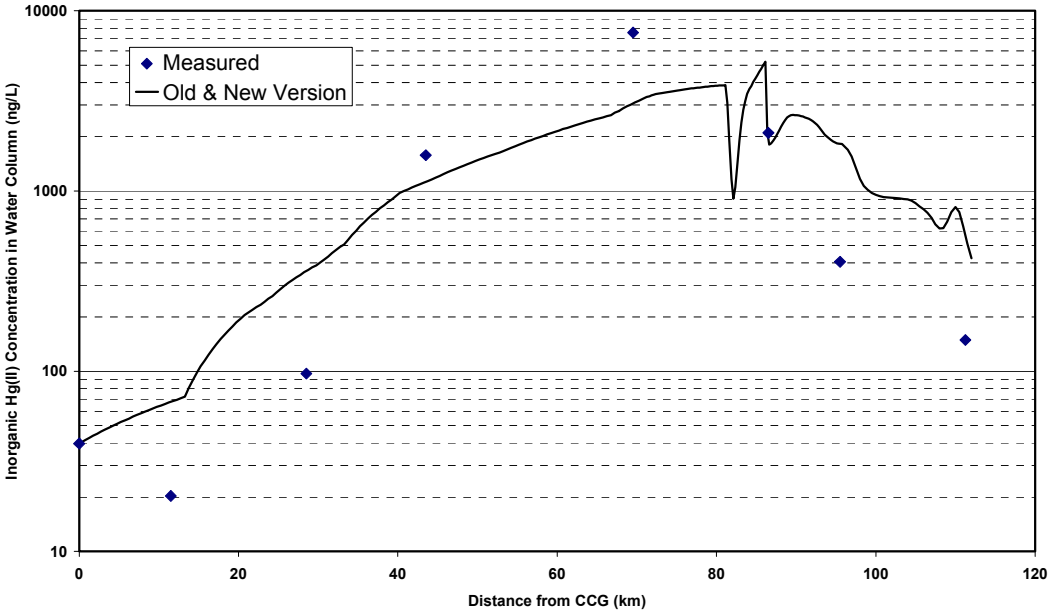

Figure 7-5. High flow (June 10, 1995) IFMTFM verification for inorganic Hg(II) (parameter λ_1) in channel banks for 'old' and 'new' code versions

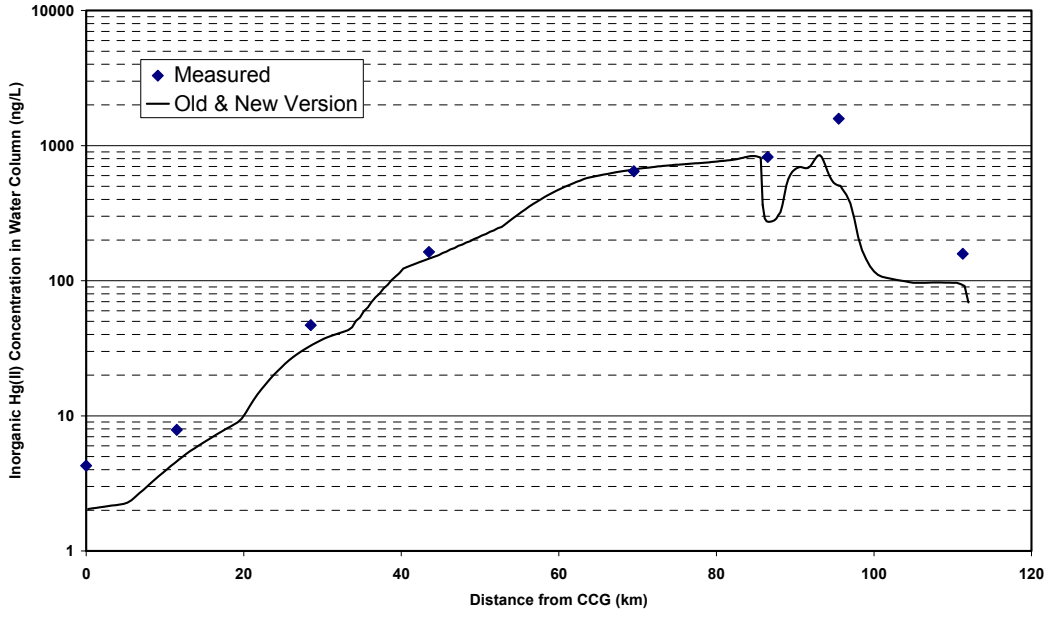

Figure 7-6. Low flow (June 16, 1994) IFMTFM verification for inorganic Hg(II) (parameter λ_1) in channel banks for 'old' and 'new' code versions

as equal to the demethylation rate within bed sediments, and the bank methylation rate is varied and calibrated on. In discussing the required changes to the WASP input data file for the 'new' version of the IFMTFM code, it was mentioned that input data limitations allow a maximum of four separate methylation / demethylation rates based on segment classifications. In the 'old' input file, the methylation and demethylation rates varied as indicated in Table 7-2. Note that methylation and demethylation are not simulated in the water column, as conditions are no sufficiently anoxic.

Table 7-3 indicates the rate coefficients used in the 'new' version. The addition of bank segments to the IFMTFM and the allowance for methylation and demethylation within these segments requires specification of the reaction rate constants within bank sediments. Specification of K_{20} rates for bank segments in the 'new' code requires the removal of one of the previous four K_{20} values; K_{20} values for methylation and demethylation within the reservoir are therefore taken as the average of values previously specified for the upstream and downstream reservoir segments. As indicated in Table 7-3, the demethylation rate is held constant at the value used for river bed segments, and the bank methylation rate is calibrated to match observed water column samples for MeHg.

The calibrated value for the methylation K_{20} rate is 0.014 day^{-1}. This value is roughly three times greater than methylation rates observed in bed sediments, although it is noted that the demethylation rate was held constant at the value used for river bed segments. The net methylation rate, as represented by the M / D ratio is greater for bank sediments than bed sediments according to this calibration. This observation can be explained, at least in part, by the larger percentage of fine sediment within the channel banks, as compared to the channel bed. Based on field data (Heim and Warwick, 1997),

Table 7-2. Segment classification for M/D reaction constants in 'old' IFMTFM

		Methylation		Demethylation	
WASP Element Type	Model Segment Range	K_{20} (day^{-1})	Q_{10}	K_{20} (day^{-1})	Q_{10}
Water Column	1 - 273	0.0000	0.00	0.0000	0.00
River Bed	274 - 448	0.0041	2.03	0.4483	2.32
Upstream Reservoir	449 - 513	0.0011	2.03	1.3291	2.32
Downstream Reservoir	514 - 546	0.0028	2.03	1.1753	2.32

Table 7-3. Segment classification for M/D reaction constants in 'new' IFMTFM

		Methylation		Demethylation	
WASP Element Type	Model Segment Range	K_{20} (day^{-1})	Q_{10}	K_{20} (day^{-1})	Q_{10}
Water Column	1 - 273	0.0000	0.00	0.0000	0.00
River Bed	274 - 448	0.0041	2.03	0.4483	2.32
Reservoir Bed	449 - 546	0.0020	2.03	1.2522	2.32
Channel Banks	547 - 819	0.014*	2.03	0.4483	2.32

* calibration parameter

the following sediment descriptions are used in the IFMTFM model: river bed segments are modeled as 50% fine (diameter < 0.063 mm) and 50% coarse (diameter > 0.063 mm); river bank segments are modeled as 70% fine and 30% coarse; and reservoir bed and bank segments are modeled as 40% fine and 60% coarse (banks no longer distinguishable from bed). For Carson River sediments, the larger surface area of fine sediments results in increased mercury sorption (Miller et al., 1999), as indicated by the larger values shown in Figure 4-2. This higher sorption kinetic for fine particles results in a lower dissolved fraction of total mercury. Despite total mercury concentrations in the channel banks (higher percentage of fine sediment) typically one order of magnitude larger than along the channel bed, the dissolved fraction, or that fraction assumed bioavailable for methylation and demethylation reactions, is lower than in the channel bed sediments. In order to generate the amount of MeHg in the channel banks that is needed to match the water column observations, a higher methylation rate is therefore needed for input to the model. Although supporting data is not available, the calibration results are able to be justified. Also, the same result could have been achieved by lowering the demethylation rate.

Comparison of 'Old' and 'New' IFMTFM Code for MeHg Modeling

The 'old' version of the IFMTFM code required calibration on three parameters: λ_1 for inorganic Hg(II) in the channel banks, λ_2 for MeHg in the channel banks, and the threshold depth (H_T) for MeHg in the channel banks. By creating the bank elements within the 'new' IFMTFM code, methylmercury concentrations in channel banks are actively simulated and continuously updated by the model. Rather than calibrate on λ_2 and H_T, the model is only calibrated on the K_{20} rate for methylation in the channel banks. For the 'new' code, the model is calibrated using the medium flow data set (May 1994; Q = 600 cfs, 27 cms), as shown in Figure 7-7. Model verification uses the high (June 1995; Q = 1,960 cfs, 55.5 cms) and low (June 1994; Q = 62 cfs, 1.76 cms) flow data sets, as shown in Figures 7-8 and 7-9. Before the code modifications, the medium flow data set was used for λ_2 calibration (λ_2 = 4.57 μg-MeHg / Kg-soil), and the high flow data set was used for H_T calibration (H_T = 1.00 m). To facilitate comparison, IFMTFM results for 'old' and 'new' versions of the code are shown in each figure.

The environmental concerns regarding methylmercury underscore the importance of accurately modeling this species within the Carson River IFMTFM model. Channel banks have higher concentrations of mercury associated with sediment than those found within the channel bed (Miller and Lechler, 1998). Mercury is, of course, not uniformly distributed throughout the system; instead, bank concentrations vary over three orders of magnitude with localized "hot spots of contamination" (Miller and Lechler, 1998).This thesis improves the ability of the IFMTFM to simulate processes which control MeHg concentrations within channel banks. Bank erosion is then a controlling factor for water

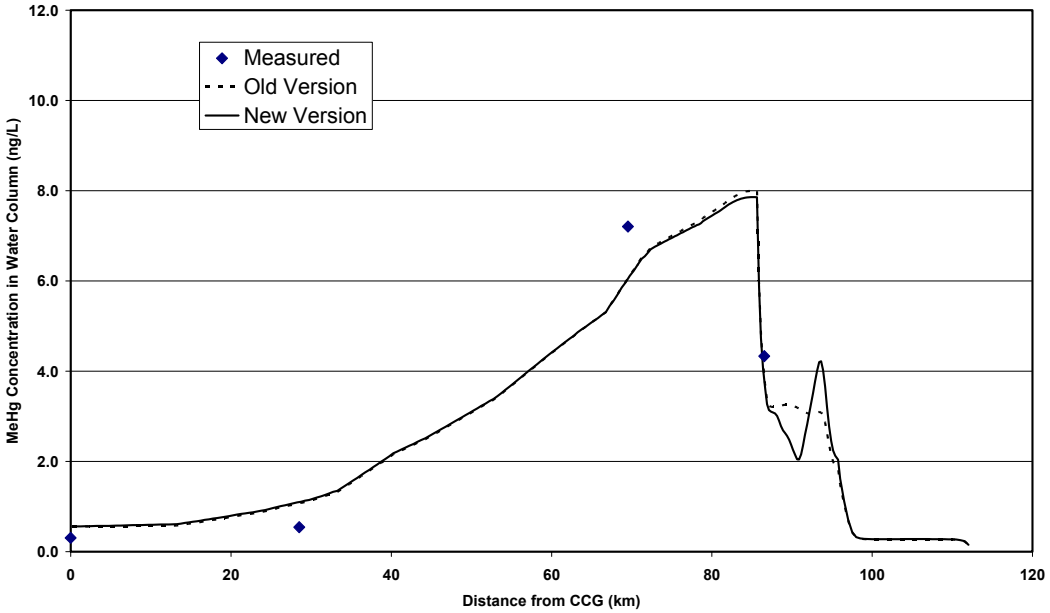

Figure 7-7. Medium flow (May 16, 1994) IFMTFM calibration for MeHg (λ_2) in channel banks ('old' code version) and K_{20} methylation rate in channel banks ('new' code version)

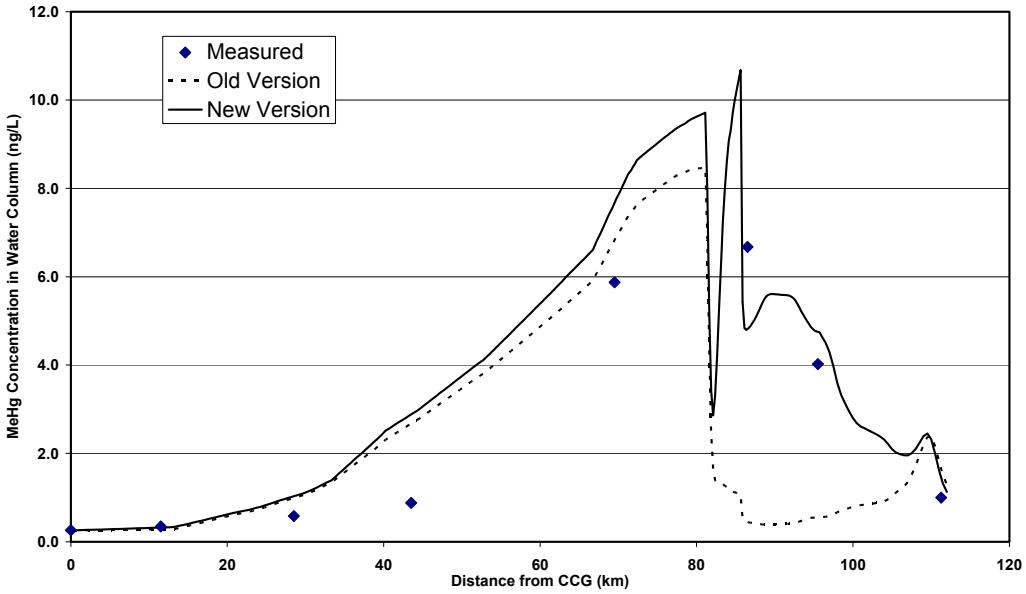

Figure 7-8. High flow (June 10, 1995) IFMTFM calibration for MeHg threshold height (H_T) in channel banks ('old code version) and verification for MeHg in channel banks ('new' code version)

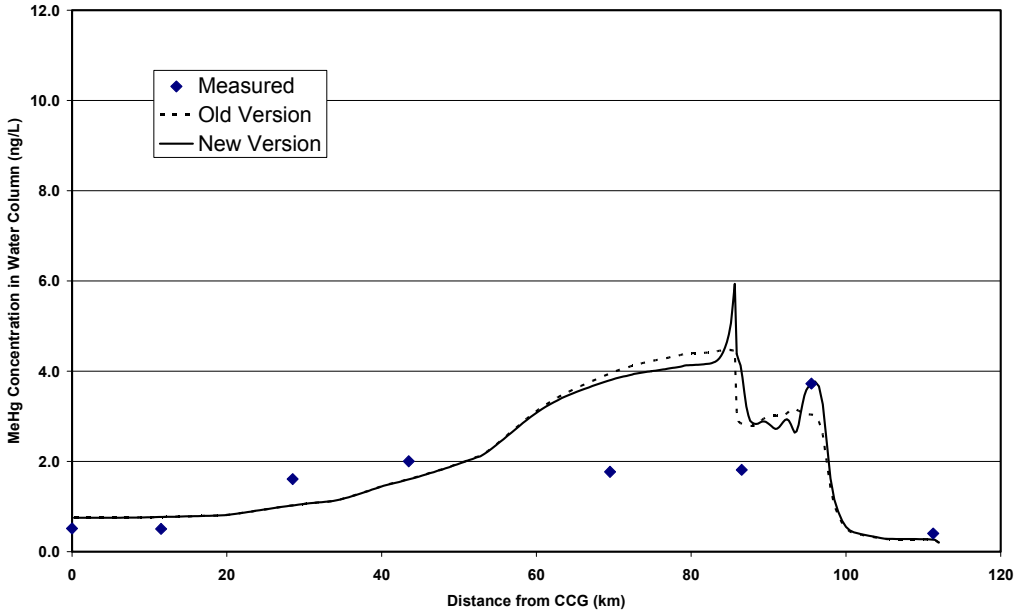

Figure 7-9. Low flow (June 16, 1994) IFMTFM verification for MeHg in channel banks for 'old' and 'new' code versions

column concentrations of mercury because of the high affinity of mercury for particulate matter.

Comparing the calibration and verification of the 'old' and 'new' code versions for water column MeHg concentrations, the 'new' code is clearly superior for matching observed concentrations of MeHg within Lahontan Reservoir, based on visual inspection of the respective model output for distances greater than 85.74 km (model segment 201) downstream of CCG. The ability of the IFMTFM to duplicate these reservoir data points is particularly important given the bioaccumulation processes occurring within the reservoir. With respect to data points between CCG and the reservoir, matching of data points between the two versions is comparable for the medium flow data set (Figure 7-7), improved by the 'new' version for the low flow data set (Figure 7-8), and diminished by the 'new'code for the high flow data set (Figure 7-9). The usefulness of a quantitative

comparison is limited by the small number of data points to which the calibration is being fit. It is additionally noted that the MeHg concentration peak at kilometer 85 in Figure 7-9 is not a model error, but rather the result of three factors: high mercury concentrations in bed and bank sediments, based on equation 4-2 and the small channel slope in the deltaic region; high reservoir stage, associated with previous high flows, and reservoir contact with bank sediments caused by this backwater effect; and high opportunity for diffusion of MeHg into the overlying water column because of low flow velocity.

Measurement error associated with the mercury sample points does not impact the perceived fit between sample data points and the IFMTFM model. Error bars for the total MeHg sample data were determined from water column samples taken on June 16, 1994 (Table 7-4, points in Figure 7-9). Samples were taken in triplicate at six locations along the Carson River mainstem (including the delta) and two locations within Lahontan Reservoir. The average error (standard deviation) for samples collected along the river is 0.056 ng/L, a value not discernable when applied to sample data points in Figures 7-7, 7-8, or 7-9. Only the data point collected at Fisherman's Point within the reservoir demonstrates a high sample standard deviation, likely the result of high sediment concentrations (poor sample uniformity) associated with a previous period of high flow.

A qualitative comparison has been considered, but more important is the ability of the 'new' code to better simulate natural processes occurring in the field. During the upgrade from 'old' version to 'new' version, no changes were made to sediment composition (in terms of percent fines and percent coarse, within channel banks or channel bed), which determine the fraction of adsorbed versus soluble and bioavailable mercury. Additionally, no changes were made to the erosion functions or values of

Table 7-4. Error associated with sample MeHg data points

Distance from CCG (km)	Mean Total MeHg* (ng/L)	Standard deviation* (ng/L)
0	0.512	0.054
11	0.505	0.067
28	1.607	0.087
44	2.001	0.074
69	1.786	0.031
87	1.813	0.023
95	3.725	1.090
111	0.400	0.033

* computed from 3 samples at each location

calibration parameters for erosion. IFMTFM parameters which remained unchanged between 'old' and 'new' code versions are summarized in Table 7-5. The modeling of MeHg within channel banks of the Carson River was changed by this thesis research. A comparison between the 'old' and 'new' versions of the IFMTFM, as related to modeling of bank MeHg, is shown in Table 7-6.

Table 7-5. Parameters unchanged between 'old' and 'new' IFMTFM versions

Channel bed:	- no erosion (vertical equilibrium) - dynamic MeHg concentrations - Hg(II), MeHg diffusion to water column
Channel banks:	- lateral bank erosion - Hg(II) constant over time - Hg(II) varies spatially: $[Hg_{in}] = \lambda_1 / S_0^{0.5}$
General:	- sediment composition unchanged - sediment transport parameters unchanged - partitioning coefficients unchanged

Table 7-6. Comparison of channel bank MeHg modeling in 'old' and 'new' IFMTFM

old' version	new' version
- MeHg temporally constant	- MeHg varies temporally with dynamic zone of active methylation
- MeHg varies spatially: $[Hg_{MeHg}] = \lambda_2 / S_0^{0.5}$	- MeHg varies spatially based on changing river stage and bank contact
- threshold depth (H_T) for MeHg	- no threshold depth for MeHg
- no diffusion of Hg to water column	- diffusion from contacted banks
- no advection of Hg water column	- advection during receding hydrographs
- calibration on λ_2 and H_T	- calibration on bank K_{20} methylation rate
- MeHg available to water columnupon bank contact	- MeHg available following 4-day microbial acclimation time

The ‘old’ version of the IFMTFM code was calibrated to MeHg concentrations in the bank, which were allowed to vary between segments but not over time. Given that the methylation and demethylation reactions are microbially-mediated, MeHg concentrations cannot be static through time. Mercury methylation is stimulated if soils are fully saturated and anoxic conditions are achieved (Gilmour and Henry, 1991; Porvari and Verta, 1994). High flow rates are too infrequent and short in duration to allow anaerobic microbes to actively methylate mercury in the upper portions of the bank sediments throughout the year. This said, there is not, however, a threshold height above which MeHg within channel banks will always be zero, as assumed by the ‘old’ code structure. The implications of this change are seen in Figure 7-10, a flood simulation for May and June of 1995 during which all flows contacted the banks above the 1.00-meter threshold depth. In the ‘old’ version of the code, the threshold height for MeHg introduction into the water column results in a dilution effect (no additional MeHg available as flows rise). The ‘new’ code version allows MeHg concentrations to be created and eroded from the upper channel banks; additionally, the time lag for microbial response (as captured by the use of the 4-day averaging window for the height of bank saturation) is evident compared to the flow hydrograph. Sample data for MeHg is not available for this time period.

For comparison, a simulation from May and June of 1994 is also included as Figure 7-11. Here, all flows have a depth less than the 1.00-meter threshold depth. The ‘old’ code version has MeHg immediately available for input to the water column as flow rises. The ‘new’ code shows a delay, following flow rising, in creating the MeHg within the channel banks and subsequent input into the channel. MeHg concentrations within contacted portions of the channel banks, previously modeled as susceptible only to

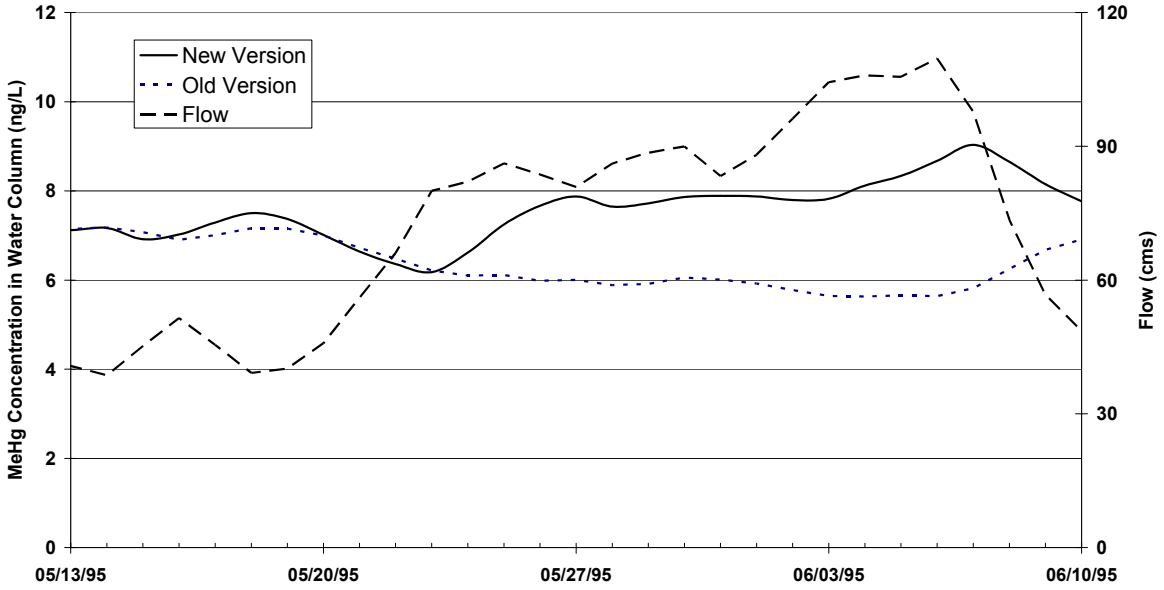

Figure 7-10. IFMTFM simulation for May / June 1995 flood event at Fort Churchill (model segment 140), illustrating MeHg dilution effect of threshold height H_T in 'old' code version

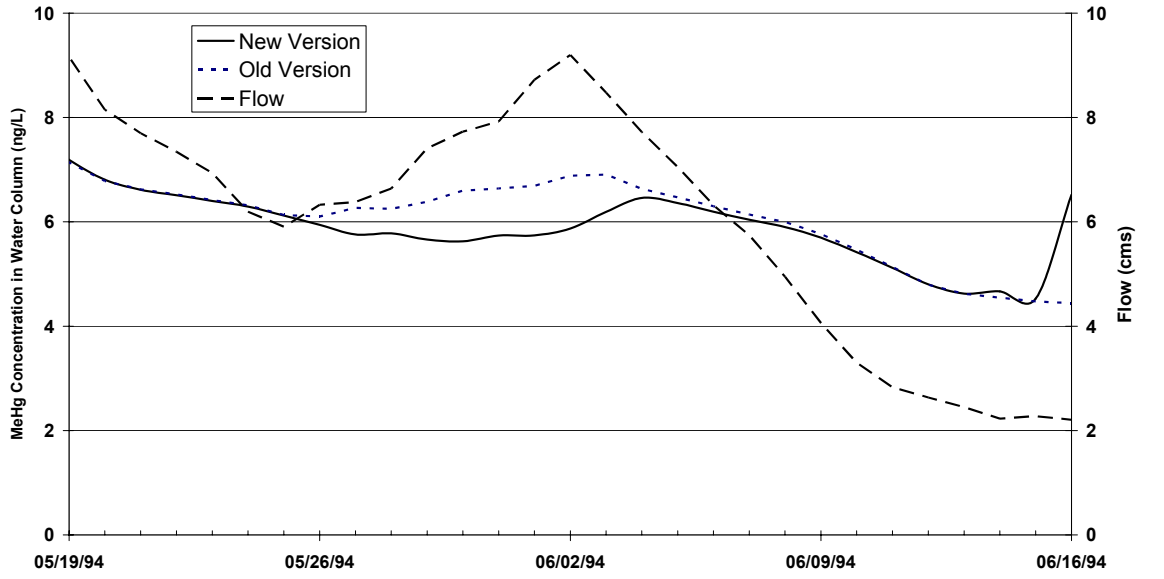

Figure 7-11. IFMTFM simulation for May / June 1994 flows at Fort Churchill (model segment 140), demonstrating time lag for MeHg response in 'new' code version

erosion, are also not temporally constant in the 'new' code. In this regard, the 'new' IFMTFM code is superior. Bank element volumes are dynamic dependent on the time-history of river stage. Methylation and demethylation processes actively occur within saturated portions of the channel banks, imparting dynamic MeHg concentrations within channel banks. MeHg concentrations now display a dependence on soil moisture conditions, as evidenced by previous field data (Figure 4-3), within both channel bed and channel bank sediments.

Contacted portions of the channel banks are no longer subject only to erosion, but the 'new' code also allows for mercury introduction to the water column through diffusion; advection of mercury to the water column is modeled during periods of a receding hydrograph. Though advection and diffusion are not the primary contributors to water column mercury concentrations (erosion), the processes no doubt do occur in the field. In addition to improving the model capabilities to simulate field processes, the 'new' code reduces the number of calibration parameters for mercury from three to two and provides an improved match to in-channel MeHg observations.

The Next Step for the IFMTFM Model

While this thesis research has addressed one IFMTFM shortcoming by adding the ability of the model to simulate dynamic methylmercury concentrations within channel banks, mercury modeling within the IFMTFM continues to have room for improvement. Two specific opportunities will be briefly discussed.

Bioavailable mercury for methylation and demethylation reactions is presently taken as equivalent to the soluble (or dissolved) fraction of total mercury. The soluble fraction is computed within MERC4 through the use of calculated partition coefficients (K_d values). Partitioning coefficients were measured only for the washload fraction of

sediment (the fine sediment) and were computed for the coarse suspended solid and bedload fractions by making use of average particle diameters and the washload results (Bonzongo, 1996a). From the original "grab" sample collected just below the water surface of the Carson River, the washload fraction and dissolved fractions were functionally defined as the sample fractions captured by a 0.45 μm sieve and passing through the sieve, respectively. The partitioning coefficient (L / mol) was calculated for MeHg and Hg(II) using equation 7-4, where $[Hg_P]$ is the concentration of mercury bound to washload particles in the sample, $[Hg_D]$ is the concentration of dissolved mercury in the sample, and [Solid] is the concentration of the solid constituent in molar units, assuming the solids are composed of iron hydroxide (FeOOH):

$$K_d = \frac{[Hg_P]}{[Hg_D]\,[Solid]} \qquad \text{(Eq. 7-4)}$$

A sediment density of 1.9 kg/L is used by the model, as computed from a measured sediment dry bulk density of 1.6 g/cm^3 (Miller et al., 1999) and assuming a porosity of 0.30 (Carroll, 1999). The IFMTFM predicts the dissolved and adsorbed fractions of MeHg and Hg(II) using this sediment characteristic and the computed K_d values. These fractions are then applied to the total mercury concentrations within bed and bank segments to determine the amount of soluble MeHg available for methylation and the amount of soluble Hg(II) available for demethylation. Methylation and demethylation kinetics then govern the dynamic concentrations of both species within bed and bank segments throughout the model domain. The modeling approach therefore makes use of the assumption that soluble methylmercury and soluble inorganic mercury is the only fraction of total mercury available to the methylating and demethylating microbial populations. More research is ongoing to determine the validity of this assumption.

Reasonably, it can be assumed that the microbes are not floating in solution but rather are themselves attached to the sediment grains, in which case they may be able to make use of some portion of adsorbed mercury as well. Again, this may explain the need to use a significantly higher methylation rate in bank elements.

After the incorporation of bank elements into the IFMTFM, one other problem also emerged. This is the problem of limited data. Data available for inorganic mercury concentrations within the channel banks along the Carson River are highly variable for multiple samples at a given site and spatially along the river (Miller and Lechler, 1998). The current IFMTFM version is calibrated to the methylation rate in the channel banks, and the model predicts spatially-variable and time-dependant MeHg concentrations. However, no sample data is available to verify these model predictions. To facilitate such a comparison, additional data on the distribution of mercury in channel banks is needed. While the model predictions are in good agreement with water column data for MeHg and Hg(II), the question remains whether the model predictions are good for the right reasons. Bank elements each possess unique Hg(II) concentrations, but doubts remain as to whether the λ_1 calibration parameter is the best modeling approach to capture the spatial variability.

CHAPTER 8
COMPARATIVE ANALYSIS: RIVMOD VERSUS FESWMS MODULE OF SMS

When the SMS model was selected as the surface water model for this project, two distinct end-products were envisioned. The first was to develop a simple relationship, to relate stage in the channel to water table level within the bank. This thesis research has concluded that the water table response to stage changes is approximately instantaneous. Given this rapid response time, the assumption is made that the free surface elevation in the channel is equal to the phreatic surface in the channel bank immediately adjacent to the channel. The saturated portion of the erodable face of the channel bank varies temporally with the river stage, and the two water surface elevations are equivalent. To incorporate this relationship into the functionality of the new IFMTFM bank elements, microbial response time for methylation and demethylation reactions was also necessarily considered. Laboratory data suggest a time period of 4 days is needed for the methylating population to become established and attain peak reaction rates (Dr. Mark Hines, personal communication). Because the M/D ratio in the channel banks is a calibration parameter, rates for methylation and demethylation reaction rates (K_{20}) values were not allowed to vary with time. Instead, the calibration parameter was taken as the peak M/D ratio, and the height of the saturated (actively methylating) portion of the channel banks is dynamically computed from the four-day moving average of the water surface elevation in the channel and the channel geometry used in RIVMOD.

The second end-product is a comparative analysis between RIVMOD predictions and SMS predictions. For the modeled Scout Camp reach, a comparison between the two

models was sought for flow depths and mean velocity to see if the simplified channel geometry and 1D nature of RIVMOD resulted in consistently high or low predictions relative to a more detailed and calibrated model. The paucity of surveyed water surface elevation data prevented calibration of the SMS model. Limitations within the SMS model also mandated the assumption of a temporally-constant head loss through the SMS model domain of 1.99 meters, irrespective of flow magnitude or antecedent flow conditions. Antecedent flow conditions are also excluded based on the model's inability to simulate element re-wetting (as would occur for rising portions of a dynamic streamflow hydrograph) without loss of numerical stability. The FESWMS-2DH model mesh created using SMS software is clearly not the accurate predictor of river stage that was originally envisioned before the start of this thesis research. The accuracy of SMS stage predictions over time cannot be quantified, as only a single data point is generated from surveyed water surface elevation data in the vicinity of the wells. Through regression analysis, shown in Figure 6-27, the observed water surface elevation at the well transect was estimated as 1252.30 meters (NAVD 88) for the streamflow of 173.8 cfs on March 9, 2001. Comparing this field observation to the rating curve prediction from SMS model results, the SMS model prediction is 15 centimeters high, at an elevation of 1252.45 meters for the water surface. A comparison between SMS and observed water surface elevations in the channel is not available for any other time during the 2001-2002 study of the Scout Camp reach of the Carson River. With these considerations in mind, the comparative analysis will still be conducted, although the limitations of the analysis are noted in advance.

Comparison of Channel Geometry along the Well Transect

In general, RIVMOD is based on a generalized channel shape (figure 3-1) and data interpolated from topographic maps, and FESWMS-2DH (SMS) is based on precise data collected using GPS. A visual comparison of the channel cross-section (at the location of Well 1) between the two models is shown in Figure 8-1. The figure is plotted by normalizing all elevations with respect to the minimum bed elevation along the respective transect. The SMS transect is extracted directly from the SMS mesh. The geometry of the main channel (below floodplain stage) in RIVMOD utilizes a simplified cross-sectional shape and average values for each geometric parameter (as indicated in Figure 3-1) and these parameters do not vary spatially. It is therefore not surprising that the model cross-sections differ in shape. In particular, the main channel width used in SMS (52.61 m) is greater than the channel width used by RIVMOD (45.50 m) by 7.11 meters, and the channel bank height in RIVMOD (3.27 m) is significantly larger than the average channel bank height in SMS (2.30 m). One potential opportunity for IFMTFM improvement would involve the collection of higher resolution cross-section data and the incorporation of this data into RIVMOD segment geometry. The Manning roughness coefficient for the main channel is equal to 0.045 within both models. This value was selected to properly calibrate the 1D RIVMOD model, but it likely high for actual field conditions. No data is available regarding the setting of this parameter, and lower values within SMS are not tested based on time constraints and model run time requirements.

Steady-State Comparisons for Velocity and Depths of Flow

Model output for velocity and depth of flow were compared for the SMS and RIVMOD models over the applicable range of the SMS model. While RIVMOD includes the ability to simulate flows spilling onto the floodplain, this capability is not available to

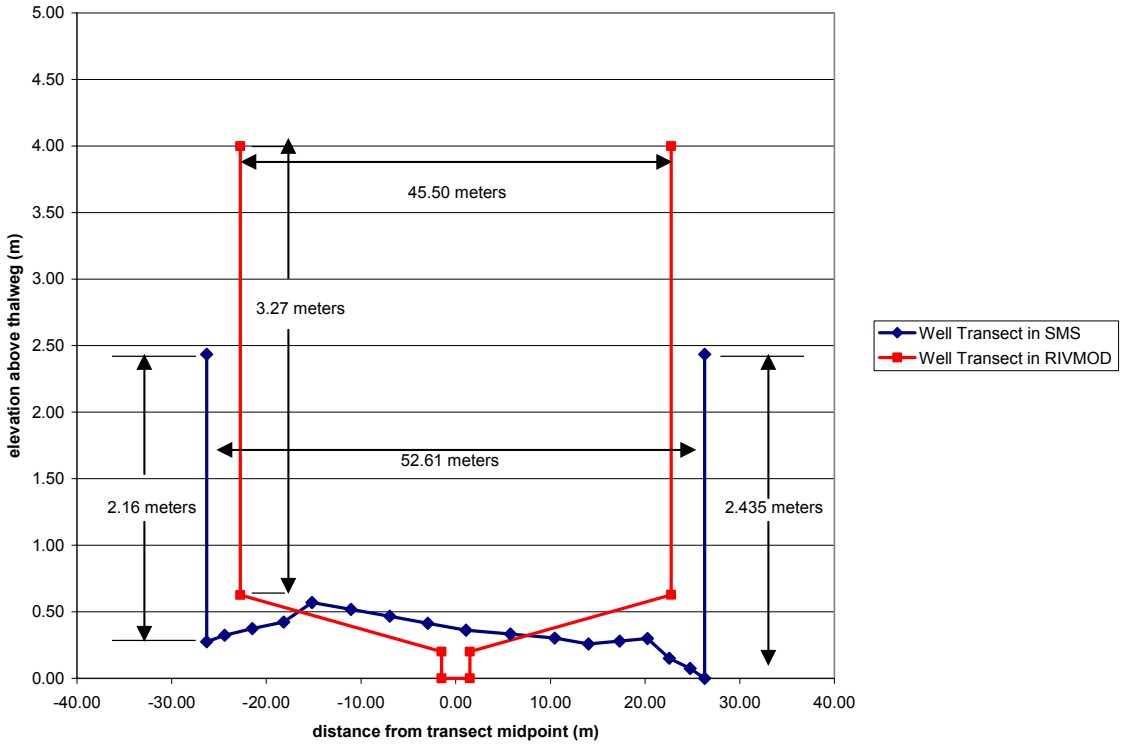

Figure 8-1. Comparison of channel geometry at well transect for SMS and RIVMOD

SMS because of the required inclusion of vertical wall model boundaries. At the well transect in SMS, channel banks on both sides of the channel are characterized by vertical walls (Figure 5-3). These walls extend upward indefinitely, but the surveyed elevation for the top of the channel bank nearest the wells (1254.15 meters,NAVD 88) is used to indicate the top of the channel banks in Figure 8-1. Based on the rating curve analysis (Figure 6-34) and associated discussion found in chapter 6 of this thesis, recall that the applicable flow range for the SMS model is 1.91 cms (67.5 cfs) to 109.6 cms (3871 cfs). The rating curve equation was developed using 0.25-meter head increments along the upstream and downstream flow boundaries, resulting in 7 data points falling within the applicable flow range of SMS. The same seven data points (discharge values) used to develop the rating curve equation for depth as a function of discharge will be used as the

basis for the comparison of SMS and RIVMOD solutions for velocity and depth at the well transect (Table 8-1).

Table 8-1. Comparison of steady-state velocity and depth output from SMS and RIVMOD

Discharge, cms (cfs)	109.6 (3871)	84.2 (2974)	63.7 (2250)	45.3 (1600)	20.8 (735)	15.2 (537)	6.85 (242)
SMS Average Velocity (m/s)	1.13	0.98	0.87	0.76	0.38	0.40	0.35
RIVMOD Average Velocity (m/s)	1.12	1.02	0.91	0.80	0.59	0.52	0.38
SMS Average Depth (m)	1.89	1.67	1.42	1.17	1.07	0.74	0.39
RIVMOD Average Depth (m)	2.53	2.21	1.92	1.63	1.16	1.03	0.78
SMS Contacted Bank Height (m)	1.75	1.53	1.28	1.03	0.93	0.60	0.25
RIVMOD Contacted Bank Height (m)	1.91	1.58	1.29	1.00	0.53	0.40	0.15
Bank Contact Difference (m)*	0.16	0.05	0.01	-0.03	-0.40	-0.20	-0.09

The following procedures were used to generate the values in Table 8-1. Both models are allowed to run to steady state before solutions are extracted. Noting that the well transect is approximately centrally-located between RIVMOD stations 152 and 153 (segment 152), RIVMOD average velocity and RIVMOD average depth are computed simply by averaging the steady-state model output for the given flow magnitudes at the two stations. The 1D RIVMOD model generates a single output value at each station for each time step. Flow depths are equivalent to the depth above the channel thalweg (elevation 0.00 meters in Figure 8-1). Contacted bank height was computed as the difference between flow depth and the elevation at the bottom of the RIVMOD vertical banks (0.63 meters). The procedure differed for SMS output. The non-uniform node spacing along the well transect required this to be considered. Model output is available at each node for velocity magnitude and flow depth above the nodal bed elevation. Depth-averaged velocity and depth vary across the channel. A simple arithmetic average would be appropriate if node spacing were uniform. This not being the case, numerical integration via the trapezoidal rule was used to compute the average velocity and flow depth for all nodes along the transect. Although all nodes do not lie perfectly on the well

transect, this simplification is reasonably made, and node locations (and thus distance between nodes) were able to be computed with respect to their distance from the left channel bank, looking upstream. The contacted bank height for SMS was computed as the difference between flow depth and the average elevation of the bottom of the SMS vertical banks in Figure 8-1 ((0.00 m + 0.275 m) / 2 = 0.1375 meters).

Velocity comparisons are shown in Figure 8-2 and Figure 8-3 for discharge values of 109.6 cms (3871 cfs) and 6.85 cms (242 cfs), respectively. At the higher flow magnitude, average velocity computed using SMS is greater than average velocity computed using RIVMOD, while the reverse is true for the lower flow magnitude. Velocity predictions between the two models differ by less than 0.05 meters per second for all but two of the seven comparisons, with significant differences of 0.12 m/s and 0.21 m/s at discharge values of 15.2 cms and 20.8 cms, respectively. Of the seven comparisons, RIVMOD velocity was exceeded by SMS velocity only at a discharge of 109.6 cms. The two models compare most favorably under high flow conditions (Q > 1000 cfs) most important for mercury modeling. Under these high flow regimes, bank erosion is the primary determinant for mercury introduction to the water column; bank erosion, as modeled within the IFMTFM, is highly correlated to velocity so that higher velocities result in ever-increasing erosion of mercury-contaminated bank material.

The changing shape of the velocity distribution (SMS node solutions) across the channel is also of note in these figures. This is the result of the bed morphology. High points along the bed present increased frictional resistance to flow, resulting in alternative preferential flow pathways where the channel is deeper. Turbulence and steep velocity

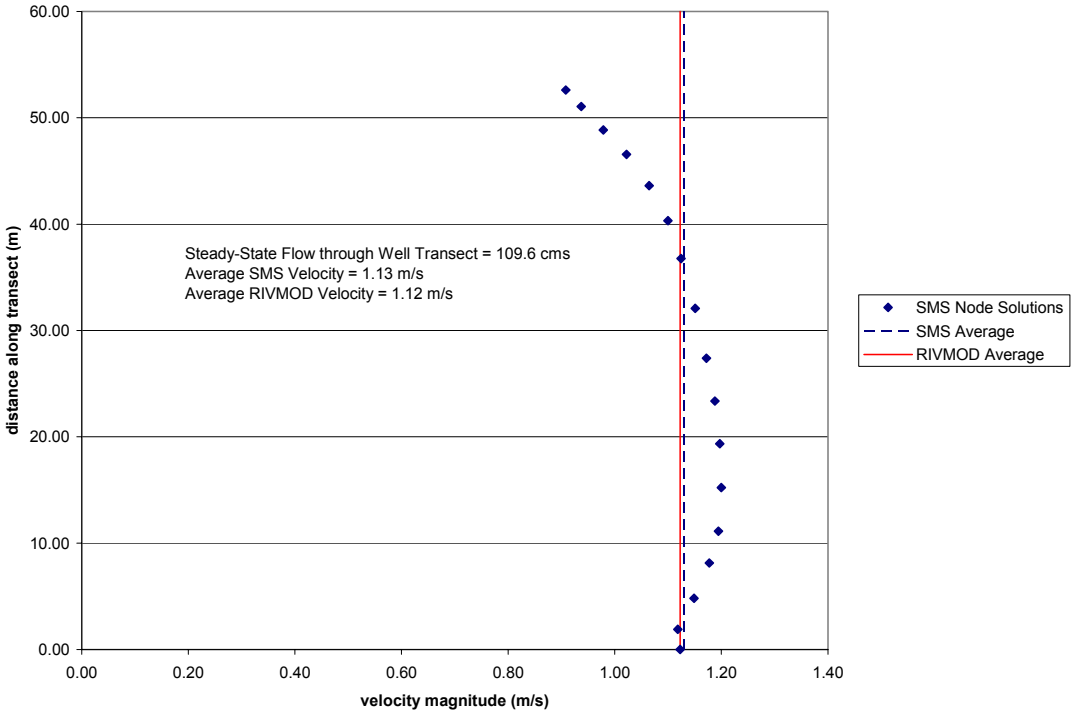

Figure 8-2. Q = 109.6 cms: comparison of steady-state velocity output from SMS and RIVMOD

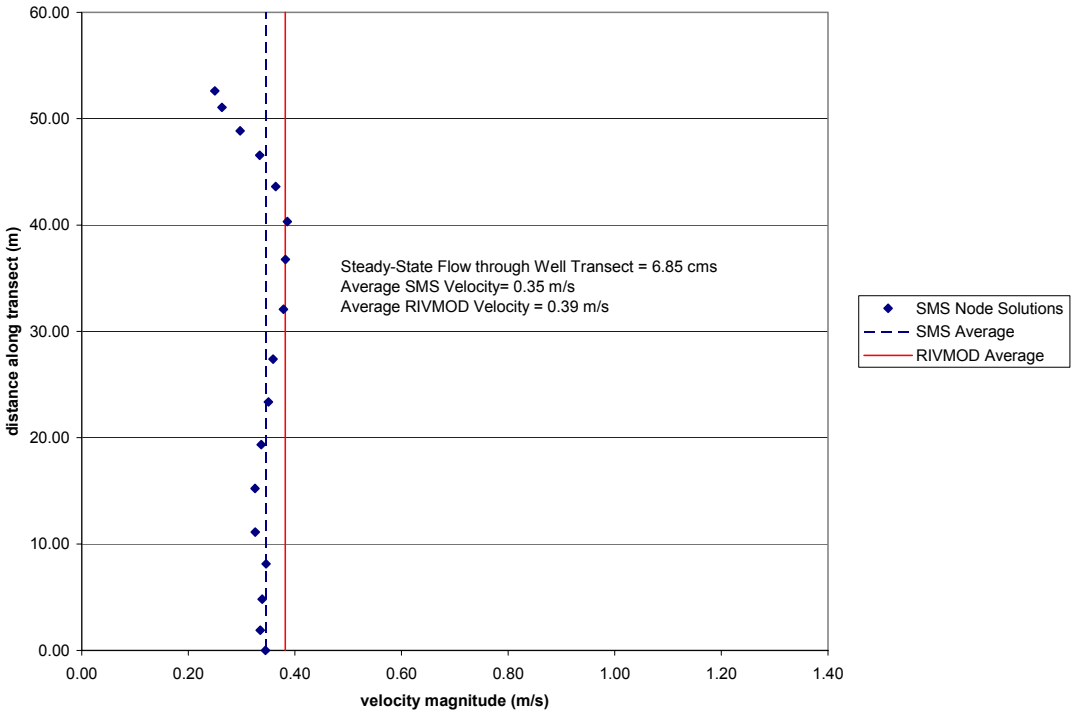

Figure 8-3. Q = 6.85 cms: comparison of steady-state velocity output from SMS and RIVMOD

gradients associated with boundary layer effects are not considered in SMS model computations; vertical walls do cause frictional shear stress and force tangential velocity at these nodes, but velocity computations exclude the boundary layer effects, and velocity is therefore not equal to zero at these no-flow boundaries.

Depth comparisons are shown in Figure 8-4 and Figure 8-5 for discharge values of 109.6 cms (3871 cfs) and 6.85 cms (242 cfs), respectively. For the seven compared discharge values, the average predicted depths by RIVMOD always exceed the average predicted depths from SMS. This is to be expected because of the lower channel width used in RIVMOD. Of more consequence is the comparison of the height of contacted channel bank between the two models, as this value will be used to predict the active methylation zone within the newly-incorporated bank elements of the IFMTFM.

The contacted height of river stage on the vertical channel banks varies between the SMS and RIVMOD models. The magnitude of this bank contact difference was previously indicated in Table 8-1. The difference is more evident when the SMS and RIVMOD predictions are plotted with respect to a line of perfect agreement, as shown in Figure 8-6. If the two models were in perfect agreement, the predicted bank contact height would be equal for the two models for each discharge, and all data points would plot on the line of perfect agreement.

Bank contact heights predicted using SMS, on average, exceed bank contact heights predicted using RIVMOD by 7.1 centimeters. Error statistics may be computed using model results shown in Table 8-1, but these statistics are of little value given the uncertainty with SMS model output. The SMS model is not properly calibrated to water surface observations, and it was necessary to assume a constant head loss across the

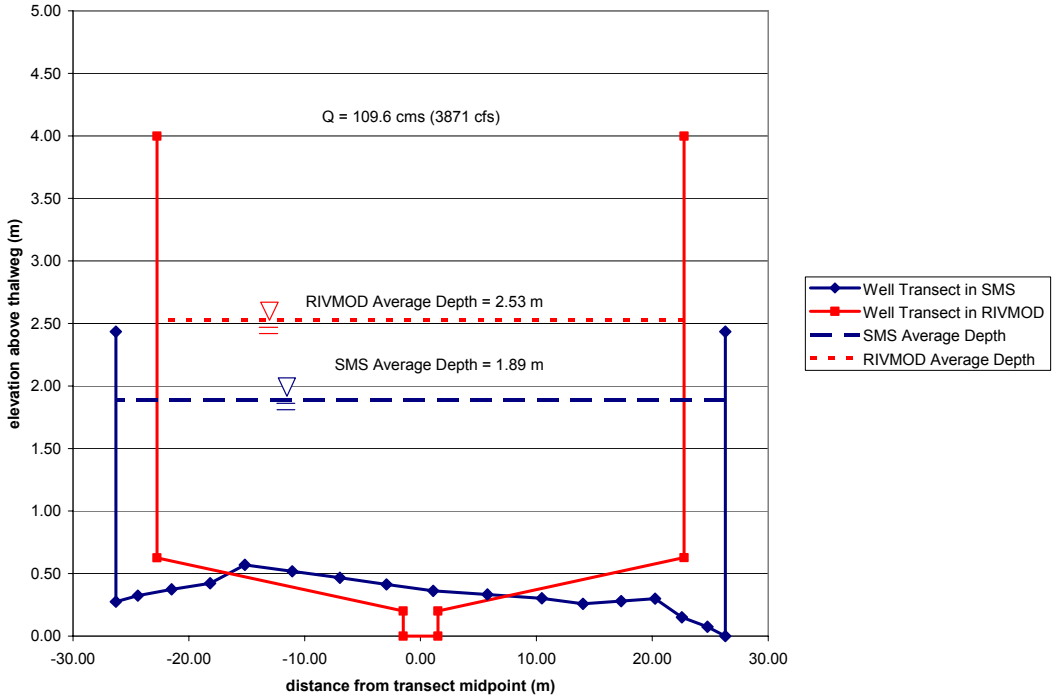

Figure 8-4. Q = 109.6 cms: comparison of steady-state depth predictions from SMS and RIVMOD

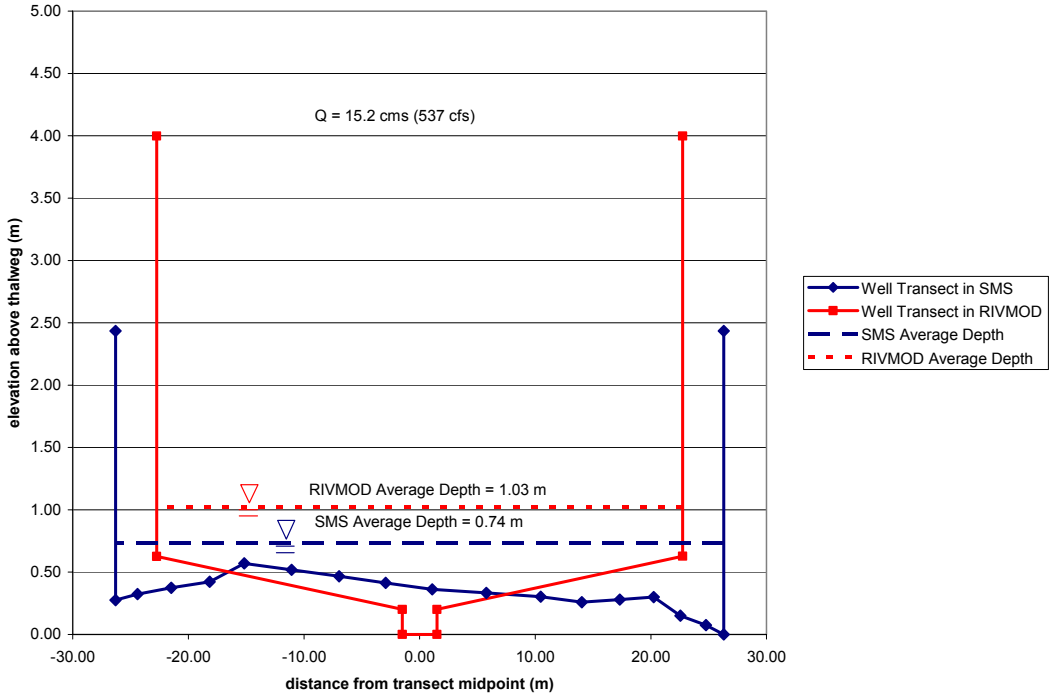

Figure 8-5. Q = 6.85 cms: comparison of steady-state depth predictions from SMS and RIVMOD

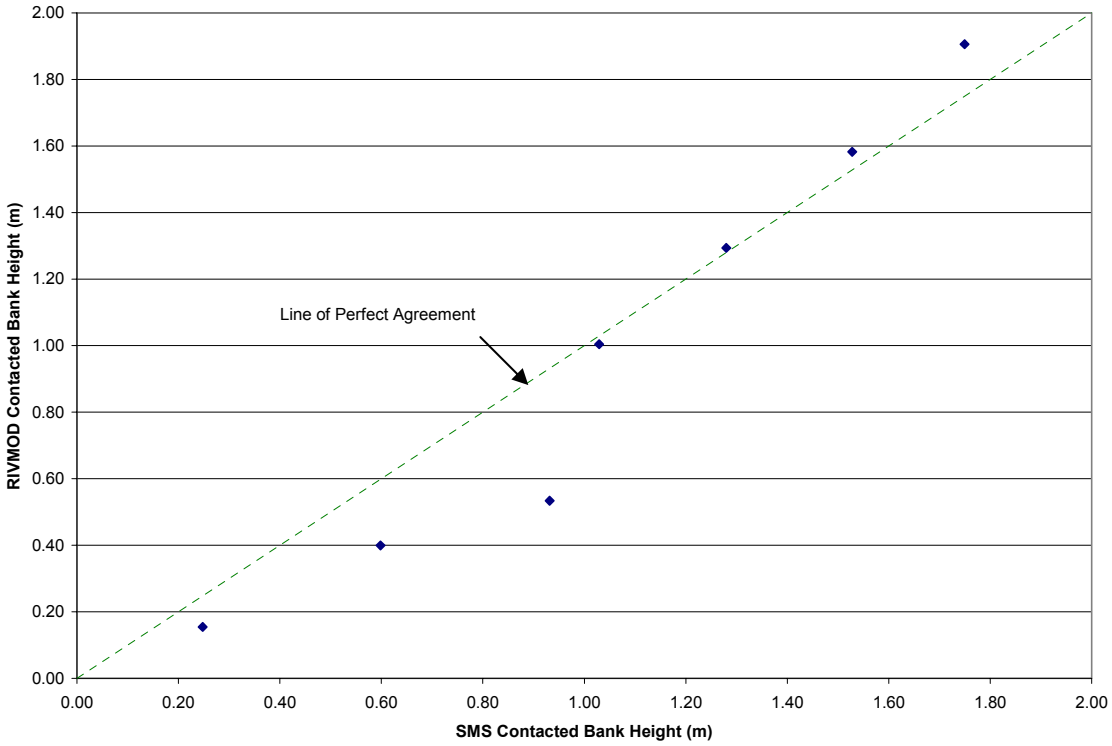

Figure 8-6. Comparison of contacted bank height predictions from SMS and RIVMOD

model domain, regardless of flow magnitude. The availability of additional calibration data would prove useful to this type of error analysis, but the required data is not available for this thesis research. Limited data and limited capabilities of the SMS model prevent an accurate quantitative comparison between the detailed SMS model (assembled from surveyed channel bathymetry) and the simplified RIVMOD model (utilizing simplified channel geometry and average parameter values). Recall, however, that the water surface elevation predicted using SMS exceeds the surveyed water surface elevation from March 9, 2001 by 15 cm. As discussed, the SMS model results include several assumptions and simplifications such that the SMS predictions represent maximum levels that could be observed in the channel. If additional data were available to correct the shortcomings of the SMS model, the two models would likely illustrate improved agreement under the high flow conditions at which bank contact is particularly

important for determination of a methylating bank zone and erosion of contaminated bank material.

Comparative Analysis and Data Limitations

The comparative analysis chapter of this thesis serves as a microcosm of the difficulties encountered throughout this thesis research. Detailed spatial and temporal modeling efforts require extensive data for model calibration. Unfortunately, for this research, the SMS model presented unforeseen limitations given the data which were available. Additional water surface elevations for different streamflow regimes would have been a valuable tool to assist in SMS model calibration and a comparison of stage predicted by SMS to water table observations and RIVMOD stage predictions. For rating curve development, measurements to validate or invalidate the accuracy of streamflows routed using RIVMOD would also have been useful. However, making use of available data, alternative analyses were able to quantify the coupling of river stage and water table oscillations.

The primary deliverable for this thesis was the incorporation of a new bank element into the IFMTFM, to relate flow history within the channel to moisture content levels observed within the channel banks. Zones of varying moisture impact methylation and demethylation kinetics, and therefore the temporal concentrations of methylmercury available to the water column. Data analysis indicated a nearly instantaneous response of the water table to streamflow oscillations, at a monitoring well 5 feet removed from the channel. The IFMTFM is only concerned with the erodable surface of the channel banks. It was assumed that for flow levels contacting the channel bank, the erodable face of the channel bank would be saturated up to a height equivalent to the river stage. To incorporate microbial acclimation time into the IFMTFM, bank element volumes vary

over time as river stage levels change. The saturated portion of the channel bank elements are computed based on the 4-day moving average of RIVMOD-predicted river stage. Incorporation of the bank element into the complete Carson River model of hydrodynamics, sediment transport, and mercury transport and cycling (IFMTFM), provides the model with a new capability to simulate temporally-variable mercury concentrations within the channel bank, reduces the model calibration procedure, and increases the accuracy of in-stream mercury predictions, while also adding to the model's ability to simulate processes actually occurring in the field.

APPENDIX A
SMS MODEL PARAMETERIZATION AND MESH EDITING

Creation of Triangular Mesh from Scatter Point Data Set

After the set of surveyed data points are imported into SMS as scatter points within the scatter module, the model user selects the coverage type under 'Data / Switch Current Model' to FESWMS and switches to the SMS river module to create and edit the mesh and parameterize the model. The options available within the SMS river module are determined by the selected coverage. In this case, FESWMS options are available and the FESWMS model is run from this module.

The software incorporates numerous automatic mesh generation techniques, of which triangulation is most suitable for a network of random survey points. The triangulation generates a mesh of either quadratic or linear triangles, with the quadratic option creating additional nodes at the midpoint of each triangle leg. A single node corresponds to each point in the scatter data set. It is possible to toggle between element types using the 'Elements / Linear <-> Quadratic' feature of the FESWMS module. Despite the implied increase in computational effort, quadratic elements are selected in order to increase numerical stability during the wetting and drying process. Triangular elements are created from the scatter point set by selecting 'Elements / Triangulate.' The triangulation process creates elements outside the desired mesh boundaries, a by-product of the non-linear shape of the channel. The model user is required to manually select and delete these extraneous elements. Thin triangles along the mesh boundary, the corner nodes of which are almost co-linear and effectively hidden, are identified according to a

thin triangle aspect ratio (perfect equilateral triangles have an aspect ratio of 1.0) set under ‘Elements / Options.’ With the default value of 0.04 unchanged, these triangular elements are selected under ‘Elements / Select Thin Triangles’ and deleted.

Transformation of Mesh from Triangular to Quadrilateral Elements

After the deletion of outer elements, the general geometric and bathymetric features of the channel can be distinguished. At this point it is useful to consider the desired mesh characteristics. The mesh must be able to simulate the areal wetting and drying of the model domain. Vertical channel banks result in a drying pattern from the floodplain to the outer channel banks to the inner channel thalweg. The final model mesh should consist of elements that are approximately parallel to the channel bank boundaries. This will allow the model domain to dry uniformly; perhaps the best analogy is the peeling of an onion. Model functionality dictates that as one node is predicted to be dry (predicted water surface below node elevation), the entire element becomes dry and incapable of transporting flow. Failure of the elements to follow this basic design will result in jagged boundaries of the water edge, isolated ponded areas, and resulting numerical divergence. Quadratic elements are best able to capture this wetting / drying front and offer improved numerical stability and a faster solution time for the model (SMS Tutorial: Version 8.0, Section 3.4). Triangular elements will be necessary is some areas to improve model wetting and drying in steep area and around bends in the channel.

At this point, the mesh is composed entirely of triangles. Quadrilateral elements are preferred because of the need to simulate element wetting and drying. Triangular elements are converted to quadrilateral elements using the ‘Element / Merge Triangles’ feature in FESWMS. Before merging triangles, the merge triangles feature angle is set under ‘Elements / Options.’ Using the SMS model default, triangles are only merged if

all angles of the resulting quadrilateral are greater than 65 °. SMS merges triangles in an iterative manner, starting with quadrilateral angles of 90 ° and working down in a step fashion, to form the best-shaped elements. The finite element method is more stable and accurate when quadrilateral elements are rectangular and triangular elements are equilateral (SMS Tutorial: Version 8.0, Lesson 3.5). Clearly, a mesh cannot consist entirely of these ideal shapes, but the elements should approach these shapes as close as possible.

To toggle between 8-noded and 9-noded (nodes at all side midpoints and in the center) quadrilateral elements, use the option under 'Elements / QUAD8 <-> QUAD9.' 9-noded quadrilateral elements decrease node spacing and should assist the finite element scheme with model convergence. For FESWMS, it is best to use 9-noded quadrilateral elements, even though both 8-noded and 9-noded quadrilaterals are supported (SMS Tutorial: Version 8.0s, Lesson 5.2). The model mesh after merging of triangles is shown in Figure A-1. With a basic mesh in hand and knowledge of the desired end product, mesh shortcomings are next addressed and remedied.

Mesh Corrections Based on Perceived Model Operation

The first round of mesh corrections is performed in advance of using the finite-element model, or, alternatively, with no water flowing in the channel. The corrections are based solely on observed needs and intuition with regard to how the model performs calculations. As mentioned previously, an abundance of points is available at each of the five cross sections. Points along the top of banks and on the floodplain are incomplete or lacking in some locations. Points at the base of vertical banks are also very limited, due to limitations associated with the surveying equipment. Lastly, channel bed features, most

notably the thalweg, are poorly represented. All of these elements are critical if water is to actually flow through the model domain and channel stage is to be accurately simulated.

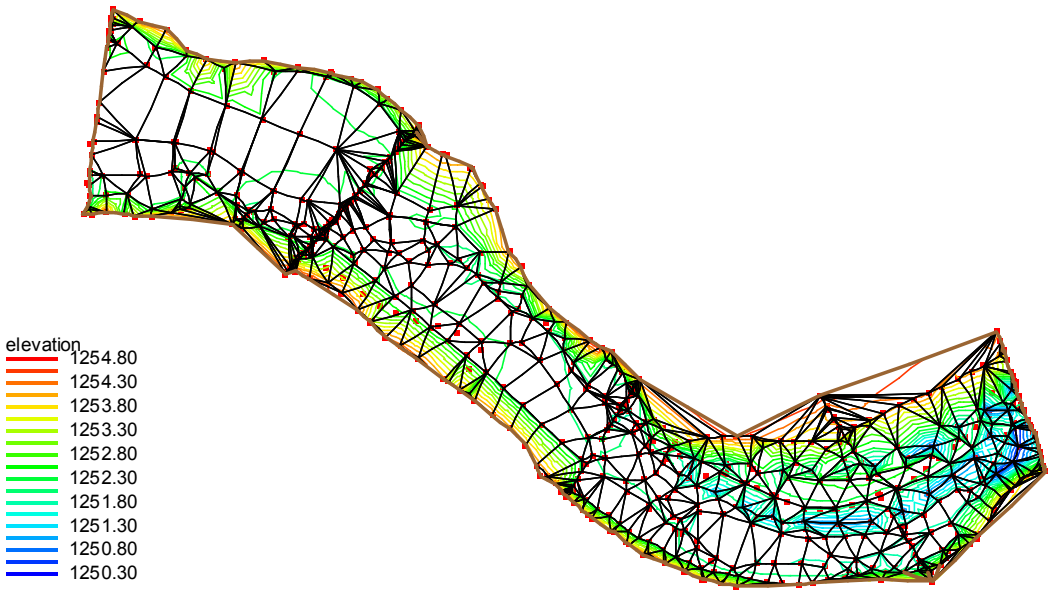

Figure A-1. Quadrilateral element mesh after initial merging triangular elements

Rectifying the Mesh with Observed Channel Geometry

The FESWMS module allows the user to manually create mesh nodes by clicking on a desired location. Within the node options dialog box, check the option to insert nodes into the triangulated mesh and retriangulate voids when deleting. By using these options, inserted nodes are automatically updated with elevations to conform to the existing elevation contours, and nodes deleted to improve the node spacing will not result in gaps in the mesh. One other model feature of note when creating new nodes is the interpolation option. This allows the user to select two nodes of known elevations and generate any number of additional nodes between with spatial position and elevation determined by linear interpolation.

Admittedly, the addition and deletion of nodes cannot be performed arbitrarily. The goal is to develop a mesh that accurately portrays the observations of channel geometry within the model domain. Were this not the case, the final model predictions of river stage, to be compared against water table stage, would be of minimal validity.

In general, water flows downhill. This is not a scientific breakthrough, but it is an important starting point for refining this model mesh. Some basic limitations to numerical modeling also need to be realized. For a given simulation, three solution values are generated for each node: water surface elevation, water depth (a function of node elevation and water surface elevation), and a velocity vector. The equations built into the SMS solution algorithm were previously reviewed, but these provide little insight compared to simple experience with using this model. The knowledge obtained from model reference manuals, model tutorials, and simple trial-and-error experimentation was used extensively during this stage of model development. With numerical modeling, a divergent solution at a single node will cause the model to crash. The important point taken from all of this is that bed elevation needs to be gradually lowered downstream in the direction of flow. Flow pathways need to be determined in advance of mesh refinement. Information from first-hand observations, photographs, names given to survey points (such as thalweg, water surface, or bank), and graphical analysis of survey data were used to discern the channel thalweg, connect thalweg points to each other, and verify that the general characteristics of the channel bed (high points and low points) are representative of what was actually observed. The channel is, of course, dynamic by its very nature, but this mesh assumes that the morphologic changes occurring over the past two years have not significantly altered the relationship between channel stage and

discharge. Having returned to the field site in October 2002, this is a valid assumption. The contour lines presented in Figure A-1 show clear evidence of thalweg location for the downstream portion of the model domain, but the thalweg location for the upper half is not clear. However, the thalweg and water edge locations were precisely surveyed for the upstream portion of this reach during July of 2001 (Figure A-2). A simple linear interpolation of the scatter points along the thalweg allows for the connection of these points within the model mesh. The remainder of the bed in these areas is fairly flat, and linear interpolation from the existing survey points allowed new nodes to be created to improve the nodal density and spacing. The bed characteristics for the downstream half of the model domain, between easting coordinates 744100 and 744300, are more complex. Given that the Scout Camp reach of the Carson River is generally oriented east-west, bed elevation plots were prepared for 50-meter subsections of this east-west distance and for each cross-section. These plots, an example of which is shown in Figure A-3, importantly show the locations of multiple low-flow channels and the high points between these channels. For these plots, the x axis is the northing coordinate (approximately perpendicular to flow direction), the y-axis is the surveyed elevation, and all available survey points are classified and plotted based on which 10-meter group they fall into along the direction of flow (as approximated by easting coordinate). The idea was to be able to see how the bed is changing along its longitudinal length, so that this variability could be captured in the model mesh.

The general bed geometry features for the cross-sections are shown in Figure A-4. Cross-section locations are indicated back on Figure 5-1. A few additional points are worthy of note following inspection of the cross-sections. Channel bed elevation is lost

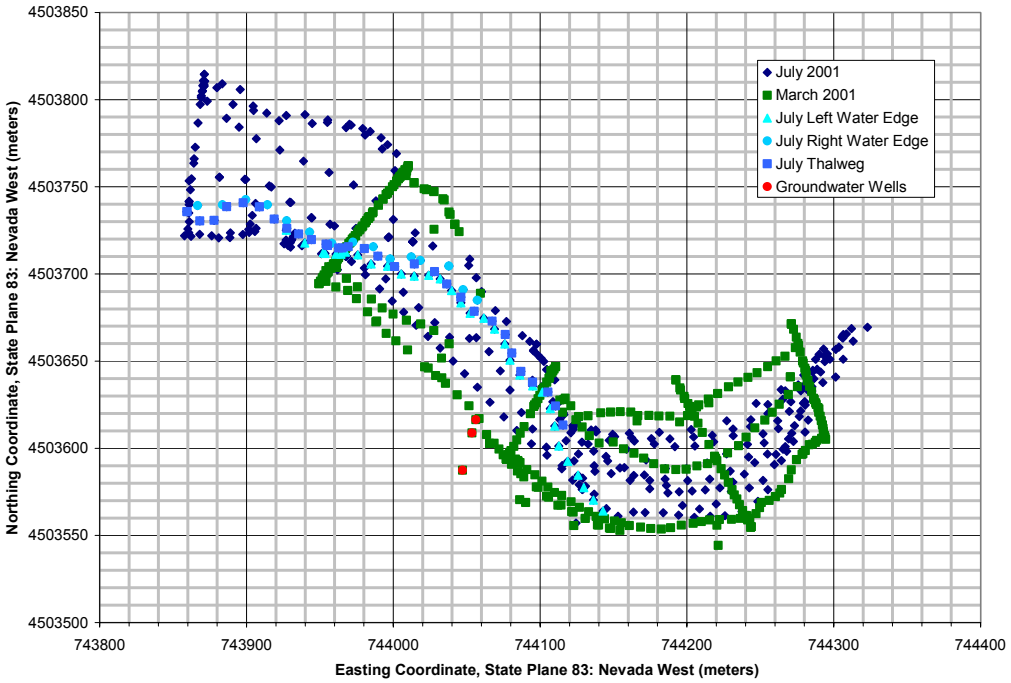

Figure A-2. Network of survey data points, indicating location of thalweg and water edge

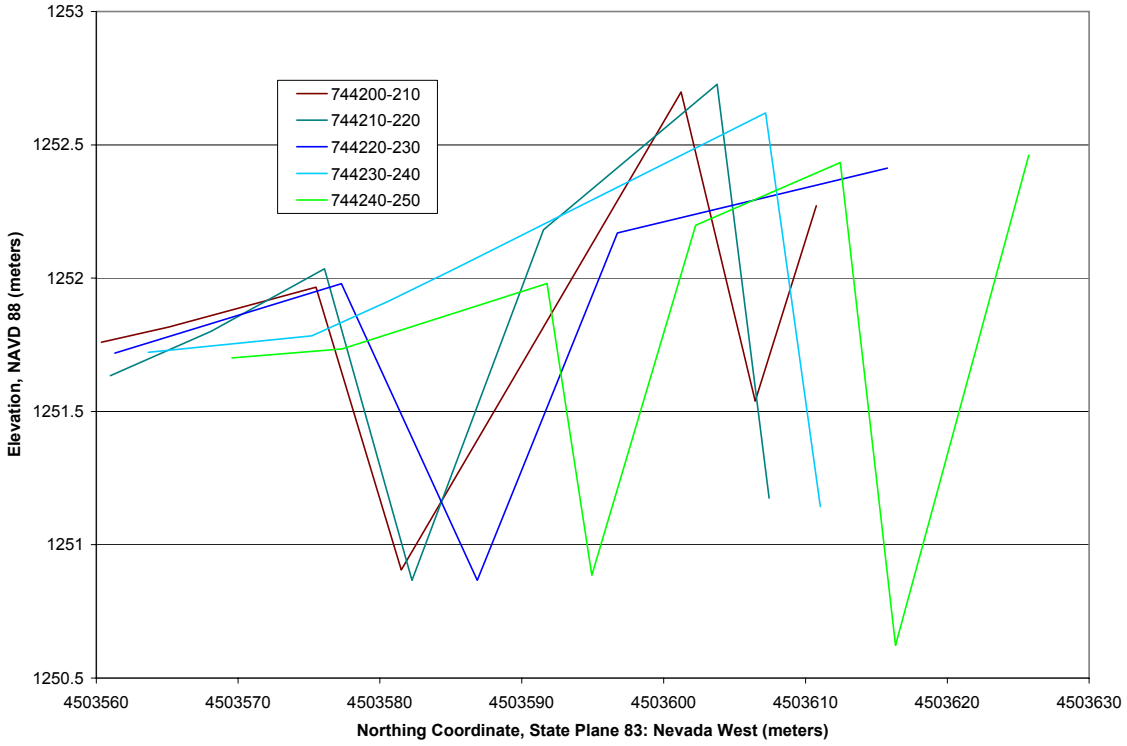

Figure A-3. Bed elevation plot indicating bed feature changes in flow direction

moving downstream, and the channel thalweg becomes more pronounced. All cross-sections show the presence of steep channel banks, with cross-section 300 the most telling example of vertical banks on both sides of the channel. Lastly, bed geometry data is not smooth because of the presence of bed forms such as dunes, depositional sandbars, and multiple low-flow channels. Again, the mesh needs to capture the general trends, but within the confines of numerical convergence. These plots allowed the removal of subjectivity associated with node insertion and deletion.

The majority of removed data points were along the five cross-sections. Points retained were deemed as representative of the cross-sectional geometry, rather than those needed to capture each bed form. Some data points from the July bed survey were also removed near the cross-sections in order to improve the union of the two temporal data sets.

The days spent surveying the Scout Camp site provided insight and photographic documentation to incorporate the vertical channel banks and steep slopes into the scatter point network. Additionally, field measurements of bank height were recorded as a component of the erosion study, during which a network of iron stakes were pounded into the vertical portions of the bank. This resource base allowed for additional nodes to be created along the tops of vertical banks (where data collection was inhibited by the cottonwood trees) and along the base of the channel banks (where the banks themselves often inhibited data collection). Linear interpolation between two surveyed points was used only as a final resort when other data was lacking.

Initial model intention was to include the capability to model flows up to the bank full level, or flows at which channel water depth is above the vertical banks. Many of

these data points along the top of channel the channel banks and on the floodplain were created subjectively or utilizing linear interpolation. Detail was not necessary, and the points simply needed to show a subtle elevation increase moving away from the channel; the goal here was to identify the flows at which bank full conditions occurred throughout the simulated reach. Given the changing nature of vegetation (roughness characteristics variable relative to sandy channel bottom), highly variable slopes, and limited data, these nodes were created using a combination of cross-section data where available, linear interpolation, and common sense.

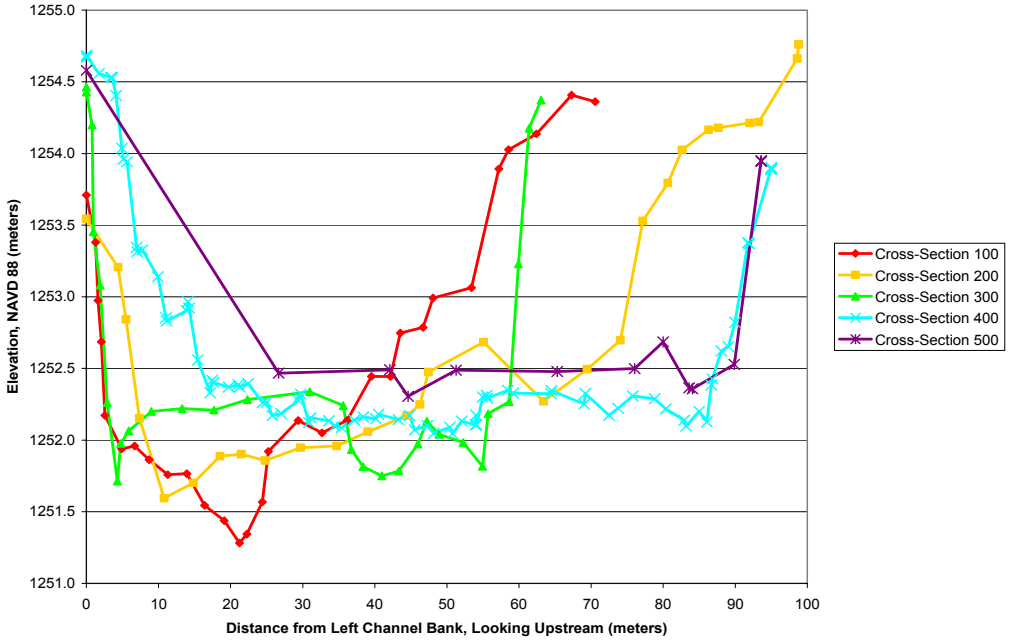

Figure A-4. Bed and bank geometry at surveyed Scout Camp cross-sections

Improvement of Node Spacing and Drying Properties

After triangulating the nodes, deleting elements outside the boundaries, merging triangles, and adding and deleting nodes to add channel morphology details, the mesh still needs additional manipulation to add to model stability. At this stage, node spacing becomes of primary importance. While some consideration of this is used during node

addition, all attempts were made to hold the locations of surveyed nodes constant. Up until this point, one primary goal was kept in mind: getting the channel geometry contours to be representative of the general observed trends and continuous. The lowest elevation contours follow the channel thalweg and low-flow channels, higher contours follow the channel bed, still higher contours come together at vertical banks, and the highest contours smoothly traverse onto the floodplain. Basically, the contour lines within the model domain resemble a topographic representation of a large bathtub, with the lowest downstream thalweg elevation representing the drain.

Recall that quadrilateral elements are preferred for two reasons: they make a more concise mesh for faster solutions, and quadrilateral elements are numerically more stable, particularly when dealing with areal wetting and drying (SMS Tutorial: Version 8.0, Lesson 3.4). Lines of quadrilateral elements should run parallel to the boundary so that the mesh will wet and dry parallel to the boundary (SMS Tutorial: Version 8.0, Lesson 3.6). Referring back to Figure A-1, several significant obstacles to developing elements of this pattern are noted. The algorithm used by SMS to triangulate nodes into elements always connects the three nodes closest to one another into a triangular element. The algorithm to merge triangles into quadrilaterals only merges triangles when all resulting quadrilateral angles exceed a user-input value, the default being 65°.

Quadrilaterals are then created in the order of increasing minimum angle. Simply put, given the variable node spacing in this mesh, the quadrilateral elements created will not run parallel to the mesh boundary and will include several triangular elements internal to the mesh. The decision was made that the mesh would be completely triangulated, including only triangular elements, and the quadrilateral elements would be

created one at a time using the features of the FESWMS user interface. The modified triangular mesh, including all node additions and deletions until this point, is shown in Figure A-5. Also shown are the underlying contours for this triangulated mesh. Note the continuous nature of the contour lines and conformity to field observations. Importantly, the mesh will be able to transport fluid through the model domain, at least in theory.

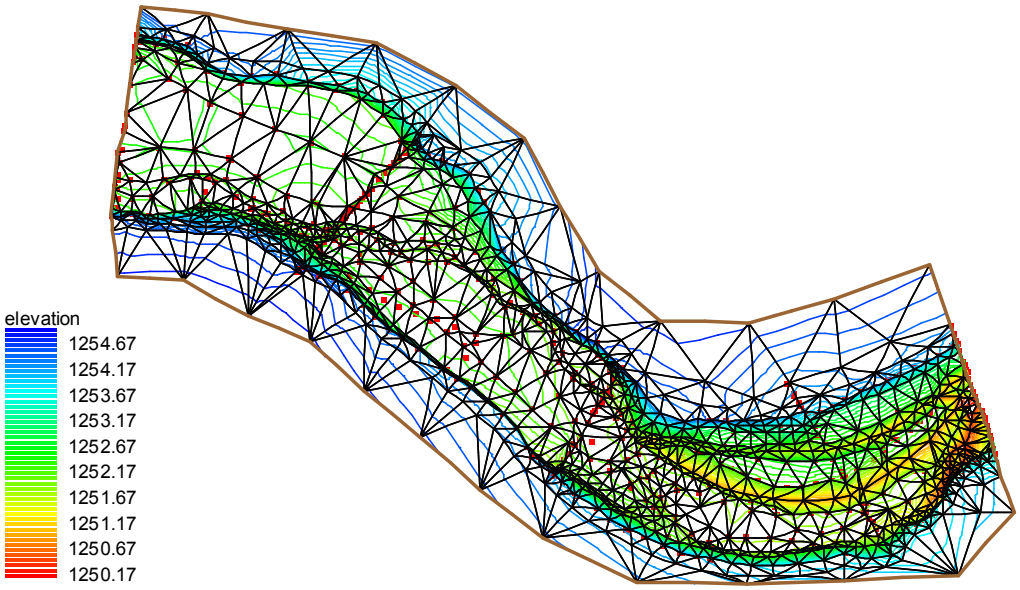

Figure A-5. Modified triangular mesh after node addition and deletion

The user interface of the FESWMS module offers several features useful to the development of a quadrilateral mesh and the improvement of node spacing. Useful at this time is to visualize the desired end-product. The rectangular mesh will need to dry parallel to the boundaries, and to enhance numerical stability, the use of triangular elements within the mesh interior will be minimized. The approach was to visualize a network of channel transects, perpendicular to the direction of channel flow. By dividing the model domain in this fashion, the overall mesh would be built one transect at a time. Flow direction is approximated by the channel thalweg. As such, getting the thalweg right was the starting point of this process. With a fairly extensive network of nodes

already in place and no large spatial gaps, linear interpolation was used to add nodes where needed so that they would fall along these transects. With the nodes in place, the split / merge tool is FESWMS was used to merge each set of two triangles into the desired quadrilaterals. The progression of this procedure is shown in Figure A-6, Figure A-7, and Figure A-8. Initially, the process was applied only to the channel bottom, working from the thalweg outward and downstream to upstream. Mesh points were deleted and inserted as needed, but data points representing actual survey observations were retained whenever possible. Admittedly, the process is tedious and time consuming, but it is made simpler with the underlying contours in place. Inserted nodes, in other words, conform to the existing lay of the land. Triangular elements are needed along bends in the channel to maintain uniform node spacing. Triangular elements are also included in a few locations to preserve details of the channel geometry.

After the main channel was completed, the process was repeated with the floodplain. Here, the lack of data required the insertion of many more nodes. The linear interpolation was used to insert multiple nodes between two known points, with the exact number based on extension of transects to the model boundaries. The process is completed working outward from the channel banks to the model boundary. The end result, the completed quadrilateral mesh, is shown in Figure A-9. For reference, the original survey points have also been shown. Some nodes were moved slightly, using the unlock node option, to improve uniformity of node spacing. These minimal alterations in node locations will not alter the final solution to within the expected error associated with the data itself. Wherever possible, original survey node locations were retained. The

framework is now developed for a quadrilateral mesh that will wet and dry parallel to the boundaries.

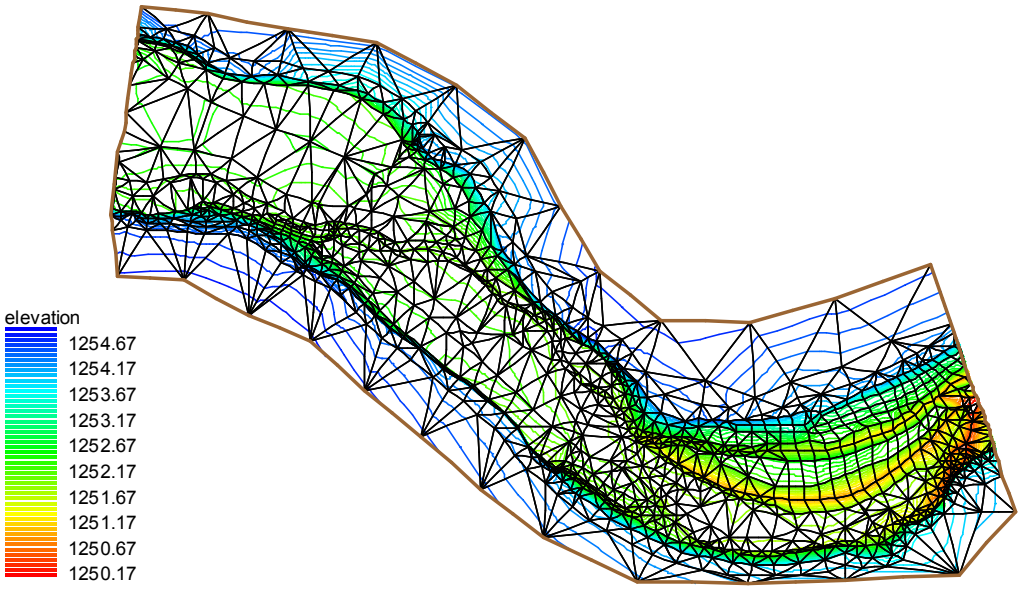

Figure A-6. Downstream main channel, quadrilateral mesh creation

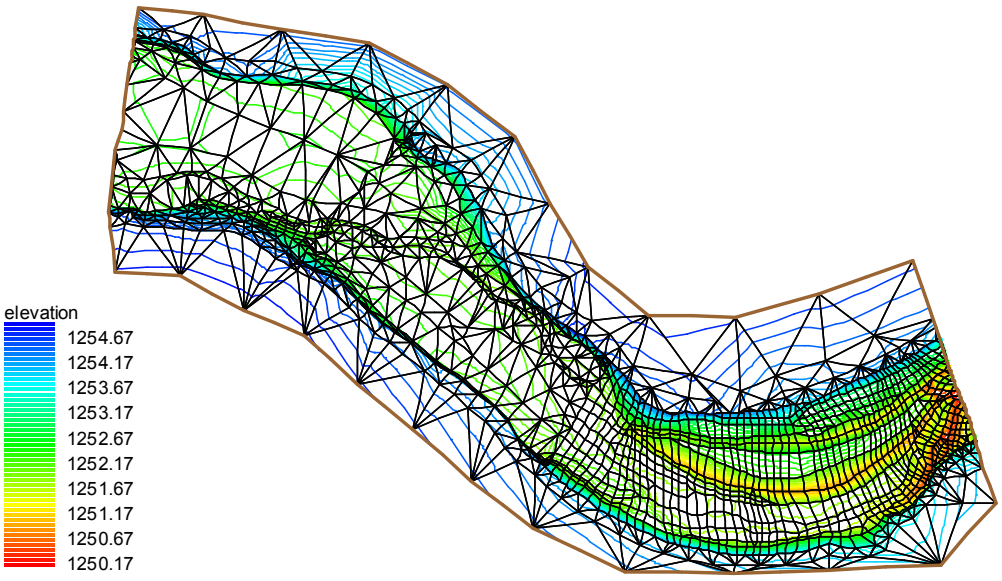

Figure A-7. Middle main channel, quadrilateral mesh creation

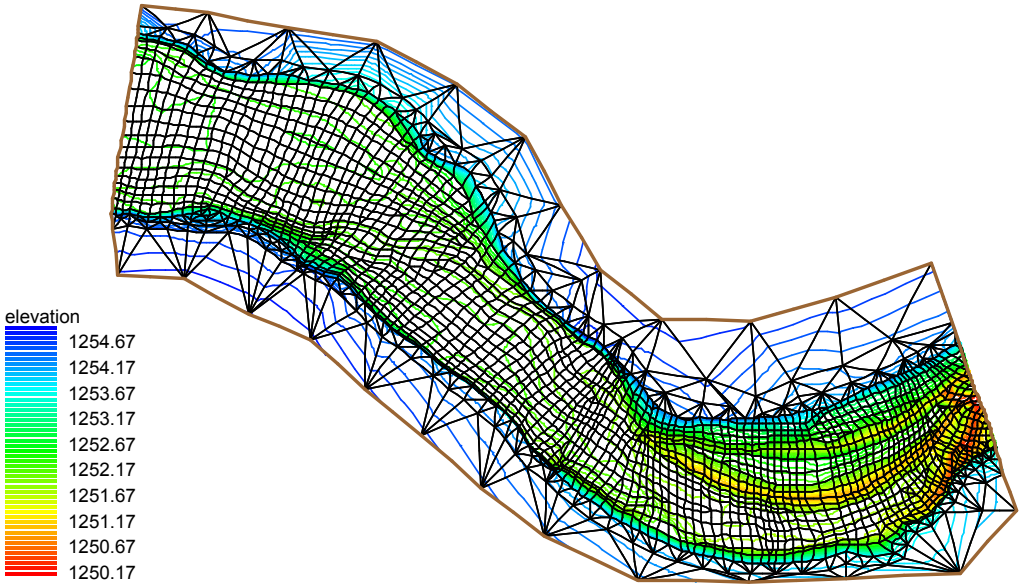

Figure A-8. Main channel complete, quadrilateral mesh creation

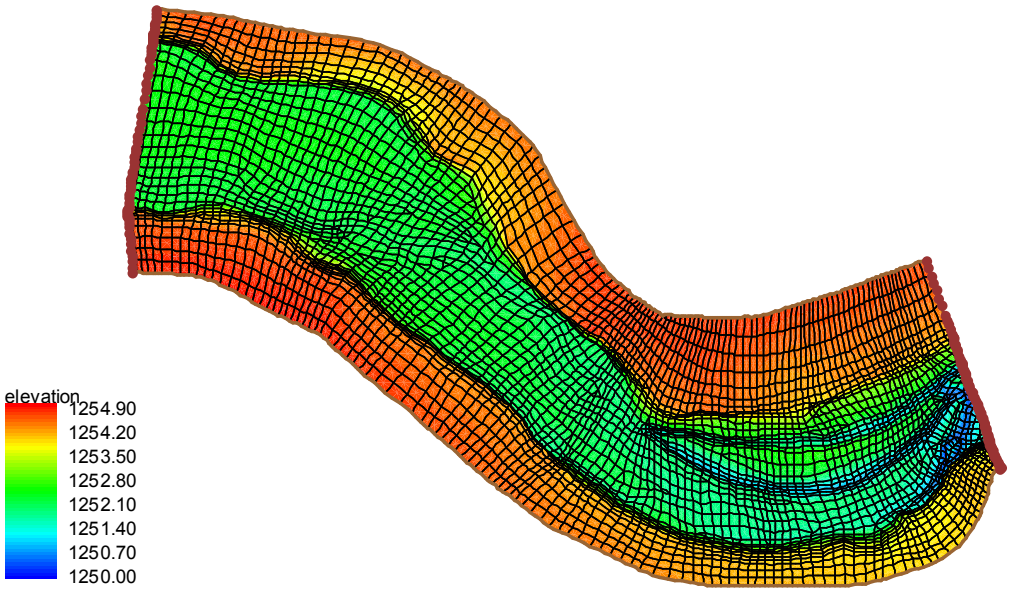

Figure A-9. Completed quadrilateral mesh with bathymetric contours

Mesh Corrections for Hydrodynamic Simulations

With the critical geometric features of the channel, including the thalweg, bed high points, steep vertical banks, rip-rap, and the floodplain, consistent between model and reality, the next process is getting the model to work and convey water. Water conveyance is accomplished through the use of boundary conditions. The finite element mesh was developed so that the upstream and downstream boundaries each approximate transects, perpendicular to flow direction. The create nodestring feature of the FESWMS toolbox is used to create a nodestring connecting all nodes along these two open boundaries, boundaries at which flow enters or leaves the mesh. Four options are available within FESWMS for boundary definition: specified flow / WSE, supercritical outflow, computed WSE, and Storm / Tide WSE (note that WSE is an abbreviation for water surface elevation). These boundary conditions will be applied at the upstream and downstream cross-sections of the Carson River model domain. The remaining model boundaries are, in essence, vertical walls. These boundaries may be applied roughness values and serve as no-flow boundaries.

A required condition for the starting a FESWMS simulation is the submergence of all nodes within the model domain. The initial water surface elevation must, therefore, be greater than the elevation of the highest node within the mesh. For the Carson River model, flow within the model domain will be subcritical ($Fr = V / (gD)^{1/2} < 1.0$). The avoidance of supercritical flow conditions at the specified upstream and downstream boundaries is the principal determinant as to the minimum initial water surface elevation that can be specified. Given that flow through the model domain will be primarily subcritical in nature (except in cases where flow depths approach zero as elements are very close to dry or recently rewet) and that tidal conditions (as needed for a river

entering an estuary or ocean modeling) are not being simulated, boundary conditions will be of two possible types: head boundary condition or flow boundary condition. FESWMS allows flow boundary conditions to be specified as constant or dynamic. While head boundary conditions are also specified as constant or dynamic, head values at a boundary nodestring can be manually input, read from a rating curve (with the independent variable flow specified), or specified using a friction slope. The friction slope option allows for a non-level water surface along the boundary. The use of the rating curve or friction slope options, do introduce additional problems, as will be later discussed.

Development of a Simple Linear Model

In order to gain experience with SMS, determine the best way to parameterize the model, and develop insight for further mesh refinement, a smaller and simpler linear model was prepared. The model captured the inner thalweg, small sloping bed, vertical banks, and floodplain which characterize the Carson River and the prepared mesh. However, the number of elements for the simple model was only a fraction of the complete model, allowing for reduced computational time and the opportunity to focus initially on the big picture. Clearly, the most obvious problem area was the steep (almost vertical) banks. A profile view of this simple model, including the same quadrilateral elements as the complete detailed model, is found in Figure A-10. Cross-sectional shape and dimensions were taken from Figure 3-1. The simple model was constructed following the same procedure as the detailed model, with the notable exception being that the input scatter points were created with respect to an arbitrary datum and based on the dimensions indicated in Figure A-10. A channel bottom slope of 0.001 (1 meter per 1000 meters of channel length) was used along the 500-meter straight channel reach. Bottom slopes and cross-sectional geometry remain uniform throughout the model domain.

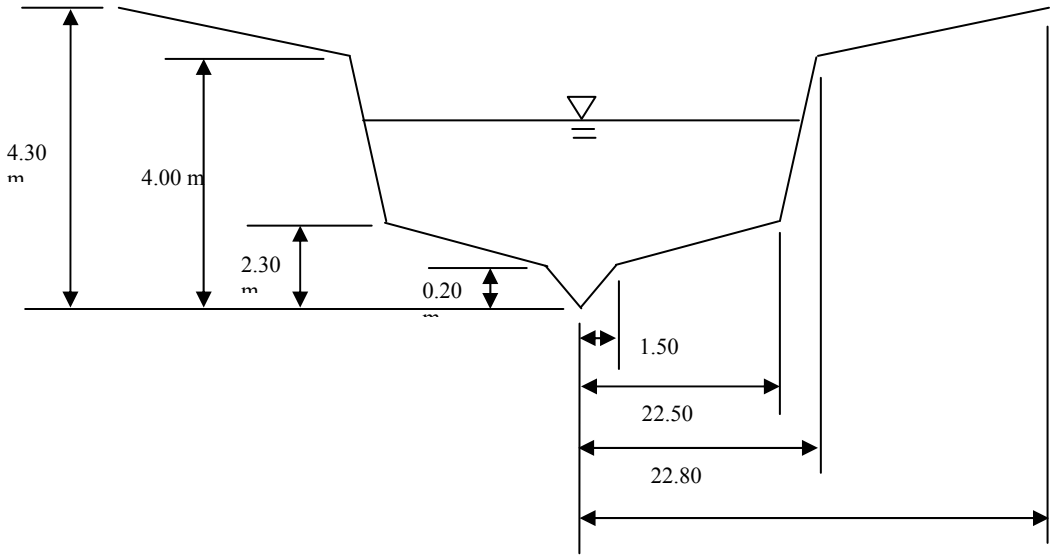

Figure A-10. Uniform Cross-Section Dimensions for Simple SMS Model Mesh

All node points were not directly calculated for the input data points. Rather, several useful features with FESWMS were used to add additional elements. The breakline feature allows for the creation of new elements by transforming mid-side nodes (selected as part of an input nodestring) into element corner nodes. The refine command allows for the division of selected quadrilateral elements into four smaller elements. Both options apply linear interpolation to existing node positions and elevations.

SMS Model Insights Provided by Simple Linear Model

Repeated experimentation using this simple model resulted in several important and useful discoveries about the modeling system operation and limitations. This experimentation yielded information about specifying boundary conditions; and the effective and efficient handling of steep channel banks.

Specification of boundary conditions

First, it is necessary to review the specification of boundary conditions. For a simple model domain, with uniform bottom slope and uniform cross-sectional geometry,

the model can easily simulate the following boundary condition specifications: upstream flow with downstream head, or upstream head with downstream head. This introduces a potential problem with reference to the modeled reach of the Carson River. While the USGS gaging station at Fort Churchill allows for a reasonable approximation of the flow at the model upstream boundary, no data is available for the downstream boundary. No stage recorder was installed at the field site, and no stage-discharge relationship is known. While the user may specify an upstream flow boundary with a downstream flow boundary, two details should be realized: travel time is a function of flow magnitude and velocity, and a numerical model specified in this fashion will be extremely unstable. The interface does allow for the specification of a rating curve boundary condition, but model reference to this as a computed water surface elevation can be misleading. In fact, the model will not independently compute this downstream head elevation based on an upstream flow condition. Rather, the rating curve relationship (stage as a function of discharge) must be specified and the constant or transient discharge values must be provided. In other words, downstream head values must be known either through direct field measurement of stage (or depth) or direct field measurement of flow. The friction slope option can only be applied across the downstream boundary, rather than along the downstream boundary. This option allows for a non-level water surface to be specified along the boundary nodestring, and the input value does not represent the water surface slope passing over the boundary, out of the model domain. The lack of stage data available for the modeled reach of the Carson River is therefore a problem in need of a solution.

Recall that the detailed model for the Scout Camp reach of the Carson River is approximately 500 meters in length. The downstream model domain boundary could presumably be extended far enough downstream so that the effects of the downstream boundary would not be felt within the current model domain. This would essentially involve creating new scatter points to extend the model mesh into a reservoir, within which the head could remain constant. Of course, given that no survey data is available for further downstream and the uncertainty as to how far would be far enough, this option was not selected. Rather, the model has a useful way to sidestep this problem. Model solutions predict a water surface elevation, water depth, and velocity vector for each node in the model domain. Using the solution velocity vectors and depths, the model calculates flow across any nodestring. Such nodestrings can include the upstream boundary, downstream boundary, or say, a nodestring across the channel at the well cross-section. With no stage data available for the downstream boundary and no means to independently calculate and verify this relationship, it was determined that the use of both upstream and downstream head boundary conditions were the best means to simulate the hydraulics of the channel. The model output could then be used to develop rating curves for the modeled reach, specifically a rating curve to predict the stage-discharge relationship for the vertical bank adjacent to the groundwater wells. The repercussions of this decision will become more evident as this discussion progresses. Of particular interest is the choice of water surface slope and the linkage between the respective boundary head conditions.

Model handling of steep vertical channel banks

The steep banks of the simple model also posed problems. A slope is necessarily applied to these banks. Within the model mesh, two points cannot be located at the same

latitude and longitude in space. Node elevations for the base and top of these banks were often not each available at a given location due to aforementioned surveying difficulties with point acquisition. Rather, some of these points are based on collaboration between field measurements, photographs, and recollection of the modeler. The SMS model will allow creation of these steep elements, but wetting and drying of these elements introduces complications.

A discussion is necessary with regard to how element wetting and drying is performed within the SMS model. The finite-difference solution scheme predicts water surface elevations for all nodes within the model domain. FESWMS parameters set in the FESWMS model control determines how elements are checked for their wet or dry status. Two specific parameters need to be defined. Default storativity is defined as the water depth below ground elevation at which a node is considered to be dry. When a node becomes dry, all elements attached to the dry node are considered dry. A zero value for storativity indicates that a node will become dry when the water surface elevation is equal to the nodal ground elevation. A positive value indicates that the element will only dry when the computed water surface is some height below the node ground elevation. Values in the range of 0.0 to 0.1 meters were used throughout the modeling process, with higher values best suited for elements possessing the steepest slopes. If the numerical model determines that an element has dried out, any flow previously passing through that element is passed over to elements that remain wet. The second notable parameter is the depth tolerance for drying. The element drying / wetting toggle is used to control how FESWMS handles changing water surface elevations. The toggle needs to be checked in the FESWMS parameters dialog box if elements are to be turned either on or off during a

given simulation. If turned on, the input depth tolerance is used to determine if a partially submerged element should or should not be included in the computational analysis. In this case, the water surface elevation for an adjacent element is higher than the minimum node elevation for the bordering dry element, presumably those nodes along this wet / dry boundary. When the water depth over any node of a dry element exceeds the depth tolerance threshold value, a previously dry element will be considered wet, at least for the purposes of the given iteration. If too many elements get classified as dry in a single iteration, the water surface elevations in the remaining elements may go up enough to incorrectly make the dry elements wet again. The shifting back and forth between wet and dry elements results in numerical instability in the solution. Such instability is particularly evident for steep elements, as shown in Figure A-11. As an illustrative example, consider node 1 going dry when the water surface drops below the node elevation by the storativity depth for one iteration, but the water depth in the adjacent element (sharing node 3) exceeding the depth tolerance for drying during the next iteration; the hatched portion will oscillate between wet and dry and the underlying element may be unable to converge or even diverge, depending on other adjacent elements.

The repeated shifts of elements from wet to dry will prevent model convergence. In cases where several adjacent elements simultaneously undergo this shifting, the magnitude of the oscillations will often progressively increase with each iteration. The resulting changes in nodal velocities and water surface elevations will eventually cause model divergence and a model crash. The problem is enhanced further during dynamic simulations in which the water surface is already changing from time step to time step.

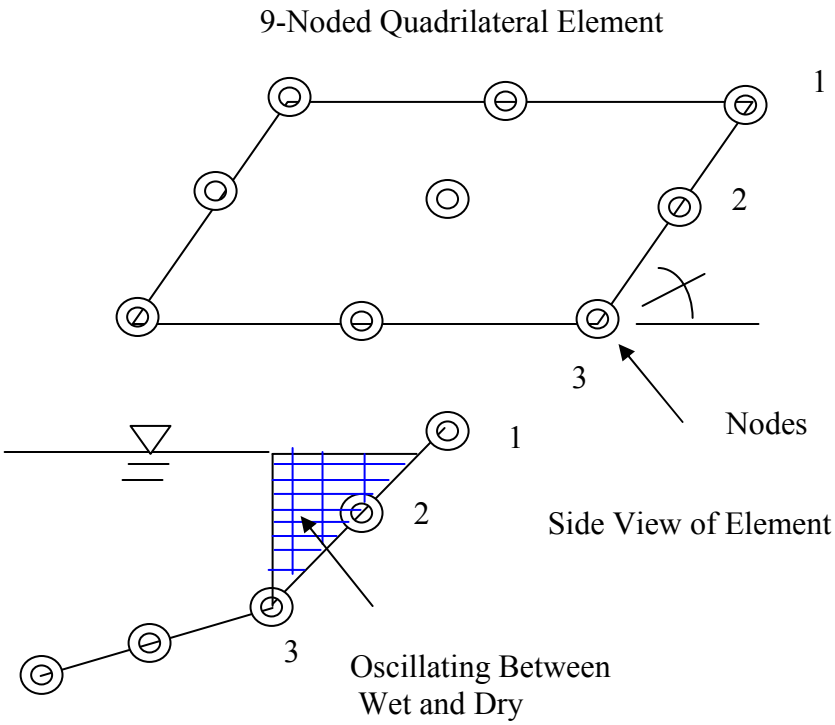

Figure A-11. Element Wet / Dry Oscillation

The problem here is the maximum iteration criteria. If the model has neither converged nor diverged during the time step, the model will advance to the next time step. Certain elements which should be wet will be dry, and certain elements which should be dry will be wet. Typically, it is only a matter of a few iterations before model divergence occurs.

Evidence of this numerical instability is found from steady state simulations of the simplified SMS mesh. Because flow is able to be lowered from floodplain levels completely down to zero, attempts were made to develop rating curves from a series of steady state simulations. The head boundary conditions were incrementally lowered for a constant water surface slope, with equilibrium flow conditions recorded. The simple mesh contained only a single element along the steep banks, but the drying of these elements causes an inconsistency in the rating curve. For a typical rating curve, increasing depth of flow is associated with increasing flow. However, the sudden drying

of theses elements when the top nodes are dry disallows flow through these elements. Equilibrium flow increases for a decreased depth of flow. This is illustrative of how sudden drying of a large portion of the elements in a model domain can significantly alter flow conditions. For the Carson River model, the bank elements would not dry simultaneously as they do here and the bank elements transport far less flow than the remaining mesh elements, but the probability of model divergence for a dynamic simulation in which several bank elements become dry is suggested.

FESWMS Model Parameterization: Element Wetting and Drying

Before running a simulation using FESWMS, a conceptual understanding of how the model performs computations combined with a few observations concerning the raw survey data allows for prediction of likely causes of model failure and modify the mesh in advance of their occurrence. Recall the model requires all mesh nodes to be initially submerged. In the model mesh shown in Figure A-9, the water surface elevation at both boundaries was to be lowered at a constant rate. Head boundary conditions would be used, and the water surface slope would be held constant as the water surface is incrementally lowered in a step fashion. Two specific probable divergence problems were identified. First, the surveyed elevation data includes high and low points along the lower floodplain. The morphology surrounding the tops of the channel banks is not at all smooth, including hills and valleys on both a large and small scale. Elevation inconsistencies will ensure a jagged wetting and drying boundary. With the model only allowing flow to pass through “wet” elements, the flow pattern from upstream to downstream will be effectively interrupted for these regions. As the model attempts to compensate through changing velocities and water depths, divergence is inevitable. Secondly, the model will experience divergence due to the aforementioned oscillation of

elements from wet to dry. The drying of a single steep bank element from a single node becoming dry would often result in an adjacent water surface computation higher than the dry node itself, and certainly an adjacent water surface depth sufficient to cause re-wetting for any small value of the depth tolerance parameter.

To circumvent these problems and retain the ability to simulate flows above the bank-full river stage, nodes were inserted to sub-divide single steep bank elements (two corner nodes at both top and bottom of a given bank) into between three and five smaller elements with vertical dimensions on the order of one-half of one meter. The depth tolerance for element re-wetting is also set to be greater than height of these steep bank elements. Of course, how realistic is this? Given that small magnitude numerical fluctuations are likely during the course of any solution, the modeler is effectively not allowing the model to self-correct these problems and re-wet an element that should be wet. In addition to assisting the model to run, justification is found in the fact that the flow through a few bank elements mistakenly turned off is negligible by comparison to the flow through the mesh as a whole. This is definitely valid at the high flows required for extensive bank contact, and the resulting water surface elevations will not be altered by any amount greater than the errors associated with the survey data points, node elevation modifications, or well data precision. In summation, this simplification should allow for simulation of a falling river stage. The jagged interface between wet and dry elements and the resulting numerical divergence proves to be a problem difficult to solve. This is a simply by-product of the nature of the channel morphology, within which elevations gradients do not follow smooth rising or falling curves. This will be a problem in need of a solution, or at least some means of control.

Modeling of Steep Channel Banks

General steps prior to start of hydrodynamic simulations

With the first round of mesh refinements in place, the mesh should be capable of simulating channel hydrodynamics. Before running the FLO2DH model used by FESWMS, a few additional steps do need to be completed. First, the model boundary should be smoothed. To prevent loss of mass through the jagged boundary of a quadratic mesh, smoothing will move the mid-side nodes along the model boundary while preserving the locations of corner nodes (SMS Tutorial: Version 8.0, Lesson 3.7). Smoothing requires the creation of a nodestring in a counter-clockwise direction between the two extreme nodes along the upstream boundary condition nodestring. The select nodestring tool is used to select this nodestring, followed by the use of the 'Elements / Smooth Nodestring' command. The process of creating and editing a finite-element mesh causes the node and element numbering to become almost random, thereby increasing the size of the matrices required by the finite element analysis codes. Renumbering the mesh restores order. After selecting the nodestring at the upstream boundary condition, the band width option is selected from the 'Elements / Renumber' option, and the mesh is renumbered. In all instances involving changes of nodes along the mesh boundary, the mesh boundary should be smoothed. Similarly, the addition or deletion of nodes from the mesh alters the node numbering, and renumbering is always the last step of the mesh creation process.

FESWMS also includes a mesh quality feature. This feature visually identifies potential problems with the finite-element mesh layout. When this option is checked under 'Display / Display Options,' an element is highlighted in a color corresponding to the criterion which it violates. Mesh quality affects the validity of a finite element

analysis. While not all problems are identified, problems known to cause model instability are identified and can be easily corrected using this quality check. Available quality checks include the following: minimum interior angle, ambiguous gradient, concave quadrilaterals, maximum slope, and element area change.

A brief discussion of each mesh quality check is herein provided (SMS Help Menu). Minimum interior angle warns of skinny triangles and skinny diamond-shaped quadrilaterals. Ambiguous gradients occur when two diagonal corner nodes of a quadrilateral are higher than the other two corner nodes, forming a saddle point along the middle of the element; these elements are undesirable because a drop of water at the middle of the element could flow downhill in two different directions. Concave quadrilaterals possess large interior angles and should never be included in the mesh. In the flow direction, a steep element slope indicates the possibility of supercritical flow; although FESWMS supports supercritical flow, supercritical conditions along boundaries specified as subcritical may cause the model to crash. In the direction perpendicular to flow, a steep element indicates possible wet / dry shocking. It is suggested that the area difference between two adjacent elements not exceed 50 percent.

Before any model simulation run, mesh quality is checked and problems are remedied. Minor dragging of nodes to a new location (limited by elements formed by bordering nodes) can be useful to alleviate minimum interior angles, concave quadrilaterals, and element area change warnings. Other remedies include addition of new nodes by linear interpolation to create smaller elements, node deletion to re-form elements, switching element shape from triangular to quadrilateral (or the reverse), or switching diagonals for two triangular elements within a quadrilateral. Maximum slope

warnings perpendicular to flow are common within the Carson River mesh and unavoidable given the nature of the channel morphology. Throughout the mesh modification process, the creation, deletion, or movement of nodes is always followed by a mesh quality check. It is a good recommendation to perform a quality check before any simulation, as it will save the loss of time associated with a foreseeable and hence avoidable model crash.

Identification of mesh problems after a hydrodynamic simulation

One clear advantage of the simple linear model was that all node elevations were effectively inserted by hand. The channel cross-section shape does not vary moving downstream. Even though the bank elements were steep (possessing nearly a 6:1 slope), the mesh elements were well constructed. Unfortunately, the steep bank elements within the Carson River model do not exhibit this same uniformity. In most cases, surveyed elevations along the tops and bottoms of banks were linearly interpolated to generate additional points along these characteristic features. Linear interpolation was additionally used to subdivide the bank elements into smaller elements in an attempt to prevent model divergence caused by simultaneous drying of elements, thereby preventing flow through the element. Given that the surveyed elevations do not smoothly rise or fall along the banks, element areas often differ substantially between adjacent element, and rows of bank elements do not typically follow the underlying contour lines. Nodal elevation changes, slope changes from one bank element to the next, and the sudden increase in flow depth during the mesh transition from floodplain elements to bank elements cause significant instabilities within the finite difference solution algorithm. Elements subject to these instabilities can be easily identified in two ways. One way is to run the FESWMS FLO2DH model, allow the model to crash, import the solution final (the .flo file) and

view the mesh properties for the time steps immediately preceding the model crash. Nodes within unstable elements will exhibit trends during these pre-crash time steps including the following: water surface elevations (or water depths) well above or below the range imposed by the boundary conditions, velocity magnitudes significantly higher than other elements within the model domain, or velocity vectors facing in directions not consistent with the principal direction of flow. These problem areas are easily identified in the solution window, as the contour range is set by default to automatically adjust based on the range for all nodes in the mesh solution. When the model is set to color fill, versus only contour lines, over the spectrum of colors, distinct color differences will jump out for these diverging nodes. Vectors for velocity solutions can also be shown for all nodes, making inconsistent velocity values literally jump off the page. Examples of diverging solutions are shown in Figures A-12, A-13, and A-14. These three figures actually represent the same solution. Note the contours as indicated in the legend. Recalling that the highest nodes of the mesh have elevations of 1254.45 meters, it is noted that all nodes in the model mesh are submerged under greater than 20 meters of water. Considering the channel morphology, as indicated in Figure A-9, water depths are predicted to be close to uniform within the main channel, excluding the increased depth at the downstream thalweg. Figure A-12 clearly shows a diverging solution with physically-unreasonable water depths, most notably along areas characterized by steep channel banks. The diverging velocity magnitudes and vectors for this same solution are evident in Figures A-13 and A-14. In the case of Figure A-14, the finite-element solution is predicting velocity vortices around the areas of extreme water surface (related to depth

and bed elevation) variation. These are physically unrealistic solutions that are output by the model, indicating the importance of quality control checks by the user.

The second means of identifying potential diverging nodes is through examination of the output file (the .prt file). Poorly formed elements may result in a negative or zero determinants that will lead to unacceptable solutions. These elements are identified during each model iteration by the following warning message: Determinant <= 0 in element X at integration point X. Diverging nodes may not immediately cause the model to crash. The maximum number of iterations for all time steps is 99, and the number of allowable iterations can be specified as any number less than 99. A few diverging nodes may not cause the model to crash, but the model will be unable to converge. With increasing numbers of iterations, however, the divergence of one node will influence adjacent nodes, and eventually the model will crash. The best solution around this problem is to inspect each final model solution to check for inconsistencies in nodal

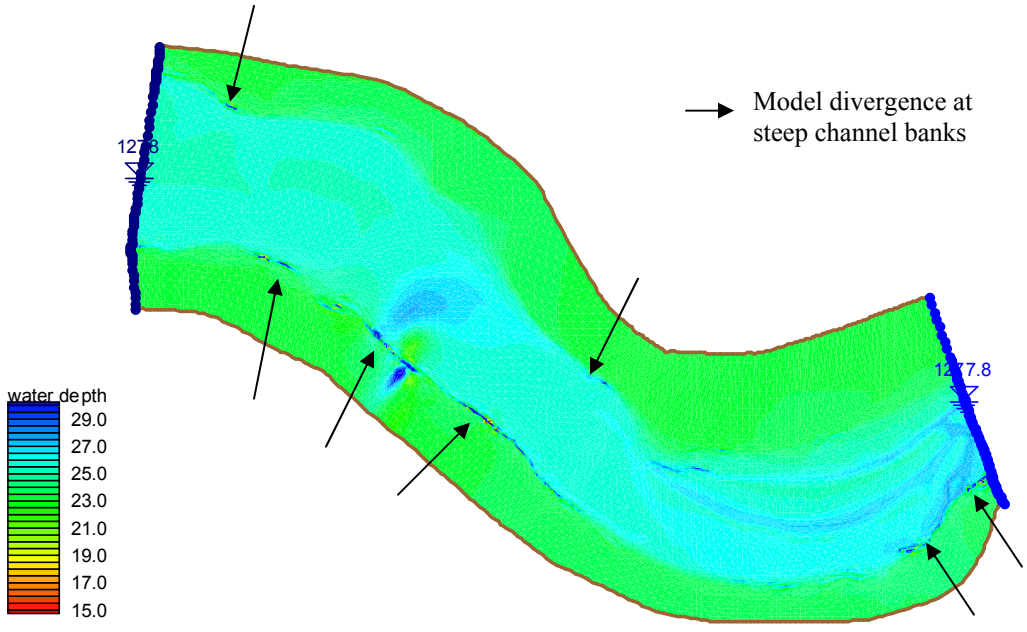

Figure A-12. Physically-unrealistic water depths along steep channel banks

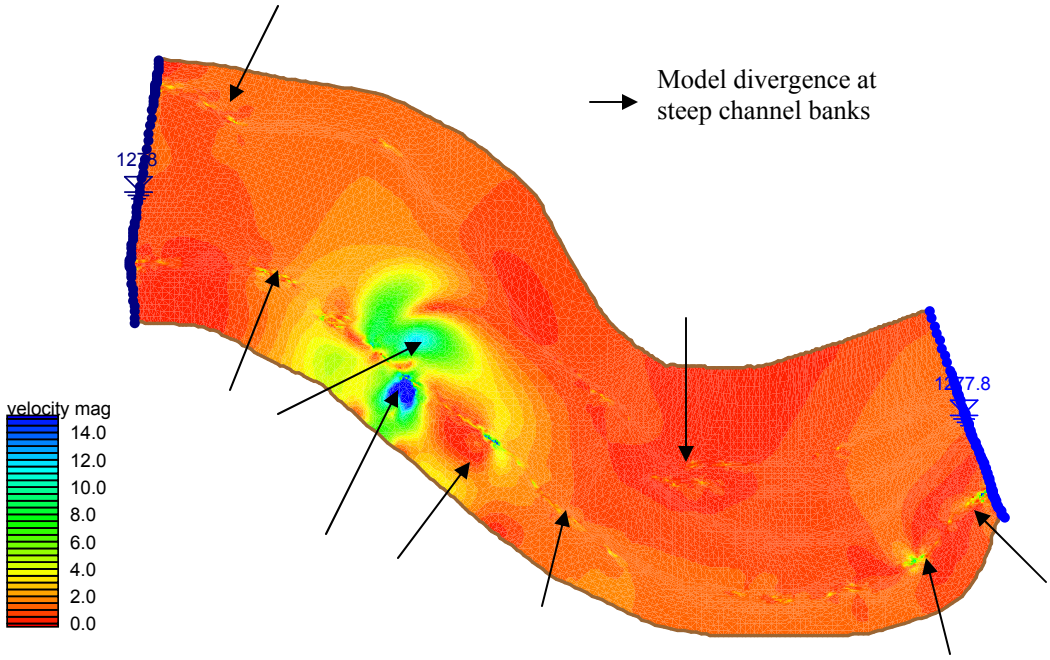

Figure A-13. Model divergence, velocity magnitude

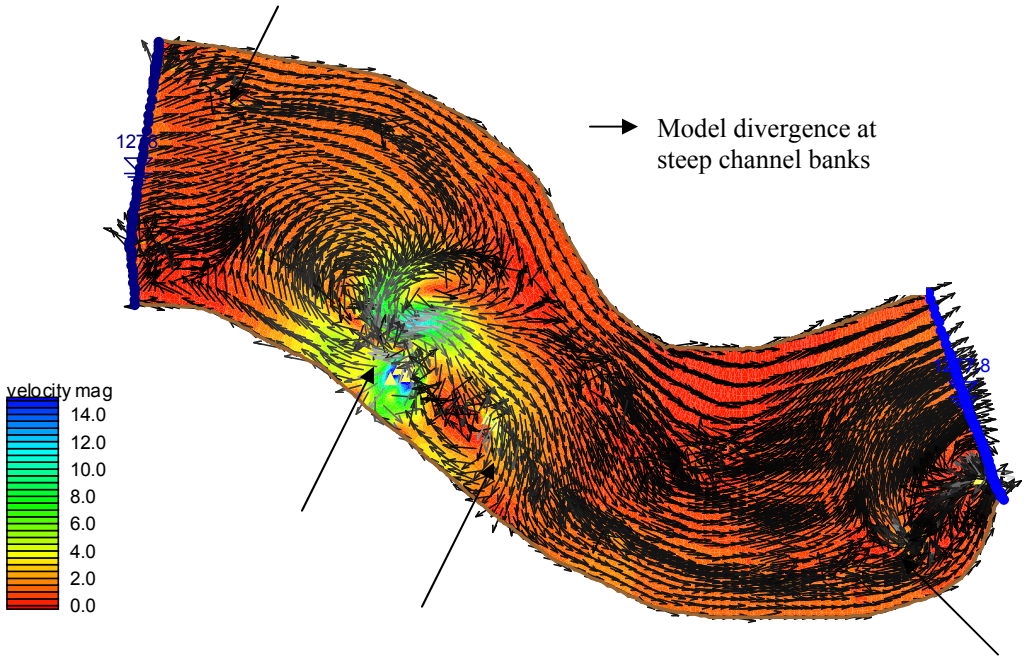

Figure A-14. Model divergence, velocity vectors

elevations or velocities. In addition to substantially increasing model run time, final water surface elevations in the solution may not be physically reasonable. Where these diverging nodes are located, the elements need to be reconstructed, either through minor node relocation to improve uniformity of adjacent element shapes or through adjustment of node elevations to smooth the elevation gradients.

Attempts to Fix the Problem Areas Identified by a Hydrodynamic Simulation

Mesh corrections are an iterative procedure. All model nodes must be submerged for the initial conditions. Initially, head boundary conditions were used for simple steady state simulations. When the maximum number of iterations was reached or the model crashed, the output .prt files were examined and diverging nodes recorded. The .prt file is created for all model runs, regardless of whether a model crash occurs. The DOS window in which FLO2DH runs only tells the model user the number of errors and warnings, explaining nothing about model divergence or a model crash. By zooming in on these diverging areas, clicking on nodes to view elevation properties, and utilizing 3D viewing angles with exaggeration in the height dimension, the diverging nodes were corrected one at a time by dragging nodes or inserting nodes to create uniform node spacing, minor modification to node elevations to smooth gradients between adjacent nodes, or some combination of both. The model would then be run again subject to the same boundary conditions to see if the correction had worked properly. The mesh would either be corrected again or the boundary conditions would be lowered and the procedure repeated. Most of these diverging nodes were present along the steep portions of the vertical banks, but steep portions of the inner channel also posed some divergence problems that required correction. Many of the divergence problems were simply a by-product of using raw survey elevations, resulting in abrupt elevation changes or poor node spacing. These

trouble spots were able to be corrected so that the steady state simulations would not crash and flows through the model domain approached constant values. However, this only held true for flow depths in excess of ten meters above the highest node elevations in the mesh. As the water surface was gradually lowered using the boundary conditions, regardless of the rate of lowering, supercritical flow warnings would arise for nodes along the steep portions of the mesh. Within a few iterations of these supercritical flow warnings reaching nodes along the boundary conditions nodestrings, the SMS model would crash.

The problem of steep banks in a finite element model

One common thread tied these problem nodes together. These nodes were all found in steep portions of the mesh, either along channel banks or channel thalweg. Other nodes did cause diverging solutions at first, but these nodes were able to be corrected using the above-discussed procedures. Given that the goal is to lower the water surface elevation to a level representing close to zero flow in the channel, the inability to lower the water surface elevation to even the levels of the highest node without model failure posed a definite problem.

Boss International hosts an online forum through which SMS model users can direct questions to technical support staff or post advice or comments from personal experience with the model. In posing a question to post to the forum, the following important information was included: general mesh characteristics, including the nature of elements along the steep channel banks; boundary conditions used, and a description of warnings preceding model failure. Feedback was collected from a combination of suggestions from other SMS model users, previous postings on the site, and a review of the model mesh by members of the Boss International technical support staff. It was

verified that steep elements cause convergence problems and noted that these elements generally do not carry much conveyance, thereby providing justification to ignore these bank elements when necessary. FESWMS assumes that mesh boundaries are no flow boundaries, able to be defined as either frictionless or not. Additional suggestions included lowering of the relaxation factor, specified under 'FESWMS Control / Iterations,' to a value of 0.01. The range for this value is 0 to 2, with a default value of 1.0. According to documentation within the SMS help menu, higher values should be used if a model demonstrates slow convergence. Smaller values can be used to increase numerical stability if a model diverges. A lower value will give a slower but more stable solution run. The technical support team did note some mesh problem areas, such as poor element construction along one channel bank (Figure A-15), but fixing of these nodes and elements still did not result in model crash prevention. Other potential alternatives were discovered by searching through the forum archives. Potential alternatives included the following: reduced nodestring length along the upstream and downstream boundaries to prevent boundary condition elements from drying, straightening of the boundary condition nodestrings to ensure perpendicularity to flow direction, shortening the overall mesh length to check if convergence is attained, turning off the wet / dry toggle for these submerged conditions, defining different roughness values for floodplain and main channel flows, and utilizing an upstream flow boundary condition. Each approach failed to solve the problems arising from the steep channel banks. The biggest piece of advice taken from the experience of other modelers was the following: if modeling of the floodplain in not critical, then eliminate the overbank areas and steep elements along the

channel edges and use a semi-slip or no-slip boundary with a vertical wall roughness appropriate to the bank condition.

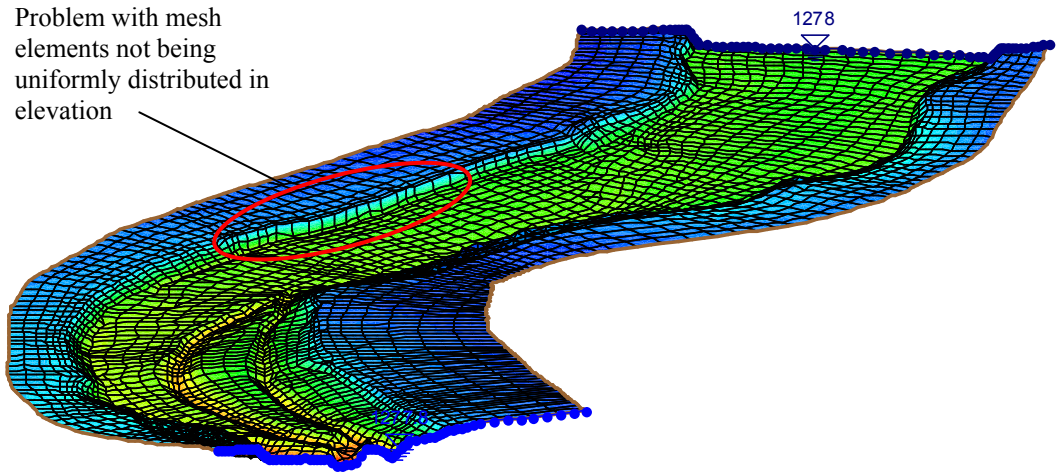

Figure A-15. Poor element construction along channel bank, 3D model illustration

A new approach for including of vertical banks in the model mesh

After repeated experimentation and consultation, it was evident that an alternate approach would be needed to solve the mounting problems related to the steep channel banks characteristic of the Carson River channel. Steep elements bring about sudden changes in water depths and velocities between adjacent nodes within steep elements, and the finite-difference algorithm of FESWMS inevitably moves toward divergence and a model crash. Realizing that the simulation of floodplain flows could result in assumptions that would bring the model results into question and noting that the maximum Carson River streamflow for the period covered by this analysis was below the bank-full level (7555 cfs at Fort Churchill, estimated using RIVMOD), it was decided that the model mesh would be significantly modified to effectively remove the floodplain elements. Besides, most of the floodplain nodes were not field surveyed and were only later added.

Additionally, FESWMS offers one feature that would prove particularly useful for this change. The model mesh includes a finite spatial area defined with a boundary. This boundary is a vertical wall with no upper limit. Flows magnitudes causing contact with the boundary are therefore not subject to elemental drying, except when water surface elevations drop below the storativity depth specified at the base of this imaginary vertical wall. A vertical wall shear coefficient is specified within the FESWMS parameters dialog box. Based on the availability of no data, it is assumed that the shear stress applied to the bottom of the channel will be the same as the shear stress applied to the vertical walls. Semi-slip conditions are selected in the FESWMS control box and a value of 1.0 (100 % of bottom stress) is entered within the FESWMS parameters box.

Mesh modification required careful planning and frequent saving of work. The model interface does not include an undo button. The deletion of nodes and elements causes the model boundary to move inward toward the main channel. Nodes cannot be inserted outside of the model boundary without starting over at the triangulation phase of mesh development, at which the outer boundaries are determined. Accidental node deletion, resulting in an undesired boundary, can therefore pose a problem. Nodes within the boundary can be created and relocated, and node elevations can be recovered from original survey data, but typically it is easier to revert to a saved version of the mesh, from prior to any undesired mesh modification. Due to the small size of many elements, notably along the steep portions of channel bank, nodes were removed one at a time.

Prior to node and element deletion, planning was needed to identify these nodes and elements. The established goal was to provide a mesh able to accurately simulate flow conditions up to bank-full conditions. First, the locations of all steep, nearly vertical

banks were identified within the detailed mesh. Photographs and field data were reviewed as an additional accuracy check. Unfortunately, vertical banks do not characterize the entire 500-meter surveyed reach of the Carson River. Portions of the Scout Camp reach included a gradual slope from channel bed to floodplain or the presence of rip-rap for erosion control. Regions characterized by vertical banks are identified with ovals in Figure A-16. These vertical banks would become vertical wall boundaries for the final mesh. The disconnectedness of these vertical features meant that all mesh boundaries could not be moved uniformly closer to the channel. Rather, the top of the vertical banks was used as a reference. The extent of mesh retained between segments of vertical banks was based on one criterion: making certain that the highest elevations in these less steep areas remained higher than the tops of the vertical banks, as known from the present model mesh. This consideration ensures that the model will have the capability to accurately simulate river flows up to the bank-full threshold. Beyond this singular criterion, mesh refinement was based on both providing a smooth model boundary for improved wetting and drying performance and also minimizing the number of elements, so as to decrease computation time. The first cut of mesh refinements to create true vertical banks is shown in Figure A-17. All mesh boundaries represent vertical walls with roughness values equivalent to those of the channel bed. Roughness values were assumed equivalent to bed roughness values used in RIVMOD for the IFMTFM, a value of 0.045. Channel banks not characterized by steep banks are maintained with transitional areas between the two bank types. Where vertical walls are present along the channel, the node elevations along these vertical walls are the surveyed or estimated elevations at the base of these features.

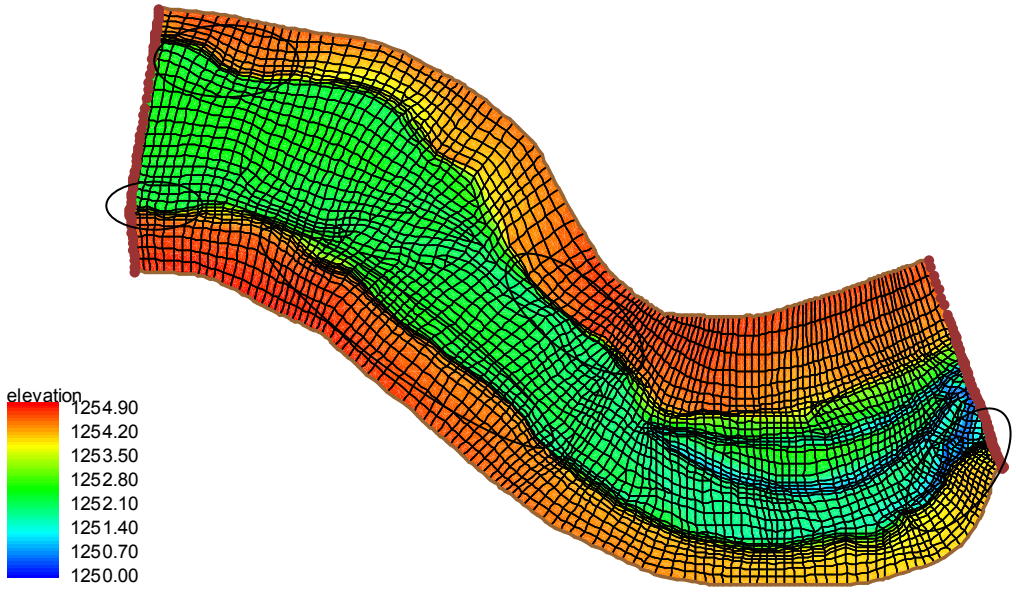

Figure A-16. Areas along Scout Camp reach characterized by steep vertical banks

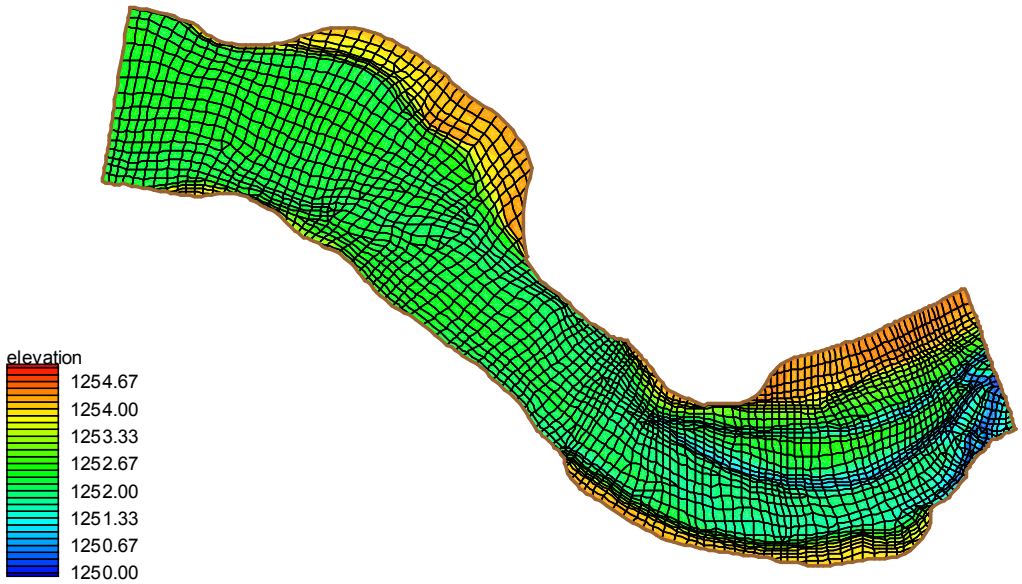

Figure A-17. Mesh alteration to incorporate vertical walls along mesh boundaries

Steady-State FESWMS Simulations, Elements Submerged

Setting of Model Parameters

With the mesh framework now in place, the next phase of mesh development revolves around lowering the water surface to simulate drying conditions. The ability to construct a model mesh in which elements dry smoothly would prove a difficult task. A couple of questions first need to be answered. Is element re-wetting important? At this point, the intention remained to have the FESWMS model simulate Carson River flows over the entire period for which water table data from the wells was available. With channel flows during this period both rising and falling, element wetting and drying would both need to be considered. A reasonable range for storativity and depth tolerance for drying was determined to be 0 – 10 cm and 10 – 30+ cm, respectively.

In simplistic terms, if the storativity is 0.0 and the depth tolerance for drying is 5 cm, the node goes dry (causing all elements that use the node to go dry) when the computed depth reaches zero. The node and associated elements remain dry until the computed depth gets above the depth tolerance value of 5 cm. If the storativity is a positive value larger than zero, the node does not go dry until the computed depth drops below the node elevation by the storativity depth. Less flow, however, is transmitted through the elements attached to the node if the depth is between zero and the storativity value, an effective negative water depth. Storativity depth must be carefully parameterized. If the computed water surface drops below the ground elevation of all nodes in an element without falling below any one node by a value larger than the storativity depth, then a "water surface elevation < 0 for node X in element Y" error will result, causing the model to crash. This functionality suggests that upper end of the storativity range will be most useful to simulate drying of elements with moderate slopes,

where the elevation shift from channel bed to floodplain levels is not as abrupt as where vertical banks are situated. Storativity values of zero are essential when stage levels move below the banks and onto the flatter channel bed. The trade-off here is the premature drying (and inability to transmit flow) of some elements within the channel thalweg, where slopes are comparable to the non-vertical channel banks.

Similar logic is used in the setting of the depth tolerance for drying. If the water depth along any side node of a "dry" element exceeds the depth tolerance value, the element will re-wet during the next iteration. Of course, the storativity value will be checked during the next iteration, and the element will likely again become dry. Additionally, dry elements adjacent to the newly wetted element can also be rewetted if the water depths are sufficient. This drying and rewetting can result in wet elements disjoint from the wet portion of the mesh. Given that the model has no means to remove water in disconnected "ponds" from the mesh, a sufficient volume of trapped water can cause several nodes to oscillate between wet and dry, often causing water surface elevations and velocities to move outside of a reasonably expected range. As the model is merely performing a series of computations without any logic checks in place, the model may not crash. The model will, however, not converge, and the errors will propagate from one iteration or time step to the next. It is critical, therefore, to visually inspect all final solutions for reasonable values and no disjoint wet elements. Under conditions where wet elements do not become disjoint, but only oscillate between wet and dry, the problem is the increase in computational time caused by the failure to converge. As the model attempts to compensate and force convergence, divergence can result. Through a trial and error procedure, depth tolerances greater than 30 cm were found to work for the

stages in which moderately-sloped banks elements remain wet, while lower values were found only to work for low flow levels close to the channel thalweg.

With the storativity and depth tolerance limitations in mind, it was decided to refine the model mesh under conditions of drying, whereby the head boundary conditions are always dropping. At this time, one was not interested in allowing the model to come to steady state through use of step function head decreases. Simple linear decreases were applied to the upstream and downstream head boundary conditions. Depending on which elements were subjected to drying, variable rates of drop were necessary. The balancing act here was to lower the stage as quickly as possible, but without a loss of model stability. Stages over the steeper portions of the mesh were able to be lowered at rates of 0.1 meters over 3 or 4 hours, as relatively few elements dry for a given time step of 15 minutes. As flows dropped to levels in which channel bed elements become dry, slower rates were needed. With the approach in place, all that remained was the determination of the head gradient between the boundary condition nodestrings. For mesh refinement purposes only, as opposed to generation of final results, a gradient of 0.2 meters was chosen. The belief was that a small gradient (0.2 meters of head loss over approximately 500 meters along the thalweg) would result in a smooth drying pattern of elements around mesh bends and steeper mesh elements. A node causing model divergence or a model crash under the most passive of conditions would clearly result in model problems under higher velocity conditions, and therefore represented a portion of the mesh in need of adjustment.

Convergence Problems Present under Submerged Conditions

While looking to lower the water surface through the model domain from completely submerged conditions to levels at which steep banks are no longer contacted,

goal number one was the removal of all warning messages from the model output file (the .prt file). The earliest model simulations used boundary condition head levels of 1265.0 and 1264.8 meters, respectively, at the upstream and downstream boundary nodestrings. The highest node elevation within the model mesh is only 1254.45 meters. All mesh nodes are clearly submerged, as mandated for a cold start (no previous solution at all nodes) simulation. A simple steady state simulation indicated 24 nodes which produced "determinant < 0" warning messages. The FESWMS manual indicates this as caused by poorly constructed elements, but the output file does not indicate any course of action. The convergence problems associated with these nodes are evident in the steady state solution. Node velocities and water depths will appear to be inconsistent with those of most adjacent elements. Figure A-18 shows an example of how easily an area of the mesh experiencing divergence problems can be identified; the figure shows water surface elevation and velocity directions for all nodes. Areas of physically-inaccurate water surface elevations will be evident. The cause of the divergence in the solution is the

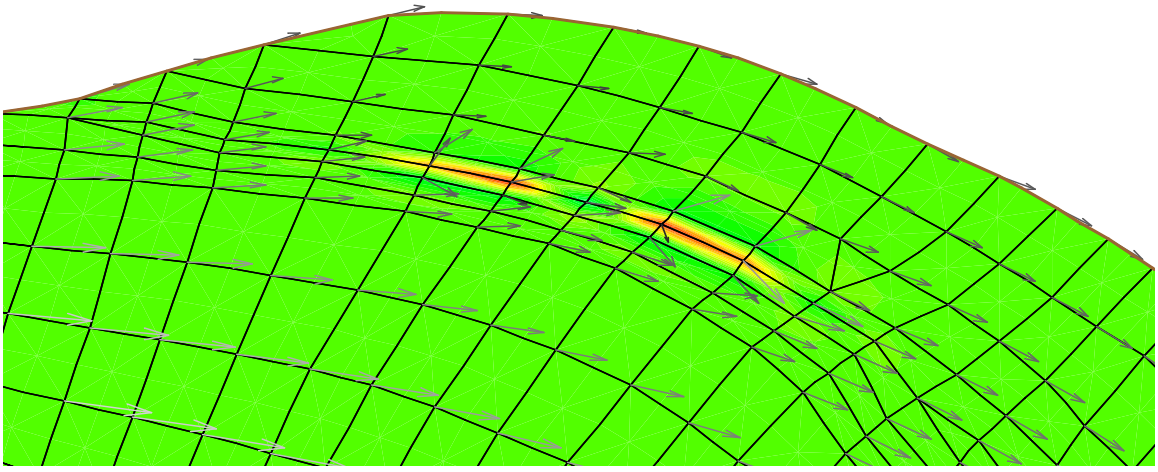

Figure A-18. Model divergence, water surface elevation and velocity vectors

survey data. Most notably along the sloping channel banks, locations submerged for only a small fraction of the year, channel morphology does not smoothly vary. Areas of deposition and erosion, including sloughed banks and preferential flow pathways, occur with high frequency. While such features are indicative of field conditions, sudden low or high points can cause divergence with the numerical solution scheme. By zooming in on these diverging elements and clicking on each node, it is simple to identify these nodes failing to follow the overall morphological trend. In these instances, adjustment of the elevation of a single node, or even a few adjacent nodes, by less than a centimeter, to better match the surrounding nodes, can solve the divergence problem. In other instances, elements were poorly shaped, with large interior angles, non-uniform node spacing, or element areas differing from adjacent elements by greater than a factor of two. On a case-by-case basis, nodes were added, deleted, or moved slightly to improve mesh characteristics. Considering the dynamic nature of the channel morphology and the fact that the survey data itself includes two collection periods, these changes are easily justified as having negligible bearing on the eventual model result of interest, river stage at the well cross-section.

Model convergence is also a concern, in an effort to minimize computation time. Recall the convergence criteria are user defined, and the values require all mesh nodes to demonstrate iteration-to-iteration variability of less than these values for "convergence" to be achieved. Values of 0.1 m^2/s and 0.05 meters were used for unit flow (both x and y directions) and water depth convergence, respectively. Per the eventual desire to accurately predict river stage, water depth convergence was of particular significance. It was found that when the above convergence criteria were satisfied, the average depth

change of all mesh nodes between iterations was typically less than one centimeter. This average value, also found in the output file, was perhaps of greater interest, but the FESWMS model does not allow convergence to be specified according to this average change. The repercussion of this model limitation is that a single diverging node for which unit flow and water depth cannot stabilize will prevent model convergence. The 10 highest nodes can be viewed from the output file. While admittedly, multiple nodes will be outside of the convergence criteria during element drying, the limitation is evident.

In an attempt to counter this limitation, the top 10 nodes were also recorded for each model simulation. In most instances, less than five nodes would stand out as having significantly larger maximum changes for unit flow and unit depth. When the same nodes top the list for both unit flow and water depth, these nodes were noted. In the same fashion as warning messages were alleviated, elements containing these elements were meticulously studied, and minor elevation changes or node spacing changes were completed.

The act of correcting nodes and elements identified by mesh quality checks, warning messages, convergence criteria listings, or simply looking at the solution is never a guarantee of model success. Mesh refinement is always an iterative procedure. Considering the general nature of the warning messages or the appearance of an unexpected mesh solution, it is never really assured that the underlying problem has been fixed. Node elevation changes were specifically made to be minimal, in an effort to preserve both the underlying survey data and the relevance of the model solution. In some cases, these adjustments would prove not enough. In some cases, seemingly fixing one problem would cause a problem with adjacent elements. After each round of

corrections, the model was started again under the same boundary conditions. Solutions were analyzed and additional corrections were made.

Convergence of the Steady-State Model for Submerged Conditions

The first sign of true progress was the attainment of convergence for a simple steady state solution for submerged conditions. The second sign of progress was the removal of all warning messages from the model output file. Warning messages, after all, are only one step removed from an error message, the latter of which cause the model to crash completely. Nodestrings created within the mesh interior were used as tools to check flow convergence. While these nodestrings are never exactly perpendicular to flow direction, they can be used to compute flow though the cross-section based on nodal velocity and water depth solutions along the nodestring (integration of flow area and velocity along a line of nodes). Comparison of flows at the boundary condition nodestrings and within the mesh interior is a useful check that a steady state solution was achieved, given that the model uses alternate criteria for convergence). Velocity vectors can also be displayed to check for nodes falling outside of the typical range, including nodes with velocity vectors not facing the direction of flow or nodes with unusually large magnitudes for velocity.

When a solution is imported into the display window using the Data Browser, several additional statistics are computed and displayed. Noting the interest in river stage for this research, the range, mean, and standard deviation of the water surface elevations are of primary interest. The use of natural boundary conditions, which allow for modest variability of water surface along the boundary nodestrings, guarantees that the water surface elevation range within the model solution will exceed the input boundary condition range. Additional variability is the result of diverging nodes within the interior

of the mesh, as the water surface should generally slope downward along the model domain. The mean water surface elevation should fall close to the average of the boundary conditions at any given time step. The water surface standard deviation will be a function of the head gradient through the model domain. For the small head gradient of 0.2 meters from upstream to downstream, the standard deviation for well-characterized solutions was typically close to 0.035 meters. Since node distribution in not uniform within the mesh and the flow path is not straight, the statistics were used a guidelines to check model reliability. For dynamic solutions, these statistics prove particularly useful as they allow identification of the exact time step at which the solution started to experience divergence difficulties. In these instances, the output text files can become too large to open using WordPad. By importing the solution and noting when the problems begin, stepping through each solution time step before and after this time enables identification of particular mesh areas in need of further refinement.

The above mesh refinement process was required to get a simple steady state model to run. No consideration of element drying has yet taken place. It is certain that mesh drying will bring about a completely new set of problems, some of which have previously been suggested in the discussions pertaining to vertical banks and the establishment of model convergence criteria. Realize, however, that the mesh problems fixed previously would each have likely guaranteed model failure when element drying began. In a sense, these problems were avoided before the start of what would become the biggest modeling challenge of this project, the simulation of mesh wetting and drying and prediction of channel stage over time, as a function of streamflow. The modified mesh with steady state solutions for velocity (vectors) and water depth (color-filled contours) are shown in

Figure A-19. Note the smooth nature of the depth variations from thalweg to vertical banks and the characteristic trend of velocity magnitudes, with highest magnitudes observed for the thalweg and lowest magnitudes where flow is the shallowest and farthest from the inner channel. The model also includes distinct material properties for the channel bed, channel banks, and floodplain areas. The channel bed and channel banks are defined by a roughness value of 0.045. The floodplain represents that portion of the model domain that is not submerged during most years and to which vegetation imparts a different roughness of 0.10. These values are taken from the RIVMOD input data files.

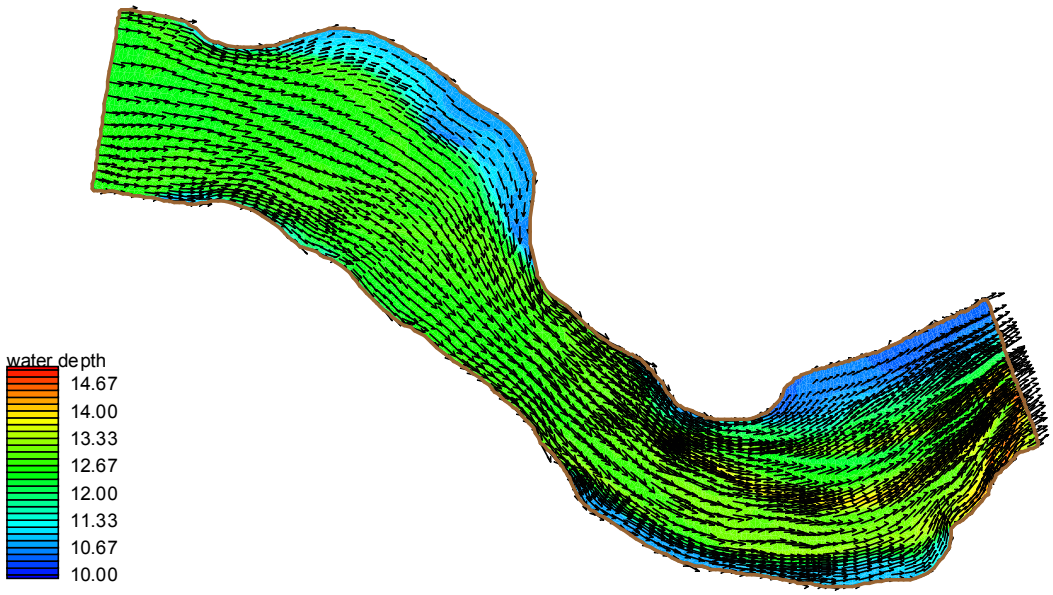

Figure A-19. Converged velocity solution, model domain submerged

Dynamic FESWMS Simulations: Lowering of the Water Table

Model Parameterization

Before testing the ability of the mesh to simulate water surface lowering and element drying, model parameters needed to be set. The ultimate goal is to create a stable model able to simulate in-channel water depths from near zero to bank full conditions. At

times, this effort will require some creativity, but some basic rules of the game need to be laid out.

Head boundary conditions will be applied at the upstream and downstream boundary nodestrings. The hydraulic head loss, or decrease in water surface elevation, along the approximately 500-meter flow path of the model domain will remain constant at 0.2 meters. The rate at which the water surface is lowered will vary, but the rate will be the same at each boundary nodestring. Because of the intrinsic instabilities associated with a jagged wet / dry boundary, boundary conditions are lowered continuously, instead of through the use of a step function whereby the model is lowered to a point and stabilized to reach a steady state. At this point, the concern is not the simulation of actual flow conditions. Rates of head decrease are chosen based on two simple criteria: the FLO2DH model being able to run to completion and the drying of elements appearing to follow the topography of the terrain. Given the potential for rapid stage change within the system, as a result of sudden upstream snowmelt, the model should possess the capability to simulate a rapid lowering of the water surface. The maximum rate of water surface lowering to maintain model stability was found to be approximately 0.1 meters per 3.0 hours. In many instances, these same 0.1-meter decreases required 4 or 5 hours (at minimum) because of the irregular nature of the channel topography. With nodestrings created to include all nodes along the upstream and downstream boundaries, boundary conditions are assigned by selecting ‘FESWMS / Assign BC.’ Within this dialog box, the following options are checked: boundary definition: specified flow / WSE. This highlights for editing the specified flow / WSE options portion of the dialog box. Check the water surface elevation box and the natural boundary circle, the latter to allow small

fluctuations, from the single specified boundary condition, in water surface elevation along the boundary. For steady state simulations, a constant water surface elevation is input. For dynamic simulations, the transient option is selected and a series of points are inserted to define the time / water surface elevation curve at the selected boundary.

Two options are available for starting the model, a cold start or a hot start. The FLO2DH model in FESWMS computes water surface elevations, water depths, and velocity vectors for all nodes in the model mesh. A cold start is used when no previous FLO2DH solution is available. By default, velocity in the x and y directions is zero for all nodes. An initial water surface elevation is assigned to all nodes not already assigned a water surface elevation by the boundary conditions. The model will converge sooner the closer this initial value is to the eventual solution. Initial water surface elevation is assigned from 'FESWMS / Model Control / Parameters' by typing a value in the appropriate box. For a cold start, the initial water surface must be greater than the elevation of the highest node in the model domain, such that all nodes are submerged. The steady state option is selected under 'FESWMS / Model Control', the maximum number of iterations is set to 99, and the model will iterate towards a solution.

For the hot start option, the initial conditions to the FLO2DH model are read from the output files (.ini and .flo file extensions). Nodes are assigned the water surface elevations and velocity vectors from a previous simulation. Several advantages are offered by this approach. Steady state simulations with unchanging boundary conditions can be repeatedly run until meeting the established convergence criteria, rather than stopping at the solution after 99 iterations. Additionally, dynamic simulations can be run for smaller time periods, and the final solution can be used as the initial conditions for the

next simulation. This keeps the output file sizes manageable for post-processing and facilitates early identification of divergence problems. Hot starts can be initialized from any time step of a previous dynamic solution. This is particularly useful in the case of relatively minor divergence problems caused by disjoint wet elements during the drying process. The output .flo file can be edited to force these disjoint elements to be dry (which would be the case in reality) at the first sign of their appearance. By saving this modified file, the model can be restarted from this middle time step, and the disjoint nodes will not be carried through future time steps. Small divergence problems can therefore be corrected and the water surface lowering can continue. By contrast, changing any of the node locations or elevations would require starting over again from a cold start with all nodes submerged. In the case of no element divergence due to drying, hot start solutions alleviate having to start over with submerged conditions. This is a time consideration. As noted, an upper limit exists for the rate of water table lowering. If it is known that the model is able to simulate higher stage levels, node modification is not a desirable choice. However, large divergence problems require node modification, re-starting of the simulation from submerged conditions, and re-lowering of the water table, with no guarantee that another drying problem will not occur. To use the hot start option, which is available for both steady state and dynamic simulations, the previous solution file is imported using the Data Browser, and the output file data sets and desired time step to be used as new initial conditions is selected under ‘FESWMS / Initial Conditions Data.’ Additionally, the .ini external file option must be selected in the FLO2DH input section under ‘FESWMS / Model Control’ and the appropriate .ini file selected.

Model parameters are also set within ‘FESWMS / Model Control.’ Required selections include the following, with the appropriate choice in parentheses: FESWMS version (FESWMS 3), FLO2DH input (.net file and .ini file for hot start simulations), run type (hydrodynamic), means to compute bottom stresses (Manning’s Equation), solution type (steady state or dynamic), slip conditions (semi-slip as next discussed), and option for higher order integration (none). The latter two of these parameters have not yet been discussed. The slip option applies no shear stress (frictionless) at the closed boundaries; no slip indicates that the shear stress at closed boundaries is so great that the tangential velocity is zero; and semi-slip allows for slip at a closed boundary unless the flow is against a vertical wall. Because the model boundaries in this model represent vertical walls, most notably at locations of steep, near-vertical banks, the no slip condition is selected to impart a non-zero frictional resistance to flow. After clicking on the Parameters box, a value of 1.0 is entered for the vertical wall shear coefficient, signifying that the shear stress on the walls is the same as on the bottom, based on roughness values assigned to elements at the base of the vertical walls. Higher order integration results in more precise solutions with a lengthier analysis time, primarily suited for dealing with curve-sided elements. Convergence criteria for unit flow and water depth are also input in this dialog box. Based on results from steady state analyses, unit flow convergence equal to 0.1 m^2/s and unit depth convergence of 0.05 m were determined to provide reliable results. The element drying / wetting option must be checked if elements dry during a simulation. The timing of element drying is determined by the input values for storativity and depth tolerance for drying. Different values are used dependant on which elements are drying. Storativity values in the range of 0.0 to 0.1 meters were used throughout the

modeling process, with higher values best suited for elements possessing the steepest slopes. Depth tolerance for drying values included a minimum of 0.1 meters for stage levels on the channel bed, 0.3 meters for stage levels along the channel banks, and values of 2.0 meters when flows approach the inner channel thalweg. These values are necessary to prevent excessive oscillation of elements between wet and dry, while not preventing re-wetting altogether.

All other parameters in FESWMS remained unchanged from the default values. This conclusion is based on a review of the physical significance of the default values (with the SMS Help menu as a reference) and an assessment of data limitations. Default values are used for the average water density and momentum flux correction coefficients. Model defaults also exclude consideration of Coriolis forces and wind conditions.

Within the iterations box under Model Control, a relaxation factor of 0.01, as recommended by other model users, is used to increase the numerical stability. Presumably due to the result of the high degree of channel variability, the FLO2DH model will crash when the default value of 1.0 is used. A time step of 15 minutes (0.25 hours) was specified. Maximum iterations were set at 30 for dynamic simulations. Element drying often prevented model convergence based on the convergence parameters, but trials indicated that this number of iterations resulted in a stable solution. The time integration factor was not changed from the default value of 0.667. The start time and end time values are in reference to transient boundary conditions assigned under dynamic simulations.

Material properties are assigned for both floodplain and channel bank elements. Manning roughness values are taken from the RIVMOD input data files, with 0.10 used

for floodplain elements and 0.045 used for elements within the confines of the main channel. Turbulence parameters, including eddy viscosity and eddy diffusivity remain at the default values.

Model Operation

Element wetting and drying: considerations and parameterization

To predict channel stage as a function of flow using SMS, the model must be capable of simulating element drying without crashing. Although the FESWMS model does include options to simulate element drying, the ability of the model to converge is dependant on the pattern in which elements dry. It is preferable for elements to dry as the layers of an onion peel, always with a smooth wet / dry boundary, as might be reasonably expected for a straight, symmetric channel with smooth elevation changes throughout. Unfortunately, these optimal characteristics do not describe the Carson River mesh. Cross-sectional area is variable, including both smooth (gradually sloping) and abrupt (vertical banks) transition zones from channel bed to floodplain. In the downstream half of the modeled reach, channel thalwegs are deeper and the inner channel elements transport a significantly greater fraction of total flow than upstream, where thalwegs are less incised and more discrete. The modeled reach is not straight, including an almost 90° curve in the downstream section. Channel morphology is not smooth, including small hills and valleys where otherwise the trends in elevation change are reversed. Portions of the channel bed include sedimentation deposits and erosional deposits from bank sloughing. With the mesh constructed from a network of survey points with irregular node spacing and from multiple time periods, some of these bed features are captured better than others.

These observations dictate the element drying pattern when the water surface is gradually lowered. Elements cannot dry along a smooth boundary. Higher areas of the bank and channel bed will become dry, unable to transport flow, before elements at lower elevations. The rows of quadrilateral elements simply cannot be constructed to follow the contours of the land. Irregular drying results in element re-wetting and the potential for wet elements that are disconnected from the main channel. The oft-jagged nature of the wet / dry boundary causes numerical divergence at corner nodes of the outermost elements. As higher elements internal to the outermost wet / dry boundary become dry, flow can no longer be transported through these elements. Effectively, water flowing from left to right is suddenly faced with flowing around an obstacle, and numerical divergence often results. Nodes internal to the active boundary nodestrings also dry in these situations, potentially impairing the ability of the model to transport flow. Drying along the boundary can result in supercritical flow conditions that can be managed by the FLO2DH model. However, supercritical flow conditions internal to the model mesh cause a model crash.

The convergence criteria have previously been discussed. The values set are strict enough that the model will never truly “converge” if the wet / dry boundary is jagged in several locations within the mesh. Rather, the model will perform the maximum number of iterations before moving forward. For this exercise, convergence qualities of the mesh were measured in an alternate fashion based on both the statistics for each imported solution and a measure of common sense. With the exception of nodes located at wet / dry element interfaces, along with natural fluctuation along the boundary nodestrings, the water surface elevations for nodes internal to the model mesh should fall in the range

between the head boundary conditions. Each imported solution is also visually inspected. Water surface elevations not in accord with neighboring nodes and velocity vectors not in line with the flow direction or possessing uncharacteristic magnitudes were noted. While such divergence is expected along the wet / dry boundary, such divergence within the submerged portion of the mesh requires corrective action to be taken. In many instances, this divergence will manifest itself by causing element re-wetting, disjoint wet elements within the mesh, and model failure. Within a dynamic solution, model divergence can be identified when the standard deviation of the water surface elevations in the solution deviates significantly from 0.035 meters, under the 0.2-meter hydraulic gradient from the boundary conditions.

Model divergence: node identification, causes, and solution examples

The ultimate goal is to develop a model able to continuously lower the water surface elevation from above bank-full to nearly zero without the model crashing or diverging to a physically-unreasonable solution. The rates of change in the head boundary conditions are allowed to vary, as needed to best handle drying of each channel feature, but the rate remains constant for both boundary conditions for each time step. In other words, the 0.2-meter hydraulic gradient is a fixed value. The process here is iterative.

The model must initialize with all nodes submerged. The water surface is then lowered by 0.1 meters over a period of between 3 and 6 hours. One cause of model failure is “water surface < 0 at node X in element Y.” When drying along the steeper elements along the rip-rap and gradually-sloping channel banks, it is not desirable for these elements to dry when only one node becomes dry, given that the elements do not perfectly follow the land contours, and a storativity value of 0.1 meters is used to allow

the elements to continue to transport flow. The 0.1-meter value is nothing more than an estimated average of elevation loss across these elements. By the time the computed water surface has fallen to 0.1 meters below the first dry node, the element is most likely transporting very little flow and allowed to become dry. Model failure occurs for less steep elements when the computed water surface falls below all element nodes, but not more than 0.1 meters below any one node. In many instances, this effect is caused by computational instabilities and can be rectified by simply drying these elements at a slower or faster rate, by altering the boundary condition time series. Elements may also re-wet (depth tolerance for drying = 0.3 meters for bank elements) and become disjoint because of similar computational instabilities associated with the 15-minute time steps. Smaller time steps are also unable to remedy this problem. Additionally, note that by altering the rate of water surface lowering closer to steady state values, the same end is achieved; the rate of change (change in boundary condition divided by time step) is the same in both cases. If the model crashes under this scenario, which is evident when looking at a dynamic solution, changing the rate of change is also an option worthy of attempt. Due to the flatter nature of elements within the channel bed, a storativity value of 0.0 meters is used, but this problem does still present itself for nodes along the downstream boundary as the model attempts to force all nodes to closely match the designated head value.

Unfortunately, most model crashes and solution inconsistencies were linked to specific diverging nodes. In these instances, the problem is typically due to problems with the node spacing and element size, node elevations that do not follow the general elevation change trend, or both. To aid with visualization, picture a line of elements, with

therefore a line of nodes along the tops and bottoms of these elements. Divergence problems arise when the elevations along a line of nodes is rising or close to steady, but within that line are one or two or three nodes representing an elevation dip. Similarly, sudden high points occurring along the downward sloping channel bed can cause divergence problems. Of course, such natural variability is not a by-product of poor survey techniques, but rather this simply captures the variability present in the Carson River system. When nodes are closely spaced together, as they are with the 3 to 5 meter typical element length in the Carson River mesh, the finite difference algorithm may be unable to compensate. Sudden elevation changes on the order of only a few centimeters can pose divergence problems. The highest density of these divergent nodes occurs along the channel banks and rip-rap because of the slower velocities, where fluid momentum is less of an influencing factor. While at first these divergent nodes may not be obvious in a solution, such problems become evident after error propagation through several iterations and time steps.

Divergent nodes may not cause immediate model failure, but error propagation does lead to divergence problems with adjacent nodes and an unreasonable model solution. Nodes diverging for these reasons are generally easily corrected by changing one or two node elevations by a few centimeters, although generally less than three centimeters. Such modest changes in the elevation of even two hundred nodes within this 12,000+ node model will negligibly alter the final solution. The changes certainly fall within the error already associated with assuming a constant channel bathymetry for modeling the streamflow, predicting stage, and facilitating a comparison with water table levels in the groundwater wells.

When a divergence problem is identified from either a visual inspection of the solution, solution statistics, or a model crash, the number of each diverging node is recorded. The output .prt file is generated after all model runs, regardless of whether a model crash occurs. This file includes the assigned model parameters; initial conditions; convergence checks; and solution water surface elevation, water depth, and velocity vector data for all 12,000+ nodes in the model mesh. Node solution data is available for each iteration of a steady state run or for any time step interval of a dynamic solution, for which the 15-minute time step was selected. Notably, the FLO2DH model can be parameterized to print out up to the top 10 nodes for the convergence check component, ranked based on value change since the previous iteration or time step. By setting this parameter to 10, the 10 nodes with the maximum changes in y-direction unit flow, x-direction unit flow, and water surface elevation can be viewed for each time step of the model solution. The average change in these values for all model nodes is also noted. For a given time step, either the final time step before a model crash or a time step at which solution divergence is identified as beginning, those nodes with the clearest convergence problems were recorded. Particular interest was given to the nodes with the maximum changes with regard to water surface elevation. If an area of the mesh is seen that consistently produces the largest changes, it is a good idea to refine the elements in this portion of the mesh to assist with model convergence. The highest ranked nodes often also appeared near the tops of the unit flow convergence check lists, and multiple nodes from the same element were not uncommon. With a list of diverging nodes in hand, the process of mesh editing can begin. Node elevations for these and adjacent nodes were modified as needed to aid model stability. Nodes were also moved to improve the

uniformity of node spacing and element shape. Nodes along the wet / dry boundary were generally ignored, as divergence is due simply to there location along this boundary and the associated numerical instability. Lastly, mesh quality was checked and any problems were corrected. The mesh was then saved under a new name.

One might inquire as to the reasoning behind editing nodes that have yet to show a definite divergence problem. Personal experience with the FESWMS FLO2DH model indicates that these nodes will eventually cause a model problem after sufficient time for error propagation. In addition, after a mesh edit, the model must be re-initialized with all nodes submerged. A series of steady state simulations are completed with all nodes submerged until the convergence criteria are met. With no element drying and mesh corrections already completed for submerged conditions, the model satisfies the convergence criteria, starting from a cold start, within three steady state runs of 99 iterations each and using previous runs as hot start files. The water surface is then lowered to the levels at which divergence or a crash occurred (with the final steady state solution as a hot start file), so as to find out if the corrections were adequate to fix the problem. If the changes were too conservative, the mesh editing, the steady state runs, and the water surface lowering will need to be repeated. The water surface elevation can not be instantaneously lowered to the desired test levels, making this process extremely time consuming. Presumably, if all was done properly, the model will not crash or diverge before this lower stage level is reached or surpassed.

Mesh editing was performed iteratively in this fashion until a lower limit was found at which the model would work properly. As more and more experience was gained with FLO2DH, some mesh problems were identified and corrected in advance of a model

crash or discovery of a divergence problem. The mesh layout prior to water surface lowering and additional mesh editing is shown again in Figure A-20. While more than 20 of these editing iterations were performed, the mesh editing procedure and problems encountered are as previously discussed.

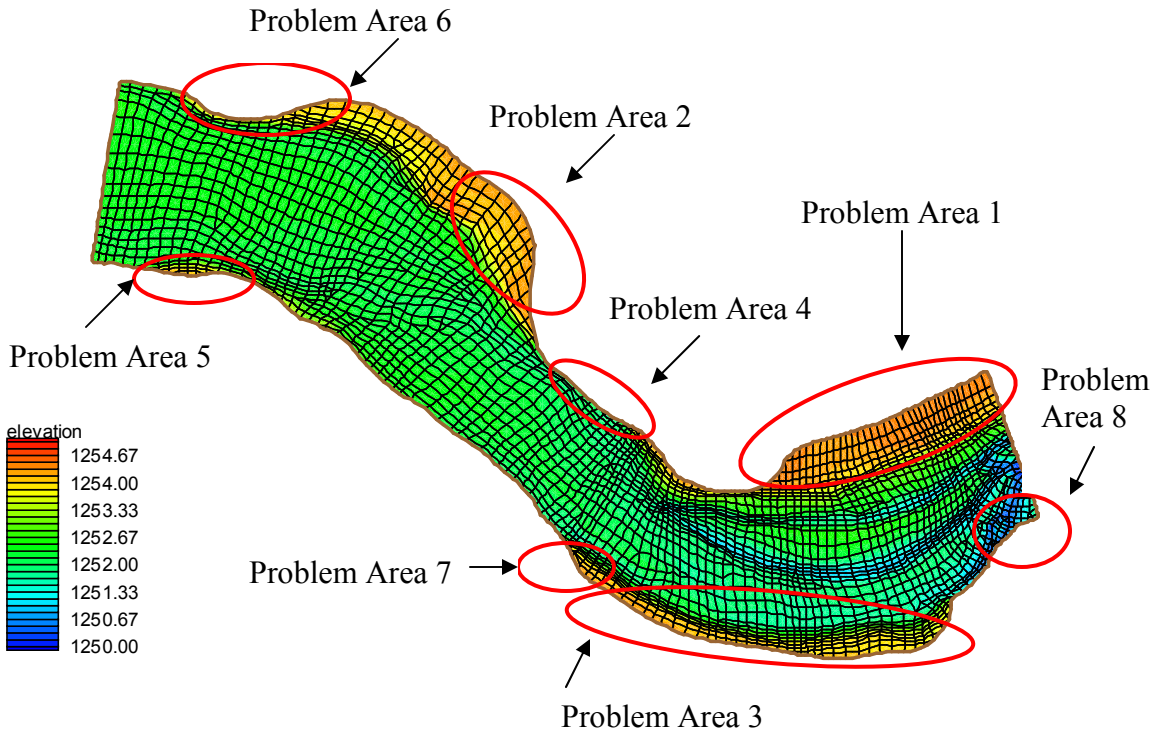

Figure A-20. Mesh structure before mesh editing to improve element drying

After considerable editing, the FLO2DH hydrodynamic model is able to simulate element drying from bank-full to the point of transition from channel banks to channel bed. The modeling experience and insight gained from fixing the many problems was next applied to the elements along the channel bed. Additional elements were added along the downstream portion of the thalwegs, to prevent too many large elements from drying within a given time step. Element density was also increased for the slope transition from bank elements to bed elements. Efforts were made to create bed elements of a fairly uniform size and rectangular shape. Triangular elements were included only

where needed around channel bends and changes in cross-sectional area, with one notable exception. Quadrilateral elements were split into triangular elements in those downstream areas in which the thalweg becomes branched. These changes assist the model in accurately simulating the channel flow under low-flow conditions. The drying of elements internal to the main body of flow, due to depositional bed features along the channel bed, requires careful mesh editing to prevent model divergence or failure when flow runs into these dynamically-changing obstacles to flow. Mesh quality was also used to correct gradient and element area problems before they could cause model divergence. Due to the flatter slope along the channel bed, except the thalweg, a storativity value of 0.0 meters and a depth tolerance for drying value of 0.1 meters were used. For flows passing primarily through thalweg elements, storativity values remained at 0.0 and depth tolerance was increased to 2.0 meters. This effectively prevents element re-wetting, but it is necessary to prevent elements from oscillating between wet and dry due the steep side slopes.

APPENDIX B
NEAR-CHANNEL WELL RESPONSE TO STREAMFLOW VARIABILITY

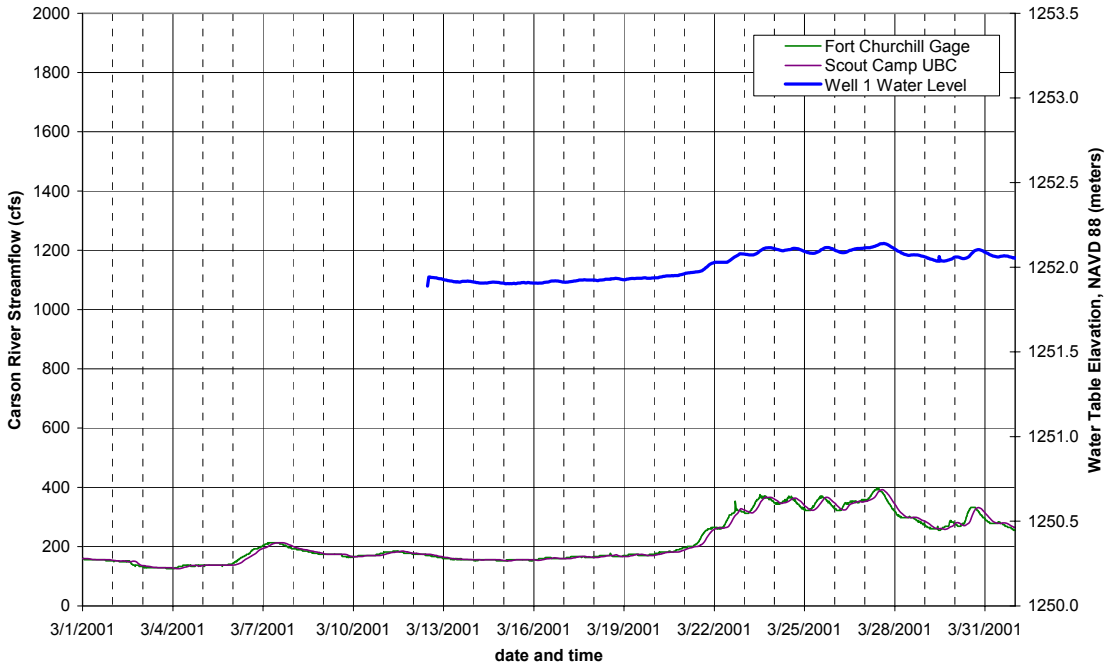

Figure B-1. March 2001

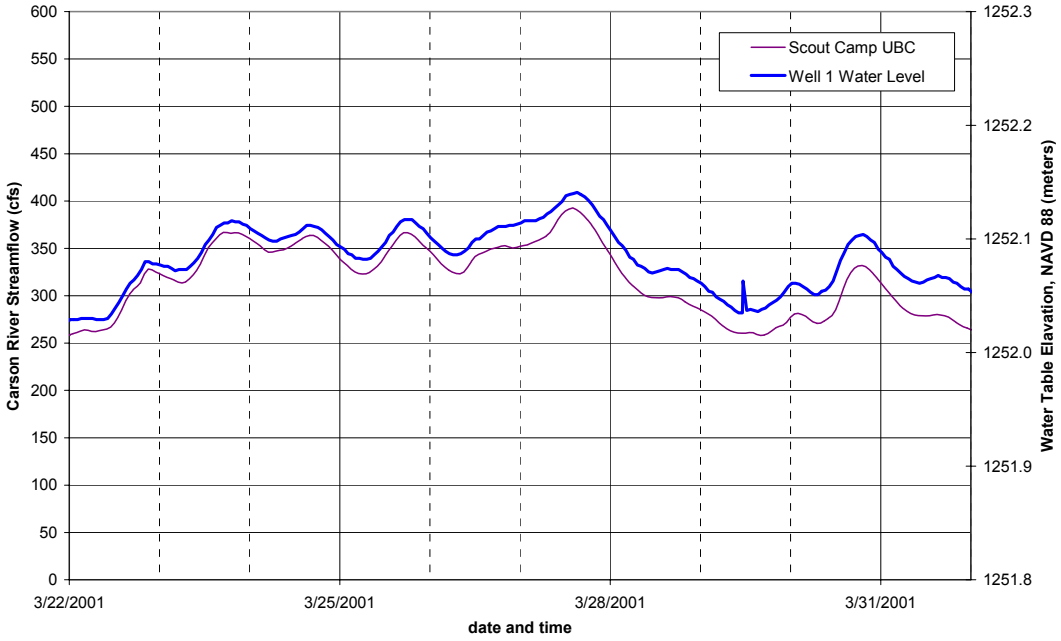

Figure B-2. March 22-21, 2001

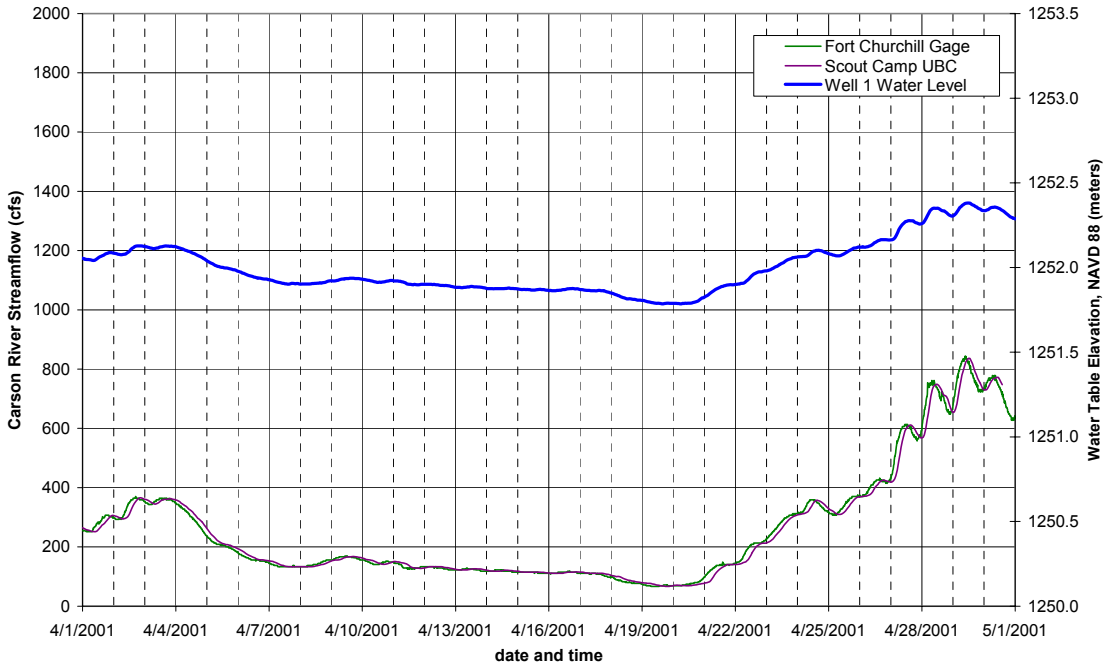

Figure B-3. April 2002

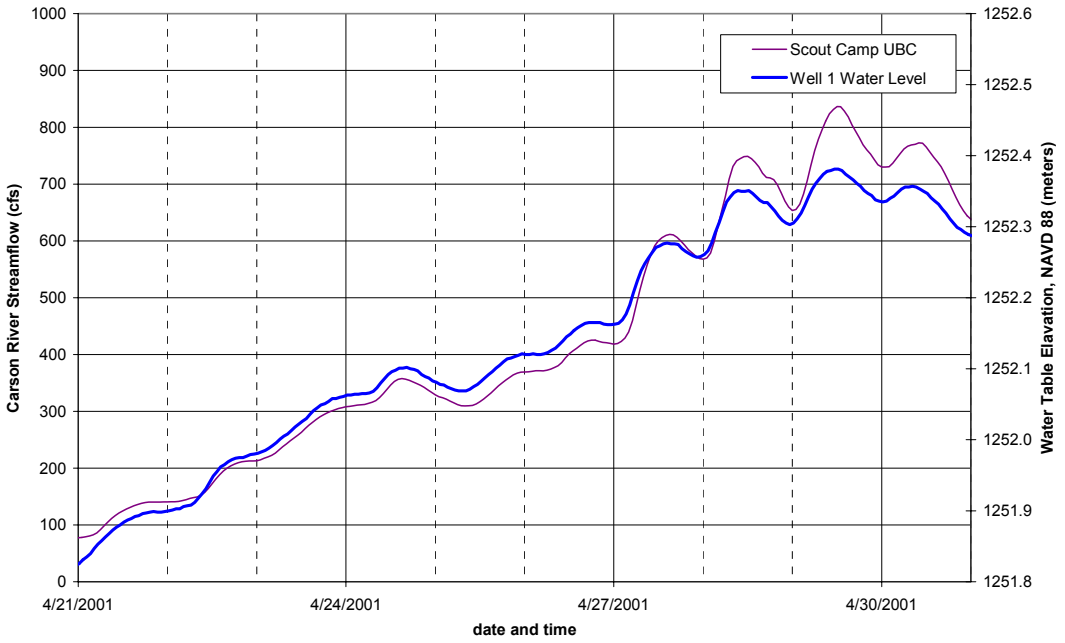

Figure B-4. April 21-30, 2001

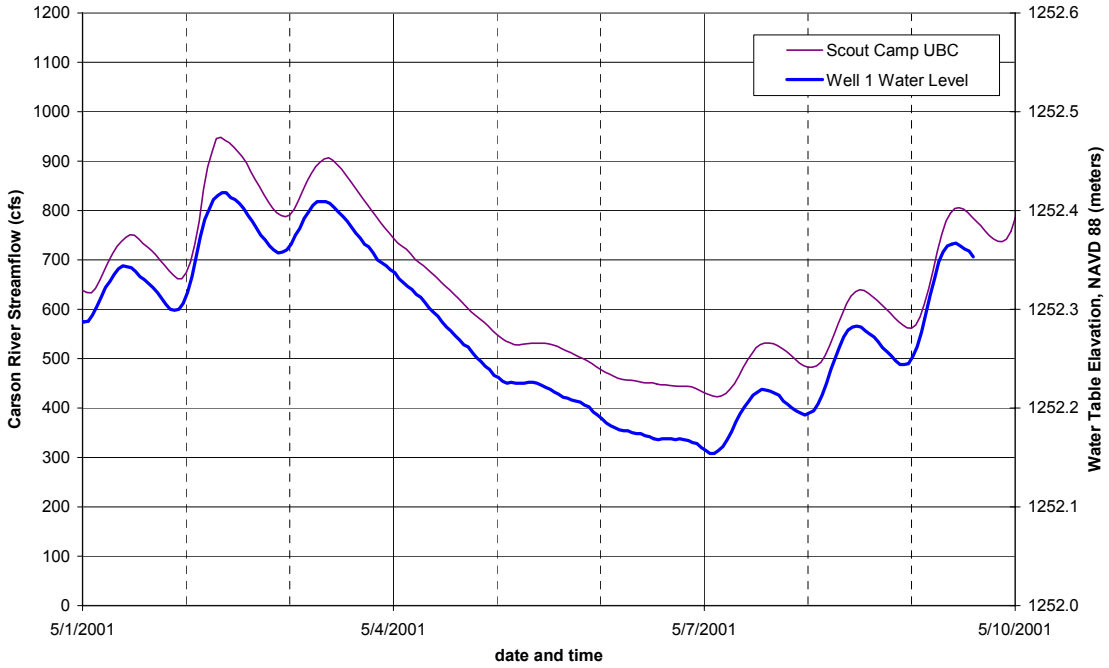

Figure B-5. May 1-9, 2001

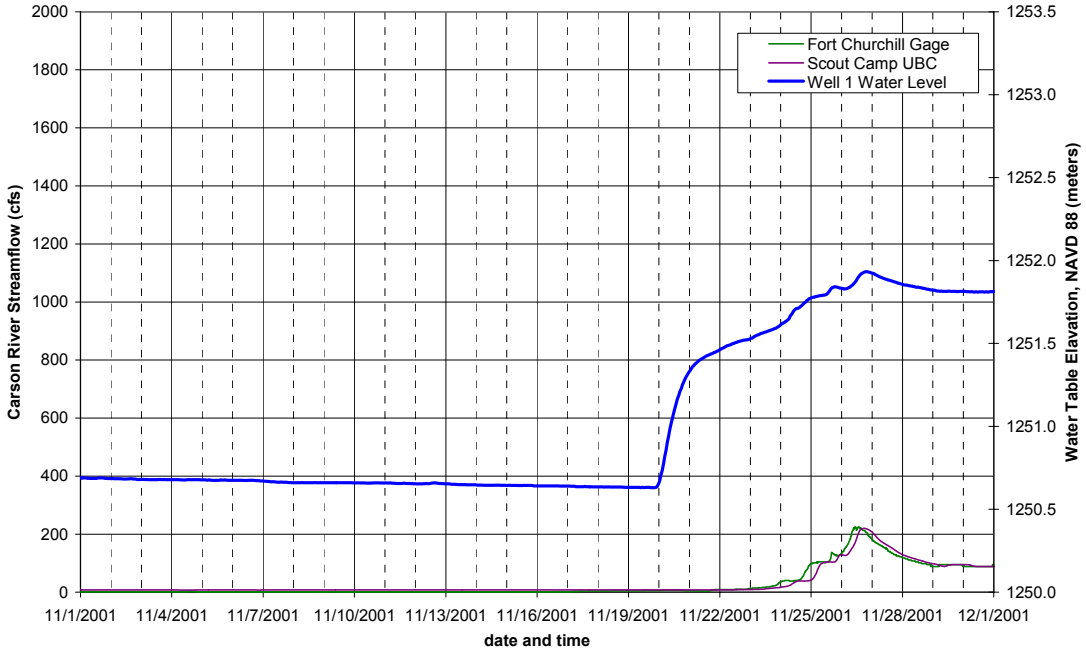

Figure B-6. November 2001

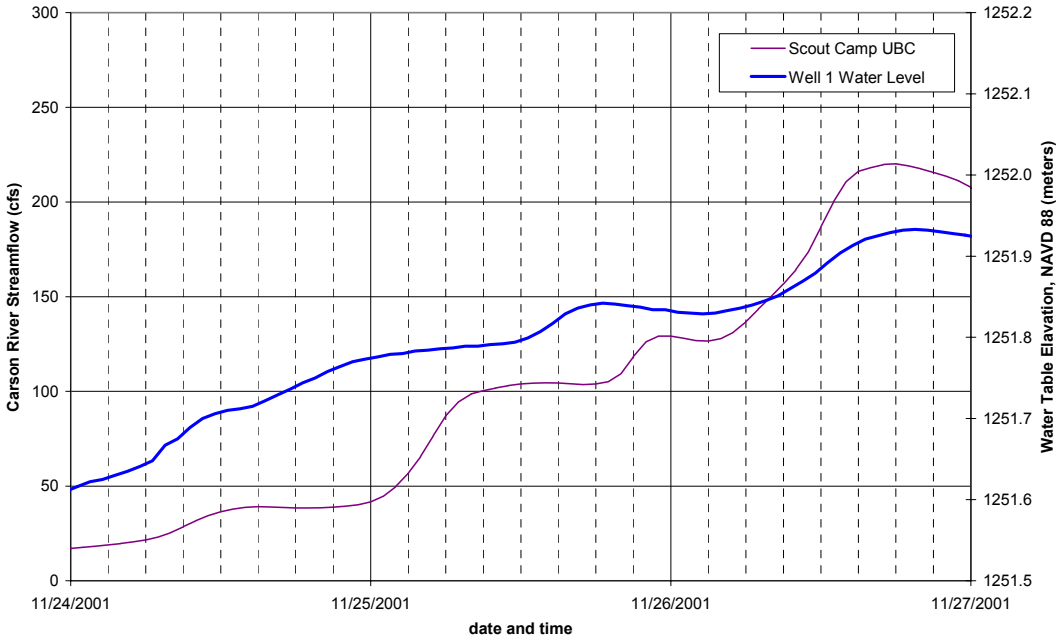

Figure B-7. November 24-27, 2001

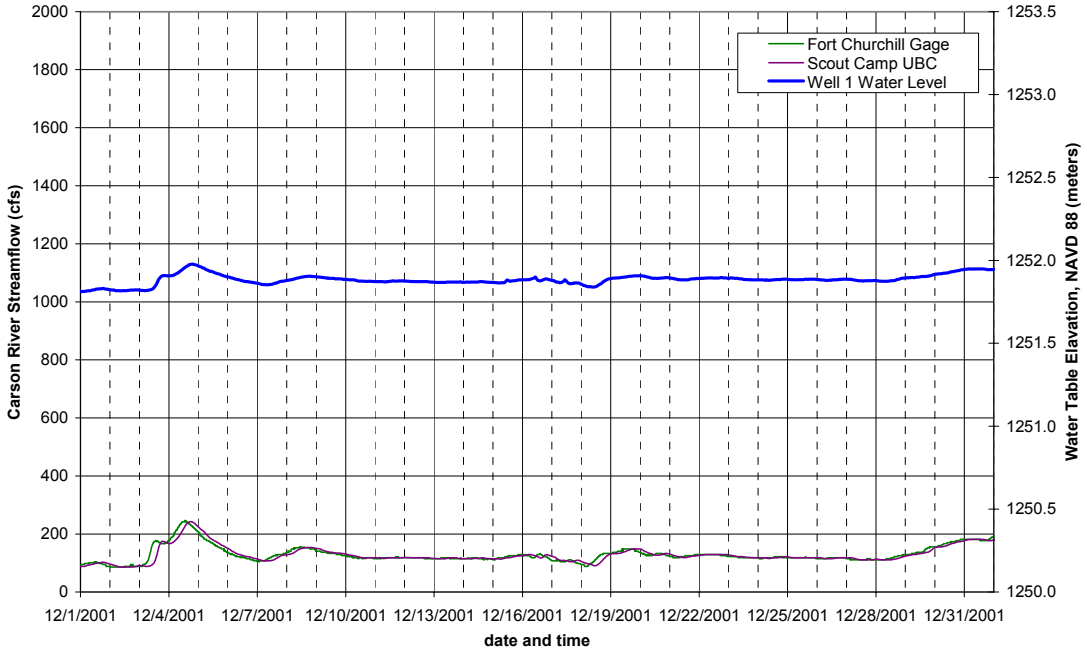

Figure B-8. December 2001

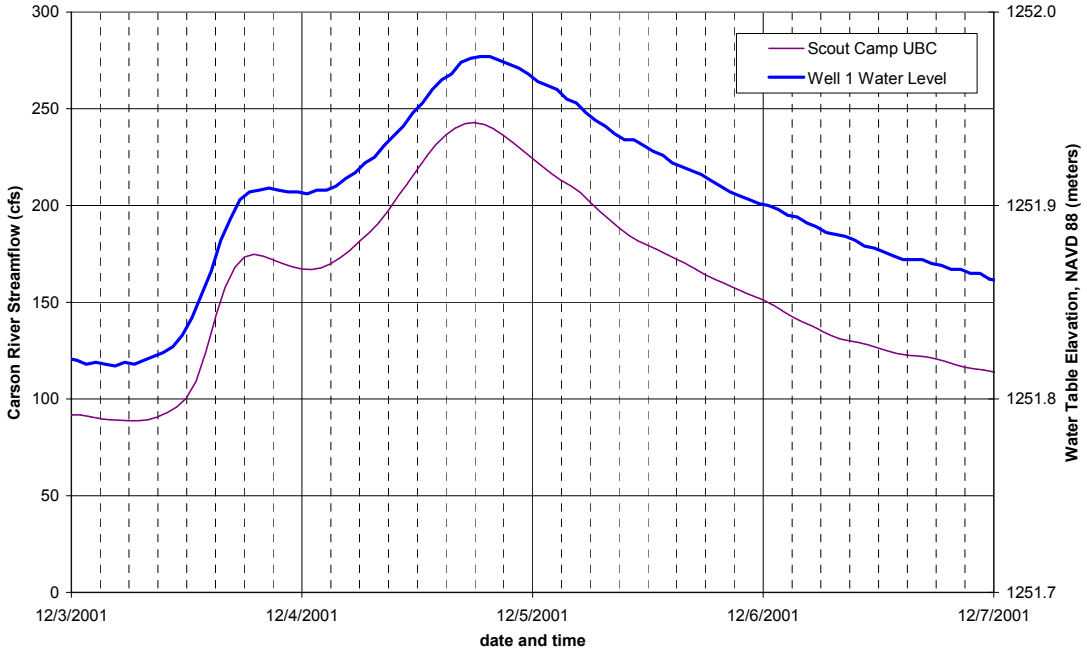

Figure B-9. December 3-6, 2001

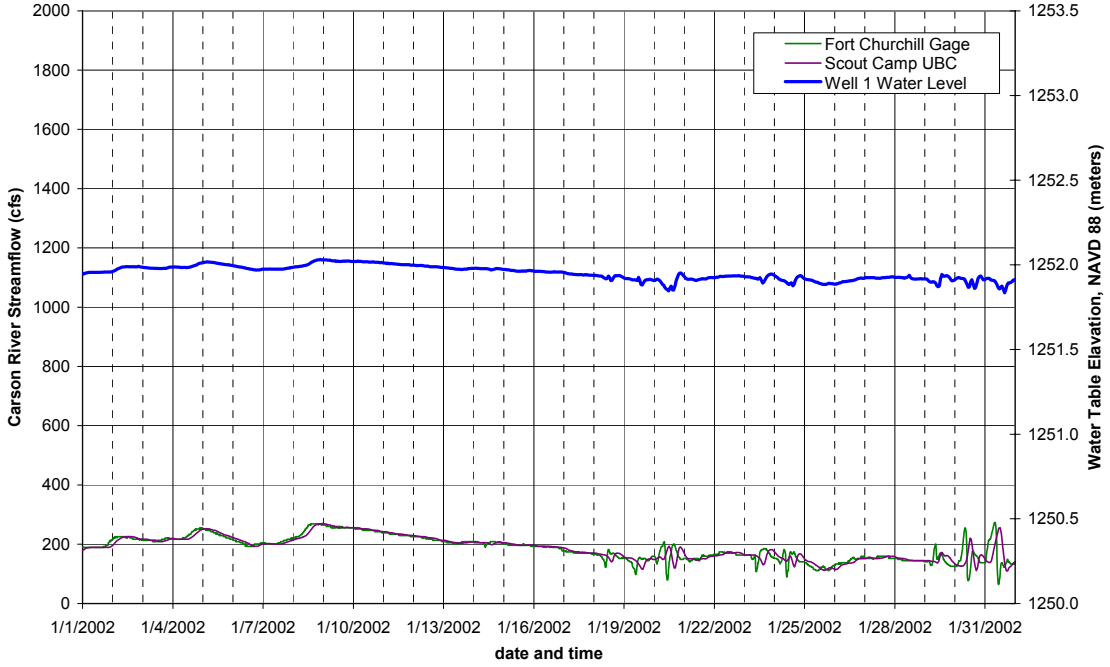

Figure B-10. January 2002

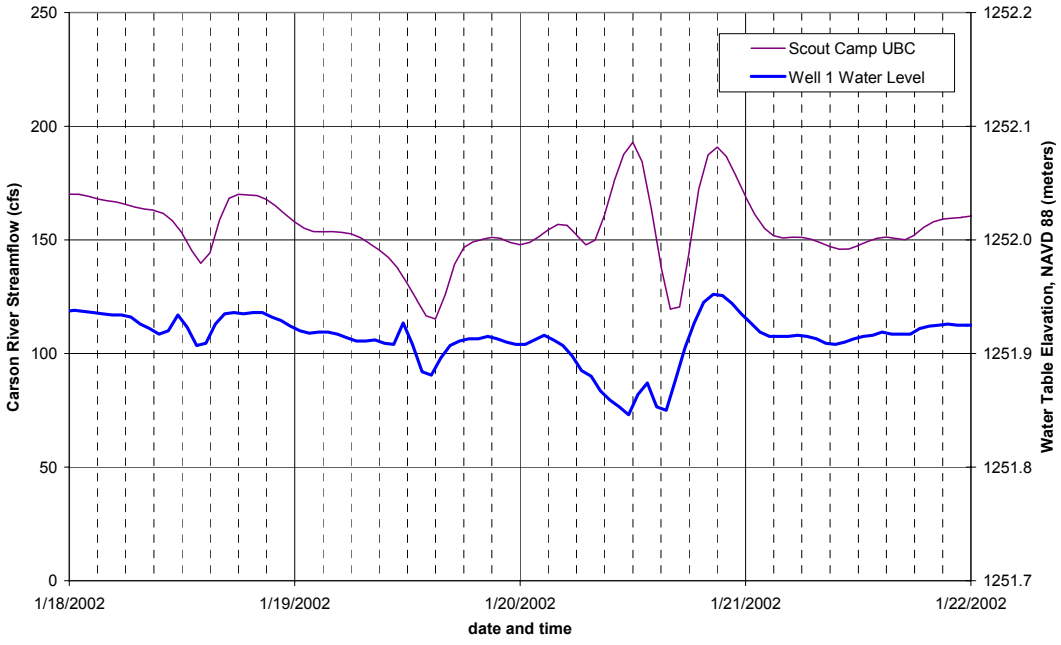

Figure B-11. January18-21, 2002

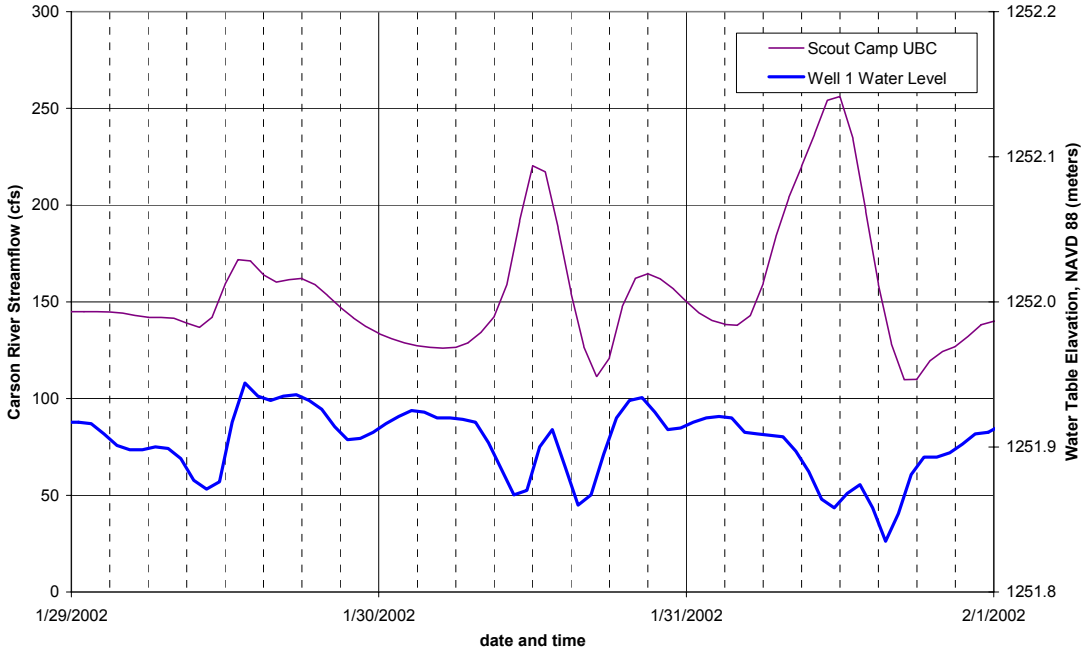

Figure B-12. January 29-31, 2002

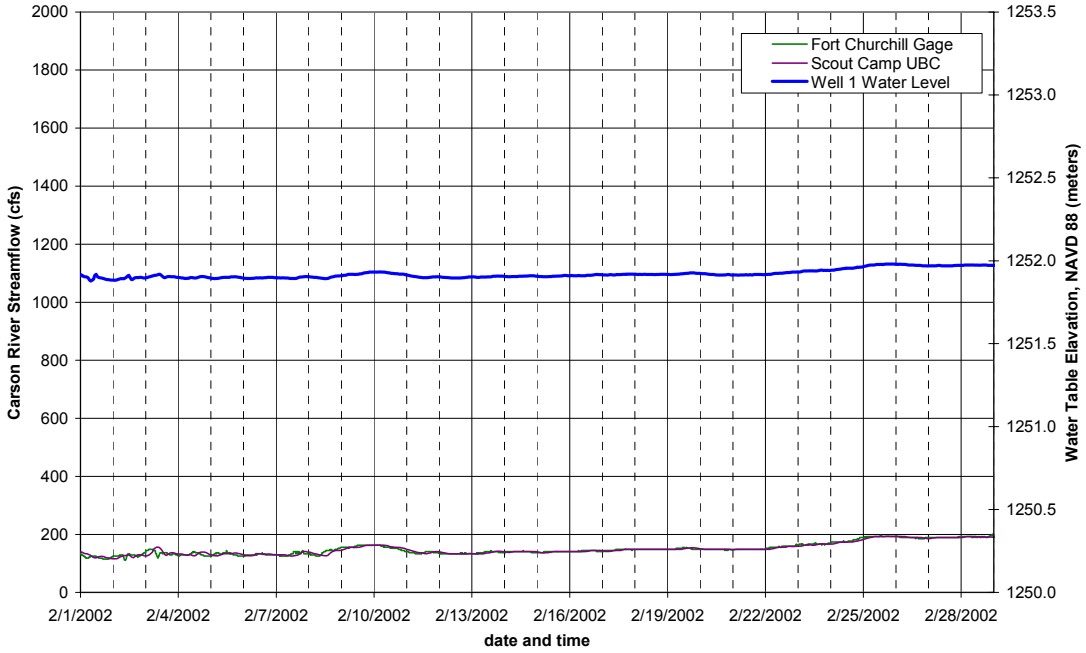

Figure B-13. February 2002

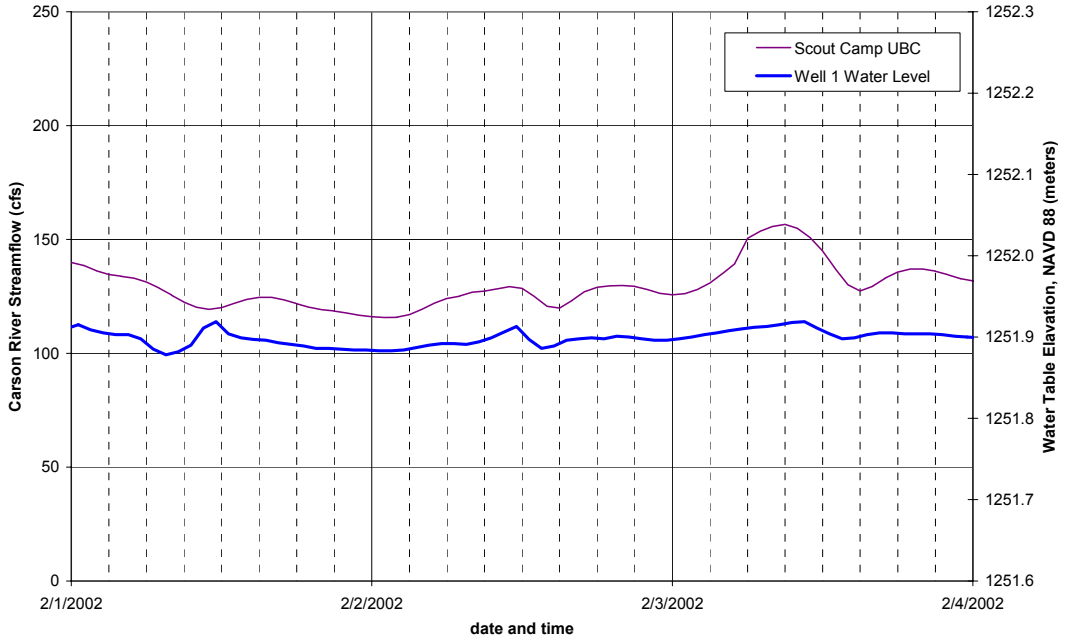

Figure B-14. February 1-3, 2002

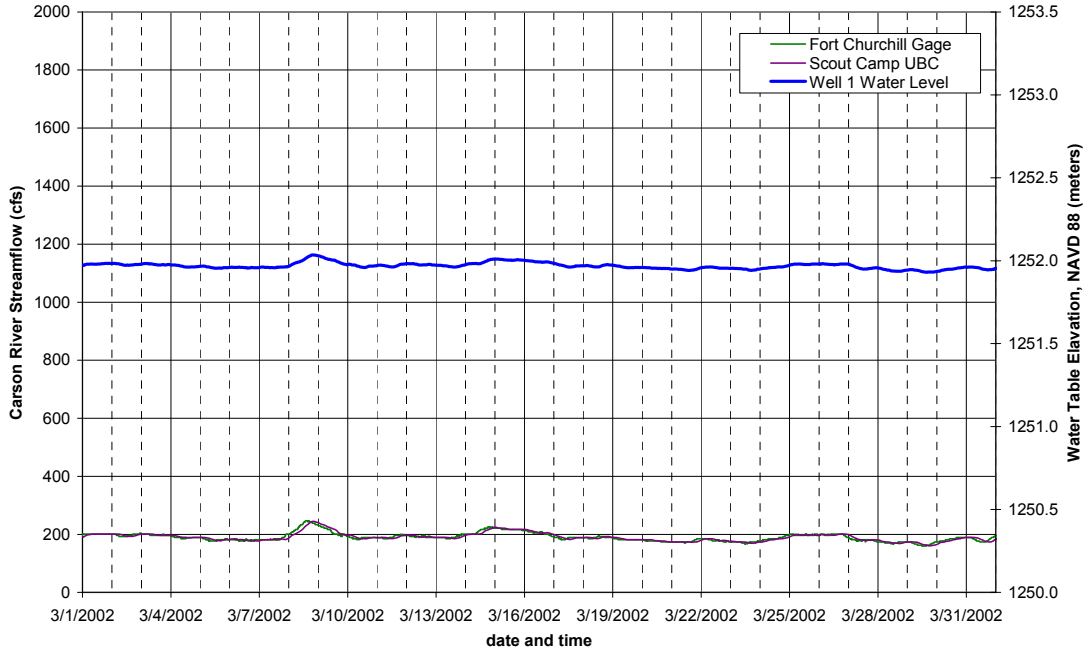

Figure B-15. March 2002

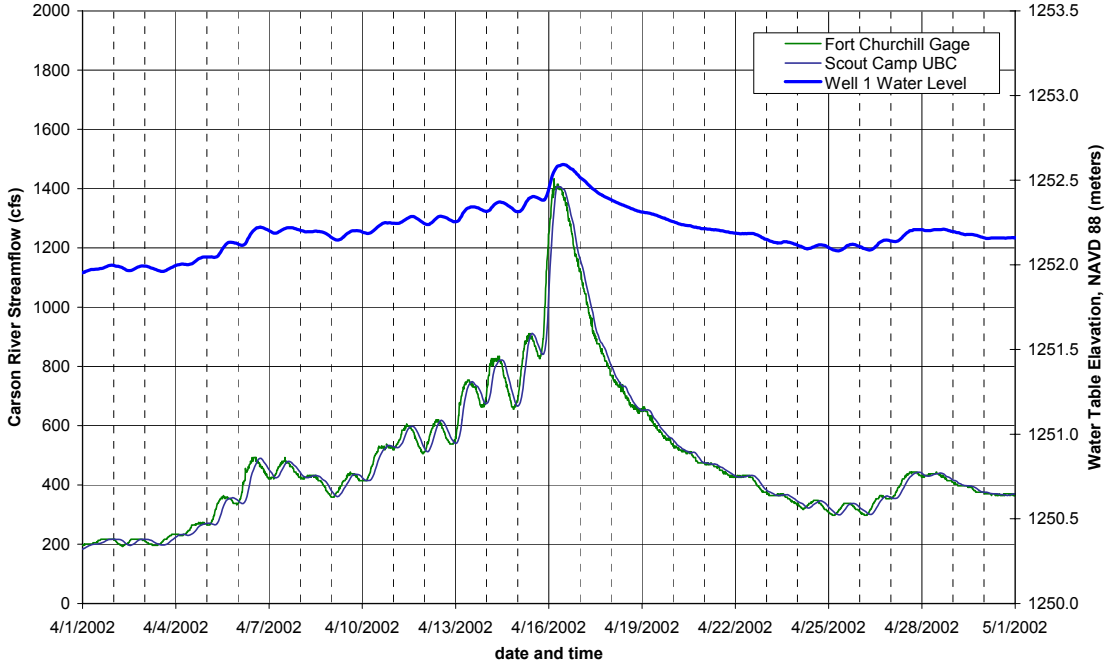

Figure B-16. Near-channel well response to streamflow variability, April 2002

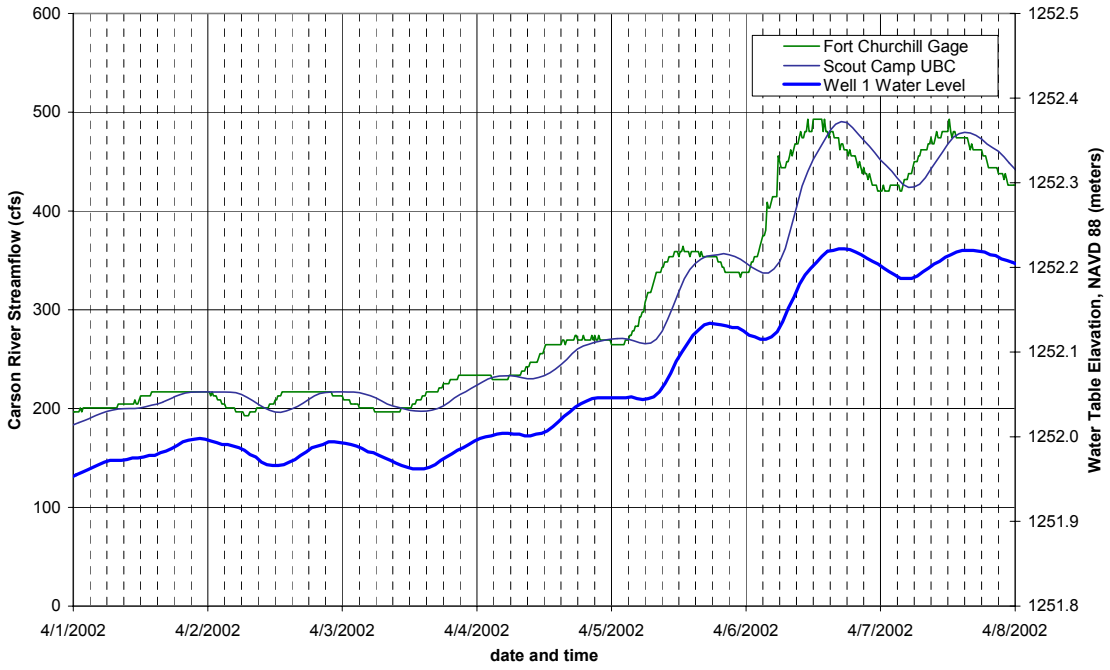

Figure B-17. April 1-7, 2002

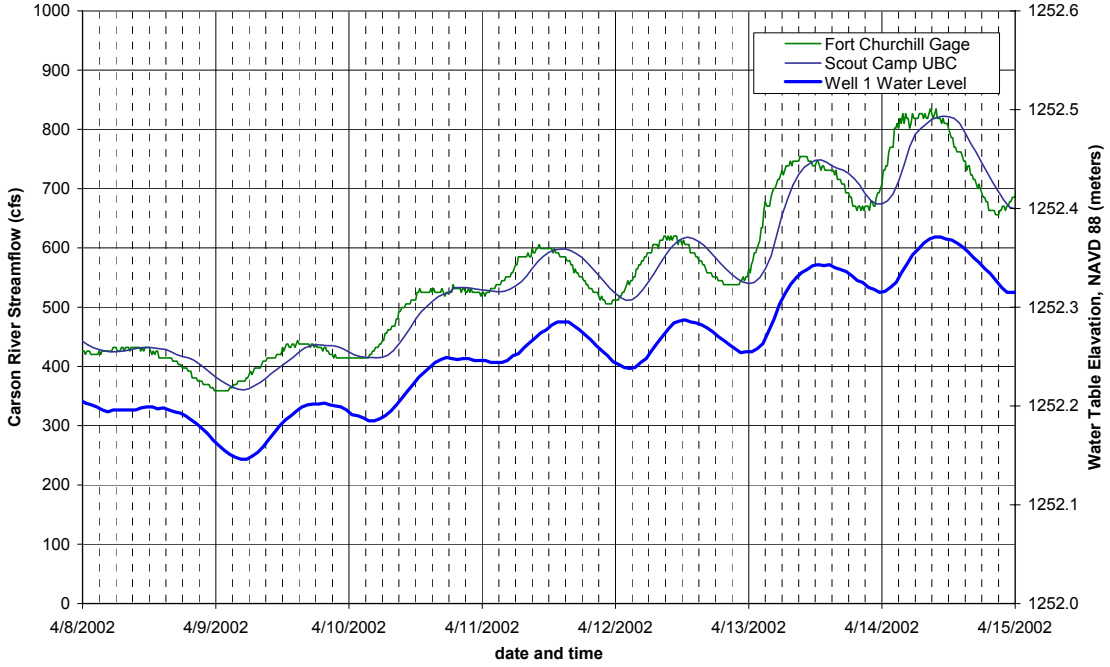

Figure B-18. April 8-14, 2002

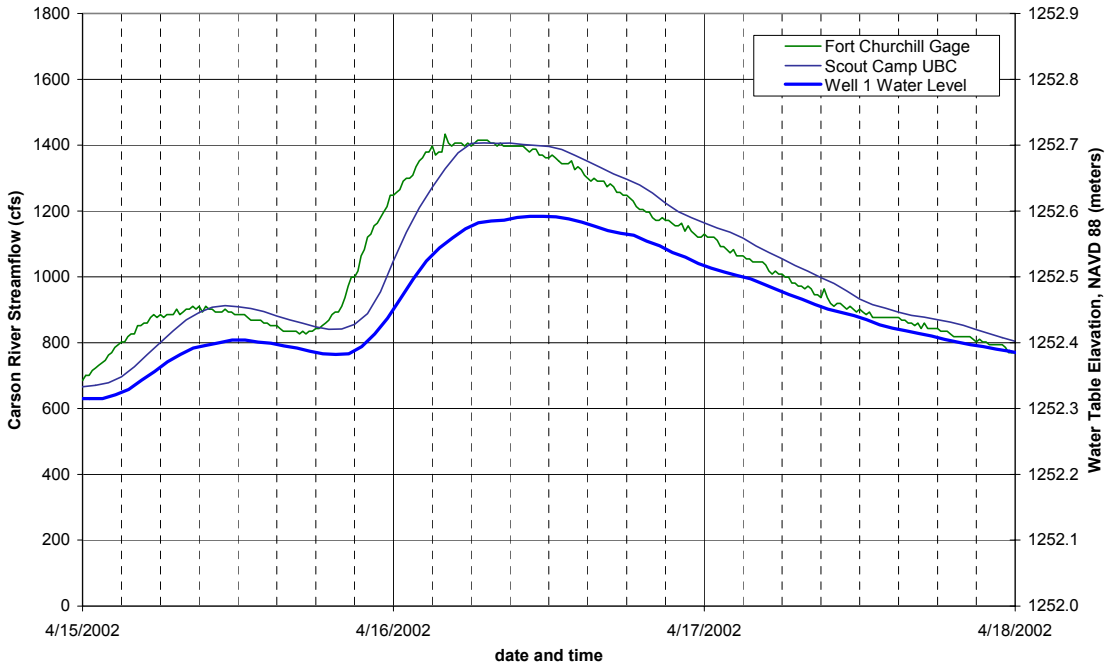

Figure B-19. April 15-17, 2002

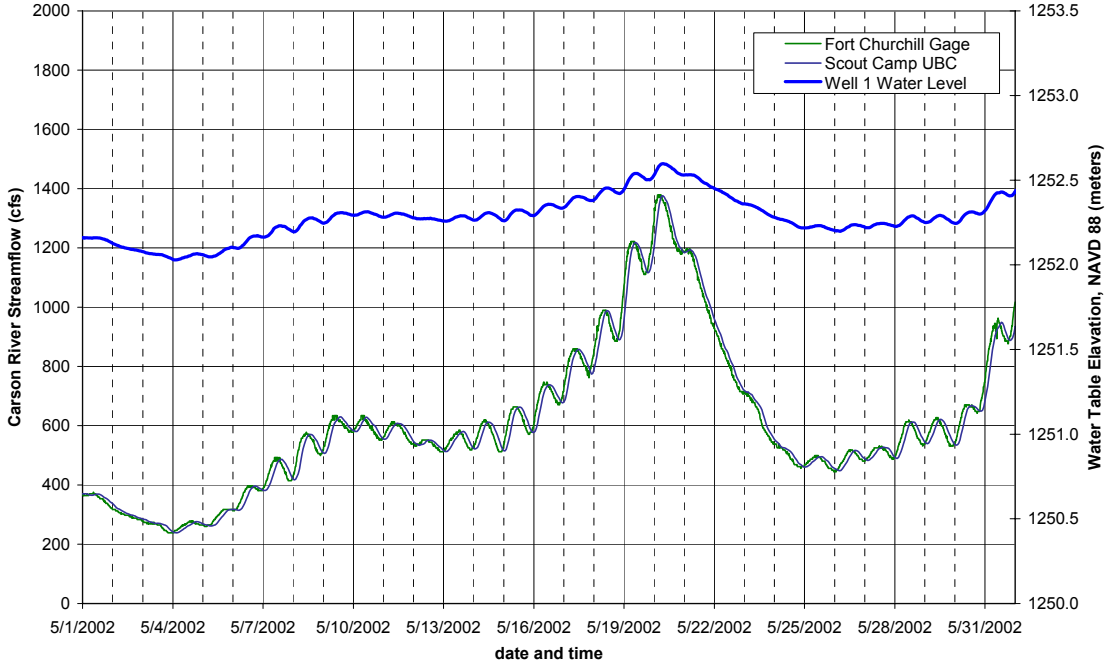

Figure B-20. May 2002

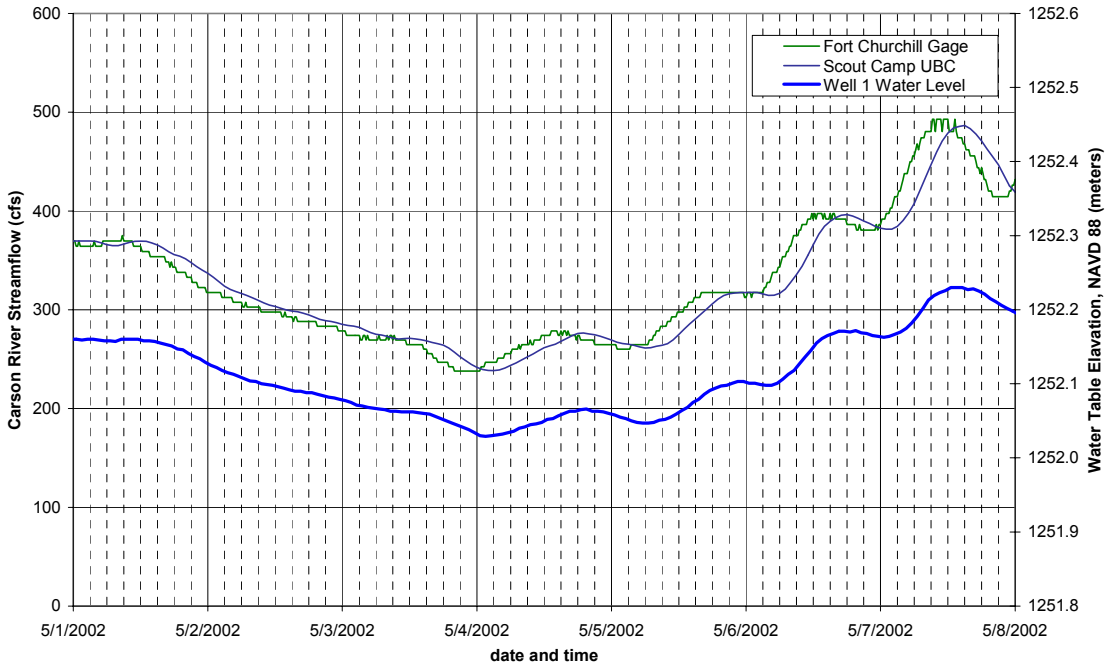

Figure B-21. May 1-7, 2002

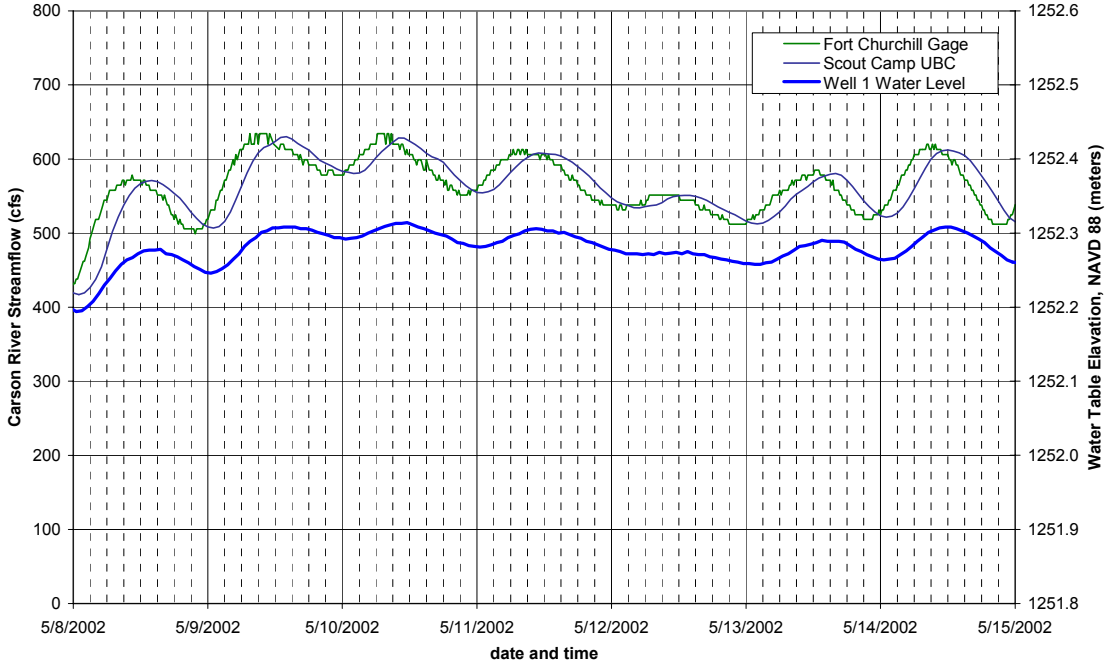

Figure B-22. May 8-14, 2002

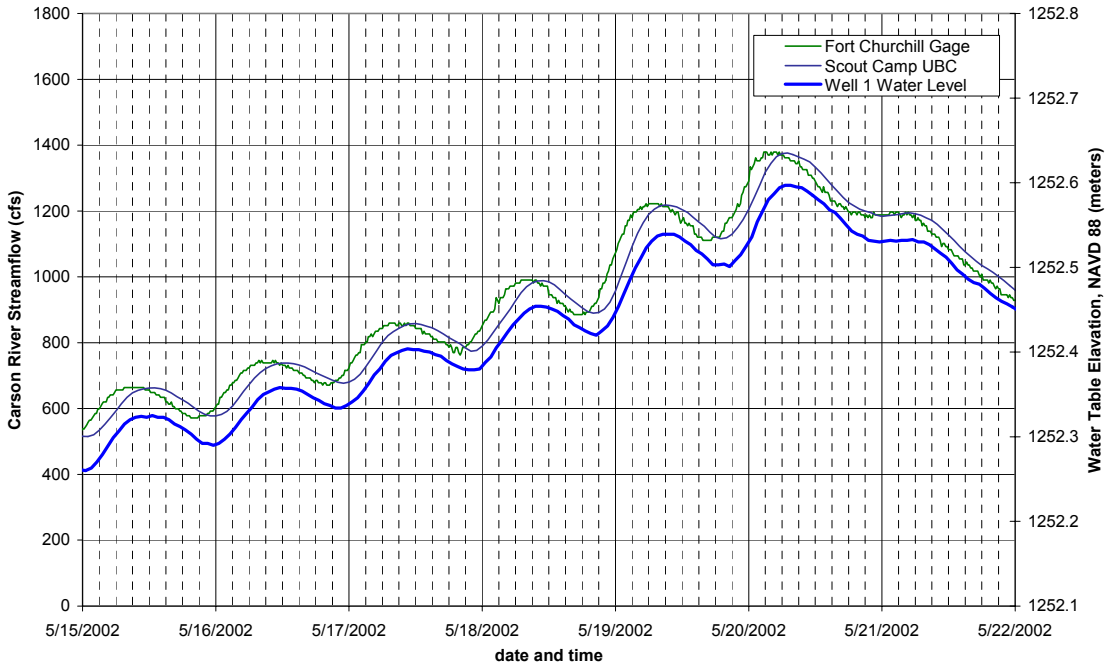

Figure B-23. May 15-21, 2002

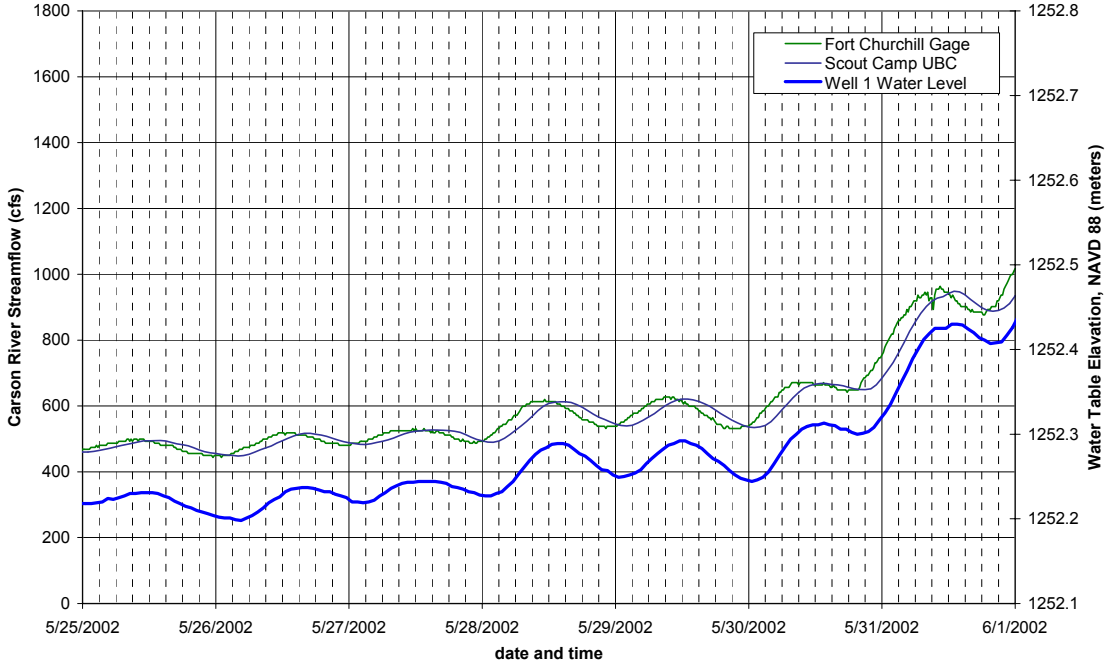

Figure B-24. May 25-31, 2002

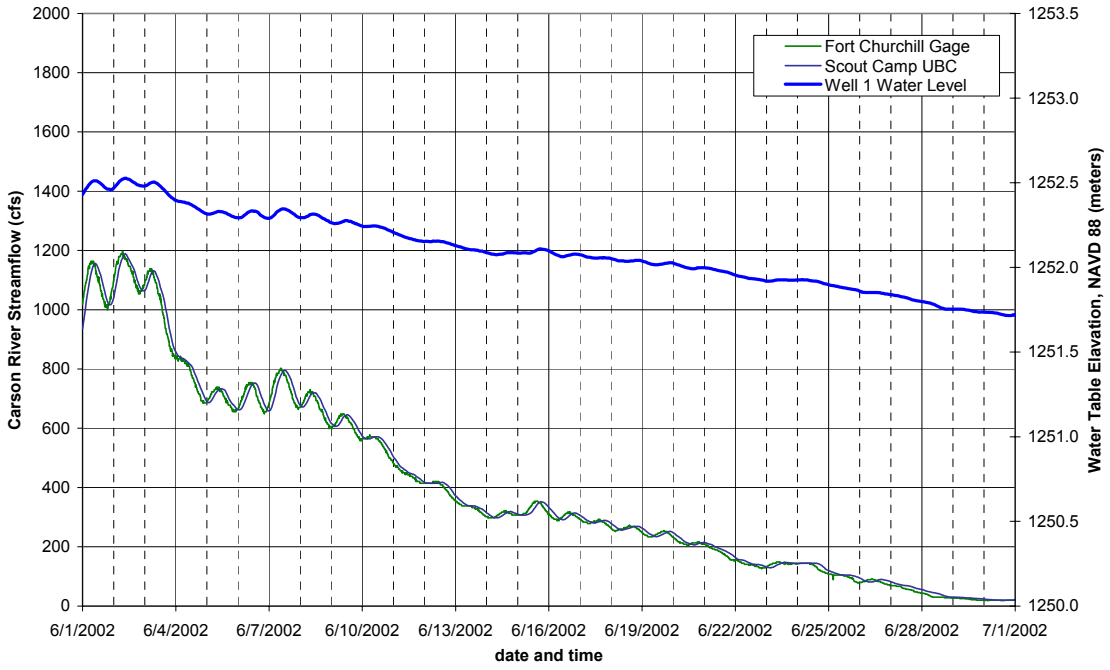

Figure B-25. June 2002

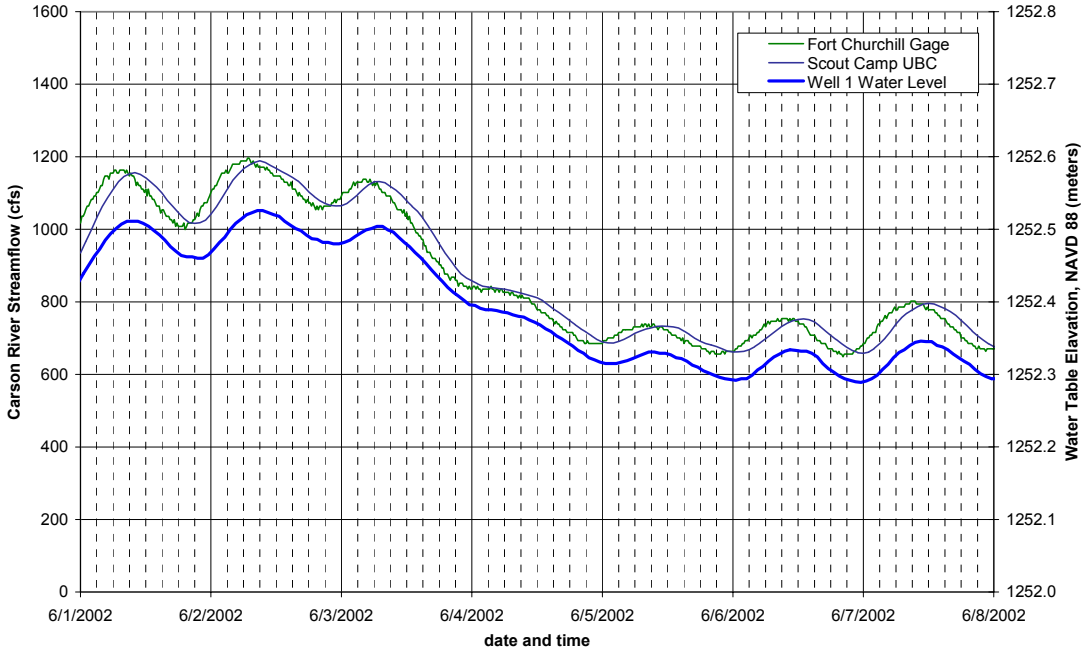

Figure B-26. June 1-7, 2002

APPENDIX C
ELEMENT DRYING AND WATER SURFACE LOWERING WITHIN COMPLETED SMS MODEL

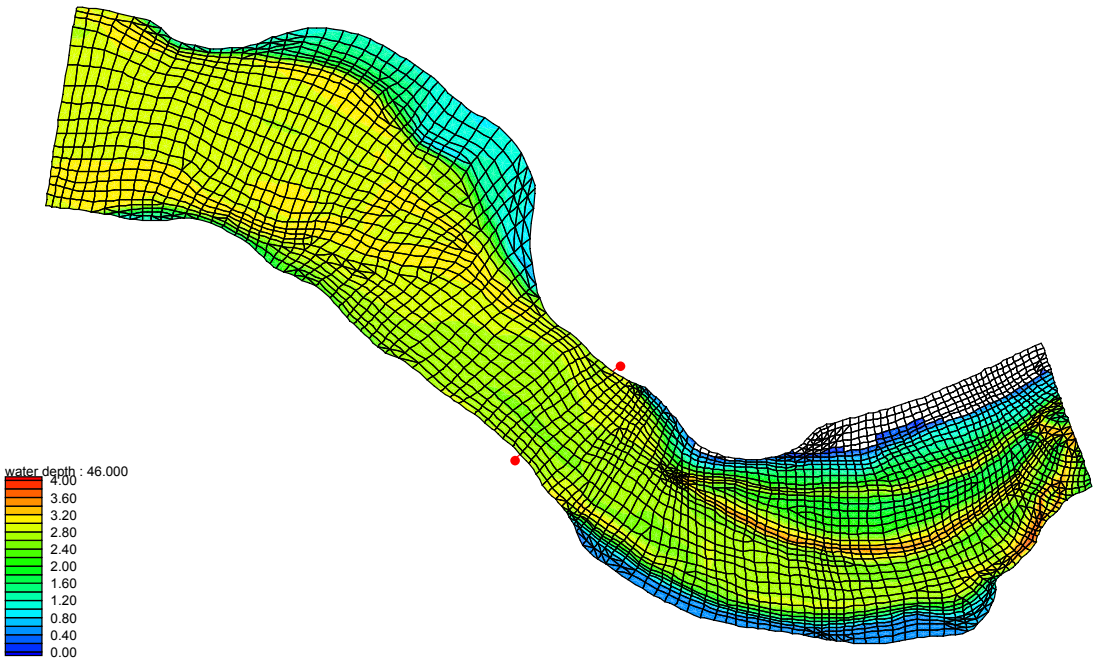

Figure C-1. Northwest channel bank

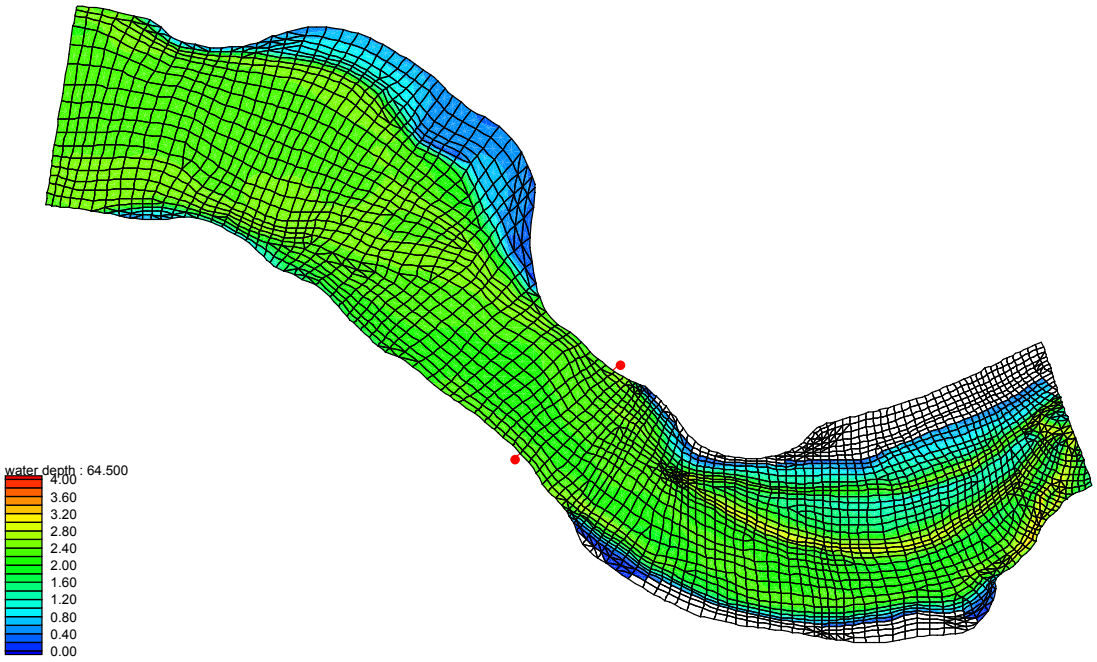

Figure C-2. Southwest channel bank rip-rap

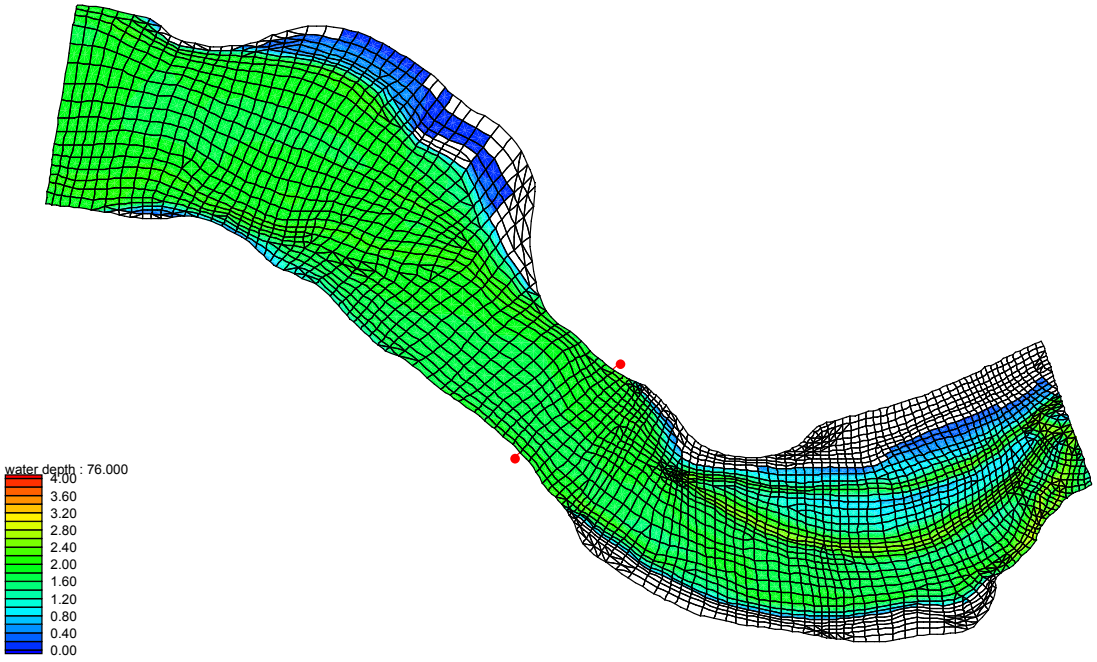

Figure C-3. North-central channel bank

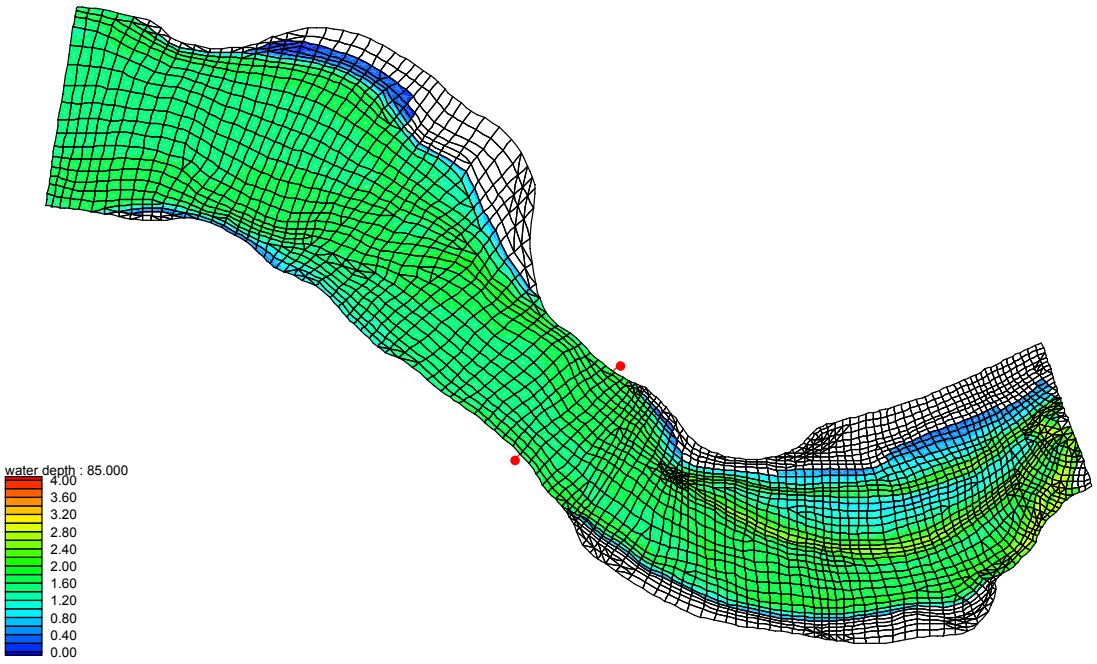

Figure C-4. Northeast channel bank

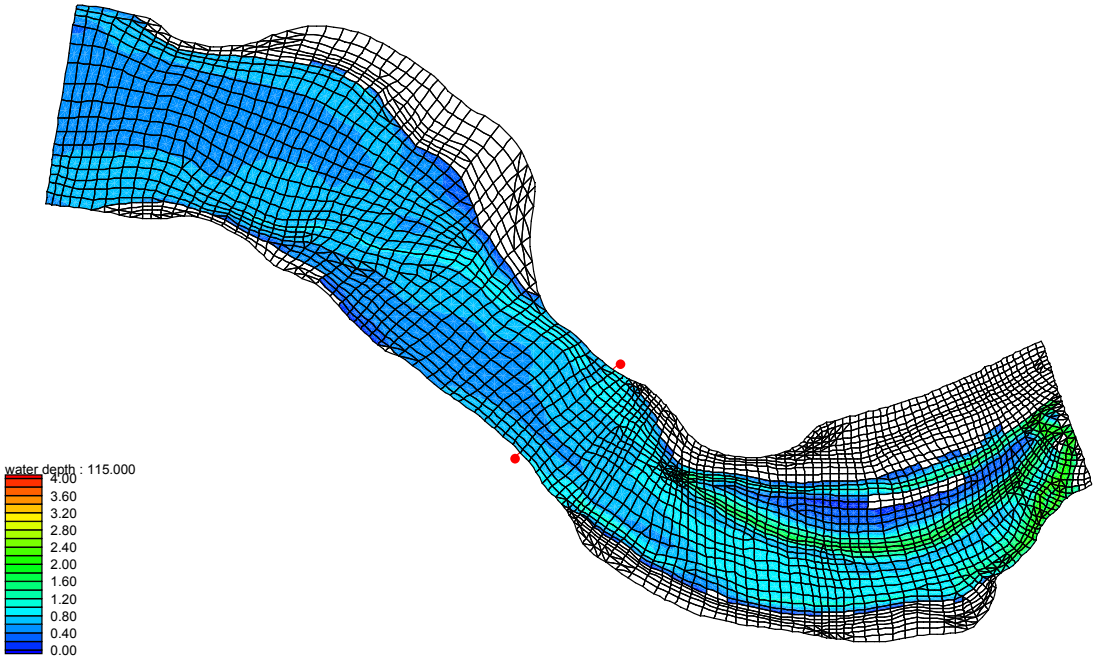

Figure C-5. Southeast channel bank

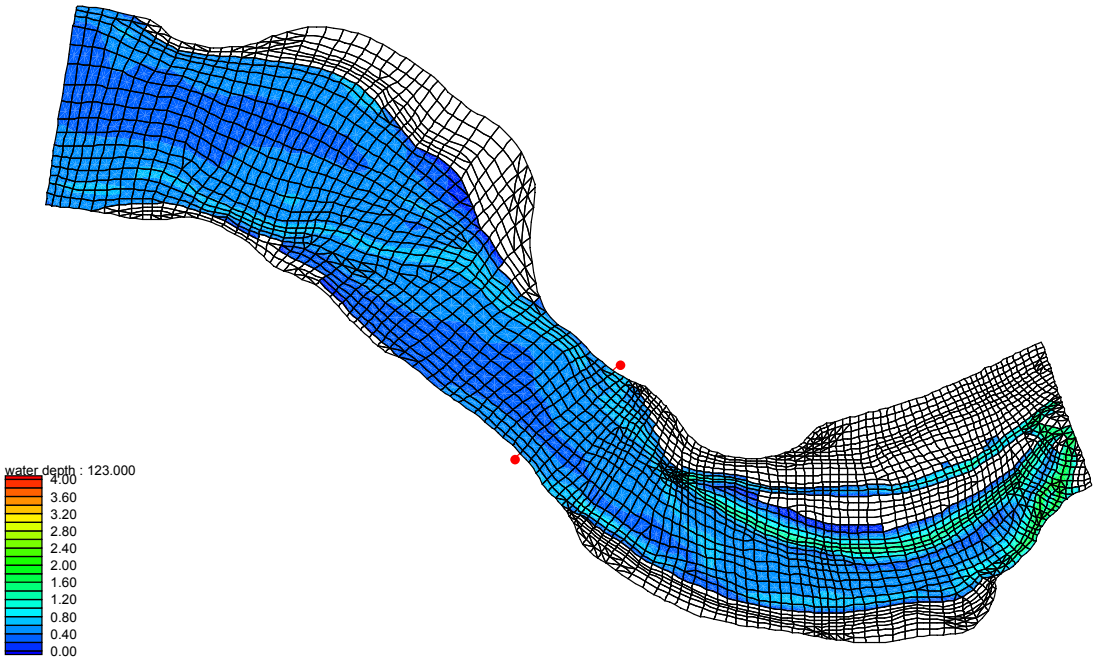

Figure C-6. Western channel bed

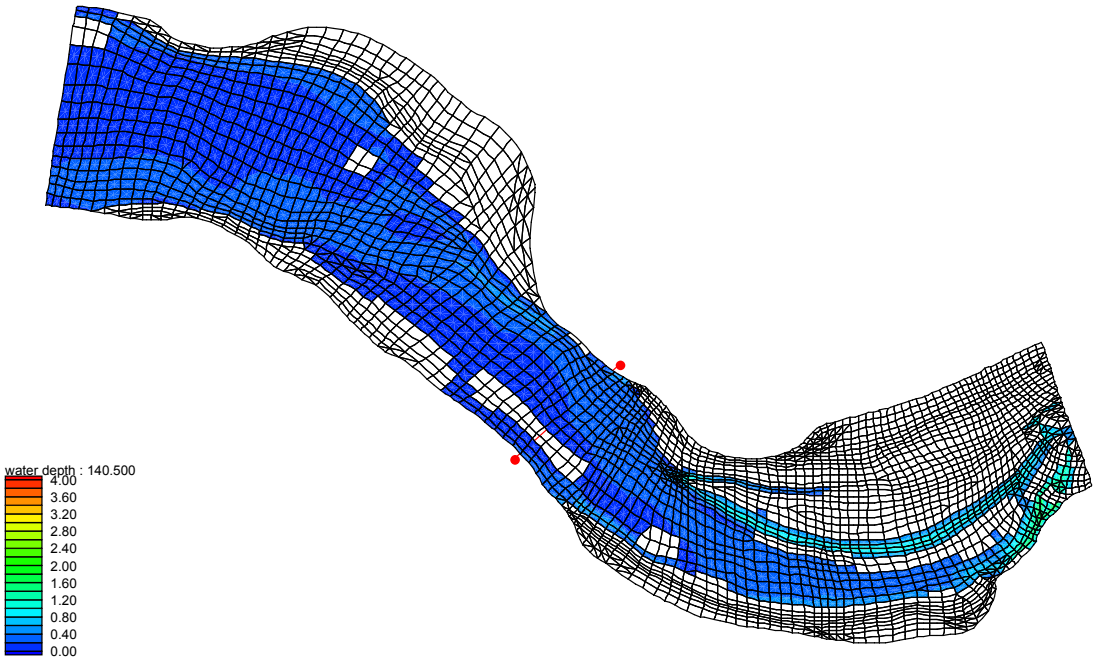

Figure C-7. Central channel bed

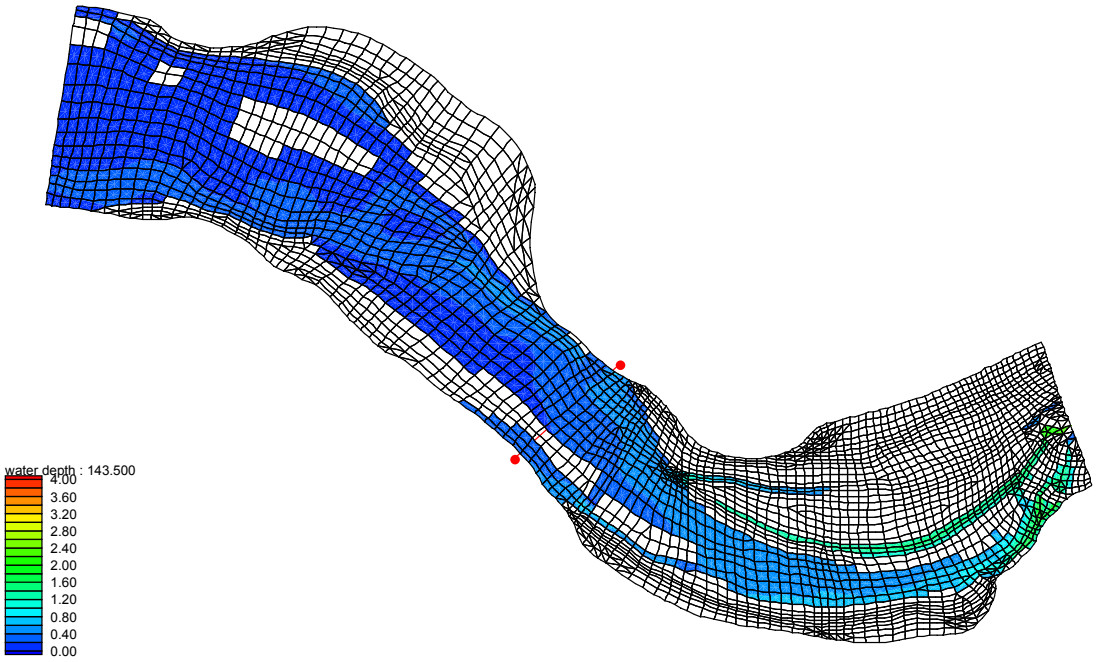

Figure C-8. Channel bed, minimum flow level for 1.99-meter head loss

LIST OF REFERENCES

Ambrose, R.B., Wool, T.A., Martin, J.P. and Schanz, R.W., 1991. WASP5.X—A Hydrodynamic and Water Quality Model: Model theory, User's Manual, and Programmer's Guide. U.S. EPA, Athens, Georgia.

Amyot, M., Kraepiel, A.M.L. and Morel, F.M.M., 1998. The Chemical Cycle and Bioaccumulation of Mercury. Annual Reviews: Ecology and Systematics, 29, 543-566.

Arteaga, F.E., 1986. Mathematical Model Analysis of the Eagle Valley Ground-Water Basin, West-Central Nevada. Nevada Division of Water Resources Bulletin 45.

Babiarz, C.L., Hurley, J.P., Benoit, J.M., Shafer, M.M., Andren, A.W. and Webb, D.A., 1998. Seasonal Influences on Partitioning and Transport of Total and Methylmercury in Rivers from Contrasting Watersheds. Biogeochemistry, 41, 237-257.

Balogh, S.J., Meyer, M.L. and Johnson, D.K., 1997. Mercury and Suspended Sediment Loadings in the Lower Minnesota River. Environmental Science and Technology, 31(1), 198-202.

Barlow, P.M., DeSimone, L.A. and Moench, A.F., 2000. Aquifer Response to Stream-stage and Recharge Variations: II. Convolution Method and Applications. Journal of Hydrology, 230, 211-229.

Bloom, N.S. and Effler, S.W., 1990. Seasonal Variability in the Mercury Speciation of Onondaga Lake (New York). Water, Air, and Soil Pollution, 53(3-4), 251-265.

Bonzongo, J.C., Heim, K.J., Chen, Y., Lyons, W.B., Warwick, J.J., Miller, G.C. and Lechler, P.J., 1996a. Mercury Pathways in the Carson River-Lahontan Reservoir System, Nevada, USA. Environmental Toxicology and Chemistry, 15(5), 677-683.

Bonzongo, J.C., Heim, K.J., Warwick, J.J. and Lyons, W.B., 1996b. Mercury Levels in Surface Waters of the Carson River-Lahontan Reservoir System, Nevada: Influence of Historic Mining Activities. Environmental Pollution, 92(2), 193-201.

Boulton, A.J., Findlay, S., Marmonier, P., Stanley, E.H. and Valett, H.M., 1998. The Functional Significance of the Hyporheic Zone in Streams and Rivers. Annual Reviews: Ecology and Systematics, 29, 59-81.

Callister, S.M. and Winfrey, M.R., 1986. Microbial Methylation of Mercury in Upper Wisconsin River Sediments. Water, Air, and Soil Pollution, 29(4), 453-465.

Carroll, R.W.H., 1999. Simulation of Mercury Transport and Fate in the Carson River, Nevada. Masters Thesis. University of Nevada-Reno, Reno, Nevada.

Carroll, R.W.H., James, A.I., Warwick, J.J. and Miller, J.R., in press. Modeling Erosion and Overbank Deposition During Extreme Flood Conditions on the Carson River, Nevada. Journal of Hydrology.

Carroll, R.W.H. and Warwick, J.J., 2001. Uncertainty analysis of the Carson River mercury transport model. Ecological Modeling, 137, 211-224.

Carroll, R.W.H., Warwick, J.J., Heim, K.J., Bonzongo, J.C., Miller, J.R. and Lyons, W.B., 2000. Simulation of Mercury Transport and Fate in the Carson River, Nevada. Ecological Modeling, 125, 255-278.

Chen, Y., Bonzongo, J.C., Lyons, W.B. and Miller, G.C., 1997. Inhibition of Mercury Methylation in Anoxic Freshwater Sediment by Group VI Anions. Environmental Toxicology and Chemistry, 16(8), 1568-1574.

Chen, Y., Bonzongo, J.C. and Miller, G.C., 1996. Levels of Methylmercury and Controlling Factors in Surface Sediments of the Carson River System, Nevada. Environmental Pollution, 92(3), 281-287.

Cooper, H.H., Jr. and Rorabaugh, M.I., 1963. Changes in Ground-Water Movement and Bank Storage Caused by Flood Waves in Surface Streams. U.S. Geological Survey Professional Paper 475-B, B192-B195.

Covay, K.J., Banks, J.M., Bevans, H.E. and Watkins, S.A., 1996. Environmental and Hydrologic settings of the Las Vegas Valley Area and the Carson and Truckee River Basins, Nevada and California. U.S. Geological Survey Water-Resources Investigations Report 96-4087.

de Magalhaes, M.E. and Tubino, M., 1995. A Possible Path for Mercury in Biological Systems: The oxidation of Metallic Mercury by Molecular Oxygen in Aqueous Solutions. The Science of the Total Environment, 170(3), 229-239.

Dever, R.J., Jr. and Cleary, R.W., 1979. Unsteady-State, Two-dimensional Response of Leaky Aquifers to Stream Stage Fluctuations. Advances in Water Research, 2, 13-18.

Fetter, C.W., 2001. Applied Hydrogeology. Prentice Hall, Inc., Upper Saddle River, New Jersey.

Fitzgerald, W.F. and Clarkson, T.W., 1991. Mercury and Monomethylmercury: Present and Future Concerns, Global Atmospheric Change and Human Health. Environmental Health Perspectives, 96, 159-166.

Fitzgerald, W.F. and Mason, R.P., 1997. Biogeochemical Cycling of Mercury in the Marine Environment. In: A. Sigel and H. Sigel (editors), Mercury and its Effects on Environment and Biology-Metal Ions in Biological Systems. Marcel Dekker, Inc., pp. 53-111.

Freeze, R.A., 1971. Three-dimensional, Transient, Saturated-Unsaturated Flow in a Groundwater Basin. Water Resources Research, 7(2), 347-366.

Freeze, R.A. and Cherry, J.A., 1979. Groundwater. Prentice-Hall, Inc, Englewood Cliffs, New Jersey.

Froehlich, D.C., 2000. Finite Element Surface-Water Modeling System: Two-Dimensional Flow in a Horizontal Plane, Version 2, User's Manual.

Fuller, C.C. and Harvey, J.W., 2000. Reactive Uptake of Trace Metals in the Hyporheic Zone of a Mining-Contaminated Stream, Pinal Creek, Arizona. Environmental Science and Technology, 34(7), 1150-1155.

Gill, G.A. and Bruland, K.W., 1990. Mercury Speciation in Surface Freshwater Systems in California and Other Areas. Environmental Science and Technology, 24(9), 1392-1400.

Gill, M.A., 1985. Bank Storage Characteristics of a Finite Aquifer Due to Sudden Rise and Fall of River Level. Journal of Hydrology, 76, 133-142.

Gilmour, C.C. and Henry, E.A., 1991. Mercury Methylation in Aquatic Systems Affected by Acid Deposition. Environmental Pollution, 71, 131.

Gilmour, C.C., Henry, E.A. and Mitchell, R., 1992. Sulfate Stimulation of Mercury Methylation in Freshwater Sediments. Environmental Science and Technology, 26(11), 2281-2287.

Govindaraju, R.S. and Koelliker, J.K., 1994. Applicability of Linearized Boussinesq Equation for Modeling Bank Storage under Uncertain Aquifer Parameters. Journal of Hydrology, 157, 349-366.

Hall, F.R. and Moench, A.F., 1972. Application of the Convolution Equation to Stream Aquifer Relations. Water Resources Research, 8(2), 487-493.

Hantush, M.S., 1967. Flow of Groundwater in Relatively Thick Leaky Aquifers. Water Resources Research, 3, 583.

Hantush, M.M., Harada, M. and Marino, M.A., 2001. Modification of Stream Flow Routing for Bank Storage. EPA/600/A-01/052.

Harada, M., Hantush, M.M. and Marino, M.A., 2000. Hydraulic Analysis on Stream-Aquifer Interaction by Storage Function Models. EPA/600/A-00/071.

Heim, K.J. and Warwick, J.J., 1997 Simulating Sediment Transport in the Carson River and Lahontan Reservoir, Nevada, USA. Journal of the American Water Resources Association, 33(1), 177-191.

Hoffman, R.J. and Thomas, K.A., 2000. Methylmercury in Water and Bottom Sediment Along the Carson River System, Nevada and California, September 1998. U.S. Geological Survey Water-Resources Investigations Report 00-4013.

Hornberger, G.M., Ebert, J. and Remson, I., 1970. Numerical Solution of the Boussinesq Equation for Aquifer-Stream Interaction. Water Resources Research, 6(2), 601-608.

Hosseinipour, E.Z. and Martin, J.L., 1990. RIVMOD—A One-dimensional Hydrodynamic and Sediment Transport Model: Model Theory and User's Manual.

Hudson, J.M., Gherini, S.A., Watras, C.J. and Porcella, D.B., 1994. Modeling the Biogeochemical Cycle of Mercury in Lakes: The Mercury Cycling Model (MCM) and its Application to the MTL Study Lakes. In: Watras, C.J. and Huckabee, J.W. (editors), Mercury Pollution: Integration and Synthesis. Lewis Publishers, Boca Raton, New York, pp. 473-523.

Hunt, B., 1990. An Approximation for the Bank Storage Effect. Water Resources Research, 26(11), 2769-2775.

Hurley, J.P., Benoit, J.M., Babiarz, C.L., Shafer, M.M., Andren, A.W., Sullivan, J.R., Hammond, R. and Webb, D.A., 1995. Influences of Watershed Characteristics on Mercury Levels in Wisconsin Rivers. Environmental Science and Technology, 29(7), 1867-1875.

Jones, J.B., Jr. and Holmes, R.M., 1996. Surface-Subsurface Interactions in Stream Ecosystems. Trends in Ecology and Evolution (TREE), 11(6), 239-242.

Kennedy, E.J., 1984. Discharge Ratings at Gaging Stations. Techniques of Water-Resources Investigations of the United States Geological Survey, Chapter A10.

Lechler, P.J., Miller, J.R., Hsu, L. and Desilets, M.O., 1997. Mercury Mobility at the Carson River Superfund Site, West-Central Nevada, USA: Interpretation of Mercury Speciation Data in Mill Tailings, Soils, and Sediments. Journal of Geochemical Exploration, 58, 259-267.

Lin, H.J., Richards, D.R., Talbot, C.A.,Yeh, G., Cheng, J., Cheng, H. and Jones, N.L., 1996. FEMWATER: A Three-Dimensional Finite Element Computer Model for Simulating Density-Dependant Flow and Transport in Variably Saturated Media, Version 3.0.

Marino, M.A., 1975. Digital Simulation Model of Aquifer Response to Stream Stage Fluctuation. Journal of Hydrology, 25, 51-58.

Martin, J.L., 1992. MERC4: A Mercury Transport and Kinetics Model: Model Theory and User's Guide. U.S. EPA, Athens, Georgia.

Marvin-DiPasquale, M. and Oremland, R.S., 1999. Methylmercury Formation and Degradation in Sediments of the Carson River System, Interim Report I. U.S Geologic Survey Water Resources Division, Menlo Park, CA.

Matilainen, T., 1995. Involvement of Bacteria in Methylmercury Formation in Anaerobic Lake Waters. Water, Air, and Soil Pollution, 81(1-4), 757-764.

Maurer, D.K., 1986. Geohydrology and Simulated Response to Ground-water Pumpage in Carson Valley, a River-dominated Basin in Douglas County, Nevada and Alpine County, California. U.S. Geological Survey Water-Resources Investigations Report 86-4328.

Meade, R.H., Moody, J.A. and Stevens, J.H.H., 1995. Contaminants in the Mississippi River 1987-1992. U.S. Geological Survey Circular 1133.

Miller, J., Barr, R., Grow, D., Lechler, P., Richardson, D., Waltman, K. and Warwick, J., 1999. Effects of the 1997 Flood on the Transport and Storage of Sediment and Mercury within the Carson River Valley, West-Central Nevada. The Journal of Geology, 107, 313-327.

Miller, J.R. and Lechler, P.J., 1998. Mercury Partitioning within Alluvial Sediments of the Carson River Valley, Nevada: Implications for Sampling Strategies an Tropical Environments. In: J.W.e. al. (editor), Geochemistry of Tropical Environments. Springer-Verlag, pp. 211-233.

Miller, J.R., Lechler, P.J. and Desilets, M., 1998. The Role of Gepmorphic Processes in the Transport and Fate of Mercury in the Carson River Basin, West-Central Nevada. Environmental Geology, 33(4), 249-262.

Miller, J.R., Rowland, J., Lecher, P.J., Desilets, M. and Hsu, L., 1996. Dispersal of Mercury-Contaminated Sediments by Geomorphic Processes, Sixmile Canyon, Nevada, USA: Implications to Site Characterization and Remediation of Fluvial Environments. Water, Air, and Soil Pollution, 86, 373-388.

Moench, A.F. and Barlow, P.F., 2000. Aquifer Response to Stream-stage and Recharge Variations: I. Analytical Step-response Functions. Journal of Hydrology, 230, 192-210.

Moench, A.F., Sauer, V.B. and Jennings, M.E., 1974. Modification of Routed Streamflow by Channel Loss and Base Flow. Water Resources Research, 10(5), 963-968.

Morel, F.M.M. and Hering, J.G., 1993. Principles and Applications of Aquatic Chemistry. John Wiley and Sons, New York, NY.

Morel-Seytoux, H.J., 1975. A Combined Model of Water Table and River Stage Evolution. Water Resources Research, 11(6), 968-972.

Neuman, S.P., 1975. Analysis of pumping test data from anisotropic unconfined aquifers considering delayed gravity response. Water Resources Research, 11, 329-342.

Neuman, S.P. and Witherspoon, P.A., 1969. Applicability of current theories of flow in leaky aquifers. Water Resources Research, 5, 817-829.

Neuman, S.P. and Witherspoon, P.A., 1971. Analysis of Nonsteady Flow with a Free Surface Using the Finite Element Method. Water Resources Research, 7(3), 611-623.

Nevada Division of Water Planning (NDWP), 1996. Carson River Chronology.

Perkins, S.P. and Koussis, A.D., 1996. Stream-Aquifer Interaction Model with Diffusive Wave Routing. Journal of Hydraulic Engineering, 210-218.

Pinder, G.F. and Sauer, S.P., 1971. Numerical Solution of Flood Wave Modification Due to Bank Storage Effects. Water Resources Research, 7(1), 63-70.

Porvari, P. and Verta, M., 1994. Methylmercury Production in Flooded Soils: A Laboratory Study. Water, Air, and Soil Pollution, 80(1-4), 765-773.

Schaefer, D.H. and Whitney, R., 1992. Geological Framework and Ground-water Conditions in Basin-fill Aquifers of the Dayton Valley and Churchill Valley Hydrographic Areas, Western Nevada. U.S. Geological Survey Water-Resources Investigations Report 91-4072.

Serrano, S.E. and Workman, S.R., 1998. Modeling Transient Stream/Aquifer Interaction with the Non-linear Boussinesq Equation and its Analytical Solution. Journal of Hydrology, 206, 245-255.

Sharp, J.M., Jr., 1977. Limitations of Bank-Storage Model Assumptions. Journal of Hydrology, 35, 31-47.

SMS: Surface Water Modeling System, Tutorial: Version 8.0, 2000. Brigham Young University – Environmental Modeling Research Laboratory.

Squillace, P.J., 1996. Observed and Simulated Movement of Bank-Storage Water. Ground Water, 34(1), 121-134.

Stordal, M.C. and Gill, G.A., 1995. Determination of Mercury Methylation Rates using a 203-Hg Radiotracer Technique. Water, Air, and Soil Pollution, 80(1-4), 725-734.

Thomann, R.V.and Mueller, J.A., 1987. Principles of Surface Water Quality Monitoring and Control. Harper Collins Publishers, New York, New York, pp. 549.

Tindall, J.A. and Kunkel, J.R., 1999. Unsaturated Zone Hydrology for Scientists and Engineers. Prentice-Hall, Inc., Upper Saddle River, New Jersey.

Trexler, D.T., 1977. Geologic Map, Carson City Quadrangle. Nevada Bureau of Mines and Geology Urban Map Series, Carson City Folio, Map 1Ag, scale 1:24000.

United States Department of Health and Human Services (USDHHS), 1997. Toxicological Profile for Mercury. Public Health Service.

United States Environmental Protection Agency (USEPA), 1997. Mercury Study Report to Congress, Volume III: Fate and Transport of Mercury in the Environment. EPA-452/R-97-003.

USEPA, 2000. Mercury Research Strategy. EPA/600/R-00/073.

United States Geological Survey (USGS), 1995. Mercury Contamination of Aquatic Ecosystems. U.S. Geological Survey Fact Sheet 216-95.

USGS, 1997. Flood of January 1997 in the Carson River Basin, California and Nevada. U.S. Geological Survey Fact Sheet 183-97.

van Rijn, L.C., 1984a. Sediment Transport, Part I: Bed Load Transport. Journal of Hydraulic Engineering, 110(10), 1431-1456.

van Rijn, L.C., 1984b. Sediment Transport, Part II: Suspended Load Transport. Journal of Hydraulic Engineering, 110(11), 1613-1641.

Warwick, J.J. and Heim, K.J., 1995. Hydrodynamic Modeling of the Carson River and Lahontan Reservoir, Nevada. Water Resources Bulletin, 31(1), 67-77.

Watras, C.J., Bloom, N.S, Claas, S.A., Morrison, K.A, Golmour, C.C. and Craig, S.R., 1995a. Methylmercury Production in the Anoxic Hypolimnion of a Dimictic Seepage Lake. Water, Air, and Soil Pollution, 80(1-4), 735-745.

Watras, C.J., Morrison, K.A., Host, J.S. and Bloom, N.S., 1995b. Concentration of Mercury Species in Relationship to other Site-Specific Factors in the Surface Waters of Northern Wisconsin Lakes. Limnology and Oceanography, 40(3), 556-565.

Wayne, D.M., Warwick, J.J., Lechler, P.J., Gill, G.A. and Lyons, W.B., 1996. Mercury Contamination in the Carson River, Nevada: A Preliminary Study of the Impact of Mining Wastes. Water, Air, and Soil Pollution, 92, 391-408.

Whiting, P.J. and Pomeranets, M., 1997. A Numerical Study of Bank Storage and its Contribution to Streamflow. Journal of Hydrology, 202, 121-136.

Wise, W.R., Clement, T.P. and Molz, F.J., 1994. Variably Saturated Modeling of Transient Drainage: Sensitivity to Soil Properties. Journal of Hydrology, 161, 91-108.

Workman, S.R., Serrano, S.E. and Liberty, K., 1997. Development and Application of an Analytical Model of Stream/Aquifer Interaction. Journal of Hydrology, 200, 149-163.

Xun, L., Campbell, N.E.R. and Rudd, J.W.M., 1987. Measurements of Specific Rates of Net Methylmercury Production in the Water Column and Surface Sediments of Acidified and Circumneutral Lakes. Canadian Journal of Fisheries and Aquatic Sciences, 44, 750-757.

Yeh, W.W-G., 1970. Nonsteady Flow to a Surface Reservoir. ASCE Journal of Hydraulics, 96(3), 609-618.

Zillioux, E.J., Porcella, D.B. and Benoit, J.M., 1993. Mercury Cycling and Effects in Freshwater Wetland Ecosystems. Environmental Toxicology and Chemistry, 12, 2245-2264.

Zitta, V.L. and Wiggert, J.M., 1971. Flood Routing in Channels with Bank Seepage. Water Resources Research, 7(5), 1341-1345.

Zlotnik, V.A. and Huang, H., 1999. Effect of Shallow Penetration and Streambed Sediments on Aquifer Response to Stream Stage Fluctuations (Analytical Model). Ground Water, 37(4), 599-605.

BIOGRAPHICAL SKETCH

Daniel Eugene Crawford was born in Jacksonville, Florida on February 22, 1978. Raised in Jacksonville, he departed to attend the University of Florida in the Fall of 1996. This was the best of times to be a Gator football fan. He graduated with a B.S. in environmental engineering in the Fall of 2001. Staying on for another 2 years, he completed the requirements for his M.E. in environmental engineering in the Spring of 2003.